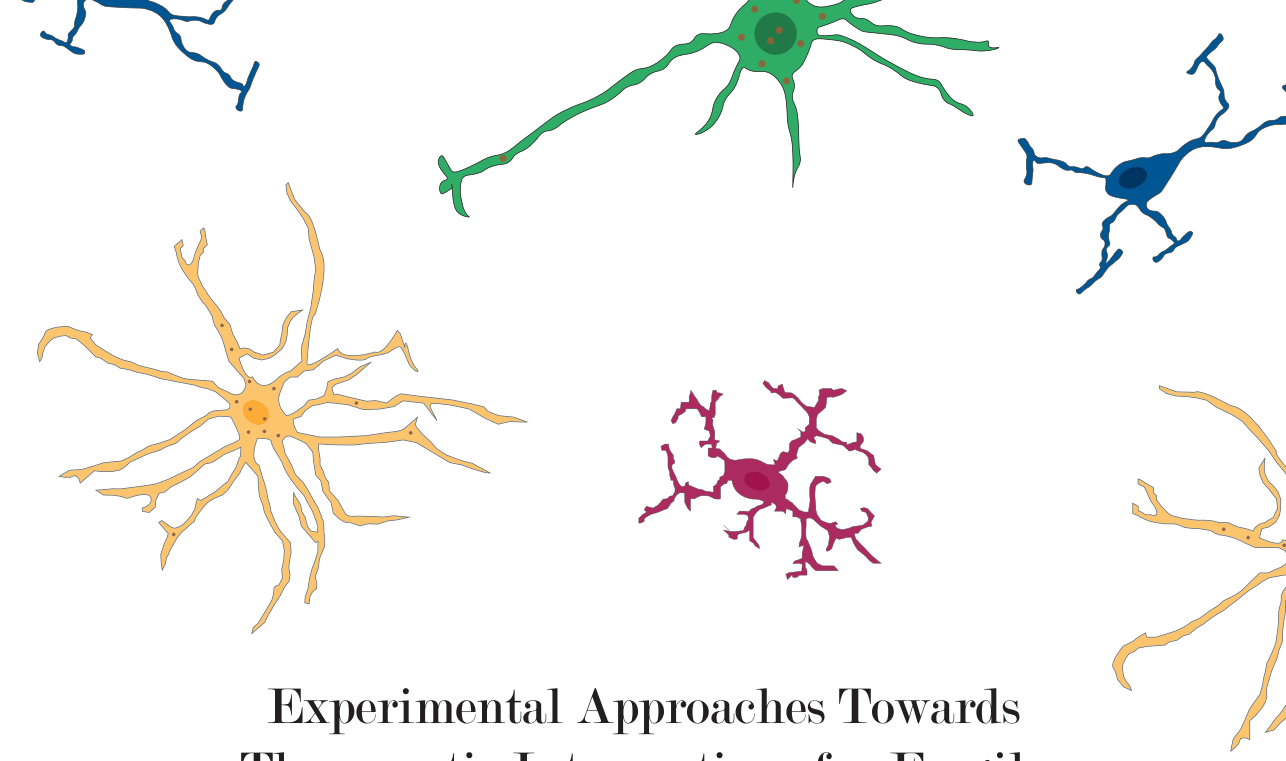

Experimental Approaches Towards Therapeutic Interventions for Fragile X-associated Tremor and Ataxia Syndrome

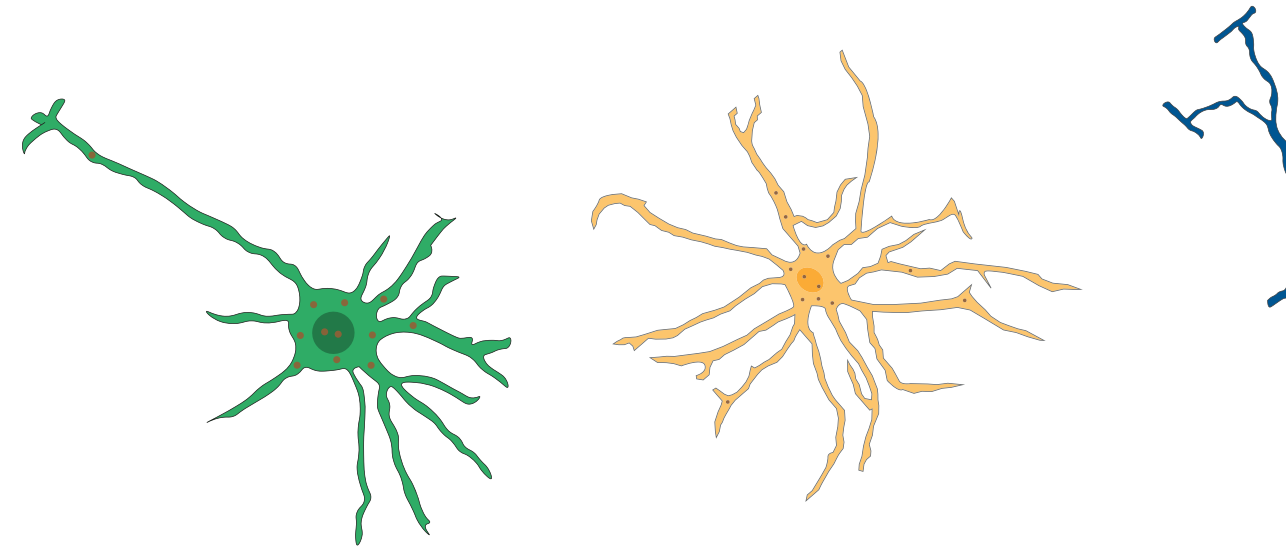

Saif Haify

Experimental Approaches Towards Therapeutic Interventions for Fragile X-associated Tremor and Ataxia Syndrome

Saif Nadim Nasser Haify

The work described in this thesis was performed at the Department of Clinical Genetics in the Erasmus Medical Center, Rotterdam, the Netherlands.

The studies presented in this thesis were financially supported by:

- Department of Clinical Genetics, Erasmus MC, Rotterdam, the Netherlands

The production costs of this thesis were supported by:

- Erasmus University, Rotterdam, the Netherlands
- Department of Clinical Genetics, Erasmus MC, Rotterdam, the Netherlands
- Fragiele X Vereniging Nederland

ISBN: 978-94-6423-249-3
Author: Saif N. Haify
Cover design: Woutje M. Berdowski
Lay-out: Saif N. Haify and ProefschriftMaken || www.proefschriftmaken.nl
Printing: ProefschriftMaken || www.proefschriftmaken.nl

Experimental Approaches Towards Therapeutic Interventions for Fragile X-associated Tremor and Ataxia Syndrome

Experimentele benaderingen richting therapeutische interventies voor het fragile X-geassocieerde tremor en ataxie syndroom

Proefschrift

ter verkrijging van de graad van doctor aan de
Erasmus Universiteit Rotterdam
op gezag van de
rector magnificus

prof. dr. F.A. van der Duijn Schouten

en volgens besluit van het College voor Promoties
De openbare verdediging zal plaatsvinden op

dinsdag 6 juli 2021 om 10:30 uur

door

Saif Nadim Nasser Haify

geboren te Bagdad, Irak

Erasmus University Rotterdam

Promotiecommissie

Promotor:	Prof. dr. R. Willemsen
Overige leden:	Prof. dr. R.F. Kooy Prof. dr. J.M. Kros Prof. dr. I. Huitinga
Copromotor:	Dr. R.K. Hukema

Table of Contents

List of abbreviations

1a	9-hydroxy-5,11-dimethyl-2-(2-(piperidin-1-yl)ethyl)-6H-pyrido[4,3- b] carbazol-2-ium
1C5	mouse monoclonal anti-FMRpolyG antibody
2'-OMe	2'-O-methyl
3PN	tripronuclear
8FM	mouse monoclonal anti-FMRpolyG antibody
9FM	mouse monoclonal anti-FMRpolyG antibody
ABC	avidin-biotin complex
AD	Alzheimer's disease
ADHD	attention deficit hyperactivity disorder
ALS	amyotrophic lateral sclerosis
AON	antisense oligonucleotide
ASD	autism spectrum disorder
ASFMRP	antisense translated proline-rich peptide
ASFMRpolyA	antisense RAN translated polyalanine containing peptide
ASFMRpolyP	antisense RAN translated polyproline containing peptide
ASFMRpolyR	antisense RAN translated polyarginine containing peptide
BAI	Beck anxiety inventory test
BBB	blood-brain-barrier
BC1	brain cytoplasmic 1
BDS	behavioral dyscontrol scale
C9ALS/FTD	*C9ORF72*-linked ALS/FTD
C9ORF72	chromosome 9 open reading frame 72
CA3	cornu ammonis 3
CamKII-α	Ca^{2+}/calmodulin-dependent protein kinase II alpha
Cas9	CRISPR-associated protein 9
CBD	corticobasal degeneration
CCS	corpus callosum splenium
CGG_n	expanded CGG-repeat
CMV	cytomegalovirus
CNS	central nervous system
COS7	CV-1 Origin SV40 cells (African green monkey kidney cells)
CRISPR	clustered regularly interspaced short palindromic repeat
CSF	cerebrospinal fluid
CUGBP1	CUG-repeat binding protein 1
CytC	cytochrome C
DG	dentate gyrus
DGCR8	DiGeorge syndrome critical region 8

DICER	endoribonuclease digestion enzyme or helicase with RNase motif
DM	myotonic dystrophy
DMSO	dimethyl sulfoxide
DNA	deoxyribonucleic acid
DOX	doxycycline
DROSHA	class II ribonuclease III enzyme
E1	ubiquitin-activating enzyme
E2	ubiquitin-conjugating enzyme
E3	ubiquitin ligase
EAAT1	excitatory amino acid transporter 1
EGFP	enhanced green fluorescent protein
eIF4A	eukaryotic initiation factor 4A
ELISA	enzyme linked immuno sorbent assay
EM	electron microscopy
EMSA	electrophoretic mobility shift assay
ER	endoplasmatic reticulum
ESc	embryonic stem cell
FACS	fluorescence-activated cell sorting
FISH	fluorescent in situ hybridization
FLAIR	fluid-attenuated inversion recovery
FM	full mutation
FMR1	fragile X mental retardation 1 gene
FMRP	fragile X mental retardation protein
FMRpolyA	RAN translated polyalanine containing peptide
FMRpolyG	RAN translated polyglycine containing peptide
FMRpolyR	RAN translated polyarginine containing peptide
FRAP	fluorescence recovery after photobleaching
FRAXA	folate-sensitive fragile X site
FTD	fronto temporal dementia
FXANC	fragile X-associated neuropsychiatric conditions
FXAND	fragile X-associated neuropsychiatric disorders
FXS	fragile X syndrome
FXPAC	fragile X premutation associated conditions
FXPOI	fragile X-associated primary ovarian insufficiency
FXTAS	fragile X-associated tremor and ataxia syndrome
FXVAC	fragile X various associated conditions
GABA	gamma-aminobutyric acid
GFAP	glial fibrillary acidic protein
GPX1	glutathione oxidase 1
H&E	hematoxylin and eosin

HBB	hemoglobin subunit beta
HD	Huntington's disease
HNRNP	heterogenous nuclear ribonucleoprotein
HSP	heat shock protein
ICV	intracerebroventricular
ID	intellectual disability
IF	immunofluorescence
IHC	immunohistochemistry
IP	intra-peritoneal
IQR	inter-quartile range
IT	intrathecal
KI	knock-in
KO	knock-out
LAP2β	lamina-associated polypeptide 2 beta
LCM	laser capture microdissection
LC-MS/MS	liquid chromatography - tandem mass spectrometry
LNA	locked nucleic acids
m^7G cap	7-methylguanosine 5′-cap
MALDI-TOF	matrix assisted laser desorption ionization time of flight
MBP	maltose-binding protein
MCP sign	bilateral white matter degeneration in the middle cerebellar peduncle
miRNA	microRNA
MBNL-1	muscle blind-like protein 1
MEF	mouse embryonic fibroblast
mGluR5	metabotropic glutamate receptor 5
MRI	magnetic resonance imaging
MSA-C	multiple system atrophy cerebellar subtype
NER	nucleotide excision repair
NfL	neurofilament light chain
NF	neurofilament
NMDA	N-methyl-d-aspartate
NT	non-transgenic
NTF1	rabbit monoclonal anti-FMRpolyG antibody
OCD	obsessive-compulsive disorder
OPCA	olivopontocerebellar atrophy
OPMD	oculopharyngeal muscular dystrophy
ORF	open reading frame
P26	ubiquitin
P/S	penicillin/streptomycin
PBMC	peripheral blood mononuclear cell

PBST	phosphate-buffered saline Tween-20
PD	Parkinson's disease
PEI	polyethyleneimine
PFA	paraformaldehyde
PIC	pre-initiation complex
PM	premutation
PpIX	porphyrin protoporphyrin IX
PPIG	peptidylprolyl isomerase G
PrP	protease-resistant protein
Pur-α	purine-rich element binding protein
PS	phosphorothioate
RAN	repeat-associated non-AUG
RBP	RNA-binding protein
RNA	ribonucleic acid
RNP	ribonucleic particles
ROS	reactive-oxygen species
rtTA	reverse tetracycline-controlled transactivator
RT-qPCR	reverse transcriptase – quantitative polymerase chain reaction
SAM68	src-associated substrate during mitosis of 68-kDa
SCA	spinocerebellar ataxia
SCW	Stroop color-word test
SDS-PAGE	sodium dodecyl sulphate – polyacrylamide gel electrophoresis
SN	substantia nigra
SNCA	synuclein alpha
SNP	single nucleotide polymorphism
SPNR	spermatid perinuclear RNA-binding protein
SRSF	serine/arginine-rich splicing factor
TDB	tail digestion buffer
TDP-43	TAR (transactive response) DNA-binding protein 43
TRA2A	transformer-2 protein homolog alpha
TRE	tetracycline responsive element
TTS	Tris/Tricine/SDS
TX	Triton-X 100
UBA	ubiquitin-associated domain
UPS	ubiquitin-proteasome system
UTR	untranslated region
VAD	vascular dementia parkinsonism
VMH	ventromedial hypothalamus
WT	wild-type
Xq27.3	position 27.3 on the long arm of the X-chromosome
YAC	yeast artificial chromosome

Scope of this manuscript

In 2001, R.J. Hagerman described five elderly men carrying a fragile X premutation displaying similar symptoms of differing severity: a progressive intention tremor, cerebellar dysfunction, cognitive decline, and Parkinsonism associated with generalized brain atrophy. This case study led to the discovery of a new progressive neurodegenerative syndrome called fragile x-associated tremor and ataxia syndrome (FXTAS). Since then, many studies have been conducted to further understand and identify the underlying disease mechanisms of FXTAS. Two potential disease mechanisms have been extensively described over the past 20 years. The first mechanism proposed is the RNA gain-of-function mechanism. Elevated levels of *FMR1* mRNA containing the expanded CGG-repeat sequester RNA-binding proteins in RNA foci preventing these proteins from performing their normal cellular function. The second proposed mechanism is repeat-associated non-AUG (RAN) initiated translation of the *FMR1* mRNA containing the expanded CGG-repeat. This results in the production of a toxic polyglycine peptide, called FMRpolyG, and subsequent formation of inclusion bodies in neurons and astrocytes. Additional mechanistic understanding of FXTAS disease pathology, using cellular and animal models, is necessary to identify potential targets for future therapies as well as new reliable biomarkers. To date, only general symptomatic treatments are available for FXTAS. The ultimate goal is to develop a targeted therapeutic intervention for patients with FXTAS.

The general aim of this manuscript is to advance our knowledge of FXTAS pathogenesis and neuropathology caused by the expression of FMRpolyG and its accumulation in intranuclear inclusions using a new relevant neuronal cell model and new FXTAS mouse models. In addition, we developed a new sandwich-ELISA to detect soluble and insoluble FMRpolyG protein fractions in post-mortem FXTAS brain tissue. This will allow for more accurate measurements of FMRpolyG levels and potentially may aid in the search for reliable biomarkers for FXTAS. Finally, a new small molecule therapeutic intervention is proposed in this thesis that is capable of reducing FMRpolyG levels *in vitro* and *in vivo*. The results described in this thesis will aid the search for potential biomarkers and the future development of effective targeted therapeutic interventions for FXTAS.

CHAPTER 1

In vitro and *in vivo* models to identify molecular pathways in Fragile X-associated Tremor and Ataxia Syndrome.

Saif N. Haify[1], Teresa Botta Orfila[2], Renate K. Hukema[1] and Gian Gaetano Tartaglia[3,4,5,6,7]

[1] Department of Clinical Genetics, Erasmus MC, Rotterdam, Netherlands.
[2] Biological Fluids Bank of the Institut d'Investigacions Biomèdiques August Pi i Sunyer (IDIBAPS), Barcelona, Spain.
[3] Centre for Genomic Regulation (CRG), The Barcelona Institute for Science and Technology, Barcelona, Spain.
[4] Institució Catalana de Recerca i Estudis Avançats (ICREA), Barcelona, Spain.
[5] Department of Biology 'Charles Darwin', Sapienza University of Rome, Rome, Italy.
[6] Department of Neuroscience and Brain Technologies, Istituto Italiano di Tecnologia, Genoa, Italy.
[7] Universitat Pompeu Fabra (UPF), Barcelona, Spain.

Frontiers in Molecular Biosciences 2020 Mar 11;7:31
(adapted and extended version for this thesis)

Abstract

Fragile X-associated tremor and ataxia syndrome (FXTAS) is a late-onset neurodegenerative monogenetic disorder caused by a 55–200 CGG-repeat expansion (premutation; PM) in the 5' untranslated region of the *Fragile X mental retardation 1* (*FMR1*) gene resulting in a progressive development of tremors, cerebellar gait ataxia, and a spectrum of neuropsychological problems. This highly disabling disease is quite common in the general population with an estimation of about 20 million PM carriers worldwide. The chances of developing FXTAS increase dramatically with age. The main neuropathological hallmark of FXTAS is the presence of ubiquitin-positive intranuclear inclusions in neurons and astrocytes throughout the brain. Protein analysis studies have identified over thirty proteins that can be found in these intranuclear inclusions and are believed to contribute to FXTAS pathology through sequestration of important RNA-binding proteins to CGG-repeat RNA. More recently, the role of a repeat-associated non-AUG (RAN) translated polyglycine peptide (FMRpolyG) has been elucidated. This chapter provides a comprehensive overview of *in vitro* and *in vivo* approaches that contributed to our current understanding of FXTAS pathology. These approaches have yielded substantial information about FXTAS pathology and, consequently, many markers have emerged to play a key role in understanding the disease mechanism. Since both the gene and pathogenic trigger, an expansion of CGG-repeats in *FMR1* RNA, causing FXTAS are known, it is an interesting disease to develop targeted therapeutic interventions for. Yet, current therapies are limited to symptomatic treatment of FXTAS pathology. Integration of the different *in vitro* and *in vivo* approaches is expected to provide crucial information about the value of these markers as either therapeutic target or fluid biomarker, essential to monitor therapeutic interventions in the future.

The *FMR1* gene

The fragile X site on the X-chromosome was first described in 1969 by Lubs [1] and in 1991 Verkerk discovered and fully sequenced the *Fragile X mental retardation 1* (*FMR1*) gene [2]. The *FMR1* gene derives its name from the folate-sensitive fragile site (FRAXA) on the long (q) arm of the X-chromosome that was later identified as Xq27.3. The *FMR1* gene is indisputably associated with the Fragile X syndrome (FXS) which is one of the most common forms of inherited mental retardation and autism, with an approximated prevalence of 1:7000 males and 1:11000 females [3-5]. The full mutation (FM; expansion of CGG-repeat >200 units) is associated with the FXS phenotype. The *FMR1* gene consists of 17 exons and is approximately 38kb in size. The mRNA transcript is sized approximately 4kb and contains almost 2kb of coding sequence. The *FMR1* gene sequence and amino acid configuration is highly conserved as is evidenced by its presence in many species beside human beings such as *M. musculus* (mouse), *D. rerio* (zebrafish), *X. laevis* (frog), *D. melanogaster* (fruit fly) and *G. gallus* (chicken) [2, 6-11].

Verkerk and colleagues speculated that the fragile site on the X-chromosome is a repeat of variable length. Subsequent sequence analysis of the *FMR1* gene proved this speculation to be correct, which resulted in the identification of a variable number of CGG repetitions to be present in the 5'-untranslated region (UTR) of the *FMR1* gene. To date, we know that the CGG-repeat in the 5'-UTR region has polymorphic characteristics which can be classified into three different forms based on the size of the repeat: healthy unaffected individuals (<55 CGG-repeats), premutation (PM) carriers (55-200) and the FM (>200 CGG-repeats) (**Fig. 1**) [12]. In the general population, transmission of the normal repeat length occurs in a stable manner. During maternal transmission the common and intermediate CGG-repeat lengths may increase in number resulting in larger repeat sizes in offspring with increasing instability of the *FMR1* gene [13, 14]. PM alleles, especially CGG-repeats larger than 90 repetitions, are unstable when maternally transmitted and usually expand in the next generation to the FM [15]. To date, repeat lengths of 59 CGGs is the smallest size known to expand to the FM in the next generation in a family with FXS [12, 16]. The CGG-repeat locus can be interrupted by one or more AGG triplets which results in less instability of the allele during transmission from parent to offspring [17]. Since the molecular characterization of the CGG-repeat in 1991, most forms of the repeat have been well studied in all populations. Nevertheless, more prospective studies worldwide are needed to better understand the risks of the disease-causing effects of CGG-repeat expansions.

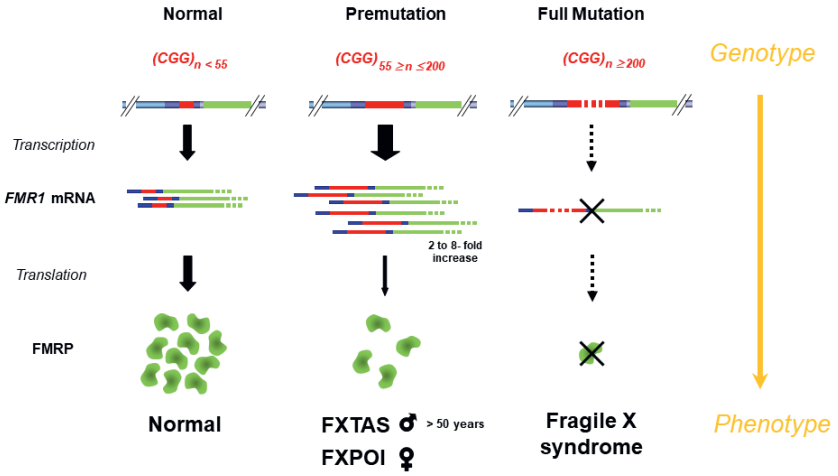

Figure 1 | Classification of the CGG trinucleotide repeat in the 5'-UTR region of the *FMR1* gene. In the general population individuals have less than 55 CGG-repeats in the 5'-UTR region of the *FMR1* gene. Premutation (PM) carriers have between 55-200 CGG-repeats which results in elevated *FMR1* mRNA levels, a moderate decrease in FMRP production and an increased risk for older male PM carriers of developing the Fragile X-associated tremor and ataxia syndrome (FXTAS). Female PM carriers can develop fragile X-associated premature ovarian insufficiency (FXPOI). Individuals with the full mutation (FM) have repeat sizes of over 200 CGG-repeats. FM carriers have silenced *FMR1* transcription due to DNA hypermethylation and consequently produce no FMRP resulting in the fragile X syndrome (FXS). Figure is adapted from [18].

Prevalence studies of PM alleles are usually conducted in relatively small cohorts within a country and predominantly associated with the Caucasian population [19]. It is relatively hard to estimate a prevalence in the general population since population differences such as racial background and ethnicity are usually not taken into account. In addition, most PM carriers are currently diagnosed by coincidence after having children with the FXS. It is assumed that in the general population PM carriers on average occur in frequencies of 1:250 in females and 1:850 in males [3, 20-22]. PM carriers are at risk of developing several fragile X-associated disorders like Fragile X-associated tremor and ataxia syndrome (FXTAS) and Fragile X-associated primary ovarian insufficiency (FXPOI). However, the most common detrimental symptoms of PM carriers which are the physical and psychiatric problems, are often left unmentioned. Therefore, Randi Hagerman recently proposed a third fragile X-associated clinical domain, the Fragile X-associated neuropsychiatric disorders (FXAND) to cover all physical and neuropsychiatric conditions seen in PM carriers [23]. It is important to highlight that many PM carriers feel stigmatized by the term "disorders" as many of these conditions observed in PM carriers are also common in the general population. In addition, FXAND can be confusing as it defines both physical and neuropsychiatric problems. During the 2019 European Fragile X Network (EFXN) conference which was held in Rotterdam, researchers and physicians proposed alternative

terminology for PM associated conditions to meet the need of all PM carriers as well as aid researchers and physicians in medical research terminology and diagnosis. Fragile X premutation associated conditions (FXPAC) has been proposed as a new term to describe the wide range of clinical conditions associated with the PM [24]. While FXTAS and FXPOI remain specific examples of FXPAC, it is proposed that FXAND should be replaced with two new terms: *1)* Fragile X-associated neuropsychiatric conditions (FXANC); and *2)* Fragile X various associated conditions (FXVAC) to cover non-psychiatric conditions including auto-immune conditions, chronic fatigue and fibromyalgia.

Fragile X Mental Retardation Protein (FMRP)

The *FMR1* gene codes for the Fragile X mental retardation protein (FMRP) that is necessary for development of normal neuronal functioning, and is involved in synaptic neuroplasticity [25, 26]. Epigenetic inactivation of the *FMR1* gene containing a FM via methylation results in transcriptional silencing and absence of FMRP production which leads to FXS. Lack of FMRP, results in a disturbance of translational regulation and a disruption in the composition of the normal protein environment, particularly in the synapse. PM carriers on the other hand have 2 to 8-fold elevated *FMR1* mRNA levels and normal, sometimes even slightly reduced, levels of FMRP [27]. The FMRP protein is widely expressed in all cells with relatively higher expression in neurons. It is known that FMRP plays an important role in many biological pathways but its role in transport and translational efficiency of specific mRNAs is extensively described in literature [28-33]. The absence of FMRP in neurons results in misregulation and mistrafficking of a subset of mRNAs into the synapse which is proposed to contribute to the mental retardation seen in FXS.

FMRP is mainly distributed in the cytoplasm, however *in vitro* and *in vivo* experiments have also shown that FMRP can be found in the nucleus [34-38]. *In vitro* studies showed that FMRP binds with high affinity and low specificity to approximately 4% of mammalian brain mRNAs, with a preference for poly-G sequences [6, 30, 39, 40]. FMRP also interacts with ribosomes attached to the endoplasmic reticulum (ER) and with free ribosomes found in cytoplasm at the bases of dendrites and within dendritic spines [37, 38, 41, 42]. This interaction between FMRP and ribosomes is mRNA dependent and is facilitated via large ribonucleic particles (RNP). In addition, studies in post-mortem brain tissue from FXS patients showed abnormal dendritic spines with abnormal shape and size compared to brain tissue from healthy individuals indicating a maturation and maintenance role for FMRP in the formation of dendritic spines [43]. Through a Dutch-Belgian Consortium an *Fmr1* knock-out (KO) mouse model was generated to study the role of FMRP. These mice lack a functional copy of the *Fmr1* gene resulting in lack of FMRP production and hence provide a good model for understanding the cellular function of the FMRP protein [44]. *In*

vitro cortical neurons and *in vivo* studies with the *Fmr1* KO mouse lacking FMRP confirm aberrant formation of dendritic spines in post-mortem brain tissue of FXS patients [45, 46]. The association of low FMRP levels and psychotic features is interesting since FMRP deficits correlate with earlier age of onset and lower IQ in those with schizophrenia without an *FMR1* mutation [47].

Clinical characteristics associated with the premutation

Diagnostic criteria for FXTAS

FXTAS only occurs in individuals who carry the PM in the 5'-UTR region of the *FMR1* gene. Therefore, it is of essence that individuals considered for diagnosis are confirmed PM carriers. Initially diagnostic criteria were determined on first hand descriptions from clinicians familiar with FXS and FXTAS [48, 49]. Although this form of identification has helped tremendously in identifying affected individuals, FXTAS patients were often missed by physicians for two very important reasons. First, since FXTAS is a relatively new disease, many physicians were not familiar with the clinical presentation of the disorder. And second, because the clinical presentation is so variable, often FXTAS patients are misdiagnosed. In 2003 Jacquemont and colleagues analyzed clinical, radiological and molecular data of 20 PM carriers [50]. Due to this work from Jacquemont and earlier clinical studies from the Hagerman group in 2001 and Brunberg and colleagues in 2002, an initial list of FXTAS diagnostic criteria was put together [48, 49]. This list of diagnostic criteria was revised in 2013 at the First International Conference on the *FMR1* Premutation: Basic Mechanisms and Clinical Involvement, and published in the journal of neurodevelopmental disorders in 2014 [51].

Diagnosis of a PM carrier requires genetic counseling of the patient and their family. Guidelines to aid the clinician during the genetic counseling on who to test for FXTAS are presented in **Table 1** (table adapted from [52]). Once the guidelines apply to an individual, the next step is to diagnose this patient based on radiological and clinical outcomes from the diagnostic criteria for FXTAS presented in **Table 2** (table adapted from [52]). The probability of an individual having FXTAS is classified in three different classes, defined as followed: *(1)* **possible case of FXTAS** when a PM individual is presented with one minor radiological sign plus one major clinical symptom; *(2)* **probable case of FXTAS** when a PM individual is presented with either one major radiological sign and one minor clinical symptom or has the two major clinical symptoms; and lastly *(3)* **definite case of FXTAS** when a PM individual is presented with one major radiological sign and one major clinical symptom. The major radiological symptoms are white matter lesions in the middle cerebellar peduncle (MCP) and/or in the brainstem. The major clinical symptoms are intention tremors and cerebellar gait ataxia [50, 52]. The corpus callosum splenium (CCS)

sign is not widely recognized as a radiological manifestation but several studies propose evidence in patients that the CCS should be a major radiological criterion for FXTAS [53-55]. Minor radiological symptoms are white matter lesions in cerebral white matter and generalized atrophy of the brain [50, 52]. Minor clinical symptoms are Parkinsonism, short-term memory loss and executive function deficits [50, 52]. Also, peripheral neuropathy is considered a minor clinical symptom [50]. Beside the importance of radiological and clinical symptoms, the presence of eosinophilic ubiquitin-positive intranuclear inclusions in neurons and astrocytes throughout the entire brain of FXTAS patients is considered a major neuropathological hallmark. This major neuropathological hallmark is of great importance in deceased unidentified 'FXTAS cases' where the individual has passed away without a proper diagnosis by a physician. Although according to the criteria intranuclear inclusions are a major hallmark, there is still some debate regarding the presence of intranuclear inclusions and their role in the pathogenesis of FXTAS. In other neurodegenerative disorders including Alzheimer's disease [56], Parkinson's disease [57] and Huntington disease [58] researchers have proposed that intranuclear inclusions may have a protective role, even enhancing degradation of aberrant proteins while others rather claim intranuclear inclusions to be disease-causing inducing neuronal cell death [59-62]. We generated a new transgenic brain-specific inducible mouse model to study the role of intranuclear inclusions on behavior. This topic is discussed in **chapter 3** of this manuscript.

Table 1: Physician guidelines on who to test for FXTAS (adapted from [52])

Clinical features	Additional clinical features	Criteria 1	Criteria 2
Intention tremor	Cerebellar ataxia, Parkinsonism or dementia	Age ≥ 50 years	Unknown cause
Cerebellar ataxia	-	Age ≥ 50 years	Unknown cause
Dementia	Cerebellar ataxia, Parkinsonism or intention tremor	Age ≥ 50 years	Unknown cause
Multiple FXTAS signs	Middle cerebellar peduncle (MCP) sign, patient/family history of premature ovarian insufficiency or family history with *FMR1* associated disorders		
Multiple system atrophy: cerebellar subtype (MSA-C; former name olivopontocerebellar atrophy (OPCA)), especially if patient has intention tremor or longer than expected disease duration			

Table 2: FXTAS diagnostic criteria for *FMR1* PM carriers; adapted from [52])

Diagnostic categories	
Possible FXTAS	One minor radiological sign + one major clinical symptom
Probable FXTAS	One major radiological sign + one minor clinical symptom or two major clinical symptoms
Definite FXTAS	One major radiological sign + one major clinical symptom
Symptom types	
Radiological signs	
Major	MRI white matter lesions in middle cerebellar peduncles (MCPs) and/or in the brain stem
Minor	MRI white matter lesions in cerebral white matter
Minor	Moderate to severe generalized atrophy
Clinical signs	
Major	Intention tremor
Major	Cerebellar gait ataxia
Minor	Parkinsonism
Minor	Moderate to severe short-term memory deficiency
Minor	Executive function deficit
Neuropathological hallmark	
Major	Round/oval eosinophilic FMRpolyG-positive and/or ubiquitin-positive intranuclear inclusions in neurons and astrocytes throughout the entire brain

Biomarkers for FXTAS

The diagnostic criteria for FXTAS comprise clinical, radiological and neuropathological features [50, 63]. These features are currently used to diagnose FXTAS patients as well as to identify unidentified FXTAS cases post-mortem. Neuroimaging using magnetic resonance imaging (MRI) is currently often used by physicians to diagnose FXTAS cases. FXTAS is considered a progressive white matter neurodegenerative disorder, clinically characterized by cerebellar gait ataxia. Bilateral white matter degradation in the MCP (MCP sign) on T2-weighted MRI or FLAIR images is the major radiological hallmark of FXTAS [50]. The MCP sign can also be seen on MRI in asymptomatic PM carriers, along with generalized cerebellar atrophy in the neocortex and brainstem [64-67]. Decreased MCP width with and without CCS hyperintensity has been proposed as an MRI biomarker for FXTAS [53-55]. These radiological features have often been correlated to other measures of brain pathophysiology including plasma metabolite concentrations [68]. However, unfortunately both MCP sign and CCS hyperintensity are not specific for FXTAS and are seen in other disorders, including sporadic olivopontocerebellar atrophy (OPCA) and spinocerebellar ataxia (SCA) [49, 69]. Additional clinical assays and genetic testing are necessary for a reliable diagnosis of PM carriers with FXTAS. Recent reports show that increase in mitochondrial activity in cultured lymphoblasts from PM carriers may

represent early stages of white matter lesions in PM carriers [70]. Combining MRI data with molecular changes in PM carriers with and without FXTAS may allow for better prediction tools in PM carriers that are at risk of developing FXTAS.

Alterations in the concentrations or ratios of specific metabolites in human fluid compartments could well reflect the pathophysiological changes in progressive disorders. Researchers have identified several plasma metabolites and their ratios in PM carriers as potential fluid biomarkers for brain associated pathophysiology [71]. The plasma metabolic ratios of oleamide and isocitrate seemed to discriminate PM carriers with FXTAS from those that do not show FXTAS symptoms [71]. Later reports of the observed plasma metabolites and their ratios in PM carriers with FXTAS delineate mitochondrial dysfunction and the role for neurodegeneration in PM carriers [72]. Changes in the plasma metabolite concentrations are also reported for other mitochondrial diseases [73]. This is consistent with reports of mitochondrial dysfunction in KI mouse models of the PM and in PM carriers [74-76]. However, future research in more PM carriers with and without FXTAS is necessary to test whether this ratio can be used as diagnostic marker for FXTAS or has a potential prognostic value in terms of identifying PM carriers that will develop FXTAS later in life from those that will not develop FXTAS. Metabolic profiling studies in PM carriers reported recently that the majority of metabolites found in PM carriers that hold prognostic value for the early prediction of FXTAS onset include lipids [77]. Several pathways of the lipid metabolism are involved in mitochondrial bio-energetics and are indeed impaired in PM carriers with FXTAS [77]. Although plasma metabolite alterations may be used as potential fluid biomarkers for FXTAS, plasma metabolites are also very sensitive to secondary manipulation of supplement (ab)use including vitamins, minerals, alcohol but also medications that are often prescribed to PM carriers with and without FXTAS. Future research is warranted to find better diagnostic biomarkers for PM carriers with and without FXTAS. Aberrant disease-causing proteins that are produced from the *FMR1* mRNA containing an expanded CGG-repeat may also be potential diagnostic biomarkers. The polyglycine (FMRpolyG) protein is produced from the expanded CGG-repeat (discussed later on in the introduction) and is abundantly present in protein aggregates in a variety of organs including the brain of PM carriers with and without FXTAS [78-81]. In **chapter 6**, we show that for the first time we are able to quantitatively measure FMRpolyG protein levels in FXTAS post-mortem brain tissue and discuss the potential role of the FMRpolyG protein as a prognostic and/or pharmacodynamic biomarker in FXTAS.

Fragile X-associated Tremor and Ataxia Syndrome (FXTAS)

PM carriers were initially considered clinically to be unaffected and only at risk of transmitting the PM allele to the next generation. In 2002, Hagerman described several PM carrier cases with a subtle phenotype [18]. To date, we know that PM carriers are also clinically affected, and can develop a variety of neuropathological symptoms including

the progressive neurodegenerative disorder FXTAS. The probability of developing FXTAS as a PM carrier increases with age and CGG-repeat size [82]. Approximately 30-50% of older males and 8-16% of female PM carriers over the age of 50 develop FXTAS [20, 83-85]. Also, approximately 20% of female PM carriers are at risk of developing FXPOI [86, 87]. Taking the prevalence of older male PM carriers and the percentage of these males potentially developing FXTAS, a rough estimation of 1:2000-3000 older males in the general population may develop FXTAS. Considering these numbers, FXTAS may be one of the more common progressive neurodegenerative disorders in older adults worldwide [85]. FXTAS disease severity is associated with increased age and disease onset is inversely correlated with CGG-repeat length [48, 50, 88]. The role of other risk factors potentially contributing to the development of FXTAS in PM carriers are not yet very clear. The use of neurotoxic agents like pesticides and chemotherapeutics, addictive substances like alcohol, opioids, cocaine and methamphetamine but also narcotic substances and anti-epileptic drugs could indirectly increase progression of the disease or just enhance specific neurological and neuropsychiatric outcomes in FXTAS patients [89-93]. The fact that epigenetic factors can interfere one way or the other with genetics is common knowledge in the medical field but since the discovery of FXTAS the contribution and understanding of additional risk factors in FXTAS patients has been minimal. Nevertheless, it is advised and even necessary that clinicians describe FXTAS cases in the outmost detail to better understand these risk factors in FXTAS cases in the future.

FXTAS patients are generally characterized by progressive intention tremors and cerebellar gait ataxia, which are proposed to be major clinical diagnostic criteria for FXTAS disease pathology. Other more minor neurological clinical features are Parkinsonism associated with generalized brain atrophy, cerebellar dysfunction, and some individuals may suffer from cognitive decline ranging from mild frontal executive and memory deficits to global dementia [25, 48, 94]. Some FXTAS patients experience emotional impairments like depression and anxiety [95-97] while predominantly male FXTAS patients are presented with extreme anger episodes but can also be apathic [98]. In 2004, the first female PM carrier cases with FXTAS were described [84, 99]. Female PM carriers show a lower probability of developing FXTAS, perhaps because of the protective effect of the normal *FMR1* allele on the unaffected X-chromosome [100]. The presence of a normal *FMR1* allele is also the likely cause of the less severe clinical phenotype seen in female FXTAS patients, as compared to male patients with FXTAS. Also, hormones like estrogen might have an alleviating effect on disease severity [84]. Nevertheless, female FXTAS cases have been described with the typical intention tremors and cerebellar gait ataxia seen in male FXTAS patients. However, all female cases had normal or high IQs and none showed any signs of dementia [84]. Next to typical FXTAS symptoms, several comorbidities have been reported to be associated with the PM including: higher prevalence of diabetes [101], sleep apnea [101], hypertension and cardiac arrhythmias with increased risk of vascular dementia [102],

chronic fatigue [103], thyroid dysfunction [83, 102], seizures [104], auto-immune disorders [102], migraine headaches [105], peripheral neuropathy [50], fibromyalgia [83, 102, 106], impotency [48, 107], cognitive and executive impairment [108, 109] and problems with numerical processing and magnitude estimates [110]. In addition, young PM carriers are reported with neurodevelopmental symptoms including attention deficit hyperactivity disorder (ADHD), autism spectrum disorder (ASD) and intellectual disability (ID) [111, 112]. There is no clear consensus about why young PM carriers have these symptoms but it is hypothesized that elevated *FMR1* mRNA levels may cause these problems [18, 23]. Another hypothesis is that these developmental deficits in young PM carriers may be caused by a partial deficiency in FMRP production [113]. Elevated *FMR1* mRNA and/or reduced FMRP levels seem to play an important role in clinical features among PM carriers rather than CGG-repeat size alone. However, larger CGG-repeat expansions can affect translation efficiency of the *FMR1* mRNA resulting in less FMRP [114, 115]. Fmrp measurements in the Dutch KI mouse model support the idea that lower Fmrp levels correlate with higher CGG-repeat lengths (>150x CGGs) [116]. Both reduced FMRP levels and elevated *FMR1* mRNA levels contribute to alterations in the limbic function and underactivity of the amygdala of young and adult PM carriers [117]. Lowered activity of the amygdala on functional MRI has indeed been shown to correlate with reduced levels of FMRP in young PM carriers [118]. More recently, subtle visual dysfunction in PM carriers was explained by decreased FMRP levels [119]. All these observations indicate a primary role for reduced FMRP levels during development in PM carriers. In addition to neurodevelopmental problems, mental health problems such as anxiety, depression and obsessive-compulsive disorder (OCD) features have also been associated with increased *FMR1* mRNA levels and/or reduced FMRP levels in adult PM carriers with and without FXTAS [120]. Mental health conditions associated with fragile X conditions are discussed in the next section.

Fragile X-associated Neuropsychiatric Conditions (FXANC)

Extensive molecular and mitochondrial studies carried out in PM carriers have increased our understanding about the molecular pathology including calcium dysregulation, mitochondrial pathology, oxidative stress, chronic DNA damage repair, and inclusion formation in the brain can be linked to the psychiatric problems often seen in PM carriers [121-124]. Initially it was thought that manifestation of psychiatric problems like depression and increased anxiety during adulthood in PM carriers, were related to increased stress of raising an affected FXS child or dealing with a parent who has FXTAS [125-127]. Although, increased stress may indeed intensify psychiatric problems in these individuals, we now know that mental health problems manifest as an intrinsic feature in over 40% of the PM carriers before neurological problems develop in those with FXTAS [95, 118, 120, 128-131]. Neuropsychiatric conditions in the PM are currently classified as FXAND [23] but this classification does not discriminate between neuropsychiatric problems and non-psychiatric conditions reported in PM carriers [24]. Therefore, it would

be advised to subcategorize neuropsychiatric conditions under the umbrella of FXANC and the various non-psychiatric conditions reported in PM carriers under FXVAC.

Depression and anxiety disorders are often accompanied with neurodevelopmental problems and are the most common mental health problems seen in PM carriers with and without FXTAS [95, 96, 131-135]. Therefore, it is not unexpected that elevated *FMR1* mRNA levels and/or reduced FMRP levels also contribute to the neuropsychiatric conditions reported in PM carriers. Both male and female PM carriers experience anxiety problems and anxiety symptoms typically begin during childhood [95, 96, 132]. More recently, a large study with 35 PM carriers between the ages 5 and 23 showed that more than 70% of the participating PM carriers met the criteria for at least one anxiety disorder including generalized anxiety disorder, specific phobia, social phobia or OCD [132]. Anxiety may also be related to the sensitivity that PM carriers experience with environmental stimuli, something that was noted in babies with the PM [113]. One study reported PM carriers with a mild deficit in GABA inhibition which may intensify anxiety symptoms through sensory stimuli [136]. Cao and colleagues showed that enhanced glutamate activity in PM neurons lead to calcium dysregulation [137]. Calcium is involved in the metabolic function of mitochondria during early neuronal development [74]. Moreover, one study found decreased cerebellar expression of the astrocytic glutamate transporter excitatory amino acid transporter 1 (EAAT1), as well as decreased expression of the metabotropic glutamate receptor 5 (mGluR5) in 16 post-mortem FXTAS brains compared to controls [138]. It is thought that primarily decreased uptake of glutamate may result in excitotoxicity and disruption of neuronal networks. More secondary effects come from decreased expression of the mGluR5 receptor, which is a translational target of FMRP. This could well explain both the psychiatric and neurological deficits observed in PM carriers in line with the lowered levels of FMRP found in the cerebellum of PM carriers [117, 118].

The elevated prevalence of depression in both male and female PM carriers is a clear feature of the PM, however, depression symptoms often manifest earlier in female carriers [111, 129, 139]. According to several large studies, the elevated prevalence of depression shows a significant positive correlation with CGG-repeat size [95, 96, 131, 140, 141]. However, the onset of depression symptoms is not associated with CGG-repeat size [128]. The median onset age of depressive symptoms as well as rates of depression in individuals with the PM are significantly higher when compared to controls and to the general population [128, 133]. In the context of neurodegeneration, PM carriers have smaller brain volumes and are more prone to stress factors later on in life, which may explain the onset of depression at later age. Smaller brain volumes could be explained by neurodegeneration due to elevated levels of *FMR1* mRNA in the brain [120]. However, the neurodegenerative role of accumulating proteins including the translated non-canonical FMRpolyG protein cannot be ruled out (discussed later on in the introduction). Either way, cellular toxicity affects

the limbic system and induces depression with aging, as seen in other neurodegenerative disorders like Huntington's disease [142]. One plausible explanation for the earlier onset of depressive symptoms in female PM carriers may be the intense stress of parenting children with FXS, especially if the child has severe autism related symptoms and/or aggression towards the mother [128]. However, other studies showed that depressive symptoms can also manifests before having children with FXS, implicating that the risk for mood disorders in PM carriers may be independent of having stress due to raising children with FXS [143]. Moreover, feelings of guilt of being a PM carrier may also be stressful and intensify depressive symptoms in these patients. Therefore, it is recommended that female PM carriers undergo early screening for depression and receive the necessary psychological care before becoming parents to minimize depression symptoms [144]. Other genetic factors, such as allelic variants in background genes or single nucleotide polymorphisms (SNPs), may impact the incidence of depression or anxiety in PM carriers [97]. Future studies are necessary to understand the impact of environmental factors, (epi) genetic factors and molecular changes on neuropsychiatric disorders in PM carriers.

Treatment guidelines for FXTAS

Intervention in FXTAS is limited to symptomatic therapy as there is no effective treatment available. The main focus of clinicians currently is to reduce symptoms in FXTAS patients and slow down the progression of the disease. Current medications are based on their effectiveness in other disorders that have similar symptoms as seen in FXTAS. For example, FXTAS patients with severe action tremors respond very well to beta-blockers and anti-epileptic drugs such as primidone [145]. However, if treatment with beta-blockers or anti-epileptic drugs fails to improve tremor symptoms, second line treatment with topiramate, which is usually used for the treatment of migraine, may be opted for symptomatic treatment in FXTAS patients [52, 145]. Deep brain stimulation is more invasive but can also be considered in the treatment of action tremors [63, 121]. Many FXTAS patients suffer from anxiety and increased stress. Benzodiazepines such as alprazolam are used to reduce anxiety in these patients. These symptoms can also intensify the action tremors seen in FXTAS and therefore alprazolam is often used to secondarily reduce tremors as well [146]. Medications for cerebellar dysfunction can be considered such as amantadine, buspirone, varenicline, riluzole, or ampyra, although there is no proof of their efficacy in treating FXTAS patients [147]. Treatment of psychiatric symptoms with selective serotonin inhibitors may be effective [147]. Treatment regimens for FXTAS patients should be personalized due to the variable presentation of symptoms and the fact that there is no effective therapy at this moment.

Fragile X-associated Premature Ovarian Insufficiency (FXPOI)

Short after the discovery of the *FMR1* gene, Cronister and collegues [86] observed that female PM carriers have a 20-fold increase in the incidence of menopause before the age of

40 and are at risk of developing premature ovarian infertility or FXPOI [148, 149]. Although FXPOI is outside the scope of this work, it is worth mentioning that this reproductive condition is recognized as the leading heritable form of early infertility. Studying the mechanism of FXPOI has proven to be more difficult than for FXTAS, due to the relative rarity of suitable human samples or appropriate animal models. FXPOI cases, similar to FXTAS, have increased levels of *FMR1* mRNA and the risk of developing premature ovarian failure appears to increase with increasing length of the CGG-repeat between 55 and 99 CGGs [150-152]. Interestingly, this association is lost or even is reversed after CGG-repeat sizes over 100 [87, 153]. In the Dutch KI mice 40-week-old ovarian cells showed a 5-fold increase in *Fmr1* mRNA expression and a 2-fold reduction in Fmrp [79]. Histopathological analysis of 40-week-old mouse ovaria showed ubiquitin-positive inclusions co-localizing with FMRpolyG-positive inclusions in stromal cells suggesting that repeat associated non-AUG (RAN) translation (discussed later on in the introduction) may play a role in FXPOI as well. FMRpolyG-positive inclusions were also present in ovarian stromal cells of a woman with FXPOI [79]. Hoffman *et al.* [150] showed that the development of the primordial follicles remains unaffected in FXPOI patients, but that there is a rapid loss of all follicles in different stages, suggesting that the problem is inherent to the ovaries. Also, there are abnormalities of the follicles, including reduced size and number of granulosa cells. In the Dutch KI mice, we have previously shown that the number of healthy growing follicles was not affected but the number of atretic large antral follicles was increased by nearly 9-fold in 40-week-old KI mice [79]. In addition, ovulations in these mice reduced with 40% and the mice that still ovulated had a reduced number of fresh corpora lutea [79]. These observations in mice and FXPOI patient ovaria form an important basis to further study the underlying pathogenic mechanisms of FXPOI.

The pathogenesis of FXTAS

The most prominent neuropathological hallmark of FXTAS is the presence of eosinophilic, ubiquitin-positive intranuclear inclusions in neurons and astroglia throughout the brain upon post-mortem histological analysis [59, 78, 80, 81]. Intranuclear inclusions were also found in systemic organs of FXTAS patients, including testicular glands, kidneys, adrenal gland, heart, thyroid, and pituitary glands [78, 79, 107, 154-156]. Additional neuropathological features found in FXTAS include reduced number of Purkinje cells, Bergmann gliosis, axonal swelling in the granular cell layer of the cerebellum, and prominent cortical and subcortical white matter pathology [80, 81]. Protein composition studies of the intranuclear inclusions revealed more than thirty other proteins to be present in the inclusions [157].

In vitro and animal models have played a critical role in revealing the mechanisms of FXTAS pathogenesis. The two widely accepted molecular mechanisms in FXTAS pathophysiology are CGG-repeat-mediated RNA gain-of-function toxicity [48, 50, 81, 158] and protein toxicity through RAN translation (**Fig. 2**) [59]. RNA gain-of-function toxicity mechanism leads to the sequestration of specific RNA-binding proteins (RBPs). RAN translation results in the production of several toxic polypeptides of which FMRpolyG is the best studied [159, 160]. FMRpolyG co-localizes with ubiquitin in inclusions throughout the brain in neurons and astrocytes of FXTAS patients [59]. Although RNA toxicity and RAN-translation are the main mechanisms, other molecular mechanisms have been proposed to contribute to the pathology including antisense *FMR1* mRNA RAN translation [161], mitochondrial dysfunctions and elevated reactive oxygen species [74-76, 123, 162], and hyperactivation of R-loop-induced DNA damage response [163, 164].

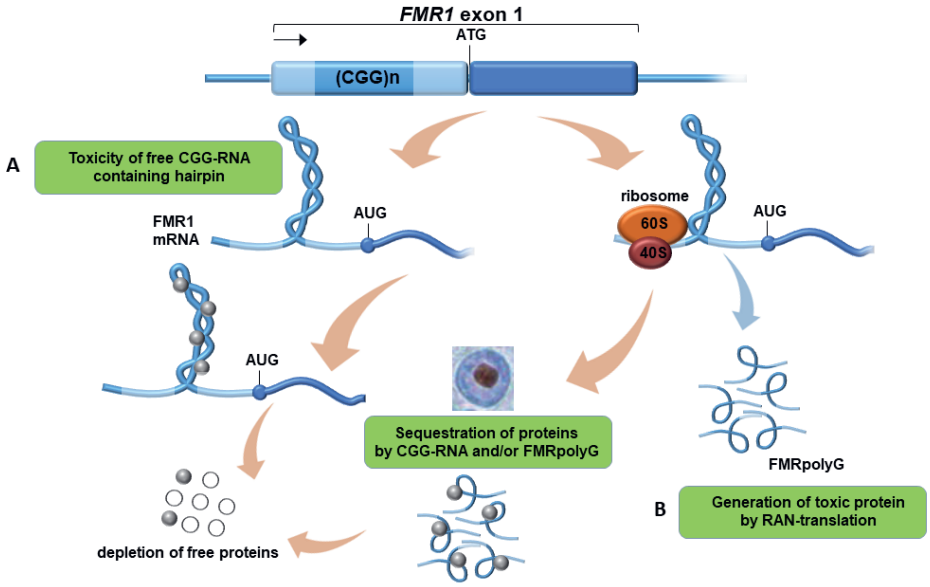

Figure 2 | Proposed mechanisms of CGG-repeat toxicity in PM carriers. (A) CGG-repeat mediated RNA toxicity and sequestration model: RNA-binding proteins (RBPs) are sequestered through their interactions with the expanded CGG-repeat *FMR1* mRNA. These proteins can in turn recruit other crucial proteins. The net result of the sequestration of these proteins is that they are unavailable to carry out their normal functions and critical cellular processes are thereby altered or blocked. **(B)** Toxic polypeptide model: the ribosome translation initiation complex stalls near the CGG-repeat hairpin formed on the *FMR1* mRNA. This promotes the repeat-associated non-AUG (RAN) translation of *FMR1* mRNA using a near-AUG start site. This results in a frame shift and the production of amongst others the polyglycine-containing polypeptide (FMRpolyG) that somehow interferes with normal cell function or may be directly toxic.

RNA gain-of-function toxicity and sequestration mechanism

PM carriers with and without FXTAS are characterized by 2 to 8-fold elevated *FMR1* mRNA levels in blood while the *FMR1* protein (FMRP) levels appear to remain at, or slightly below, normal levels [27, 114]. RNA gain-of-function mechanism has been proposed in which CGG RNA transcripts are cytotoxic. Several studies show that overexpression of *FMR1* mRNA or overexpression of normal length CGG-repeats does not result in toxicity [162, 165]. Toxicity can solely be attributed to the presence of the expanded CGG-repeat RNA. Indeed, ectopic expression in Purkinje neuron-specific transgenic mice expressing the expanded CGG-repeat RNA in context of eGFP and *Fmr1* mRNA, show that the expanded CGG-repeat RNA outside the context of the *Fmr1* mRNA can induce neuronal pathology in mammalian disease system [60]. More specifically, ectopic expression of a CGG-repeat expansion in the PM range is sufficient to induce formation of intranuclear inclusions, reduce cell viability, trigger neuronal cell death (*e.g.,* Purkinje cell loss) and result in behavioral deficits in these mice [60, 166, 167].

Also, increased levels of *FMR1* mRNA are found within intranuclear inclusions in brain sections of individuals with FXTAS [80, 81, 168]. CGG-repeat RNA sequesters important RBPs and prevents other essential proteins from their normal function in the cell [168]. Based on studies in human post-mortem brain tissue and animal models, like the mouse and *Drosophila*, several RBPs have been identified including heterogeneous nuclear ribonucleoprotein (HNRNP)-A2/B1 and CUGBP1 [169], purine-rich element binding protein alpha (Pur-α) [170, 171], DGCR8 and DROSHA [172], and SAM68 [173]. Iwahashi and colleagues [157] also identified an extensive list of proteins found in intranuclear inclusions in the frontal cortex of FXTAS patients including muscle blind-like protein 1 (MBNL-1) and several lamin-associated proteins including lamin A/C isoform 1, neurofilament protein and internexin neuronal intermediate filament protein.

Through direct association CGG-repeat RNA interacts with HNRNP-A2/B1, which is a key regulator protein in RNA metabolism [157, 169, 170, 174]. Studies show that overexpression of PM CGG-repeat RNA in *Drosophila* is sufficient to induce neurodegeneration and a dosage and repeat length dependent rough-eye phenotype [175]. Overexpression of the HNRNP-A2/B1 suppresses these toxic effects induced by the CGG-repeat RNA [169]. Also, the sequestration of HNRNP-A2/B1 by CGG-repeat RNA in neurons impairs dendritic delivery of known HNRNP-A2/B1 targeted mRNAs [176]. The HNRNP-A2/B1 can also function as indirect interactor between CGG-repeat RNA and other cellular proteins like the CUG binding protein (CUGBP1, also known as CELF1). CUGBP1, a RBP that binds CUG repeats and implicated in myotonic dystrophy type 1 (DM1) [177]. Upon binding of CUGBP1 to HNRNP-A2/B1, CUGBP1 is unable to perform its pre-mRNA alternative splicing function [178]. Furthermore, CUGBP1 is also involved in maintaining mRNA stability and translation [179]. In transgenic FXTAS *Drosophila,* CUGBP1 induces neurotoxicity through

interaction with CGG-repeat RNA via HNRNP-A2/B1. Interestingly, overexpression of CUGBP1 rescues CGG-repeat RNA induced neurodegeneration in *Drosophila* [169].

Another binding partner of HNRNP-A2/B1 is the TAR DNA binding protein 43 (TDP-43). TDP-43 does not interact directly with CGG-repeat RNA and is also not found in (intra)nuclear inclusions [157, 180]. TDP-43 is essential in mammalian development and is generally assumed to be involved in transcriptional repression and DNA repair mechanisms. Although overexpression of human TDP-43 itself can elicit neurodegeneration, studies reported that overexpression of TDP-43 partially rescues the neurodegeneration induced by CGG-repeat RNA through sequestration with HNRNP A2/B1 in a *Drosophila* model of FXTAS [180, 181]. While HNRNP A2/B1 orthologs are necessary for TDP-43 dependent rescue, overexpression of HNRNP A2/B1 itself is capable of suppressing CGG-repeat RNA toxicity even when expression of *Tbph*, the fly homologue of TDP-43, is suppressed [180]. In addition, TDP-43 expression is downregulated in Purkinje cells of PM transgenic mouse model implicating the importance of this protein in FXTAS [181]. Thus, the ability of CGG-repeat RNA to bind HNRNP A2/B1 could promote neurotoxicity by both direct interaction with HNRNP A2/B1, and indirectly by sequestering HNRNP A2/B1 binding partners.

DiGeorge syndrome critical region 8 (DGCR8) protein is a double stranded RBP that interacts directly with PM range CGG-repeats and facilitates microRNA (miRNA) processing in the cell [172]. DGCR8 forms a complex with DROSHA [182]. DROSHA is a type III RNase that is involved in miRNA biogenesis [182]. DROSHA binds primary miRNA transcripts and processes these primary miRNAs into precursor miRNAs [183]. Precursor miRNAs are then processed into mature miRNAs by the DICER enzyme [172]. DGCR8 or DROSHA, which one is not clear, recruit the src-associated substrate during mitosis of 68-kDa (SAM68) RBP [172]. SAM68 regulates miRNA processing in the nucleus from precursor miRNA alternative splicing to nuclear export of the mature miRNAs. Overexpression of PM range CGG-repeat RNA results in sequestration and depletion of DGCR8, DROSHA and SAM68 in neuronal cells leading to reduced processing of primary miRNAs and consequently, reduced levels of mature miRNAs and increased cell death *in vitro* as well as in brain sections of FXTAS patients [172, 173]. While overexpression of DGCR8 rescues neuronal cell death *in vitro*, overexpression of SAM68 does not rescue this phenotype suggesting that overall dysregulation of miRNA processing could be contributing to FXTAS pathogenesis and not dysregulated SAM68-mediated splicing per se [172, 173].

Another protein found in intranuclear inclusions is Pur-α. Pur-α is a cytoplasmic RBP and single-stranded DNA-binding protein that regulates neuronal mRNA transport and translation in the cell and plays a crucial role in the DNA-replication process [170]. In a *Drosophila* model of FXTAS expressing an expanded CGG-repeat, the Pur-α protein is localized within cytoplasmic inclusions [170]. Interestingly, overexpression of Pur-α in the

Drosophila rescues CGG-repeat mediated neurodegeneration [170]. Moreover, the lack of Pur-α in KO mice results in a developmental delay with severe tremors and seizures after birth [184, 185]. Also, the expression and distribution of axonal and dendritic proteins is altered in these mice [184, 185]. Pur-α is also found to co-localize with ubiquitin-positive intranuclear inclusions in both human post-mortem brain sections and mouse models expressing PM range CGG-repeats [170]. In *Drosophila*, neuronal apoptosis caused by the expanded CGG-repeat arose in part as a consequence of Pur-α sequestration by the expanded CGG-repeat preventing it from its normal function [170]. Pur-α may also interact with other regulating proteins that suppress CGG-repeat induced toxicity. Proteomic analysis identified the Rm62 protein as such a modulator of CGG-repeat mediated toxicity [186]. The Rm62 protein is an ortholog for the p68 RNA helicase in humans which is involved in pre-mRNA splicing, RNA interference and nucleocytoplasmic shuttling in the cell [187-191]. Overexpression of Rm62 can suppress neurotoxicity induced by the expanded CGG-repeat in the *Drosophila* FXTAS model while the expanded CGG-repeat can inhibit the posttranscriptional expression of Rm62 [186]. The decrease in Rm62 protein expression leads to increased nuclear retention of mRNAs that are normally exported outside the nucleus by Rm62 such as the *heat shock chaperone (HSP) 70* mRNA as well as mRNAs involved in stress and immune responses [186]. The HSP70 protein is also found in intranuclear inclusions in FXTAS post-mortem brain tissue as well as in FXTAS animal models [175, 186]. Interestingly, a recent report shows that the HSP70 protein forms intracellular complexes with the FMRpolyG protein in fibroblasts from a living FXTAS patient [192]. HSP70 can function as a marker for the presence of a protective cellular defense mechanisms against intranuclear inclusions in FXTAS. All these findings together suggest that the sequestration of many RBPs to the expanded CGG-repeat RNA in inclusions may directly or indirectly stimulate neurodegeneration in FXTAS.

Protein gain-of-function mechanism

An alternative mechanism by which proteins aggregate/accumulate in intranuclear inclusions in FXTAS brain is based on a noncanonical protein translation initiation mechanism known as RAN translation [59, 193]. RAN-translation was first observed with the CAG-repeat in SCA8 where the expanded repeat is translated in the absence of a canonical AUG start codon [194]. Since then, *in vitro* and *in vivo* studies have shown that RAN translation may be a potential disease mechanism for several other neurodegenerative protein aggregation disorders like SCA3, DM1, FXTAS and *C9ORF72* linked amyotrophic lateral sclerosis and frontotemporal dementia (ALS/FTD) [59, 194-197]. RAN translation initiation requires several essential factors including a methylated 5′ terminal structure (m^7G cap) that recruits the pre-initiation complex (PIC) to the 5′ end of the mRNA, the eukaryotic translation initiation factor 4A (eIF4A) and the 40S ribosomal scanning complex [198]. CGG-induced RAN translation of *FMR1* mRNA is, except for the non-AUG start codon, mechanistically similar to canonical translation but less efficient,

with the degree of efficiency dependent on the reading frame [198]. Studies in HeLa cells and *Drosophila* show that CGG-repeat RAN translation from the 5'-UTR of *FMR1* can generate three different homomeric polypeptides including polyarginine (FMRpolyR) from the +0 (CGG) reading frame, polyglycine (FMRpolyG) from the +1 (GGC) reading frame, and polyalanine (FMRpolyA) from the +2 (GCG) reading frame [59]. The +1 and +2 reading frames seem the most efficient in *in vitro* translation tests, with initiation occurring primarily at two near-cognate start codons upstream of the repeat: an ACG and a GUG for the +1 reading frame and within the repeat itself for the +2 reading frame, as introducing a stop codon immediately in front of the repeat had no impact on translation at all [59, 193, 198]. Initiation in the +0 reading frame only occurred when a canonical AUG start codon was presented in front of the CGG-repeat. In absence of the canonical AUG start codon, no product could be detected from this frame in healthy and PM range CGG-repeat lengths [59, 198]. Although theoretically three polypeptides can be produced in both cultured cells and animal models of FXTAS, in inclusions in FXTAS patient brains only the FMRpolyG and FMRpolyA protein can be observed using immunofluorescence and immunohistochemistry stainings [59, 199]. For all three reading frames, repeat length correlates with peptide size [198]. FMRpolyG and FMRpolyA are both prone to length-dependent aggregation in cellular and animal models [59, 78, 193, 198]. While increased repeat length does not or just modestly correlate with increased translation efficiency for the FMRpolyG protein, FMRpolyA is more efficiently translated with increased CGG-repeats [59, 193].

More recently, studies showed that RAN translation can also occur from all three reading frames in the 3' antisense *FMR1* mRNA containing an expanded CGG-repeat [161]. Canonical AUG antisense translation of the antisense *FMR1* mRNA results in the production of a N-terminus truncated antisense proline-rich peptide (ASFMRP) [200]. The ASFMRP protein is found in intranuclear inclusions in FXTAS brain [200]. Removing the AUG results in RAN translation from antisense *FMR1* mRNA in three different polypeptides: polyproline (ASFMRpolyP, +0 reading frame), polyarginine (ASFMRpolyR, +1 reading frame) and polyalanine (ASFMRpolyA, +2 reading frame) [200]. In contrast to sense *FMR1* mRNA RAN translation, all antisense polypeptides seem to be more efficiently translated with increased CGG-repeat lengths [200]. The increased translation efficiency may possibly be due to the guanine-cytosine ratio (*i.e.,* more cytosine than guanine) in the antisense transcript and consequently the CGG-repeat RNA secondary structure that is formed. In transfected COS7 cells, increasing CGG-repeat size causes ASFMRpolyR to re-localize from the cytoplasm to the nucleolus, and ASFMRpolyA to re-localize from the cytoplasm to the nucleus [200]. Transfected COS7 cells show clear formation of intranuclear inclusions positive for all ASFMR polypeptides [200]. In contrast, the ASFMRpolyP and ASFMRpolyA proteins but not the ASFMRpolyR protein could be detected in intranuclear inclusions, predominantly in neurons, in post-mortem FXTAS brain, and both proteins co-localized

with ubiquitin and other ubiquitinated proteins in these intranuclear inclusions [199, 200]. There is still some debate regarding toxic effects of all ASFMR polypeptides. First, polyA rich peptides are known to be involved in various human genetic diseases such as oculopharyngeal muscular dystrophy (OPMD) [201, 202]. Since FMRpolyA is known to impair protein quality systems in cellular systems [203], ASFMRpolyA may also have a toxic role in FXTAS. Second, dipeptides containing arginine (*i.e.,* poly-GR, poly-PR) are reported for *C9ORF72*-linked ALS/FTD to induce toxicity through oxidative stress by binding mitochondrial ribosomal proteins, inhibit proteasome activity, disrupt the nuclear lamina, and interfere with a variety of cellular processes including pre-mRNA splicing and ribosomal biogenesis [204-208]. Whether ASFMRpolyR induces toxicity in FXTAS pathogenesis needs further research, especially since poly-R alone is reported to have some neuroprotective properties [209]. Finally, proline-rich dipeptides (*i.e.,* poly-PR, poly-GP, poly-PA and poly-PG) induced toxicity is only observed in *C9ORF72*-linked ALS/FTD [207, 208]. Nevertheless, a protective function for polypeptides containing proline is reported. In polyQ diseases, poly-P can protect against misfolded proteins, notably preventing aggregation of huntingtin, and even favoring oligomerization of neuroprotective proteins [210, 211]. Altogether, these findings strongly suggest that RAN translation of *ASFMR* mRNA and the ASFMR polypeptides are also involved in FXTAS pathogenesis but more research is needed to warrant their roles.

The best described and characterized RAN product is the toxic FMRpolyG protein. FMRpolyG is a small protein having a 12 amino acid N-terminus and a 42 amino acid C-terminus, which is proposed to modulate the toxicity of FMRpolyG [193]. The length of the polyglycine stretch is the equivalent of the number of CGGs in the repeat. When the polyglycine stretch is expressed without its surrounding native sequences, FMRpolyG still aggregates in inclusions but with a milder phenotype in cells and the *Drosophila* model [193]. These results indicate an important yet not very clear role for the surrounding structures, with a toxicity modulating role for the C-terminus. The C-terminus also interacts with lamin-associated proteins like the lamina-associated polypeptide 2 beta (LAP2β). Both C-terminus and FMRpolyG protein interact with LAP2β disrupting the cellular lamina structure and inducing toxicity [193]. Inclusion protein composition studies show that lamin-associated proteins like lamin A/C are also found in intranuclear inclusions in FXTAS brain sections, and that neurons in FXTAS brain show abnormal nuclear lamina architecture [157, 167]. All these findings together suggest that disruption of the nuclear lamina contributes to FXTAS pathogenesis. Moreover, in *C9ORF72*-linked ALS/FTD and Huntington's disease, RAN translation products also result in disruption of the nuclear architecture and nucleocytoplasmic transport [212-214]. RAN translation of the CGG-repeat occurs predominantly in the FMRpolyG reading frame [193, 198, 215]. At least 60 to 70 CGG-repeats are required to detect the FMRpolyG protein after immunoblotting [193]. The FMRpolyG protein is present in intranuclear inclusions in cellular and animal

models as well as in neurons and astrocytes throughout the brain of FXTAS patients. CGG-repeat mediated RAN translation induced toxicity due to production of the FMRpolyG protein in mammalian cellular models, the *Drosophila* and transgenic mice. The Todd lab showed that enhancing the expression of the CGG-repeat by placing an AUG start codon upstream of the CGG-repeat resulted in more inclusion formation, increased cell death in cell cultures and a rough-eye phenotype including retinal degradation in the *Drosophila* [59]. This was supported by the fact that placing a STOP codon immediately after the near-cognate start codon and before the CGG-repeat preluded toxicity, with no observation of inclusion formation in cellular models and loss of the rough eye phenotype in the *Drosophila* model [59]. Similar results were obtained when the CGG-repeat is placed in the 3'UTR region in the *Drosophila* [59]. Also, a STOP codon introduced in mice upstream of the CGG-repeat in the +1 reading frame resulted in reduced formation of inclusions and lower expression of the FMRpolyG protein [59]. This observation was further supported by reports of behavioral deficits in mice only expressing the FMRpolyG protein but not in mice expressing only the expanded CGG-repeat RNA (mouse model reviewed in section "PM and FXTAS mouse models") [193]. Expression of the expanded CGG-repeat RNA and the production of the FMRpolyG protein in the mice resulted in locomotor deficiency with increased falling from the rotarod, decreased ability of traction from the hind limbs and decreased grip strength while only expression of the expanded CGG-repeat RNA without the formation of the FMRpolyG protein did not result in any behavioral deficits [193]. Furthermore, mice expressing FMRpolyG had a shorter lifespan, approximately 10 months, while mice that only expressed the CGG-repeat RNA exhibited normal longevity. Histopathological analysis revealed some Purkinje cell loss and also evidence of neuroinflammation in 10-month-old mice expressing both the CGG-repeat RNA and the FMRpolyG protein but not in CGG-repeat RNA only mice. Interestingly, mice expressing the FMRpolyG protein in the brain also developed obesity probably due to dysfunction of the hypothalamus, as this area had the most expression of CGG-repeat RNA and FMRpolyG production [193]. The hypothalamus also showed the earliest FMRpolyG protein presence when compared to other organs [193]. Also, recently we found that astroglia-specific expression of the FMRpolyG protein in mice resulted in the formation of FMRpolyG-positive intranuclear inclusions in the astrocytes and Bergmann glia accompanied with a deficit in motor performance on the ladder-rung test (**chapter 2**, [61]). It is worth mentioning that all studies presented here are mainly overexpression studies. However, these observations indicate a primary toxic role for the FMRpolyG protein in FXTAS pathogenesis. Nevertheless, the potential disease-causing contribution of the CGG-repeat RNA cannot be fully excluded.

Altered protein quality control pathway due to the FMRpolyG protein has also been suggested as a mechanism to contribute to FXTAS pathology. Several products from the ubiquitin-proteasome system (UPS) like ubiquitin, HSP70 and αβ-crystallin are found

to accumulate in intranuclear inclusions in FXTAS [157]. In *Drosophila,* CGG-repeat-induced neurodegeneration is enhanced by impairment of the UPS due to the presence of FMRpolyG and not the expression of CGG-repeat RNA only [59, 203]. Overexpression of Hsp70 resulted in reduction in CGG-repeat-induced toxicity [203]. In cellular models, overexpression of FMRpolyG results in a diminished UPS while inhibiting RAN translation resulted in an almost normally functioning UPS [203]. This suggests that FMRpolyG production via RAN translation affects the protein quality control system through UPS and may therefore contribute to FXTAS pathogenesis.

More recently, the adaptive ISR pathway has been proposed as a regulator of RAN translation in *C9ORF72*-ALS/FTD and FXTAS [159, 160]. Several types of integrated cellular stress responses like viral infections, misfolded proteins and oxidative stress activate stress-specific kinases, which then can phosphorylate the canonical translation initiation factor eIF2α, effectively inhibiting global translation in repeat expressing cells and neurons. The presence of CGG-repeat RNA in the cell is also considered a stressful event. Importantly, expression of construct containing PM range CGG-repeat is sufficient to induce formation of stress granules in cells. This stress granule induction requires eIF2α phosphorylation and is associated with a reduction in global protein translation in repeat expressing cells and neurons [160]. Similar events were found with the G_4C_2 repeat in *C9ORF72*-ALS/FTD and CUG-repeat in DM1 [216-218]. This indicates that any process within the cell with the potential to induce the phosphorylation of eIF2α can upregulate CGG-repeat mediated RAN translation and downregulate canonical mRNA translation [160]. Also, enhanced RAN translation of FMRpolyG via the ISR is dependent on the presence of a near cognate start codon, as introducing a canonical AUG start codon upstream of the CGG-repeat abolishes this effect [160]. Several activators of the ISR such as tunicamycin upregulate RAN translation of the CGG-repeat in the +1 and +2 reading frames [160]. All together this suggests that activation of the ISR pathway upregulates RAN translation in the cell, and consequently further activates cellular stress pathways to create a feed-forward loop that drives neurodegeneration.

In vitro prediction models

In vitro approaches to predict molecular interactions occurring in FXTAS

Protein interaction with CGG-repeats can be determined by several experimental *in vitro* approaches. The success in discovering new findings is influenced by the technical capacity to preserve the natural characteristics of the protein-RNA partners, such as the secondary and tertiary structure, electrostatic and hydrophobic interactions, hydrogen bonding, rate of transcription of RNA and translation of protein. We refer the reader to advanced reviews for details related to the experimental methods [219].

CGG-repeats form hairpins *in vitro* [220]. UV-monitored structure melting indicates that they are more stable than hairpins formed by CAG-, CUG- or CCG-repeats. Although the *in vivo* structure might differ, due to interactions with proteins and other molecules, crystallography supports the model that CGG-repeats have intermolecular duplexes [221]. Several validation and identification methods can help us discover and analyze interacting proteins of the CGG-repeat such as RNA pull-down and protein microarrays.

RNA pull-down to detect CGG-repeats interactions

The RNA pull-down consists on a selective extraction of a protein-RNA complex from a whole sample lysate, by using high-affinity tags like biotin on the RNA molecule. After tagging the known interaction partner, RNA, the RBPs complexed with it are purified by using agarose or magnetic beads. To identify which proteins are associated with expanded CGG-repeats, Sellier et al. adopted an *in vitro* approach [173]. Proteins extracted from mouse brain and COS7-cell nuclei were captured on streptavidin resin coupled to biotinylated *in vitro*-transcribed RNA composed of 60xCGG-repeats, eluted, separated on SDS–PAGE gels and identified by MALDI-TOF analysis. More than 20 proteins were identified, including a heat-shock protein and several RBPs, such as SRSF (1, 4, 5, 6, 7 and 10), MBNL-1 and HNRNP-G [173]. The list of interactors (**Fig. 3A**) included SPNR, HNRNP-A1, HNRNP-A2/B, HNRNP-C, HNRNP-D, HNRNP-E and HNRNP-H [173].

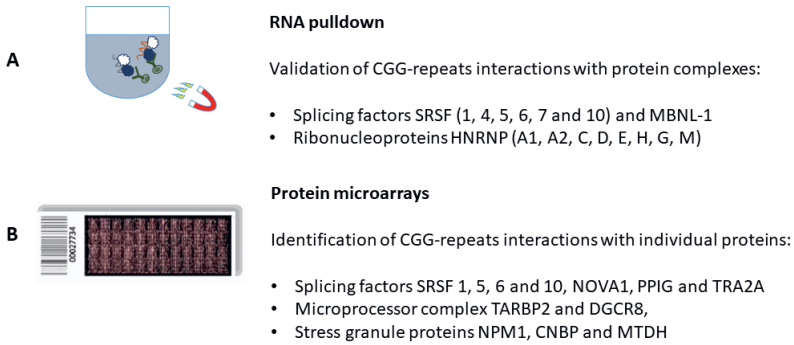

Figure 3 | *In vitro* methods to identify protein interactors of expanded CGG-repeats in the *FMR1* mRNA. (A) RNA pull-down followed by mass-spectrometry reveals the most abundant protein interactors of *FMR1* 5'-UTR. **(B)** The protein microarray approach allows to probe labeled *FMR1* 5'-UTR against the entire human proteome, revealing targets that are poorly abundant in the cell.

Protein microarrays to detect *FMR1* interactions

Protein microarray technology was used to detect RBP interactions with the first *FMR1* exon [222]. In this approach, individual human proteins, expressed in a eukaryotic system and subsequently purified, are isolated in separated nitrocellulose chambers and the

RNA labelled with Cy5 is used for probing [223]. Both expanded (79xCGG, PM range) and normal (21xCGG) repeats were probed on independent replicas and the 3'-UTR of a similar length transcript, SNCA, was used as a control for the specificity of RBP interactions [223].

Using fluorescence intensities to measure binding affinities [224], previously identified partners SRSF 1, 5 and 6 ranked in the top 1% of all interactions, followed by KHDRBS3 (2%) and MBNL-1 (5%). The overall list included 85 RBPs showing an enrichment in gene ontology terms related to splicing activity, as reported by *clever*GO [225] and includes several SRSF proteins, PCBP 1 and 2, HNRNP-A0 and F, NOVA1, PPIG and TRA2A (**Fig. 3B**).

RNA electrophoretic mobility shift assay (RNA-EMSA) to validate individual protein interactions with CGG-repeats

In the RNA-EMSA assay protein-RNA interactions are detected as migration differences in gel electrophoresis: the RNA probe is labeled by radioactivity or by fluorescent or chemiluminescent dyes, and incubated with the whole protein extract from cell lysate, in different concentrations of the first one. In case the RNA is selectively bound to proteins, the electrophoretic band will differ from a negative control, as a migration shift. In this assay, an experimental secondary approach is performed, by assessing competitive binding: an excess of unlabeled RNA is incubated with the binding reaction and in case the shifted signal decreases, there is evidence for specificity of the binding.

Using RNA-EMSA, the binding of HNRNP A2 to 105xCGG-repeats was studied in the presence of the *brain cytoplasmic 1* (*BC1*) RNA involved in neuronal translational [176]. Differently from 105xCGG-repeats, the 105xCGG-repeats competed with binding of *BC1* RNA to HNRNP-A2, which indicates impairment of neuronal function. Using 105xCGG-repeats at levels comparable to *FMR1* abundance in PM disease cells, the authors showed that distal dendritic delivery of *BC1* RNA is significantly reduced while 105xCGG-repeats had no effect on dendritic BC1 targeting [176].

RNase H protection approach to characterize the *FMR1* R-loop

The RNase H protection approach is used to detect DNA and RNA fragments in cell lysates. RNase H cleaves the target RNA molecule at a specific site hybridized with a DNA probe. In these specific sites, if a protein is bound, the hybridization is blocked, therefore no cleavage by RNase H will occur.

It has been observed that transcription through the GC-rich *FMR1* 5'-UTR region favors formation of a three-stranded nucleic acid structure, composed of a DNA:RNA called R-loop formation, with the nascent RNA assembling with the template DNA strand [164]. Using DNA:RNA immunoprecipitation of genomic DNA from cultured human dermal fibroblasts with both normal and PM alleles, the authors reported for *FMR1* R-loop formation. As

expected for R-loop formation, treatment with purified recombinant human RNases H1 and H2 eliminated DNA-RNA interaction [164].

Fluorescent in situ hybridization co-localization (FISH) to localize CGG-repeats in the cell

Fluorescent *in situ* hybridization (FISH) co-localization techniques require knowing in advance which RNA and protein interaction will be studied. This technique is commonly used in FXTAS research as it allows verifying where CGG-repeats localize with other molecules. By means of FISH coupled to immunofluorescence it has been shown that CGG expansions and TRA2A significantly co-localize in COS7 cells [222]. Similarly, co-localization of MBNL-1, KHDRBS1 and HNRNP-G within CGG aggregates was observed in COS7 cells [173]. By contrast, other *in vitro* identified candidates such as SPNR, HNRNP-A1, HNRNP-A2/B, HNRNP-C, HNRNP-D, HNRNP-E and HNRNP-H have been shown by FISH to have poor co-localization with CGG-repeats [173]. Several proteins, including a number of heat-shock proteins, HNRNP-A2/B1, CUGBP1, lamin A/C and maltose-binding protein (MBP) were found to localize with ubiquitin-positive inclusions in CGG-expressing *Drosophila*, KI mouse model and in FXTAS patients. Some of the co-localizations are model dependent. Indeed, it should be noted that Pur-α co-localizes with cytoplasmic CGG-repeats in flies [170] but not in mammalian cells, where it is strictly nuclear [173]. So, given the propensity of Pur-α to interact with CGG-repeats [226], it is possible that its subcellular localization prevents physical interaction with RNA.

PM and FXTAS mouse models

The development of animal models has provided the field with important clinical but also molecular information regarding the pathology associated with CGG-repeat expansions on *FMR1* FXS, PM carriers and FXTAS. Over the past 10 to 15 years many well-characterized mouse models have shown that RNA toxicity and RAN translation could indeed contribute to disease pathology. These mouse models also allowed us to characterize FXTAS disease pathogenesis and progression together with the underlying neurobiological changes and to develop and test highly potential targeted therapeutic interventions. This part of the review will describe the current available mouse models for FXTAS with their specific aspects, advantages and limitations, and what insights they have provided over the past years into disease mechanism.

The Dutch KI mouse

The first mouse model generated to exhibits much of the pathology seen in affected PM carriers and in FXTAS pathology at the genetic level as well as the histopathological and molecular level was the Dutch mouse knock-in (CGG_{dut} KI) model. This mouse model was

developed in Rotterdam at the Erasmus MC in the Netherlands. This model was generated by replacing the endogenous murine *Fmr1* 8xCGG-repeat with a human 98xCGG-repeat containing the human *FMR1* flanking regions. The *Fmr1* mouse promoter was left unchanged. This was done by homologous recombination in embryonic stem (ES) cells [227, 228]. Upon paternal and maternal transmission, the CGG_{dut} KI mouse showed mild instability of the CGG-repeat with both short expansions and contractions present [228-230]. The CGG_{dut} KI mice (**Fig. 4A**) have been bred into a C57BL/6J and FVB background over several generations to establish lines with expanded alleles greater than 450xCGGs [228, 231]. Although repeat lengths of more than 450CGGs were found, no increased methylation of the *Fmr1* gene has been reported. When examining these mice at the histopathological level clear ubiquitin-positive intranuclear inclusions could be shown similar to what is found in FXTAS patients. As mentioned before FXTAS patients are characterized with elevated *FMR1* mRNA and slightly decreased FMRP protein. Although FXTAS is considered to be a late-onset neurodegenerative disorder, some phenotypes of the disease in patients and in the CGG_{dut} KI mouse could suggest that FXTAS might also have features of a neurodevelopmental disorder. Developmental abnormalities during the PM stage such as altered learning and memory may contribute to the late manifestation of FXTAS. For example PM carriers have a smaller hippocampus that correlates with impaired performance in standardized tests of memory [148]. Hippocampal neurons with an abnormal dendritic morphology have been observed in FXTAS neurons at a time of development when nuclear inclusions are not detectable yet. When observing hippocampal neurons from the CGG_{dut} KI mouse researchers found cortical migration to be affected in these mice and that these neurons upon culturing display shorter dendrites and have a reduced dendritic complexity [122, 232-235]. Recently, the impact of elevated *Fmr1* mRNA levels on the morphology of dendrites and axons was studied more in depth [236]. Indeed, these morphological phenotypes are associated with increased levels of *Fmr1* mRNA because upon treatment with shRNAs specifically targeting the *Fmr1* mRNA these phenotypes are rescued. In addition, proteomic analysis in the CGG_{dut} KI mouse showed that upon rescue of *FMR1* mRNA levels a large number of important RBPs such as Tia1, HNRNPll, and ROAA could be normalized. Other rescued proteins are Rab-GTPases, which are critical for synaptic function in neurons in brain developmental disorders. Also, Aldh4a1/P5CDH and Samm50, which are involved in mitochondrial dysfunction, were found to be deregulated in these mice confirming previous hypotheses indicating the important role of mitochondria in FXTAS pathology. All these proteins provide possible future pharmacological targetable molecules for early therapeutic intervention for FXTAS. More research focusing on other aspects of neurodevelopment in FXTAS such as the role of FMRP in the PM stage is necessary before one can categorize FXTAS to also be a neurodevelopmental disorder. Altogether, the CGG_{dut} KI mouse model nicely recapitulates the histopathology and molecular changes observed in patients [227, 231].

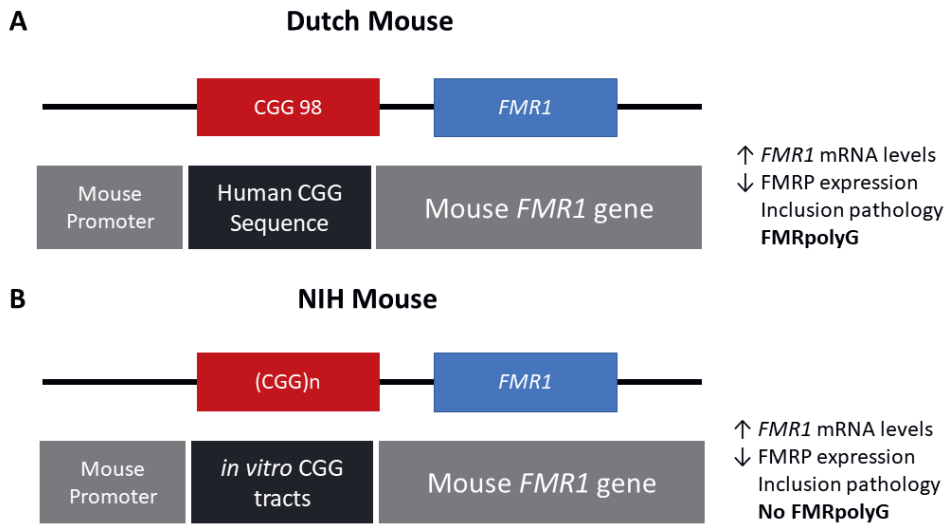

Figure 4 | Schematic drawings representing the genetic constructs designed for the Dutch and NIH CGG KI PM mouse models. (A) The Dutch mouse model has an intact mouse promoter followed by a human genetic sequence flanking the inserted CGG-repeat expansion upstream of the mouse *Fmr1* gene. **(B)** The NIH CGG KI mouse has an *in vitro* generated CGG-repeat expansion inserted to replace the mouse 8xCGG also keeping the mouse *Fmr1* gene and promoter intact. In both mouse models there is immunodetection of ubiquitin-positive intranuclear inclusions.

The NIH KI mouse

The National Institutes of Health developed a second KI mouse model (CGG_{nih} KI) (**Fig. 4B**) with a CGG-repeat length between 118-120xCGGs by generating a CGG-repeat flanked by S*fi* I sites and then ligating this CGG-repeat into the target construct with exon 1 of the mouse *Fmr1* gene in the correct orientation minimalizing changes to the mouse regions flanking the CGG-repeat, the gene itself and the promoter [150, 227, 237]. This resulted in these mice having a translational TAA stop codon upstream of the CGG-repeat. This TAA stop codon is present in the endogenous mouse *Fmr1* gene but not in the human *FMR1* gene. These mice, similar to the CGG_{dut} KI mouse show moderate intergenerational expansions with elevated *Fmr1* mRNA levels and decreased FMRP levels at the molecular level without any methylation of the *Fmr1* gene. Importantly, histopathological analysis revealed less ubiquitin-positive intranuclear inclusions being present in these mice compared to the CGG_{dut} KI mouse [227, 237].

Purkinje cell specific mouse model

A Purkinje cell specific mouse model was generated to provide evidence that the expanded CGG-repeat is necessary to cause FXTAS pathology similar to human and distinguish these effects seen from possible alterations in the *Fmr1* gene. To do so transgenic mice were

generated specifically expressing a CGG-repeat in the context of *Fmr1* (L7-CGG90-*Fmr1*) or in context of the enhanced green fluorescent protein (L7-CGG90-EGFP) in Purkinje neurons in the cerebellum using the L7/pcp-2 promoter (**Fig. 5**) [60]. With these two lines it would be possible to determine whether ectopic expression of a 90xCGG expanded repeat would cause neurodegeneration in the cerebellum or not. Significant Purkinje cell loss was observed in both the L7-CGG90-*Fmr1* and L7-CGG90-EGFP mice. Ubiquitin-positive intranuclear inclusions being the hallmark of FXTAS could be found in Purkinje cells of both the lines with the expanded CGG-repeat but not in the control mice suggesting an essential role for the expanded CGG-repeat and RNA in inclusion formation. It is assumed that the proteasome degradation pathway is involved in FXTAS disease progression in humans since essential proteins involved in this pathway are found in ubiquitin-positive inclusions [229]. Inclusions in the Purkinje cell specific mice contained as well the 20S core complex of the proteasome, Hsp40 and Rad23b protein, which is a known protein of the ubiquitin-mediated proteasome degradation pathway. Behavioral examination revealed that mice expressing the expanded CGG-repeat mRNA in the Purkinje cells had an impaired motor performance on the rotarod test. These neuropathological and behavioral observations provide evidence that expression of the CGG-repeat mRNA is sufficient to cause Purkinje cell dysfunction and loss of neurons similar to that reported in FXTAS patients [81]. Although there might be a connection between intranuclear inclusion formation and in this case Purkinje cell death, such a conclusion may only be made upon understanding the role of other essential proteins present in these inclusions.

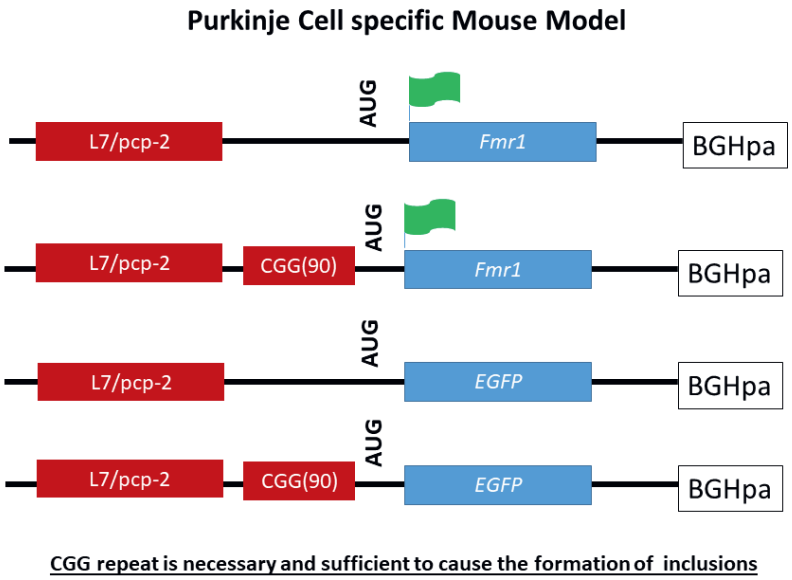

Figure 5 | Schematic representation of the Purkinje cell specific expression constructs in the context of *Fmr1* or EGFP. The transgenes were driven by the Purkinje cells specific L7/pcp-2 promoter. A human genomic *FMR1* DNA fragment containing a 90xCGG-repeat was inserted upstream of the *Fmr1* or EGFP coding region between the transcriptional and translational start sites. The *Fmr1* containing transgenes have a FLAG epitope engineered into the 5'-region of the gene. A BGH polyadenylation (pa) site was inserted in the 3'-region of all transgenes.

FMRpolyG and CGG-RNA transgenic mice

To further elaborate on the two hypotheses regarding the pathogenic mechanism in PM and FXTAS pathology based on expression of mutant *FMR1* mRNA bearing an expanded CGG-repeat a new mouse model was suggested. How *FMR1* mRNA containing expanded CGG-repeats is pathogenic was still unclear. To study this, the lab of Charlet Berguerand at the Institut de Génétique et de Biologie Moléculaire et Cellulaire (IGBMC) in France created two transgenic mouse models (**Fig. 6**). The first model contains the full human 5'-UTR of *FMR1* with expanded 99xCGG-repeats that express both the CGG-RNA as well as the FMRpolyG protein (**Fig. 6A**). The second line referred to as the mutant line also expresses 99xCGG-repeats, but without the non-canonical ACG start-codon and the surrounding 5'-UTR sequence region only expressing the CGG-RNA and no protein (**Fig. 6B**) [193]. Both transgenic mouse lines have a CAG promotor inserted within the *Rosa26* locus and expression is controlled by a loxP-polyadeneylation cassette [193]. Using the ubiquitously and embryonically expressed Cre recombinase resulted in deletion of the loxP cassette, which led to high expression of transgene RNA throughout the brain, heart and liver, with less expression in skeletal muscle and the kidneys. Transgene RNA expression is the same in both transgenic mouse lines. The full human *FMR1* 5'-UTR transgenic mice showed

upon histological analysis FMRpolyG protein nuclear aggregates that co-localize with ubiquitin in the brain [193]. The mutant *FMR1* 5′-UTR mice did not show these aggregates. The occurrence of CGG RNA *foci* in the brain of both mouse models (**Fig. 6**) is slightly lower compared to other previously reported mouse models [173, 193]. FMRpolyG protein also accumulated in other tissue than the brain, which is similar to what our group reported regarding FMRpolyG aggregates in non-CNS tissues in FXTAS patients [78]. Other sense proteins such as the polyalanine (FMRpolyA) and polyarginine (FMRpolyR) peptides from other reading frames were not observed in these mice. There is to some extent neuronal cell death and little loss of Purkinje neurons in the mice expressing CGG-RNA and the FMRpolyG protein but not in the mice expressing only CGG-RNA [193].

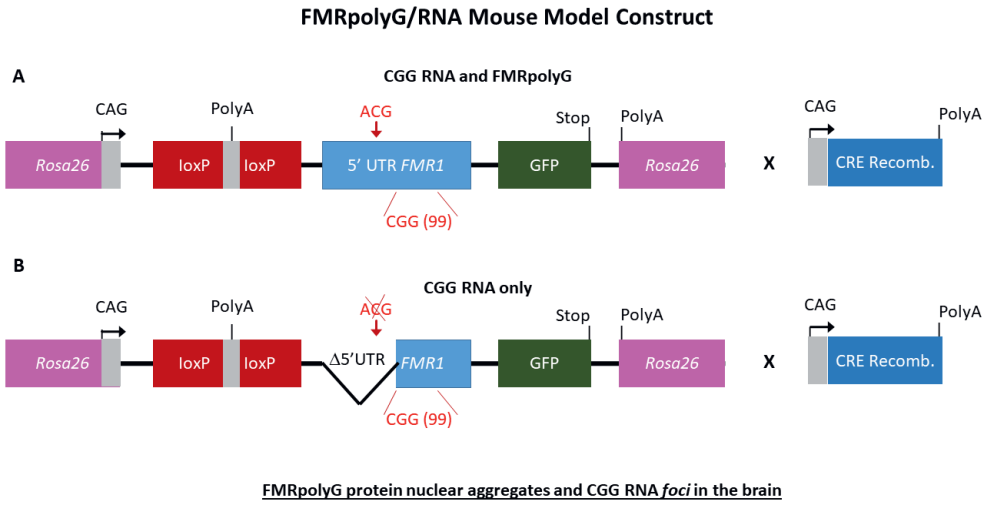

Figure 6 | Schematic representation of the mouse transgene constructs. Both mice present inclusions in the brain containing either FMRpolyG or CGG-repeat RNA only. Expression of FMRpolyG is pathogenic in mice. Immunohistochemistry in cerebellum and hippocampus of 6-month-old double transgenic **(A)** CMV-Cre/5′-UTR-99xCGG-GFP mice show clear staining for ubiquitin and FMRpolyG in intranuclear inclusions while **(B)** CMV-Cre/Δ5′-UTR-99xCGG-GFP transgenic mice only show intranuclear *foci* containing CGG-repeat RNA without FMRpolyG.

FMR1 overexpressing mice

FMR1 mRNA toxicity is mentioned several times before to be one of the hypothesis causing FXTAS pathology and is supported by elevated levels of *FMR1* mRNA with an expanded CGG-repeat [18]. It could be that toxicity occurs due to expression of an expanded CGG-repeat or because of just elevated *FMR1* mRNA levels independent of the CGG-repeat being present. The *Drosophila* model shows that repeat length is a direct cause of pathology since longer repeats show extreme retina pathology while short repeats result in little pathology [175]. To confirm these findings in mice, transgenic mice

were generated overexpressing *FMR1* mRNA with a normal length CGG-repeat consisting of 29xCGGs [238]. Human *FMR1* cDNA with 29xCGG-repeats under control of a SV40/T7 promoter was injected in oocytes to generate these transgenic 29xCGG mice with 20- to 100-fold increase in *FMR1* mRNA in tissues such as liver, cerebral cortex and cerebellum. Although these mice express extreme levels of *FMR1* mRNA, there was no significant difference in general activity or anxiety-related behaviors in open-field tests, which suggests that expression of *FMR1* mRNA alone is not enough to induce pathology but that a CGG-repeat expansion is necessary for pathology to occur.

A yeast artificial chromosome (YAC) containing the full-length human *FMR1* gene was used to generate transgenic mice overexpressing *FMR1* mRNA to study the toxic effect of *FMR1* mRNA as well as to study CGG-repeat instability [239, 240]. These mice were generated by direct microinjection of purified YAC DNA containing a 92xCGG-repeat isolated from an adult male permutation carrier into the pro-nuclei of fertilized FVB/N mouse oocytes and then transferred into foster mice which eventually led to identifying a mouse line having a repeat bearing 90xCGGs [239]. These YAC mice show a 2- to 3-fold increase in expression of *FMR1* mRNA and a 10- to 15-fold increase in FMRP protein production [240, 241]. Importantly to mention is that histological analysis presented no changes in overall brain morphology due to overexpression of *FMR1* mRNA or FMRP. When YAC mice were crossed with *Fmr1* KO mice lacking FMRP protein, some of the pathological features attributed to the absence of FMRP could be reversed and even overcorrected which also resulted in some abnormal behaviors. The authors attributed phenotype to overexpression of FMRP but the high levels of *Fmr1* mRNA could also have contributed to these behavioral effects [241].

Inducible mouse models

As mentioned, before it was not yet clear whether overexpression of RNA bearing normal CGG-repeat length or an expanded CGG-repeat is sufficient to induce toxicity in animal models and how to translate results in mice to the PM and FXTAS pathology. To further elaborate on this question two additional doxycycline inducible transgenic mouse models were generated. Both mouse models consisted of two transgenic mouse lines differing in the promoter used. The main advantage of both models is that expression of the transgene can be switched on and off using doxycycline. The first mouse line expresses the tetracycline response element (TRE) and the other line expressing the reverse tetracycline-controlled transactivator protein (rtTA), which can be activated using doxycycline or a doxycycline-derivative in drinking water or food. The TRE-element was coupled to an expanded CGG-repeat in frame with eGFP while the rtTA was coupled to a hnRNP promoter. Both mouse lines were crossbred generating double transgenic offspring with ubiquitous expression of 90xCGG-repeat RNA (hnRNP-rtTA/TRE-90xCGG-eGFP; **Fig. 7**). Strange enough these mice died within five days after induction of the

transgene using doxycycline. After histopathological analysis of the liver and molecular analysis two markers, cytochrome C (CytC) and glutathione oxidase (GPX1), could be identified being affected in the livers with increased steatosis, mitochondrial dysfunction and subsequent apoptosis. Due to the early death of these mice no neuropathology could be observed. In summary this mouse model taught us that *in vivo* expression of expanded CGG-repeat RNA leads to severe toxicity in the liver by affecting reactive-oxygen species (ROS) signaling [162].

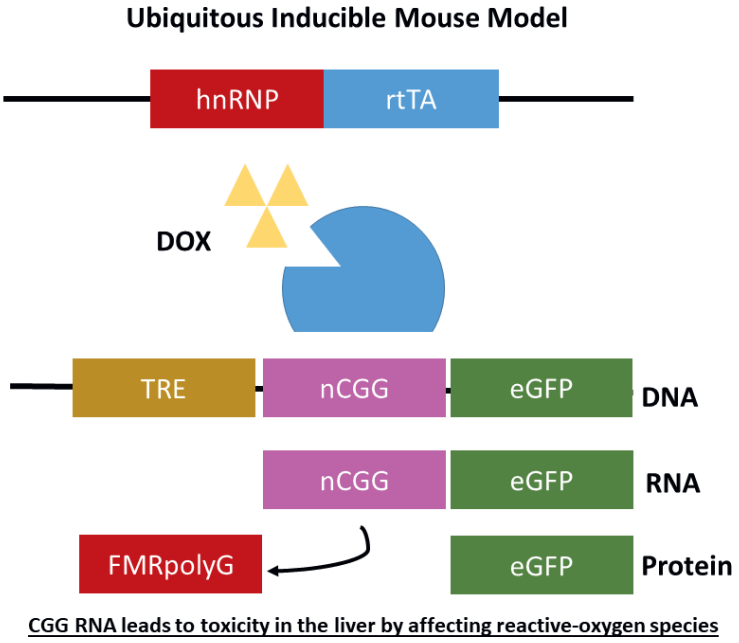

Figure 7 | Ubiquitous expression of expanded CGG-repeat (nCGG) RNA in inducible transgenic mouse model. The Tet-On system was used to generate double transgenic mice expressing an expanded CGG-repeat at the RNA level in all tissues. Expression of rtTA is controlled by the hnRNP promoter on a transgene. In contrast, brain specific expression of the nCGG RNA in inducible mice is controlled by either the specific prion protein (PrP) or the *CamKII-α* promoter. Upon DOX administration rtTA will be activated and can bind the Tet Responsive Element (TRE) on another transgene, inducing expression of the nCGG at the RNA level and eGFP at the protein level. FMRpolyG is produced through RAN-translation of the nCGG RNA.

Since FXTAS pathology is considered to be a neurodegenerative disease, it was clear that the next step would be to generate a brain specific doxycycline inducible mouse model expressing RNA containing an expanded CGG-repeat. For this a brain specific prion protein (PrP)-rtTA driver was used to activate expression of normal length CGG RNA or expanded CGG-repeat RNA fused to eGFP [165, 242]. The PrP promoter drives expression

in glial cells and neurons in the CNS. Compared to the hnRNP-rtTA mouse line, these mice could be treated for several weeks with doxycycline without any apparent liver toxicity. The RNA bearing an expanded CGG-repeat was expressed the strongest in the cerebellum, hippocampus and striatum. Examining brain sections showed ubiquitin-positive intranuclear inclusions co-localizing with FMRpolyG-positive intranuclear inclusions. Inclusion formation was followed in time showing increasing numbers and size when mice were treated longer with doxycycline. Other FXTAS-related proteins such as 20S core complex of the proteasome, Hsp40 and Rad23b could also be found co-localizing with the ubiquitin-positive aggregates. Our lab could show that introducing a wash-out period at an early stage was enough to halt and even reverse inclusion body formation. When repeating the wash-out step at a later point in time disease pathology could only be halted but not reversed [165, 242]. Upon doxycycline induction the brain specific inducible mice had deficits in the compensatory eye movements. By turning of expression of the RNA with an expanded repeat this functional phenotype could be stopped [165]. After doxycycline induction double transgenic brain specific inducible mice performed poorly on the rotarod test indicating that motor performance is affected, more specifically motor coordination and motor learning which was also in line with the high number of intranuclear inclusions observed in lobule X of the cerebellum. When examined in the open-field test for emotional disturbance these mice were more anxious but had no deficits in emotional learning nor memory impairments correlating with intranuclear inclusions found in the amygdala and the hippocampus [165]. Behavioral phenotype and rescue were paralleled by the intranuclear inclusions formed in several brain regions such as lobule X of the cerebellum, the central amygdala and basolateral nuclei region of the amygdala, and hippocampal sub-regions such as the dentate gyrus (DG) and cornu ammonis 3 (CA3) region of the hippocampus [242]. Turning off transgene expression could halt functional phenotype and even reverse neuropathology if intervened at an early stage potentially suggesting that brain region specific therapeutic intervention might be beneficial for FXTAS patients in the future [242]. More recently, we generated a new brain specific doxycycline inducible mouse model that is controlled by the *CamKII-α* promoter. These mice form FMRpolyG-positive intranuclear inclusions in the hippocampus, the striatum, the hypothalamus, the inferior and superior colliculus but not in the cerebellum. Surprisingly, any behavior associated with these brain regions was absent potentially suggesting an early protective role for inclusions. This mouse model will be further discussed in **chapter 3**.

Astrocyte-specific mouse model

The FXTAS field has been provided with many interesting mouse models but there are still questions left unanswered. One interesting question in the field concerns the specific role of astrocytes in FXTAS pathology. What is the role of astroglial cells in FXTAS? Is for example expression of an expanded CGG-repeat enough to induce pathology? FXTAS

patient brains have inclusions throughout the entire brain, in neurons but also in astroglial cells such as the Bergmann glia in the cerebellum [229]. Although the CGG_{dut} KI mouse model of FXTAS recapitulates most aspects see in FXTAS, these mice have relatively few numbers of astrocytes with intranuclear inclusions. Therefore, a transgenic mouse model specifically expressing the expanded CGG-repeat RNA in astroglia was missing. This transgenic mouse line with a C57BL/6j background was generated through pronuclear injection using an astrocyte-specific *Gfa2* promoter to induce expression of an expanded 99xCGG-repeat fused to an eGFP marker gene only in astrocytes [61]. Immunocytochemical analysis of eGFP expression patterns show expression of 99xCGG RNA was restricted to astroglia and Bergmann glia only and was not present in neurons, microglia or oligodendrocytes. Ubiquitin-positive and FMRpolyG-positive inclusions were observed in the nucleus of astroglia with inclusion bodies also being present in the cytoplasm of astrocyte processes. Although astrocytes with inclusion bodies were low in number, they were widely distributed in the brain such as in the neocortex, cerebellum and occasionally in subcortical regions in the hypothalamus and some brain stem nuclei. These mice had no sign of Purkinje neuronal dropout as well as no ubiquitin-positive inclusions in Purkinje cells could be found [61, 193]. This study was the first of its kind to provide evidence of FXTAS related RAN-translation products being present in mouse astroglia. Surprisingly, these mice also had ubiquitin-positive intranuclear inclusions in neurons even though there was no leaky expression in neurons of the *Gfa2*-promotor and these cells did not express the expanded 99xCGG RNA suggesting a prion-like spread of pathology, similar to what is seen in other models, from astrocytes to neurons by a cell-to-cell transfer mechanism [243]. Several behavioral tests were performed to examine neurological disease phenotypes associated with FXTAS pathology. These mice had difficulty with basic gait parameters such as stance time and range of motion. Also, when placed on the ladder rung test their motor performance was clearly affected. These mice did not suffer from any emotional disturbance nor memory learning deficits. Although this model presents evidence of key hallmarks of FXTAS pathology, more work is necessary to further elaborate on the role of astroglia in FXTAS disease pathology. This mouse model will be further discussed in depth in **chapter 2**.

References

1. Lubs, H.A., *A marker X chromosome.* Am J Hum Genet, 1969. **21**(3): p. 231-44.
2. Verkerk, A.J., et al., *Identification of a gene (FMR-1) containing a CGG repeat coincident with a breakpoint cluster region exhibiting length variation in fragile X syndrome.* Cell, 1991. **65**(5): p. 905-14.
3. Hunter, J., et al., *Epidemiology of fragile X syndrome: a systematic review and meta-analysis.* Am J Med Genet A, 2014. **164A**(7): p. 1648-58.
4. *United States Center for Disease Control (CDC) website: http://www.cdc.gov/ncbddd/fxs/data.html*. Accessed November 2020.
5. Jin, X. and L. Chen, *Fragile X syndrome as a rare disease in China - Therapeutic challenges and opportunities.* Intractable Rare Dis Res, 2015. **4**(1): p. 39-48.
6. Ashley, C.T., et al., *Human and murine FMR-1: alternative splicing and translational initiation downstream of the CGG-repeat.* Nat Genet, 1993. **4**(3): p. 244-51.
7. Price, D.K., et al., *The chicken FMR1 gene is highly conserved with a CCT 5'-untranslated repeat and encodes an RNA-binding protein.* Genomics, 1996. **31**(1): p. 3-12.
8. Wan, L., et al., *Characterization of dFMR1, a Drosophila melanogaster homolog of the fragile X mental retardation protein.* Mol Cell Biol, 2000. **20**(22): p. 8536-47.
9. Shtang, S., M.D. Perry, and M.E. Percy, *Search for a Caenorhabditis elegans FMR1 homologue: identification of a new putative RNA-binding protein (PRP-1) that hybridizes to the mouse FMR1 double K homology domain.* Am J Med Genet, 1999. **84**(3): p. 283-5.
10. Lim, J.H., et al., *Developmental expression of Xenopus fragile X mental retardation-1 gene.* Int J Dev Biol, 2005. **49**(8): p. 981-4.
11. van 't Padje, S., et al., *Characterisation of Fmrp in zebrafish: evolutionary dynamics of the fmr1 gene.* Dev Genes Evol, 2005. **215**(4): p. 198-206.
12. Maddalena, A., et al., *Technical standards and guidelines for fragile X: the first of a series of disease-specific supplements to the Standards and Guidelines for Clinical Genetics Laboratories of the American College of Medical Genetics. Quality Assurance Subcommittee of the Laboratory Practice Committee.* Genet Med, 2001. **3**(3): p. 200-5.
13. Yrigollen, C.M., et al., *AGG interruptions and maternal age affect FMR1 CGG repeat allele stability during transmission.* J Neurodev Disord, 2014. **6**(1): p. 24.
14. Oberle, I., et al., *Instability of a 550-base pair DNA segment and abnormal methylation in fragile X syndrome.* Science, 1991. **252**(5009): p. 1097-102.
15. Ashley-Koch, A.E., et al., *Examination of factors associated with instability of the FMR1 CGG repeat.* Am J Hum Genet, 1998. **63**(3): p. 776-85.
16. Nolin, S.L., et al., *Familial transmission of the FMR1 CGG repeat.* Am J Hum Genet, 1996. **59**(6): p. 1252-61.
17. Yrigollen, C.M., et al., *AGG interruptions within the maternal FMR1 gene reduce the risk of offspring with fragile X syndrome.* Genet Med, 2012. **14**(8): p. 729-36.
18. Hagerman, R.J. and P.J. Hagerman, *The fragile X premutation: into the phenotypic fold.* Curr Opin Genet Dev, 2002. **12**(3): p. 278-83.

19. Crawford, D.C., J.M. Acuna, and S.L. Sherman, *FMR1 and the fragile X syndrome: human genome epidemiology review.* Genet Med, 2001. **3**(5): p. 359-71.
20. Jacquemont, S., et al., *Penetrance of the fragile X-associated tremor/ataxia syndrome in a premutation carrier population.* JAMA, 2004. **291**(4): p. 460-9.
21. Cronister, A., et al., *Prevalence and instability of fragile X alleles: implications for offering fragile X prenatal diagnosis.* Obstet Gynecol, 2008. **111**(3): p. 596-601.
22. Sherman, S.L., *Premature ovarian failure in the fragile X syndrome.* Am J Med Genet, 2000. **97**(3): p. 189-94.
23. Hagerman, R.J., et al., *Fragile X-Associated Neuropsychiatric Disorders (FXAND).* Front Psychiatry, 2018. **9**: p. 564.
24. Johnson, K., J. Herring, and J. Richstein, *Fragile X Premutation Associated Conditions (FXPAC).* Front Pediatr, 2020. **8**: p. 266.
25. Grigsby, J., *The fragile X mental retardation 1 gene (FMR1): historical perspective, phenotypes, mechanism, pathology, and epidemiology.* Clin Neuropsychol, 2016. **30**(6): p. 815-33.
26. Davis, J.K. and K. Broadie, *Multifarious Functions of the Fragile X Mental Retardation Protein.* Trends Genet, 2017. **33**(10): p. 703-714.
27. Tassone, F., et al., *Elevated levels of FMR1 mRNA in carrier males: a new mechanism of involvement in the fragile-X syndrome.* Am J Hum Genet, 2000. **66**(1): p. 6-15.
28. Brown, V., et al., *Microarray identification of FMRP-associated brain mRNAs and altered mRNA translational profiles in fragile X syndrome.* Cell, 2001. **107**(4): p. 477-87.
29. Darnell, J.C., et al., *Fragile X mental retardation protein targets G quartet mRNAs important for neuronal function.* Cell, 2001. **107**(4): p. 489-99.
30. Laggerbauer, B., et al., *Evidence that fragile X mental retardation protein is a negative regulator of translation.* Hum Mol Genet, 2001. **10**(4): p. 329-38.
31. Li, Z., et al., *The fragile X mental retardation protein inhibits translation via interacting with mRNA.* Nucleic Acids Res, 2001. **29**(11): p. 2276-83.
32. Schaeffer, C., et al., *The fragile X mental retardation protein binds specifically to its mRNA via a purine quartet motif.* EMBO J, 2001. **20**(17): p. 4803-13.
33. Miyashiro, K.Y., et al., *RNA cargoes associating with FMRP reveal deficits in cellular functioning in Fmr1 null mice.* Neuron, 2003. **37**(3): p. 417-31.
34. Eberhart, D.E., et al., *The fragile X mental retardation protein is a ribonucleoprotein containing both nuclear localization and nuclear export signals.* Hum Mol Genet, 1996. **5**(8): p. 1083-91.
35. Fridell, R.A., et al., *A nuclear role for the Fragile X mental retardation protein.* EMBO J, 1996. **15**(19): p. 5408-14.
36. Sittler, A., et al., *Alternative splicing of exon 14 determines nuclear or cytoplasmic localisation of fmr1 protein isoforms.* Hum Mol Genet, 1996. **5**(1): p. 95-102.
37. Willemsen, R., et al., *Association of FMRP with ribosomal precursor particles in the nucleolus.* Biochem Biophys Res Commun, 1996. **225**(1): p. 27-33.
38. Bakker, C.E., et al., *Immunocytochemical and biochemical characterization of FMRP, FXR1P, and FXR2P in the mouse.* Exp Cell Res, 2000. **258**(1): p. 162-70.

39. Siomi, H., et al., *The protein product of the fragile X gene, FMR1, has characteristics of an RNA-binding protein.* Cell, 1993. **74**(2): p. 291-8.
40. Brown, V., et al., *Purified recombinant Fmrp exhibits selective RNA binding as an intrinsic property of the fragile X mental retardation protein.* J Biol Chem, 1998. **273**(25): p. 15521-7.
41. Feng, Y., et al., *Fragile X mental retardation protein: nucleocytoplasmic shuttling and association with somatodendritic ribosomes.* J Neurosci, 1997. **17**(5): p. 1539-47.
42. Weiler, I.J., et al., *Fragile X mental retardation protein is translated near synapses in response to neurotransmitter activation.* Proc Natl Acad Sci U S A, 1997. **94**(10): p. 5395-400.
43. Nakayama, A.Y., M.B. Harms, and L. Luo, *Small GTPases Rac and Rho in the maintenance of dendritic spines and branches in hippocampal pyramidal neurons.* J Neurosci, 2000. **20**(14): p. 5329-38.
44. Consortium, T.D.-B.F.X., *Fmr1 knockout mice: a model to study fragile X mental retardation. The Dutch-Belgian Fragile X Consortium.* Cell, 1994. **78**(1): p. 23-33.
45. Comery, T.A., et al., *Abnormal dendritic spines in fragile X knockout mice: maturation and pruning deficits.* Proc Natl Acad Sci U S A, 1997. **94**(10): p. 5401-4.
46. Nimchinsky, E.A., A.M. Oberlander, and K. Svoboda, *Abnormal development of dendritic spines in FMR1 knock-out mice.* J Neurosci, 2001. **21**(14): p. 5139-46.
47. Kovacs, T., O. Kelemen, and S. Keri, *Decreased fragile X mental retardation protein (FMRP) is associated with lower IQ and earlier illness onset in patients with schizophrenia.* Psychiatry Res, 2013. **210**(3): p. 690-3.
48. Hagerman, R.J., et al., *Intention tremor, parkinsonism, and generalized brain atrophy in male carriers of fragile X.* Neurology, 2001. **57**(1): p. 127-30.
49. Brunberg, J.A., et al., *Fragile X premutation carriers: characteristic MR imaging findings of adult male patients with progressive cerebellar and cognitive dysfunction.* AJNR Am J Neuroradiol, 2002. **23**(10): p. 1757-66.
50. Jacquemont, S., et al., *Fragile X premutation tremor/ataxia syndrome: molecular, clinical, and neuroimaging correlates.* Am J Hum Genet, 2003. **72**(4): p. 869-78.
51. Hall, D.A., et al., *Emerging topics in FXTAS.* J Neurodev Disord, 2014. **6**(1): p. 31.
52. Leehey, M.A., *Fragile X-associated tremor/ataxia syndrome: clinical phenotype, diagnosis, and treatment.* J Investig Med, 2009. **57**(8): p. 830-6.
53. Hall, D.A., et al., *The Corpus Callosum Splenium Sign in Fragile X-Associated Tremor Ataxia Syndrome.* Mov Disord Clin Pract, 2017. **4**(3): p. 383-388.
54. Renaud, M., et al., *Relevance of corpus callosum splenium versus middle cerebellar peduncle hyperintensity for FXTAS diagnosis in clinical practice.* J Neurol, 2015. **262**(2): p. 435-42.
55. Apartis, E., et al., *FXTAS: new insights and the need for revised diagnostic criteria.* Neurology, 2012. **79**(18): p. 1898-907.
56. Castellani, R.J., et al., *Reexamining Alzheimer's disease: evidence for a protective role for amyloid-beta protein precursor and amyloid-beta.* J Alzheimers Dis, 2009. **18**(2): p. 447-52.
57. Tanaka, M., et al., *Aggresomes formed by alpha-synuclein and synphilin-1 are cytoprotective.* J Biol Chem, 2004. **279**(6): p. 4625-31.

58. Bjorkoy, G., et al., *p62/SQSTM1 forms protein aggregates degraded by autophagy and has a protective effect on huntingtin-induced cell death.* J Cell Biol, 2005. **171**(4): p. 603-14.
59. Todd, P.K., et al., *CGG repeat-associated translation mediates neurodegeneration in fragile X tremor ataxia syndrome.* Neuron, 2013. **78**(3): p. 440-55.
60. Hashem, V., et al., *Ectopic expression of CGG containing mRNA is neurotoxic in mammals.* Hum Mol Genet, 2009. **18**(13): p. 2443-51.
61. Wenzel, H.J., et al., *Astroglial-targeted expression of the fragile X CGG repeat premutation in mice yields RAN translation, motor deficits and possible evidence for cell-to-cell propagation of FXTAS pathology.* Acta Neuropathol Commun, 2019. **7**(1): p. 27.
62. Wenzel, H.J., et al., *Ubiquitin-positive intranuclear inclusions in neuronal and glial cells in a mouse model of the fragile X premutation.* Brain Res, 2010. **1318**: p. 155-66.
63. Hall, D.A., et al., *Update on the Clinical, Radiographic, and Neurobehavioral Manifestations in FXTAS and FMR1 Premutation Carriers.* Cerebellum, 2016. **15**(5): p. 578-86.
64. Cohen, S., et al., *Molecular and imaging correlates of the fragile X-associated tremor/ataxia syndrome.* Neurology, 2006. **67**(8): p. 1426-31.
65. Rivera, S., G. Stebbins, and J. Grigsby, *Radiological findings in FXTAS*. 2010. p. 55-66.
66. Famula, J.L., et al., *Presence of Middle Cerebellar Peduncle Sign in FMR1 Premutation Carriers Without Tremor and Ataxia.* Front Neurol, 2018. **9**: p. 695.
67. Battistella, G., et al., *Brain structure in asymptomatic FMR1 premutation carriers at risk for fragile X-associated tremor/ataxia syndrome.* Neurobiol Aging, 2013. **34**(6): p. 1700-7.
68. Shelton, A.L., et al., *Middle Cerebellar Peduncle Width-A Novel MRI Biomarker for FXTAS?* Front Neurosci, 2018. **12**: p. 379.
69. Quattrone, A., et al., *MR parkinsonism index predicts vertical supranuclear gaze palsy in patients with PSP-parkinsonism.* Neurology, 2016. **87**(12): p. 1266-73.
70. Loesch, D.Z., et al., *Novel Blood Biomarkers Are Associated with White Matter Lesions in Fragile X-Associated Tremor/Ataxia Syndrome.* Neurodegener Dis, 2017. **17**(1): p. 22-30.
71. Giulivi, C., et al., *Plasma Biomarkers for Monitoring Brain Pathophysiology in FMR1 Premutation Carriers.* Front Mol Neurosci, 2016. **9**: p. 71.
72. Giulivi, C., et al., *Plasma metabolic profile delineates roles for neurodegeneration, pro-inflammatory damage and mitochondrial dysfunction in the FMR1 premutation.* Biochem J, 2016. **473**(21): p. 3871-3888.
73. Crippa, B.L., et al., *Biochemical abnormalities in Pearson syndrome.* Am J Med Genet A, 2015. **167A**(3): p. 621-8.
74. Kaplan, E.S., et al., *Early mitochondrial abnormalities in hippocampal neurons cultured from Fmr1 pre-mutation mouse model.* J Neurochem, 2012. **123**(4): p. 613-21.
75. Napoli, E., et al., *Altered zinc transport disrupts mitochondrial protein processing/import in fragile X-associated tremor/ataxia syndrome.* Hum Mol Genet, 2011. **20**(15): p. 3079-92.
76. Ross-Inta, C., et al., *Evidence of mitochondrial dysfunction in fragile X-associated tremor/ataxia syndrome.* Biochem J, 2010. **429**(3): p. 545-52.

77. Zafarullah, M., et al., *Metabolic profiling reveals dysregulated lipid metabolism and potential biomarkers associated with the development and progression of Fragile X-Associated Tremor/ Ataxia Syndrome (FXTAS).* FASEB J, 2020. **34**(12): p. 16676-16692.
78. Buijsen, R.A., et al., *FMRpolyG-positive inclusions in CNS and non-CNS organs of a fragile X premutation carrier with fragile X-associated tremor/ataxia syndrome.* Acta Neuropathol Commun, 2014. **2**: p. 162.
79. Buijsen, R.A., et al., *Presence of inclusions positive for polyglycine containing protein, FMRpolyG, indicates that repeat-associated non-AUG translation plays a role in fragile X-associated primary ovarian insufficiency.* Hum Reprod, 2016. **31**(1): p. 158-68.
80. Greco, C.M., et al., *Neuropathology of fragile X-associated tremor/ataxia syndrome (FXTAS).* Brain, 2006. **129**(Pt 1): p. 243-55.
81. Greco, C.M., et al., *Neuronal intranuclear inclusions in a new cerebellar tremor/ataxia syndrome among fragile X carriers.* Brain, 2002. **125**(Pt 8): p. 1760-71.
82. Leehey, M.A., et al., *FMR1 CGG repeat length predicts motor dysfunction in premutation carriers.* Neurology, 2008. **70**(16 Pt 2): p. 1397-402.
83. Rodriguez-Revenga, L., et al., *Penetrance of FMR1 premutation associated pathologies in fragile X syndrome families.* Eur J Hum Genet, 2009. **17**(10): p. 1359-62.
84. Hagerman, R.J., et al., *Fragile-X-associated tremor/ataxia syndrome (FXTAS) in females with the FMR1 premutation.* Am J Hum Genet, 2004. **74**(5): p. 1051-6.
85. Jacquemont, S., et al., *Aging in individuals with the FMR1 mutation.* Am J Ment Retard, 2004. **109**(2): p. 154-64.
86. Cronister, A., et al., *Heterozygous fragile X female: historical, physical, cognitive, and cytogenetic features.* Am J Med Genet, 1991. **38**(2-3): p. 269-74.
87. Sullivan, A.K., et al., *Association of FMR1 repeat size with ovarian dysfunction.* Hum Reprod, 2005. **20**(2): p. 402-12.
88. Tassone, F., et al., *CGG repeat length correlates with age of onset of motor signs of the fragile X-associated tremor/ataxia syndrome (FXTAS).* Am J Med Genet B Neuropsychiatr Genet, 2007. **144B**(4): p. 566-9.
89. Paul, R., et al., *Early onset of neurological symptoms in fragile X premutation carriers exposed to neurotoxins.* Neurotoxicology, 2010. **31**(4): p. 399-402.
90. O'Dwyer, J.P., et al., *Fragile X-associated tremor/ataxia syndrome presenting in a woman after chemotherapy.* Neurology, 2005. **65**(2): p. 331-2.
91. Muzar, Z., et al., *Addictive substances may induce a rapid neurological deterioration in fragile X-associated tremor ataxia syndrome: A report of two cases.* Intractable Rare Dis Res, 2014. **3**(4): p. 162-5.
92. Muzar, Z., et al., *Methadone use in a male with the FMRI premutation and FXTAS.* Am J Med Genet A, 2015. **167**(6): p. 1354-9.
93. Saldarriaga, W., et al., *Phenobarbital use and neurological problems in FMR1 premutation carriers.* Neurotoxicology, 2016. **53**: p. 141-147.
94. Berry-Kravis, E., et al., *Fragile X-associated tremor/ataxia syndrome: clinical features, genetics, and testing guidelines.* Mov Disord, 2007. **22**(14): p. 2018-30, quiz 2140.

95. Roberts, J.E., et al., *Mood and anxiety disorders in females with the FMR1 premutation.* Am J Med Genet B Neuropsychiatr Genet, 2009. **150B**(1): p. 130-9.
96. Hunter, J.E., et al., *Investigation of phenotypes associated with mood and anxiety among male and female fragile X premutation carriers.* Behav Genet, 2008. **38**(5): p. 493-502.
97. Hunter, J.E., et al., *The FMR1 premutation and attention-deficit hyperactivity disorder (ADHD): evidence for a complex inheritance.* Behav Genet, 2012. **42**(3): p. 415-22.
98. Bacalman, S., et al., *Psychiatric phenotype of the fragile X-associated tremor/ataxia syndrome (FXTAS) in males: newly described fronto-subcortical dementia.* J Clin Psychiatry, 2006. **67**(1): p. 87-94.
99. Zuhlke, C., et al., *FMR1 premutation as a rare cause of late onset ataxia--evidence for FXTAS in female carriers.* J Neurol, 2004. **251**(11): p. 1418-9.
100. Berry-Kravis, E., et al., *Fragile X-associated tremor/ataxia syndrome in sisters related to X-inactivation.* Ann Neurol, 2005. **57**(1): p. 144-7.
101. Hamlin, A., et al., *Sleep apnea in fragile X premutation carriers with and without FXTAS.* Am J Med Genet B Neuropsychiatr Genet, 2011. **156B**(8): p. 923-8.
102. Coffey, S.M., et al., *Expanded clinical phenotype of women with the FMR1 premutation.* Am J Med Genet A, 2008. **146A**(8): p. 1009-16.
103. Summers, S.M., et al., *Fatigue and body mass index in the Fragile X premutation carrier.* Fatigue: Biomedicine, Health & Behavior, 2014. **2**(2): p. 64-72.
104. Bailey, D.B., Jr., et al., *Co-occurring conditions associated with FMR1 gene variations: findings from a national parent survey.* Am J Med Genet A, 2008. **146A**(16): p. 2060-9.
105. Au, J., et al., *Prevalence and risk of migraine headaches in adult fragile X premutation carriers.* Clin Genet, 2013. **84**(6): p. 546-51.
106. Leehey, M.A., et al., *Fibromyalgia in fragile X mental retardation 1 gene premutation carriers.* Rheumatology (Oxford), 2011. **50**(12): p. 2233-6.
107. Greco, C.M., et al., *Testicular and pituitary inclusion formation in fragile X associated tremor/ataxia syndrome.* J Urol, 2007. **177**(4): p. 1434-7.
108. Seritan, A.L., et al., *Risk Factors for Cognitive Impairment in Fragile X-Associated Tremor/Ataxia Syndrome.* J Geriatr Psychiatry Neurol, 2016. **29**(6): p. 328-337.
109. Grigsby, J., et al., *Cognitive profile of fragile X premutation carriers with and without fragile X-associated tremor/ataxia syndrome.* Neuropsychology, 2008. **22**(1): p. 48-60.
110. Kim, S.Y., et al., *Altered neural activity of magnitude estimation processing in adults with the fragile X premutation.* J Psychiatr Res, 2013. **47**(12): p. 1909-16.
111. Farzin, F., et al., *Autism spectrum disorders and attention-deficit/hyperactivity disorder in boys with the fragile X premutation.* J Dev Behav Pediatr, 2006. **27**(2 Suppl): p. S137-44.
112. Clifford, S., et al., *Autism spectrum phenotype in males and females with fragile X full mutation and premutation.* J Autism Dev Disord, 2007. **37**(4): p. 738-47.
113. Wheeler, A.C., et al., *Developmental profiles of infants with an FMR1 premutation.* J Neurodev Disord, 2016. **8**: p. 40.

114. Kenneson, A., et al., *Reduced FMRP and increased FMR1 transcription is proportionally associated with CGG repeat number in intermediate-length and premutation carriers.* Hum Mol Genet, 2001. **10**(14): p. 1449-54.
115. Primerano, B., et al., *Reduced FMR1 mRNA translation efficiency in fragile X patients with premutations.* RNA, 2002. **8**(12): p. 1482-8.
116. Brouwer, J.R., et al., *CGG-repeat length and neuropathological and molecular correlates in a mouse model for fragile X-associated tremor/ataxia syndrome.* J Neurochem, 2008. **107**(6): p. 1671-82.
117. Hessl, D., et al., *Amygdala dysfunction in men with the fragile X premutation.* Brain, 2007. **130**(Pt 2): p. 404-16.
118. Hessl, D., et al., *Decreased fragile X mental retardation protein expression underlies amygdala dysfunction in carriers of the fragile X premutation.* Biol Psychiatry, 2011. **70**(9): p. 859-65.
119. Keri, S. and G. Benedek, *Why is vision impaired in fragile X premutation carriers? The role of fragile X mental retardation protein and potential FMR1 mRNA toxicity.* Neuroscience, 2012. **206**: p. 183-9.
120. Hessl, D., et al., *Abnormal elevation of FMR1 mRNA is associated with psychological symptoms in individuals with the fragile X premutation.* Am J Med Genet B Neuropsychiatr Genet, 2005. **139B**(1): p. 115-21.
121. Hagerman, R.J. and P. Hagerman, *Fragile X-associated tremor/ataxia syndrome - features, mechanisms and management.* Nat Rev Neurol, 2016. **12**(7): p. 403-12.
122. Berman, R.F., et al., *Mouse models of the fragile X premutation and fragile X-associated tremor/ataxia syndrome.* J Neurodev Disord, 2014. **6**(1): p. 25.
123. Song, G., et al., *Altered redox mitochondrial biology in the neurodegenerative disorder fragile X-tremor/ataxia syndrome: use of antioxidants in precision medicine.* Mol Med, 2016. **22**: p. 548-559.
124. Robin, G., et al., *Calcium dysregulation and Cdk5-ATM pathway involved in a mouse model of fragile X-associated tremor/ataxia syndrome.* Hum Mol Genet, 2017. **26**(14): p. 2649-2666.
125. Franke, P., et al., *Genotype-phenotype relationship in female carriers of the premutation and full mutation of FMR-1.* Psychiatry Res, 1998. **80**(2): p. 113-27.
126. Franke, P., et al., *Fragile-X carrier females: evidence for a distinct psychopathological phenotype?* Am J Med Genet, 1996. **64**(2): p. 334-9.
127. Sobesky, W.E., et al., *Molecular/clinical correlations in females with fragile X.* Am J Med Genet, 1996. **64**(2): p. 340-5.
128. Seritan, A.L., et al., *Ages of Onset of Mood and Anxiety Disorders in Fragile X Premutation Carriers.* Curr Psychiatry Rev, 2013. **9**(1): p. 65-71.
129. Rodriguez-Revenga, L., et al., *Evidence of depressive symptoms in fragile-X syndrome premutated females.* Psychiatr Genet, 2008. **18**(4): p. 153-5.
130. Bourgeois, J.A., et al., *A review of fragile X premutation disorders: expanding the psychiatric perspective.* J Clin Psychiatry, 2009. **70**(6): p. 852-62.
131. Bourgeois, J.A., et al., *Lifetime prevalence of mood and anxiety disorders in fragile X premutation carriers.* J Clin Psychiatry, 2011. **72**(2): p. 175-82.
132. Cordeiro, L., et al., *Anxiety disorders in fragile X premutation carriers: Preliminary characterization of probands and non-probands.* Intractable Rare Dis Res, 2015. **4**(3): p. 123-30.

133. Seritan, A.L., et al., *Psychiatric Disorders Associated with Fxtas.* Curr Psychiatry Rev, 2013. **9**(1): p. 59-64.
134. Bourgeois, J.A., et al., *Cognitive, anxiety and mood disorders in the fragile X-associated tremor/ataxia syndrome.* Gen Hosp Psychiatry, 2007. **29**(4): p. 349-56.
135. Chonchaiya, W., et al., *Increased prevalence of seizures in boys who were probands with the FMR1 premutation and co-morbid autism spectrum disorder.* Hum Genet, 2012. **131**(4): p. 581-9.
136. Conde, V., et al., *Abnormal GABA-mediated and cerebellar inhibition in women with the fragile X premutation.* J Neurophysiol, 2013. **109**(5): p. 1315-22.
137. Cao, Z., et al., *Enhanced asynchronous Ca(2+) oscillations associated with impaired glutamate transport in cortical astrocytes expressing Fmr1 gene premutation expansion.* J Biol Chem, 2013. **288**(19): p. 13831-41.
138. Pretto, D.I., et al., *Reduced excitatory amino acid transporter 1 and metabotropic glutamate receptor 5 expression in the cerebellum of fragile X mental retardation gene 1 premutation carriers with fragile X-associated tremor/ataxia syndrome.* Neurobiol Aging, 2014. **35**(5): p. 1189-97.
139. Hunter, J.E., J.K. Rohr, and S.L. Sherman, *Co-occurring diagnoses among FMR1 premutation allele carriers.* Clin Genet, 2010. **77**(4): p. 374-81.
140. Johnston, C., et al., *Neurobehavioral phenotype in carriers of the fragile X premutation.* Am J Med Genet, 2001. **103**(4): p. 314-9.
141. Kenna, H.A., et al., *High rates of comorbid depressive and anxiety disorders among women with premutation of the FMR1 gene.* Am J Med Genet B Neuropsychiatr Genet, 2013. **162B**(8): p. 872-8.
142. Ross, C.A. and S.J. Tabrizi, *Huntington's disease: from molecular pathogenesis to clinical treatment.* Lancet Neurol, 2011. **10**(1): p. 83-98.
143. Kraan, C.M., et al., *Neurobehavioural evidence for the involvement of the FMR1 gene in female carriers of fragile X syndrome.* Neurosci Biobehav Rev, 2013. **37**(3): p. 522-47.
144. Gossett, A., et al., *Psychiatric disorders among women with the fragile X premutation without children affected by fragile X syndrome.* Am J Med Genet B Neuropsychiatr Genet, 2016. **171**(8): p. 1139-1147.
145. Hagerman, R.J., et al., *Treatment of fragile X-associated tremor ataxia syndrome (FXTAS) and related neurological problems.* Clin Interv Aging, 2008. **3**(2): p. 251-62.
146. Gunal, D.I., et al., *New alternative agents in essential tremor therapy: double-blind placebo-controlled study of alprazolam and acetazolamide.* Neurol Sci, 2000. **21**(5): p. 315-7.
147. Rosselot, H. *Fragile X-Associated Tremor/Ataxia Syndrome (FXTAS): Consensus of the FXTAS Task Force and the Fragile X Clinical & Research Consortium*. Consensus of the FXTAS Task Force and the Fragile X Clinical & Research Consortium 2011 3-1-2018; Available from: https://fragilex.org/fxtas-consensus-document/.
148. Hagerman, P., *Fragile X-associated tremor/ataxia syndrome (FXTAS): pathology and mechanisms.* Acta Neuropathol, 2013. **126**(1): p. 1-19.
149. Fink, D.A., et al., *Fragile X Associated Primary Ovarian Insufficiency (FXPOI): Case Report and Literature Review.* Front Genet, 2018. **9**: p. 529.
150. Hoffman, G.E., et al., *Ovarian abnormalities in a mouse model of fragile X primary ovarian insufficiency.* J Histochem Cytochem, 2012. **60**(6): p. 439-56.

151. Wittenberger, M.D., et al., *The FMR1 premutation and reproduction.* Fertil Steril, 2007. **87**(3): p. 456-65.
152. Conway, G.S., et al., *Fragile X premutation screening in women with premature ovarian failure.* Hum Reprod, 1998. **13**(5): p. 1184-7.
153. Ennis, S., D. Ward, and A. Murray, *Nonlinear association between CGG repeat number and age of menopause in FMR1 premutation carriers.* Eur J Hum Genet, 2006. **14**(2): p. 253-5.
154. Gokden, M., J.T. Al-Hinti, and S.I. Harik, *Peripheral nervous system pathology in fragile X tremor/ataxia syndrome (FXTAS).* Neuropathology, 2009. **29**(3): p. 280-4.
155. Hunsaker, M.R., et al., *Widespread non-central nervous system organ pathology in fragile X premutation carriers with fragile X-associated tremor/ataxia syndrome and CGG knock-in mice.* Acta Neuropathol, 2011. **122**(4): p. 467-79.
156. Louis, E., et al., *Parkinsonism, dysautonomia, and intranuclear inclusions in a fragile X carrier: a clinical-pathological study.* Mov Disord, 2006. **21**(3): p. 420-5.
157. Iwahashi, C.K., et al., *Protein composition of the intranuclear inclusions of FXTAS.* Brain, 2006. **129**(Pt 1): p. 256-71.
158. Hagerman, P.J. and R.J. Hagerman, *The fragile-X premutation: a maturing perspective.* Am J Hum Genet, 2004. **74**(5): p. 805-16.
159. Cheng, W., et al., *C9ORF72 GGGGCC repeat-associated non-AUG translation is upregulated by stress through eIF2alpha phosphorylation.* Nat Commun, 2018. **9**(1): p. 51.
160. Green, K.M., et al., *RAN translation at C9orf72-associated repeat expansions is selectively enhanced by the integrated stress response.* Nat Commun, 2017. **8**(1): p. 2005.
161. Ladd, P.D., et al., *An antisense transcript spanning the CGG repeat region of FMR1 is upregulated in premutation carriers but silenced in full mutation individuals.* Hum Mol Genet, 2007. **16**(24): p. 3174-87.
162. Hukema, R.K., et al., *Induced expression of expanded CGG RNA causes mitochondrial dysfunction in vivo.* Cell Cycle, 2014. **13**(16): p. 2600-8.
163. Reddy, K., et al., *Determinants of R-loop formation at convergent bidirectionally transcribed trinucleotide repeats.* Nucleic Acids Res, 2011. **39**(5): p. 1749-62.
164. Loomis, E.W., et al., *Transcription-associated R-loop formation across the human FMR1 CGG-repeat region.* PLoS Genet, 2014. **10**(4): p. e1004294.
165. Hukema, R.K., et al., *Reversibility of neuropathology and motor deficits in an inducible mouse model for FXTAS.* Hum Mol Genet, 2015. **24**(17): p. 4948-57.
166. Hoem, G., et al., *CGG-repeat length threshold for FMR1 RNA pathogenesis in a cellular model for FXTAS.* Hum Mol Genet, 2011. **20**(11): p. 2161-70.
167. Arocena, D.G., et al., *Induction of inclusion formation and disruption of lamin A/C structure by premutation CGG-repeat RNA in human cultured neural cells.* Human Molecular Genetics, 2005. **14**(23): p. 3661-3671.
168. Tassone, F., C. Iwahashi, and P.J. Hagerman, *FMR1 RNA within the intranuclear inclusions of fragile X-associated tremor/ataxia syndrome (FXTAS).* RNA Biol, 2004. **1**(2): p. 103-5.

169. Sofola, O.A., et al., *RNA-binding proteins hnRNP A2/B1 and CUGBP1 suppress fragile X CGG premutation repeat-induced neurodegeneration in a Drosophila model of FXTAS.* Neuron, 2007. **55**(4): p. 565-71.
170. Jin, P., et al., *Pur α binds to rCGG repeats and modulates repeat-mediated neurodegeneration in a Drosophila model of Fragile X Tremor/Ataxia Syndrome.* Neuron, 2007. **55**: p. 556–564.
171. Aumiller, V., et al., *Drosophila Pur-alpha binds to trinucleotide-repeat containing cellular RNAs and translocates to the early oocyte.* RNA Biol, 2012. **9**(5): p. 633-43.
172. Sellier, C., et al., *Sequestration of DROSHA and DGCR8 by expanded CGG RNA repeats alters microRNA processing in fragile X-associated tremor/ataxia syndrome.* Cell Rep, 2013. **3**(3): p. 869-80.
173. Sellier, C., et al., *Sam68 sequestration and partial loss of function are associated with splicing alterations in FXTAS patients.* EMBO J, 2010. **29**(7): p. 1248-61.
174. Bekenstein, U. and H. Soreq, *Heterogeneous nuclear ribonucleoprotein A1 in health and neurodegenerative disease: from structural insights to post-transcriptional regulatory roles.* Mol Cell Neurosci, 2013. **56**: p. 436-46.
175. Jin, P., et al., *RNA-mediated neurodegeneration caused by the fragile X premutation rCGG repeats in Drosophila.* Neuron, 2003. **39**(5): p. 739-47.
176. Muslimov, I.A., et al., *Spatial code recognition in neuronal RNA targeting: role of RNA-hnRNP A2 interactions.* J Cell Biol, 2011. **194**(3): p. 441-57.
177. Timchenko, L.T., et al., *Identification of a (CUG)n triplet repeat RNA-binding protein and its expression in myotonic dystrophy.* Nucleic Acids Res, 1996. **24**(22): p. 4407-14.
178. Barreau, C., et al., *Mammalian CELF/Bruno-like RNA-binding proteins: molecular characteristics and biological functions.* Biochimie, 2006. **88**(5): p. 515-25.
179. Kuyumcu-Martinez, N.M., G.S. Wang, and T.A. Cooper, *Increased steady-state levels of CUGBP1 in myotonic dystrophy 1 are due to PKC-mediated hyperphosphorylation.* Mol Cell, 2007. **28**(1): p. 68-78.
180. He, F., et al., *TDP-43 suppresses CGG repeat-induced neurotoxicity through interactions with HnRNP A2/B1.* Hum Mol Genet, 2014. **23**(19): p. 5036-51.
181. Galloway, J.N., et al., *CGG repeats in RNA modulate expression of TDP-43 in mouse and fly models of fragile X tremor ataxia syndrome.* Hum Mol Genet, 2014. **23**(22): p. 5906-15.
182. Han, J., et al., *The Drosha-DGCR8 complex in primary microRNA processing.* Genes Dev, 2004. **18**(24): p. 3016-27.
183. Lee, Y., et al., *The nuclear RNase III Drosha initiates microRNA processing.* Nature, 2003. **425**(6956): p. 415-9.
184. Khalili, K., et al., *Puralpha is essential for postnatal brain development and developmentally coupled cellular proliferation as revealed by genetic inactivation in the mouse.* Mol Cell Biol, 2003. **23**(19): p. 6857-75.
185. Hokkanen, S., et al., *Lack of Pur-alpha alters postnatal brain development and causes megalencephaly.* Hum Mol Genet, 2012. **21**(3): p. 473-84.
186. Qurashi, A., et al., *Nuclear accumulation of stress response mRNAs contributes to the neurodegeneration caused by Fragile X premutation rCGG repeats.* PLoS Genet, 2011. **7**(6): p. e1002102.

187. Bond, A.T., et al., *Absence of Dbp2p alters both nonsense-mediated mRNA decay and rRNA processing.* Mol Cell Biol, 2001. **21**(21): p. 7366-79.
188. Ishizuka, A., M.C. Siomi, and H. Siomi, *A Drosophila fragile X protein interacts with components of RNAi and ribosomal proteins.* Genes Dev, 2002. **16**(19): p. 2497-508.
189. Lin, C., et al., *ATPase/helicase activities of p68 RNA helicase are required for pre-mRNA splicing but not for assembly of the spliceosome.* Mol Cell Biol, 2005. **25**(17): p. 7484-93.
190. Liu, Z.R., *p68 RNA helicase is an essential human splicing factor that acts at the U1 snRNA-5' splice site duplex.* Mol Cell Biol, 2002. **22**(15): p. 5443-50.
191. Wilson, B.J., et al., *The p68 and p72 DEAD box RNA helicases interact with HDAC1 and repress transcription in a promoter-specific manner.* BMC Molecular Biology, 2004. **5**(1): p. 11.
192. Bonapace, G., et al., *Intracellular FMRpolyG-Hsp70 complex in fibroblast cells from a patient affected by fragile X tremor ataxia syndrome.* Heliyon, 2019. **5**(6): p. e01954.
193. Sellier, C., et al., *Translation of Expanded CGG Repeats into FMRpolyG Is Pathogenic and May Contribute to Fragile X Tremor Ataxia Syndrome.* Neuron, 2017. **93**(2): p. 331-347.
194. Zu, T., et al., *Non-ATG-initiated translation directed by microsatellite expansions.* Proc Natl Acad Sci U S A, 2011. **108**(1): p. 260-5.
195. Zu, T., et al., *RAN proteins and RNA foci from antisense transcripts in C9ORF72 ALS and frontotemporal dementia.* Proc Natl Acad Sci U S A, 2013. **110**(51): p. E4968-77.
196. Mori, K., et al., *The C9orf72 GGGGCC repeat is translated into aggregating dipeptide-repeat proteins in FTLD/ALS.* Science, 2013. **339**(6125): p. 1335-8.
197. Ash, P.E., et al., *Unconventional translation of C9ORF72 GGGGCC expansion generates insoluble polypeptides specific to c9FTD/ALS.* Neuron, 2013. **77**(4): p. 639-46.
198. Kearse, M.G., et al., *CGG Repeat-Associated Non-AUG Translation Utilizes a Cap-Dependent Scanning Mechanism of Initiation to Produce Toxic Proteins.* Mol Cell, 2016. **62**(2): p. 314-322.
199. Krans, A., et al., *Neuropathology of RAN translation proteins in fragile X-associated tremor/ataxia syndrome.* Acta Neuropathol Commun, 2019. **7**(1): p. 152.
200. Krans, A., M.G. Kearse, and P.K. Todd, *Repeat-associated non-AUG translation from antisense CCG repeats in fragile X tremor/ataxia syndrome.* Ann Neurol, 2016. **80**(6): p. 871-881.
201. Abu-Baker, A., et al., *Involvement of the ubiquitin-proteasome pathway and molecular chaperones in oculopharyngeal muscular dystrophy.* Hum Mol Genet, 2003. **12**(20): p. 2609-23.
202. Albrecht, A.N., et al., *A molecular pathogenesis for transcription factor associated poly-alanine tract expansions.* Hum Mol Genet, 2004. **13**(20): p. 2351-9.
203. Oh, S.Y., et al., *RAN translation at CGG repeats induces ubiquitin proteasome system impairment in models of fragile X-associated tremor ataxia syndrome.* Hum Mol Genet, 2015. **24**(15): p. 4317-26.
204. Mizielinska, S., et al., *C9orf72 repeat expansions cause neurodegeneration in Drosophila through arginine-rich proteins.* Science, 2014. **345**(6201): p. 1192-1194.
205. Kwon, I., et al., *Poly-dipeptides encoded by the C9orf72 repeats bind nucleoli, impede RNA biogenesis, and kill cells.* Science, 2014. **345**(6201): p. 1139-45.

206. Lopez-Gonzalez, R., et al., *Poly(GR) in C9ORF72-Related ALS/FTD Compromises Mitochondrial Function and Increases Oxidative Stress and DNA Damage in iPSC-Derived Motor Neurons.* Neuron, 2016. **92**(2): p. 383-391.
207. Shi, K.Y., et al., *Toxic PRn poly-dipeptides encoded by the C9orf72 repeat expansion block nuclear import and export.* Proc Natl Acad Sci U S A, 2017. **114**(7): p. E1111-E1117.
208. Gupta, R., et al., *The Proline/Arginine Dipeptide from Hexanucleotide Repeat Expanded C9ORF72 Inhibits the Proteasome.* 2017. **4**(1): p. ENEURO.0249-16.2017.
209. Meloni, B.P., et al., *Poly-arginine and arginine-rich peptides are neuroprotective in stroke models.* J Cereb Blood Flow Metab, 2015. **35**(6): p. 993-1004.
210. Dehay, B. and A. Bertolotti, *Critical role of the proline-rich region in Huntingtin for aggregation and cytotoxicity in yeast.* J Biol Chem, 2006. **281**(47): p. 35608-15.
211. Siwach, P., et al., *Proline repeats, in cis- and trans-positions, confer protection against the toxicity of misfolded proteins in a mammalian cellular model.* Neurosci Res, 2011. **70**(4): p. 435-41.
212. Grima, J.C., et al., *Mutant Huntingtin Disrupts the Nuclear Pore Complex.* Neuron, 2017. **94**(1): p. 93-107 e6.
213. Zhang, K., et al., *The C9orf72 repeat expansion disrupts nucleocytoplasmic transport.* Nature, 2015. **525**(7567): p. 56-61.
214. Gasset-Rosa, F., et al., *Polyglutamine-Expanded Huntingtin Exacerbates Age-Related Disruption of Nuclear Integrity and Nucleocytoplasmic Transport.* Neuron, 2017. **94**(1): p. 48-57 e4.
215. Todd, Peter K., et al., *CGG Repeat-Associated Translation Mediates Neurodegeneration in Fragile X Tremor Ataxia Syndrome.* Neuron, 2013. **78**(3): p. 440-455.
216. Boeynaems, S., et al., *Phase Separation of C9orf72 Dipeptide Repeats Perturbs Stress Granule Dynamics.* Mol Cell, 2017. **65**(6): p. 1044-1055 e5.
217. Lee, K.H., et al., *C9orf72 Dipeptide Repeats Impair the Assembly, Dynamics, and Function of Membrane-Less Organelles.* Cell, 2016. **167**(3): p. 774-788 e17.
218. Huichalaf, C., et al., *Expansion of CUG RNA repeats causes stress and inhibition of translation in myotonic dystrophy 1 (DM1) cells.* FASEB J, 2010. **24**(10): p. 3706-19.
219. Dasti, A., et al., *RNA-centric approaches to study RNA-protein interactions in vitro and in silico.* Methods, 2019.
220. Krzyzosiak, W.J., et al., *Triplet repeat RNA structure and its role as pathogenic agent and therapeutic target.* Nucleic Acids Res, 2012. **40**(1): p. 11-26.
221. Kiliszek, A., et al., *Crystal structures of CGG RNA repeats with implications for fragile X-associated tremor ataxia syndrome.* Nucleic Acids Res, 2011. **39**: p. 7308–7315.
222. Cid-Samper, F., et al., *An Integrative Study of Protein-RNA Condensates Identifies Scaffolding RNAs and Reveals Players in Fragile X-Associated Tremor/Ataxia Syndrome.* Cell Rep, 2018. **25**(12): p. 3422-3434 e7.
223. Marchese, D., et al., *Discovering the 3' UTR-mediated regulation of alpha-synuclein.* Nucleic Acids Res, 2017. **45**(22): p. 12888-12903.
224. Cirillo, D., et al., *Quantitative predictions of protein interactions with long noncoding RNAs.* Nat Methods, 2016. **14**(1): p. 5-6.

225. Klus, P., et al., *Protein aggregation, structural disorder and RNA-binding ability: a new approach for physico-chemical and gene ontology classification of multiple datasets.* BMC Genomics, 2015. **16**: p. 1071.
226. Cirillo, D., et al., *Neurodegenerative diseases: quantitative predictions of protein-RNA interactions.* RNA, 2013. **19**(2): p. 129-40.
227. Foote, M., et al., *Fragile X-Associated Tremor/Ataxia Syndrome (FXTAS) Motor Dysfunction Modeled in Mice.* Cerebellum, 2016. **15**(5): p. 611-22.
228. Bontekoe, C.J., et al., *Instability of a (CGG)98 repeat in the Fmr1 promoter.* Hum Mol Genet, 2001. **10**(16): p. 1693-9.
229. Willemsen, R., et al., *The FMR1 CGG repeat mouse displays ubiquitin-positive intranuclear neuronal inclusions; implications for the cerebellar tremor/ataxia syndrome.* Hum Mol Genet, 2003. **12**(9): p. 949-59.
230. Brouwer, J.R., et al., *Elevated Fmr1 mRNA levels and reduced protein expression in a mouse model with an unmethylated Fragile X full mutation.* Exp Cell Res, 2007. **313**(2): p. 244-53.
231. Berman, R.F. and R. Willemsen, *Mouse models of fragile X-associated tremor ataxia.* J Investig Med, 2009. **57**(8): p. 837-41.
232. Hunsaker, M.R., et al., *Mouse models of the fragile x premutation and the fragile X associated tremor/ataxia syndrome.* Results Probl Cell Differ, 2012. **54**: p. 255-69.
233. Hunsaker, M.R., et al., *Progressive spatial processing deficits in a mouse model of the fragile X premutation.* Behav Neurosci, 2009. **123**(6): p. 1315-24.
234. Chen, Y., et al., *Murine hippocampal neurons expressing Fmr1 gene premutations show early developmental deficits and late degeneration.* Hum Mol Genet, 2010. **19**(1): p. 196-208.
235. Cunningham, C.L., et al., *Premutation CGG-repeat expansion of the Fmr1 gene impairs mouse neocortical development.* Hum Mol Genet, 2011. **20**(1): p. 64-79.
236. Drozd, M., et al., *Reduction of Fmr1 mRNA Levels Rescues Pathological Features in Cortical Neurons in a Model of FXTAS.* Mol Ther Nucleic Acids, 2019. **18**: p. 546-553.
237. Entezam, A., et al., *Regional FMRP deficits and large repeat expansions into the full mutation range in a new Fragile X premutation mouse model.* Gene, 2007. **395**(1-2): p. 125-34.
238. Fernandez, J.J., et al., *Gene expression profiles in the cerebellum of transgenic mice over expressing the human FMR1 gene with CGG repeats in the normal range.* Genet Mol Res, 2012. **11**(1): p. 467-83.
239. Peier, A.M. and D.L. Nelson, *Instability of a premutation-sized CGG repeat in FMR1 YAC transgenic mice.* Genomics, 2002. **80**(4): p. 423-32.
240. Peier, A.M., et al., *(Over)correction of FMR1 deficiency with YAC transgenics: behavioral and physical features.* Hum Mol Genet, 2000. **9**(8): p. 1145-59.
241. Spencer, C.M., et al., *Social behavior in Fmr1 knockout mice carrying a human FMR1 transgene.* Behav Neurosci, 2008. **122**(3): p. 710-5.
242. Castro, H., et al., *Selective rescue of heightened anxiety but not gait ataxia in a premutation 90CGG mouse model of Fragile X-associated tremor/ataxia syndrome.* Hum Mol Genet, 2017. **26**(11): p. 2133-2145.
243. Westergard, T., et al., *Cell-to-Cell Transmission of Dipeptide Repeat Proteins Linked to C9orf72-ALS/FTD.* Cell Rep, 2016. **17**(3): p. 645-652.

CHAPTER 2

2

Astroglial-targeted expression of the Fragile X CGG repeat premutation in mice yields RAN translation, motor deficits and possible evidence for cell-to-cell propagation of FXTAS pathology

H. Jürgen Wenzel[1], Karl D. Murray[2], Saif N. Haify[4], Michael R. Hunsaker[3], Jared J. Schwartzer[1], Kyoungmi Kim[6], Albert R. La Spada[7], Bryce L. Sopher[8], Paul J. Hagerman[5], Christopher Raske[5], Lies-Anne W.F.M. Severijnen[4], Rob Willemsen[4], Renate K. Hukema[4], Robert F. Berman[1*]

[1] Dept. of Neurological Surgery, University of California, Davis; Davis, CA, USA
[2] Dept. of Psychiatry and Behavioral Sciences, University of California, Davis; Davis, CA, USA
[3] Graduate Program in Neuroscience, Univ. of California, Davis; Davis, CA, USA
[4] Dept. of Clinical Genetics, Erasmus MC; Rotterdam, The Netherlands.
[5] Dept. of Biochemistry and Molecular Medicine, Univ. of California, Davis; Davis, CA, USA
[6] Division of Biostatistics, Dept. of Public Health Sciences, Univ. California Davis, Davis, CA USA
[7] Depts. of Neurology, Neurobiology, and Cell Biology, and the Duke Center for Neurodegeneration & Neurotherapeutics, Duke University School of Medicine, Durham, NC, USA
[8] Dept. of Neurology, University of Washington School of Medicine, Seattle, WA.

[*] Corresponding author: Robert F. Berman (rfberman@ucdavis.edu)

Acta Neuropathologica Communications 2019 Feb 26;7(1):27

Abstract

The fragile X premutation is a CGG trinucleotide repeat expansion between 55-200 repeats in the 5'-untranslated region of the *Fragile X mental retardation 1 (FMR1)* gene. Human carriers of the premutation allele are at risk of developing the late-onset neurodegenerative disorder, fragile X-associated tremor and ataxia syndrome (FXTAS). Characteristic neuropathology associated with FXTAS includes intranuclear inclusions in neurons and astroglia. Previous studies recapitulated these histopathological features in neurons in a knock-in mouse model, but without significant astroglial pathology. To determine the role of astroglia in FXTAS, we generated a transgenic mouse line (*Gfa2*-CGG99-eGFP) that selectively expresses a 99xCGG repeat expansion linked to an enhanced green fluorescent protein (eGFP) reporter in astroglia throughout the brain, including cerebellar Bergmann glia. Behaviorally these mice displayed impaired motor performance on the ladder-rung test, but paradoxically better performance on the rotarod. Immunocytochemical analysis revealed that CGG99-eGFP co-localized with GFAP and S-100ß, but not with NeuN, Iba1, or MBP, indicating that CGG99-eGFP expression is specific to astroglia. Ubiquitin-positive intranuclear inclusions were found in eGFP-expressing glia throughout the brain. In addition, intracytoplasmic ubiquitin-positive inclusions were found outside the nucleus in distal astrocyte processes. Intriguingly, intranuclear inclusions, in the absence of eGFP mRNA and eGFP fluorescence, were present in neurons of the hypothalamus and neocortex. Furthermore, intranuclear inclusions in both neurons and astrocytes displayed immunofluorescent labeling for the polyglycine peptide FMRpolyG, implicating FMRpolyG in the pathology found in *Gfa2*-CGG99 mice. Considered together, these results show that *Gfa2*-CGG99 expression in mice is sufficient to induce key features of FXTAS pathology, including formation of intranuclear inclusions, translation of FMRpolyG, and deficits in motor function.

Keywords: FXTAS, Fragile X premutation, Mouse Model, Neurodegeneration, Glia, RAN translation, FMRpolyG, Non-cell-autonomous, Electron microscopy of inclusions

Introduction

The fragile X premutation is defined as an expanded $(CGG)_n$ trinucleotide repeat in the 5'-untranslated region of the *FMR1* gene. Clinical and genetic studies of patients have indicated that carriers of the premutation allele, defined as a repeat length between 55 and 200 CGGs, are at risk of developing the late-onset neurodegenerative disorder, fragile X-associated tremor/ataxia syndrome (FXTAS) [1-3]. Elevated *FMR1* mRNA levels found in cells of premutation carriers support the concept of a "toxic" *mRNA* gain-of-function mechanism of pathophysiology in FXTAS [4], likely via sequestration of RNA-binding proteins by expanded CGG repeat-containing RNA [5]. Repeat-associated non-AUG translation (RAN) of a toxic poly-glycine-containing peptide, FMRpolyG, from the expanded-repeat mRNA may also contribute to FXTAS pathology [6, 7]. The principal clinical symptoms of FXTAS include progressive intention tremor and ataxia, peripheral neuropathy, neuropsychological involvement (anxiety, depression), and cognitive impairments and dementia at late stages of the disorder [4, 8, 9]. Radiologic changes observed by MRI include increased T2 signal (hyperintensities) in cerebral white matter and in the middle cerebellar peduncle (the "MCP sign"), as well as global brain atrophy [10]. Levels of *FMR1* mRNA are elevated and levels of FMRP are slightly decreased in FXTAS. The neuropathological hallmark of FXTAS is the presence of spherical eosinophilic intranuclear inclusions in neurons and astroglia throughout the brain that are immunoreactive for ubiquitin [11-13].

The CGG KI mouse model of FXTAS shows similar neurobehavioral features that appear to be similar to those in FXTAS [14]. These include gait ataxia and visuomotor deficits in the ladder-rung [15] and rotarod tests [16], anxiety in the open field [17] and cognitive impairment [18, 19]. They also show ubiquitin-positive spherical inclusions in neurons and astrocytes similar to those found in FXTAS brains [20, 21]. The inclusions are found throughout the brain in all neocortical regions, hippocampus, hypothalamus, brain stem nuclei (*e.g.,* reticular formation, inferior olivary and dentate nuclei) and in Bergmann glia in cerebellum [21, 22]. The topographical distribution and frequency of intranuclear inclusions increase with age and length of the CGG repeat segment, and also vary between brain regions [21, 22]. Pathology in the CGG KI mouse model differs from FXTAS pathology by the absence of tremors and the relatively few numbers of astrocytes with intranuclear inclusions [23]. Ubiquitin-positive inclusions were never observed in neurons or astroglia of WT mice in any brain region at any age [24].

To determine if expression of a CGG trinucleotide repeat expansion in astroglia is sufficient to induce pathology in astroglia, and to characterize the role of astroglia in FXTAS, we created a transgenic mouse line (*Gfa2*-CGG99-eGFP) that expresses a 99xCGG repeat expansion in astrocytes throughout the brain and in Bergmann glia in the cerebellum.

Expression is driven by an astroglia-specific *Gfa2* promoter fused to an eGFP reporter gene. In these mice, immunocytochemical analysis of eGFP expression patterns revealed that CGG99-eGFP expression co-localized with astroglia markers, but not with neuronal, microglia, or oligodendroglia markers, indicating that CGG99-eGFP expression was specific for astroglia and Bergmann glia. Double-immunostaining for ubiquitin revealed the presence of intranuclear inclusions in eGFP-positive glia throughout the brain, as well as ubiquitin-positive inclusions in the cytoplasm of astrocyte processes. Surprisingly, we also observed intranuclear inclusions in NeuN-positive neurons of the hypothalamus and neocortex, though these cells did not express the CGG99-eGFP transcript. The presence of cytoplasmic inclusions in astrocytes, ectopic inclusions and inclusions in neurons suggests a spread of pathology from astrocytes to neurons by as yet unknown mechanisms. Both glial and neuronal inclusions stained positive for the RAN translation product FMRpolyG [25, 26]. These results indicate that an expanded 99xCGG repeat in astroglia is sufficient to induce formation of ubiquitin- and FMRpolyG-positive intranuclear inclusions, key features of FXTAS pathology, and that the *Gfa2*-CGG99-eGFP mouse will be a valuable model to delineate neuron-astroglia interactions that contribute to FXTAS disease pathogenesis.

Materials and Methods

Generation of *Gfa2*-CGG99-eGFP and *Gfa2*-CGG11-eGFP mice

Transgenic mice on a C57BL/6j background were generated with an expanded CGG99 trinucleotide repeat segment (*Gfa2*-CGG99-eGFP) or a typical mouse-sized CGG11 (*Gfa2*-CGG11-eGFP) repeat sequence. For simplicity, the *Gfa*2-CGG99-eGFP mice are referred to as *Gfa2*-CGG99 and the *Gfa2*-CGG11-eGFP mice as *Gfa2*-CGG11 control mice, respectively. Wildtype (WT) non-transgenic littermates were generated from breeding the *Gfa2*-CGG99 transgenic mice with WT C57BL/6j mice. These WT littermate mice were used as controls for behavioral studies to avoid litter effects and because sufficient numbers of the *Gfa2*-CGG11 transgenic mice were not available. Genotype was verified in all mice by PCR from tail-snips. A diagram of the DNA constructs and the nucleotide sequences used for pronuclear injection are shown in **Figures 1A and 1B**, respectively. Expression vector maps are included in **Figure S1**. Expression was restricted to astrocytes and Bergmann glia using the astrocyte-specific Gfa2 promoter, with the enhanced green fluorescent protein (eGFP) reporter used to identify cells expressing the *Gfa2*-CGG99-eGFP or the normal length *Gfa2*-CGG11 transgene. The *eGFP* sequence was derived from the pBR-eGFP vector. Expression of the CGG99 and CGG11 trinucleotide repeat expansions and eGFP reporter are driven by ~ 2-kb of the human *Gfa2* promoter, which drives astrocyte-specific expression in transgenic mice [27]. cDNA derived from patient and control peripheral blood lymphocytes was used to isolate ~ 226 bp of *FMR1* 5'-UTR sequence as well as the CGG repeats, which were cloned into Blp I and Pst I restriction sites. The construct also

contains a chimeric intron upstream of eGFP to enhance expression levels. *Gfa2*-CGG11-eGFP and *Gfa2*-CGG99-eGFP clones (*i.e.,* clones 3 and 11, respectively) were digested with ApaLI and SnaBI (10 ug each) and the respective 4.8 and 5.1 kb restriction fragments were purified away from the 0.9 kb vector backbone on an agarose gel. The purified *Gfa2*-CGG11-eGFP (86 ng/ul & 1.8 260/280 ratio) and Gfa2-CGG99-eGFP (62 ng/ul & 1.8 260/280 ratio) DNA fragments were then microinjected into pronuclei of oocytes from C57BL/6J x C3H/HeJ F1 hybrids at the University of Washington Microinjection Service Laboratory. Six of the 26 *Gfa2*-CGG11-eGFP mice screened (LS-2997, LS-3006, LS-3009, LS-3011, LS-3025, LS-3030 were found to be positive for the transgene by PCR. Six of the 27 *Gfa2*-CGG99-EGFP mice screened (LS-3046, LS-3049, LS-3060, LS-3061, LS-3065, LS-3072) were also found to be positive for the transgene by PCR. The *Gfa2*-CGG11 and *Gfa2*-CGG99 mouse lines used in these experiments were selected based on matched, high expression levels by TaqMan real time PCR using primers and probes to the eGFP gene as follows: forward, 5'- GTC CGC CCT GAG CAA AGA -3'; reverse, 5'- TCC AGC AGG ACC ATG TGA TC -3'; Fam-probe, 5'- CCC AAC GAG AAG CG -3'.

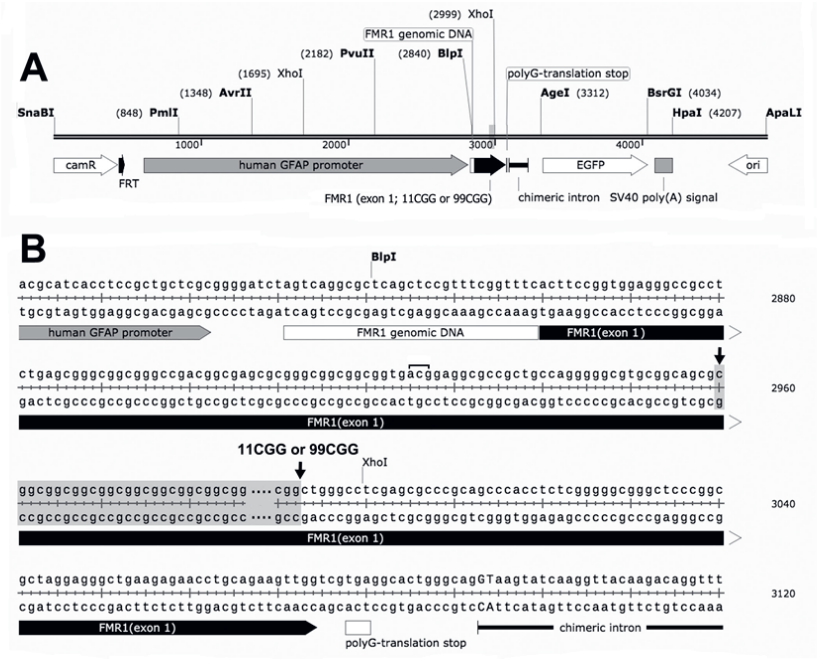

Figure 1 | Schematic representation of the transgene. (A) Diagram of a DNA fragment used for pronuclear injection with either an 11xCGG or 99xCGG trinucleotide repeat expansion on exon 1. **(B)** Nucleotide sequence of DNA construct used to make the *Gfa2*-CGG11-eGFP or *Gfa2*-CGG99-eGFP transgenic mice. The sequence contained either an 11xCGG or 99xCGG trinucleotide repeat sequence for the two transgenic mouse lines that was located between the two arrows in B. The bracketed acg sequence upstream of the repeat sequence shows the alternative translation start site supporting repeat-associated non-AUG (RAN) translation as described in [7].

Eight male *Gfa2*-CGG99 mice and five male *Gfa2*-CGG11 control mice between 4-16 months old were used for histological and molecular studies. In addition, brains of two male CGG_n knock-in (CGG128 and CGG159) and 2 WT mice 16 months of age were immunostained for ubiquitin-positive intranuclear inclusions in neurons and astroglia for comparison with *Gfa2*-CGG99 mice and *Gfa2*-CGG11 mice, as previously described [21]. Transgenic and WT mice were housed under conditions of constant temperature and a 12 / 12 h light-dark cycle, and with food and water *ad libitum*. These experiments followed the "Principles of laboratory animal care" (NIH publication No. 86-23, revised 1985), and were approved by the UC Davis Institutional Animal Care and Use Committee.

Genotyping

DNA was extracted from mouse tails by incubating with 10 mg/ml Proteinase K (Roche Diagnostics) in 300 µl lysis buffer containing 50 mM Tris-HCl, pH 7.5, 10 mM EDTA, 150 mM NaCl, 1% SDS overnight at 55oC. One hundred µl saturated NaCl was then added and the suspension was centrifuged. One volume of 100% ethanol was added, gently mixed, and the DNA was pelleted by centrifugation and the supernatant discarded. The DNA was washed and centrifuged in 500 µl 70% ethanol. The DNA was then dissolved in 100 µl milliQ-H20. CGG repeat lengths were determined by PCR using the Expanded High Fidelity Plus PCR System (Roche Diagnostics). Briefly, approximately 500-700 ng of DNA was added to 50 µl of PCR mixture containing 2.0 µM of each primer, 250 µM of each dNTP (Invitrogen), 2% DMSO (Sigma), 2.5 M Betaine (Sigma), 5 U Expand HF buffer with Mg (7.5 µM). For the CGG KI mice the forward primer was 5'-GCTCAGCTCCGTTTCGGTTTCACTTCCGGT-3' and the reverse primer was 5'-AGCCCCGCACTTCCACCACCAGCTCCTCCA-3'. For the Gfa2-CGG99 mice the forward primer was 5'- GTC CGC CCT GAG CAA AGA -3'; and the reverse primer was 5'- TCC AGC AGG ACC ATG TGA TC -3'. PCR steps were 10 min denaturation at 95oC, followed by 34 cycles of 1 min denaturation at 95°C, annealing for 1 min at 65oC, and elongation for 5 min at 75oC to end each cycle. PCR ended with a final elongation step of 10 min at 75oC. DNA CGG band sizes were determined by running DNA samples on a 2.5% agarose gel and staining DNA with ethidium bromide.

Behavioral testing

The behavioral tests used in the present study for *Gfa2*-CGG99-EGFP mice were selected to examine similar neurobehavioral deficits in FXTAS, including anxiety in the elevated plus-maze, ataxia and motor deficits in the ladder rung test, rotarod and TreadScan apparatus, and cognitive loss using contextual fear conditioning [14].

Mice

Fifteen adult wildtype (WT) and 15 *Gfa2*-CGG99 adult male mice were used for behavioral testing. The WT and *Gfa2*-CGG99 mice were littermates derived from 12 litters with no more than 3 mice taken from any litter. The mice were between 21-24 weeks of age at the

start of behavioral testing. WT littermates were used as controls as to avoid litter effects in behavioral testing, and because sufficient numbers of *Gfa2*-CGG11 transgenic mice were not available for the behavioral studies. Mice were housed individually in a climate controlled vivarium under 12:12 hr light dark cycles with food and water available *ad libitum*. Animals were tested in the order presented below.

Open-Field Locomotor Activity

Locomotor activity was measured using an automated open-field activity arena (TruScan, Coulbourn Instr., Whitehall, PA). The apparatus (27.5 x 27.5 x 37.5 cm) detects movement by recording infrared beam brakes. The number of center entries, total time in the center and periphery of the arena, and frequency of rearing were automatically scored during a 90-minute period.

Elevated Plus Maze

The maze consisted of two open arms (30 x 5 x 0.25 cm) and two closed arms (30 x 5 x 6 cm) elevated 60 cm above the floor. Mice were placed in the center of an elevated plus-maze and were allowed to freely explore the apparatus for 5 minutes while recorded by a video-tracking system (SMART, San Diego Instruments, San Diego, CA). Number of entries into open and closed arms, latency to first enter, and total time spent in open and closed arms were compared between WT and *Gfa2*-CGG99 mice.

Rotarod

Motor coordination and balance were evaluated using a Rotamex-5 rotarod with photocell detection (Columbus Instr., Columbus, OH). Prior to testing mice were given an initial training session where they were acclimated to the apparatus. Training consisted of a 120 sec trial in which the rod rotated at a constant speed of 4 RPM. Mice that fell were immediately replaced and allowed to complete the training session. Twenty-four hr later WT and *Gfa2*-CGG99 mice were placed on the rotarod at an initial speed of 4 RPM that accelerated by 1.0 RPM every 10 seconds. A trial was terminated when a mouse fell from the rod at which time the speed and latency to fall were recorded. The number of flips (*i.e.,* 360 deg rotations while grasping the rod) was also recorded. Each mouse was tested three times per day for three consecutive days. Mean performance time per day was defined as the average time the mouse remained on the rotarod across trials.

Gait Analysis

Gait abnormalities in *Gfa2*-CGG99 mice were analyzed and compared to WT mice using a motor-driven transparent treadmill affixed with high-speed digital video camera and computer-assisted software (TreadScan, CleverSys, Reston,VA). To ensure that all mice were walking, and not galloping, the treadmill speed was adjusted for each mouse but never exceeded 20 cm/s. When the mouse reached a steady gate, video of the underside

was recorded and analyzed by the system's software that identified each paw individually and calculated gait variables. Variables included stride time, defined as the time between two initial paw contacts of the same paw, stance time, the period of time the paw is in contact with the treadmill, and swing time, the portion of the stride in which the paw is not in contact with the treadmill.

Ladder Rung Task

The ladder rung apparatus tested visuomotor coordination by measuring the number of foot slips made while traversing a horizontal ladder [15]. The apparatus consisted of two 28cm tall × 65cm long black walls separated by 10 cm. The floor was elevated 10 cm from the bottom of the walls and had 43 parallel 1 mm diameter bars separated by 1.5 cm. A video camera positioned at one end of the apparatus recorded the full length of the beam floor. This allowed the experimenter to score whether the mouse's limbs extended below the beam floor as well as allowed the experimenter to observe the general posture of the mouse above the beam floor. All behavior was captured using a behavioral tracking system (SMART, San Diego Instruments, San Diego, CA). Mice were placed in the apparatus and allowed to freely explore the apparatus for 2 min. Mice typically explored the apparatus by walking the length of the apparatus, looking over the edge, and returning to the start position. The number of times a foot slipped through the beam floor was recorded and used as the dependent measure. Video recordings were later independently scored by two experimenters blinded to the genotype of the mice (intraclass correlation coefficient = 0.88, $p<0.002$).

Fear conditioning

Mice were trained in a contextual fear conditioning apparatus (Med Associates Inc., Georgia, VT). Mice underwent an initial training period consisting of 2 trials separated by a 2 minute inter-trial interval. Each trial consisted of the presence of 80dB white noise (conditioned stimulus, CS) for 30 seconds which co-terminated with a 0.5mA footshock (unconditioned stimulus, UCS) during the last 2 seconds. The testing for contextual and cued fear conditioning occurred 24 h later. For contextual conditioning, the mice were returned to the training chamber in the absence of the CS and UCS and measured for freezing behavior during a five-minute period. For cued fear conditioning, mice were placed in an altered context chamber modified by new floor and side inserts. Mice were measured for freezing during an initial 3-minute period and during a 3 min presentation of the CS. Freezing was defined as the cessation of movement other than respiration for ≥750 milliseconds.

Light microscopy/Electron microscopy/Immunocytochemistry

General tissue preparation

Histological procedures were previously described in detail [21]. In brief, mice were anesthetized with sodium pentobarbital (100 mg/kg, IP injection), then perfused with isotonic saline followed by a solution of 4% buffered paraformaldehyde (PFA), and post-fixed in the same solution for 1 hour at 4oC. The brains were cryoprotected in buffered 10% sucrose for 1 hour, followed by buffered 30% sucrose for 24 hours at 4oC, then rapidly frozen on dry ice. Thirty µm frozen sagittal sections were cut on a sliding microtome, and collected into a series of every fifth section in 30% sucrose. Single sets of sections were selected for further processing that included: cresyl violet and/or H&E staining for general histological evaluation, electron microscopy to analyze the ultrastructure of intranuclear inclusions in glia and neurons, immunocytochemistry/immunofluorescence for neuronal and glial cell markers, including ubiquitin staining used to visualize intranuclear inclusions. These ubiquitin-positive inclusions are the hallmark histopathology in FXTAS patients and are also found in astrocytes and neurons in CGG KI mice [11, 12, 22].

Immunocytochemistry

Immunocytochemical and immunofluorescence techniques were used to visualize the occurrence and distribution of intranuclear inclusions, specifically in brain astroglia and cerebellar Bergmann glia of *Gfa2*-CGG99, *Gfa2*-CGG11 control and WT mice. Subsets of alternate sections were processed for immunocytochemistry using a modification of the avidin-biotin complex (ABC)-peroxidase technique [28] as previously described [21]. Briefly, free-floating sections were rinsed in PB (pH 7.4) and pretreated with 0.1% sodium borohydride for antigen retrieval. Endogenous peroxidases were inactivated by treatment with 0.5-2% H2O2. Sections were then treated with 3% goat, horse and/or swine serum (Sigma, St. Louis, MO; DAKO, Inc., Carpinteria, CA) and 0.3% Triton X (TX) in 0.01 M PB, 0.15M NaCl, pH 7.4 (PBS) for 1 hour to reduce nonspecific staining. Following rinses in PBS, sections were incubated for 48-72 hours at 4o C in the primary antibodies: mouse monoclonal anti-glial fibrillary acidic protein (GFAP), (DAKO, Inc.), 1:2000 (1:750 for immunofluorescence (IF); rabbit polyclonal anti-S100β (Abcam, Inc., Cambridge, MA), 1:1000; mouse monoclonal anti-myelin basic protein (MBP), (Chemicon International, Inc., Temecula, CA), 1:500; mouse monoclonal anti-MAP2 (Sigma), 1:2000 (1:1000 for IF); rabbit polyclonal anti-Iba1 (ionized calcium binding adaptor molecule 1; Wako Chemicals USA, Inc., Richmond, VA), 1:2000 (1:1000 for IF); mouse-monoclonal anti-Kv2.1 (kindly provided by Dr. J.S. Trimmer; UC Davis), 1:500 for IF; rabbit polyclonal anti-eGFP (Invitrogen, A11122: 1:1000) and rabbit polyclonal antibody against ubiquitin (DAKO, Inc.), 1:2000, (1:1000 for IF) in PBS containing 1% goat, horse or swine serum, 2% BSA and 0.3% TX. Following rinses in PBS, sections were incubated in biotinylated goat or swine anti-rabbit IgG (DAKO, Inc.; Vector Laboratories, Burlingame, CA), diluted 1:500 for 24 hours at 4oC. After rinses

in PBS, sections were incubated in ABC (Elite ABC Kit, Vector Laboratories), diluted 1:500 in 2% BSA, 0.3% TX and PBS for 24 hours at 4oC. After rinses in PB followed by Tris-HCl buffers (pH 7.4; 7.6), sections were incubated in 0.025% 3,3'-diaminobenzidine (DAB, Sigma) with 0.003% H2O2 in TB (pH7.6). The incubation was stopped by rinses in TB and PB. For double-immunostaining (*e.g.,* GFAP/ubiquitin-colocalization) differently-colored chromogens were used (DAB; Vector SG Substrate Kits, Vector Laboratories). Specificity of the immunostaining was evaluated by omitting primary antibodies from the regular staining. Sections were mounted on slides, dehydrated, cleared, and cover-slipped with Permount.

Immunofluorescence staining

For single and multiplex immunofluorescent labeling of ubiquitin and neuronal/glial cell markers, frozen sections were transferred into buffered 30% and/or 10% sucrose, then rinsed in 0.1M PB and treated with 0.1% sodium borohydride for 15 min. Thereafter, sections were rinsed again with 0.1M PB and then permeabilized with 0.5% H_2O2 in 0.1M PB for 15 min followed by rinses in 0.1M PB and 0.01M PBS. Free-floating sections were treated with 10% goat serum in 0.01M PBS containing 0.3% TX-100 (vehicle) for 1 hr and then incubated overnight at 4°C in vehicle containing different combinations of mouse monoclonal/rabbit polyclonal antibodies of different IgG isotypes (see above). After rinses in 0.01M PBS and 10% goat serum (vehicle), sections were incubated in isotype-specific Alexa-conjugated secondary antibodies (1:2000): Alexa 568- and/or 488-labeled goat anti-rabbit IgG and/or Alexa 488 and/or 568-labeled goat anti-mouse IgG (Invitrogen, Carlsbad, CA) for 1-2 hrs as described previously [29]. Following rinses in vehicle, sections were mounted on gelatin-coated slides and cover-slipped with mounting medium containing DAPI (4', 6-diamidino-2-phenyindole di-lactate) for nuclear staining (Vectashield "Hard Set", Vector Laboratories).

Repeat-associated non-ATG (*i.e.,* RAN translation) translation of a novel potentially toxic peptide, FMRpolyG, was recently described in the brains of CGG KI mice [7]. Therefore, we carried out immunostaining for FMRpolyG in order to determine whether this peptide was also present in the inclusions in the *Gfa2*-CGG99 mice. Whole *Gfa2*-CGG99 and WT mouse brains were sectioned sagitally and the hemispheres were fixed overnight in 4% paraformaldehyde and embedded in paraffin according to standard protocols. Sections (6µm) were cut on a rotary microtome and deparaffinized, followed by antigen retrieval using microwave treatment in 0.01M sodium citrate. Endogenous peroxidase activity was blocked and immunostaining was performed overnight at 4°C using mouse anti-GFP (Roche 1814460; 1:1000), rabbit anti-ubiquitin (Dako Z0458; 1:250), or mouse-anti FMRpolyG (8FM) [25]; 1:10) antibodies. Antigen-antibody complexes were visualized by incubation with DAB substrate (Dako) after incubation with Brightvision poly-HRP-

linker (Immunologic). Slides were counterstained with haematoxylin and mounted with Entellan.

Multiplex immunofluorescence staining for FMRpolyG, ubiquitin, GFAP and NeuN were carried out in separate brain sections. Sections were blocked for autofluorescence with Sudan Black in 70% ethanol. Primary antibodies included rabbit-anti ubiquitin (DAKO Z0458; 1:50), mouse-anti ubiquitin (Cytoskeleton AUB01-S; 1:200), mouse-anti FMRpolyG (1:10) [25], rabbit anti-GFAP (Sigma G9269; 1:200), and mouse anti-Map2 (Roche, 1:400). Secondary antibodies included anti-rabbit Fab Alexa 488 (Life technologies A11070; 1:100) and anti-mouse Cy3 (Jackson Immuno research 715-165-150; 1:100). Nuclei were visualized with Hoechst. Analysis was done with a Leica confocal microscope and Leica Application Suite Advanced Fluorescence (LAS AF) software (Leica Microsystems, Buffalo Grove, IL).

Electron microscopy

Frozen 30µm brain sections were collected from CGG KI and *Gfa2*-CGG99 transgenic mice perfused with 4% PB-buffered PFA, post-fixed for 1hour and stored in 30% sucrose at 800C. Sets of sections were thawed and postfixed with Karnovsky fixation solution for 1hr. The sections were then postfixed with 1% buffered osmium tetroxide for 1 hour, then thoroughly rinsed with PB and dehydrated in a series of ethanol solutions and flat embedded in a mixture of Epon and Araldite between two aclar sheets for 24 hours at 70^{o}C as previously described [30]. Serial ultrathin sections were collected on TEM grids, and stained with uranyl acetate and lead citrate. Sections were then examined in a Philips 120 electron microscope. Electron microscopic images were acquired digitally using a 2k x 2k high resolution CCD camera (Gatan, Pleasanton, CA), and post-processed using Photoshop software.

Cell identification and evaluation of intranuclear inclusions

The sections were analyzed using a Nikon ECLIPSE E600 microscope with epifluorescence attachment and digital camera. Images were converted to a file format for processing as an Adobe Photoshop document. Images were analyzed to verify the presence of ubiquitin-positive intranuclear inclusions in different cell types identified with various neuronal and glial cell markers in brains of *Gfa2*-CGG99, *Gfa2*-CGG11 and WT mice. Cresyl violet and/or H&E-stained sets of brain sections from transgenic and WT mice at different ages were used for comparison and evaluation of gross anatomical differences. The different cell types in the brain were determined based on standard morphological criteria using Nissl cell staining and neuronal and glial cell markers as described previously [11, 21].

Neurons were identified by their size, large round nuclei, single or multiple nucleoli, and their abundant cytoplasm, as well as by using molecular neuronal markers (*e.g.,* NeuN, Kv2.1 channel protein). These descriptions were confirmed using electron microscopy.

Astroglia were identified by their round/ovoid nuclei with light euchromatin, and absence of nucleoli and cytoplasm. In addition, GFAP- and S100β-immunocytochemistry and/or immunofluorescence were used to identify subpopulations of astroglia based on their differing immunoreactivities (i.e, protoplasmic and/or fibrous astroglia) in different brain regions. These descriptions were confirmed using electron microscopy.

Oligodendrocytes (MBP-immunopositive cells) were identified based on their typical appearance with small, round, hyperchromatic nuclei surrounded by thin somatic cytoplasm, and their localization to white and grey matter.

Microglia were identified primarily on cellular morphology obtained from Iba1 immunostaining which displayed small cell bodies with a round nucleus and fine, ramified processes that are characteristic of resting microglia, and were clearly distinguishable from activated (but non-phagocytic) microglia and phagocytotic cells (*i.e.,* brain macrophages). For all cell types, immunocytochemical staining for ubiquitin was used to specifically label intranuclear inclusions in combination with cell-specific markers to identify the cell type (*i.e.,* neuronal and/or non-neuronal cells). Finally, all cell and inclusion types were determined and confirmed based on their ultrastructural appearance and characteristic features using electron microscopy.

Laser Capture Microdissection (LCM)

To evaluate the cellular specificity of *Gfa2*-CGG99-eGFP expression, single cell laser capture microdissection (LCM) was performed on ubiquitin-immunolabeled cells. *Gfa2*-(CGG99)-eGFP, CGG knock-in (KI) and WT mice were euthanized by lethal overdose with sodium pentobarbital after which their brains were rapidly removed and immediately frozen in OCT compound (Ted Pella Inc., Redding, CA). Coronal sections were cut at 12 µm on a cryostat (Leica Microsystems Inc., Buffalo Grove, Il). Sections were direct-mounted onto MMI Membrane Slides (Molecular Machines & Industries AG, Switzerland) and dried for 10 minutes at room temperature. Sections were then rinsed briefly in water, fixed in 70% ethanol for 1 minute, and incubated in rabbit polyclonal antibody against ubiquitin (DAKO, Inc.), 1:100 in 0.1M PB with 5% goat serum for 1 hour at room temperature. After 3 brief washes in 0.1M PB, sections were incubated in Alexa 488-labeled goat anti-rabbit secondary IgG containing 5% goat serum for 1 hour at room temperature. Finally, sections were rinsed 3x briefly in 0.1M PB, counterstained with DAPI in 0.1M PB for 1 minute and dehydrated through a descending series of alcohols. After complete drying, slides were either directly processed for LCM or stored at -80°C.

LCM was performed on coronal sections using a MMI CellCut Laser Capture Microscope (Molecular Machines & Industries AG, Switzerland). Individual neurons were captured onto isolation caps of specifically designed centrifuge tubes (MMI) and maintained frozen at -80ºC until RNA purification. Approximately 100-200 individual neurons containing ubiquitin-positive inclusions, but negative for eGFP histofluorescence, were captured from 18 tissue sections from the ventromedial hypothalamus and combined into a single PCR tube. In addition, astrocytes expressing eGFP fluorescence and bearing ubiquitin-positive inclusions were laser-captured from 10 neocortical tissue samples from *Gfa2*-CGG99-eGFP mice, combined and used as an eGFP-positive control. For comparison 100-200 cells from the amygdala of a CGG KI mouse with a CGG168 repeat expansion but no eGFP were isolated and combined as a negative control.

RNA isolation and amplification

Total RNA was isolated from LCM samples using a Qiagen RNeasy micro kit (Qiagen, Germantown, MD) according to manufacturer's recommendations. RNA quantity and quality was estimated using a NanoDrop spectrophotometer (ThermoFisher Scientific, Waltham, MA) and Agilent Bioanalyzer (Agilent Techologies Inc, Santa Clara, CA). RNA from each sample was subjected to linear amplification using Nugen Inc. SPIA technology (Nugen Tehnologies Inc., San Carlos, CA). The quantity and quality of resulting amplified cDNA was assessed using a NanoDrop and Bioanalyzer.

Semi-Quantitative Real-Time PCR

Real-time PCR was performed using an iCycler (Bio-Rad) to measure incorporation of the fluorescent dye SYBR Green I. For each reaction, a master mix of the following was made: 1× PCR buffer (QIAGEN), 400 mM dNTP, 0.5 mM forward (5'-AGTGGAGAGGGTGAAGGTGA) and reverse (5'-GGTAAAAGGACAGGGCCATC) eGFP primers (Operon), 0.01× SYBR Green I (Invitrogen), 1.5 mM MgCl2, 10 nM FITC (Bio-Rad), and 1 U of TaqDNA polymerase (QIAGEN). All PCRs were optimal for the following cycle conditions, 94°C (15 s), 60°C (30 s), and 72°C (30 s), and were run for approximately 40 cycles. After the PCR, a melting-curve analysis was performed to confirm the specificity of the PCR. In addition, samples of the PCRs were subjected to electrophoresis to verify product size and specificity. The relative quantification of RNA targets was performed as follows: The threshold cycle (Ct) at which a gene of interest first rose above background was determined and subtracted from that of the housekeeping gene, β-actin, the PCR for which was performed in a separate reaction tube. This was termed ΔCt. The ΔCt for each reaction was plotted as 2−ΔCt. Therefore, all values are for RNA expression normalized to β-actin mRNA.

Statistical analysis

Behavioral data were analyzed using R 2.14.0 language and environment. Data for each variable were examined for normality using the Shapiro-Wilk test and Kolmogorovo-

Smirnov test. Normally distributed data were analyzed by Analysis of Covariance (ANCOVA) with body weight as a covariate. If the assumption of normality of distribution was violated, then group comparisons were carried out using nonparametric rank-based ANCOVA with body weight as a covariate. The minimum levels for statistical significance set at $p<0.05$ for all statistical analyses. Data in figures are means ± standard error of the mean (SEM). Detailed statistical results for behavioral experiments are provided in **Figure S2**.

Results

Gfa2-CGG99 transgenic mice exhibit neurological and systemic disease phenotypes

Body weight

At 6 months of age when behavioral testing began *Gfa2*-CGG99 mice had significantly lower body weights (31.1 ± 1.3 g) compared to WT (39.5 ± 1.3 g), and this difference remained significant at 7 and 8 months of age ($p<0.01$) (**Fig. S2**). Body weight was therefore used as a covariate in statistical analyses. Body length did not differ between *Gfa2*-CGG99 (93.6 ± 0.6 mm) and WT mice (94.9 ± 0.5 mm) at the start of behavioral testing.

Rotarod

As shown in **Figure 2**, *Gfa2*-CGG99 mice stayed on the rotarod significantly longer (*e.g.,* A. Time to Fall) than WT mice on days 2, 3, 4, 6 & 9, but not on trial 1. A similar analysis showed that Speed to Fall (**Fig. 2B**) was significantly longer for *Gfa2* compared to WT on trials 2, 3, 4, & 9 ($p<0.05$). Numbers in parenthesis in **Figure 2A** show that *Gfa2*-CGG99 mice flipped (*i.e.,* clinging to the rotarod cylinder through complete 360 deg rotations) on 8 of 9 trials compared to only 3 of 9 trials for WT ($p<0.05$). Eleven of 15 *Gfa2* mice showed one or more episodes of flipping compared to 2 of 15 WT mice ($p<0.01$).

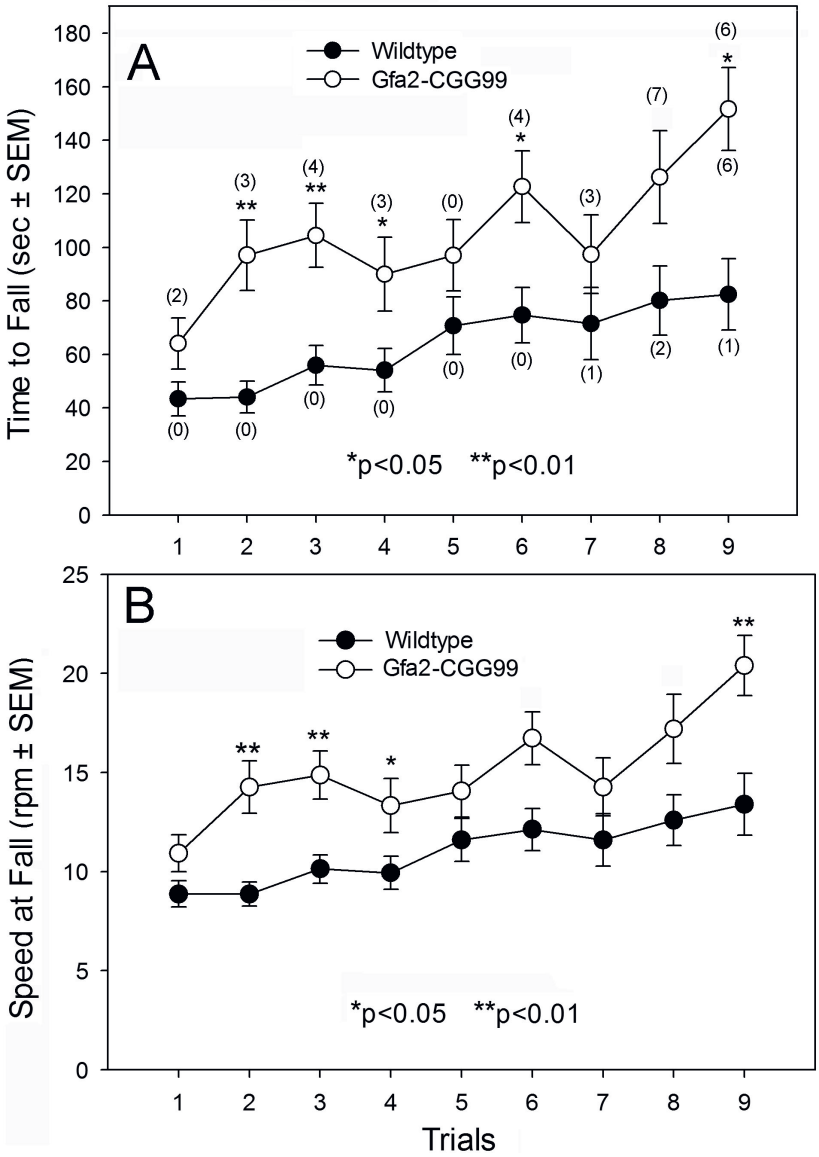

Figure 2 | Rotarod performance of *Gfa2*-CGG99 and WT mice. (A) Time to fall from the rotarod was significantly longer for *Gfa2*-CGG99 versus WT mice. In addition, *Gfa2*-CGG99 mice also showed significantly more flips (number of flips shown in parentheses) than WT mice. **(B)** The speed at which *Gfa2*-CGG99 mice fell from the rotarod was significantly higher than WT mice. * $p<0.05$, ** $p<0.01$.

Gait analysis

Gfa2-CGG99 mice differed from WT mice in several basic gait parameters measured in the TreadScan apparatus (**Fig. 3**). *Gfa2*-CGG99 mice had shorter stance times (time in contact with floor) for front-left and rear-right feet compared to wild type controls ($p<0.05$).

Maximum longitudinal deviation was significantly shorter in *Gfa2*-CGG99 mice compared to WT for the front-left ($p<0.05$), front-right ($p<0.05$) and rear-right ($p<0.05$), indicating a shortened range of motion for the *Gfa2*-CGG99 versus WT mice. No other significant gait differences were found between genotypes for any other measure. When adjusted for body weight differences these gait effects were no longer statistically significant.

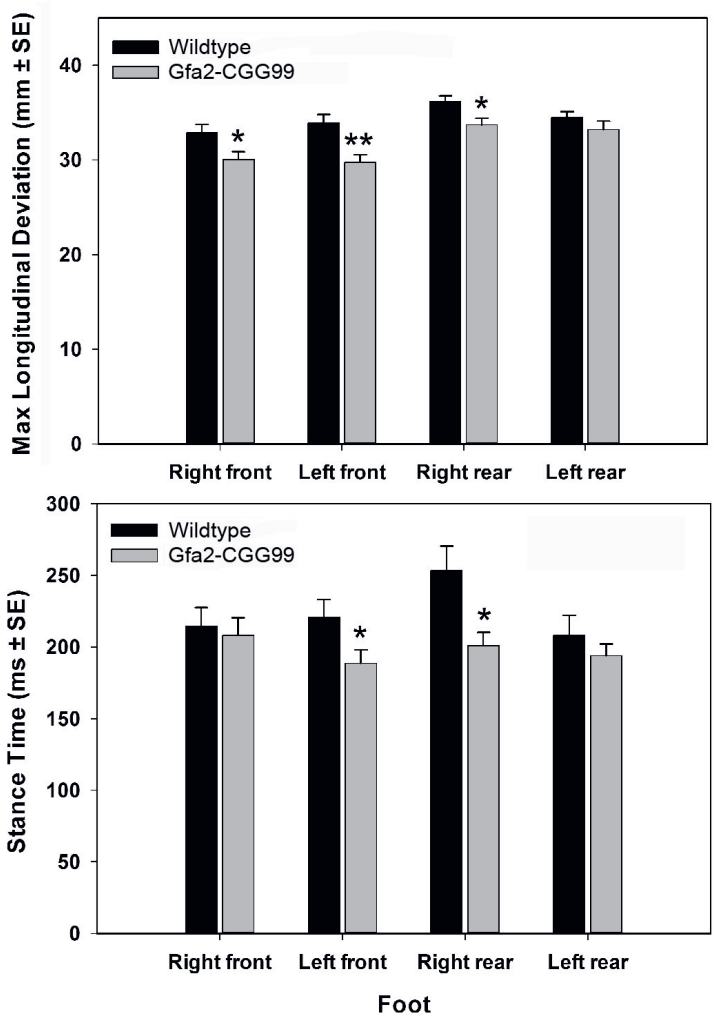

Figure 3 | Gait analysis Treadscan apparatus. (A) Maximum longitudinal deviation was significantly shorter for the right and left front and left rear feet of *Gfa2*-CGG99 mice compared to WT mice. **(B)** Stance time was significantly shorter for *Gfa2*-CGG99 compared to WT mice for the left front and right rear feet. Mice were tested at 7 months of age; $n=15$ per group. * $p<0.05$, ** $p<0.01$.

Ladder rung test

Gfa2-CGG99 mice made significantly more foot slips while crossing the ladder run apparatus compared to WT controls (**Fig. 4**). A one-way ANCOVA with body weight and locomotor activity as covariates showed that this difference between groups was statistically significant ($p<0.001$).

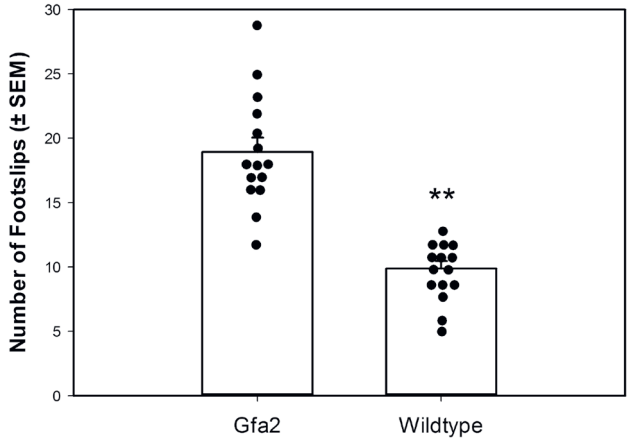

Figure 4 | Motor performance on the ladder rung test. *Gfa2*-CGG99 mice made significantly more foot slips than WT mice in the ladder rung task. Mice were tested at 8 months of age; $n=15$ per group. ** $p<0.01$.

Anxiety tests

No statistically significant differences in measures of anxiety were found between *Gfa2*-CGG99 and WT mice in the elevated plus-maze (time in open arm) or open field tests (margin time). Interestingly, *Gfa2*-CGG99 mice showed an increased frequency of rearing behaviors compared WT mice ($p<0.05$).

Contextual fear conditioning

No differences were found between WT and *Gfa2*-CGG99 mice for either contextual or cued fear conditioning.

Intranuclear inclusions in neurons and astroglia in CGG Knock-in (KI) mice

Ubiquitin-positive intranuclear inclusions are the hallmark neuropathology in FXTAS patients [1, 9], and similar appearing inclusions are found in a CGG knock-in (KI) mouse model of the fragile X premutation [22]. **Figure 5** shows representative red immunofluorescent staining for ubiquitin-positive intranuclear inclusions in neurons (arrowheads) and in astrocytes (arrow). Astrocyte was labeled immunofluorescent green for GFAP. Brain section is from layer I of the parietal cortex of a 16 months old CGG KI mouse with a 128 CGG trinucleotide repeat expansion. Ubiquitin-positive inclusions were

never observed in neurons or astroglia of WT mice used in this study, or in our previous studies in any brain region at any age [24].

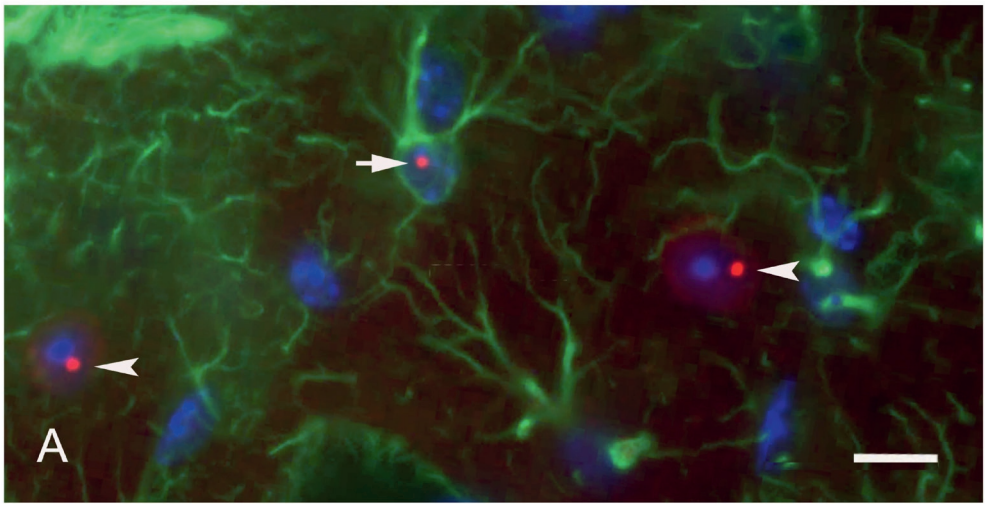

Figure 5 | Immunofluorescent labeling and ultrastructure of ubiquitin-positive intranuclear inclusions in neurons and astroglia of the CGG KI mouse. Ubiquitin-positive intranuclear inclusions (red) in a protoplasmic astroglia (green; arrow) and pyramidal neurons (arrow heads) in the neocortex of a CGG128 KI mouse. These fluorescently labeled intranuclear inclusions are shown for comparison with inclusions found in astrocytes in the *Gfa2*-CGG99 mouse brain. Ubiquitin was immunofluorescently labeled red, GFAP green, and nuclei were stained blue using DAPI. Scale bar: 10 µm.

Expression pattern of eGFP in astroglia of *Gfa2*-CGG99 and *Gfa2*-CGG11 mice

As expected, astrocytes showed green eGFP histofluorescence through the brain in *Gfa2*-CGG99-eGFP (**Fig. 6A**) and *Gfa2*-CGG11-eGFP (**Fig. 6B**) mice. This is shown for the rostral neocortex where eGFP expression was higher in *Gfa2*-CGG99 (**Fig. 6A**) compared to *Gfa2*-CGG11 mice (**Fig. 6B**). *Gfa2*-CGG99 mice showed eGFP histofluorescence in the majority of astroglia across all brain regions (*e.g.,* neocortex, hippocampus, cerebellum, brain stem nuclei). High levels of eGFP histofluorescence was seen in somata, as well as the larger processes and majority of fine processes which appeared as a "green-fluorescent cloud" around the cell body (**Fig. 6F and 6G**). Immuno-labeling astrocytes with GFAP, microglia with Iba1 and neurons with NeuN or MAP2 was carried out to determine specificity of expression of eGFP in the different cell types. The results revealed that eGFP histofluorescence was only observed in astrocytes and Bergmann glia, and not in microglia, oligodendroglia or neurons.

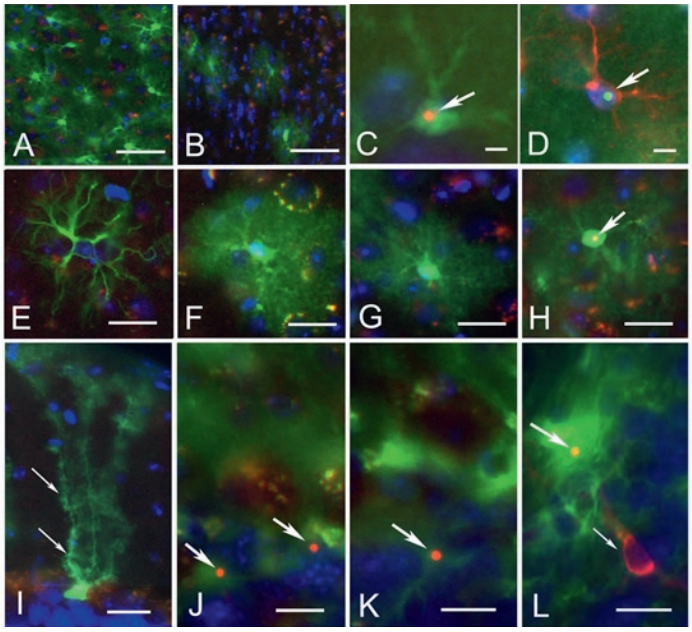

Figure 6 | Intranuclear inclusions in neocortical astrocytes and Bergmann glia in *Gfa2*-CGG99 mice. **(A-B)** EGFP histofluorescence **(green)** in neocortical astrocytes from a **(A)** Gfa2-CGG99, and a **(B)** *Gfa2*-CGG11 transgenic mouse. The majority of astrocytes in the *Gfa2*-CGG99 mouse cortex expressed eGFP, while fewer astrocytes showed expression in the *Gfa2*-CGG11 mouse. Sections were immunoreacted against ubiquitin **(red)** and nuclei stained with DAPI **(blue)**. Red/yellow fluorescent puncta are due to autofluorescence of lipofuscin granules in neurons and microglia associated with normal aging in the mouse cortex. Scale bars: 50 µm. **(C-D)** Intranuclear inclusion **(C)** in an eGFP histofluorescent *Gfa2*-CGG99 mouse astrocyte immunostained for ubiquitin **(arrow, orange/yellow)**. **(D)** Ubiquitin-stained intranuclear inclusion **(arrow, cyan)** in a *Gfa2*-CGG99 astrocyte verified as an astrocyte by staining with anti-GFAP **(red fluorescence)**. Scale bars: 5 µm. **(E-H)** Typically appearing protoplasmic astrocyte from a WT mouse immunostained for Gfap **(E, green)**. Shown for comparison with histofluorescent **(green)** *Gfa2*-CGG99 astrocytes in F-H). **(F)** Green histofluorescence in an astrocyte from a *Gfa2*-CGG11 transgenic mouse, and from a **(G)** *Gfa2*-CGG99 transgenic mouse. Both show a cloud-like histofluorescence emanating from their astrocytic processes, and neither contained a ubiquitin-positive intranuclear inclusion. **(H)** Intranuclear inclusion **(arrow, yellow)** in a green histofluorescence astrocyte from a *Gfa2*-CGG99 mouse. Although not quantified, astrocytes in *Gfa2*-CGG99 mice with inclusions appeared to show less green eGFP histofluorescence compared to astrocytes without inclusions (compare green histofluorescence in G and H). Scale bars 10 µm. **(I-L)** EGFP histofluorescence **(green)** in cerebellar Bergmann glia from a *Gfa2*-CGG11 **(I)** and Gfa2-CGG99 **(J)** transgenic mouse. In bottom panel, **(I)** note the green histofluorescence in the soma and radial glial processes of the Bergmann glia in the *Gfa2*-CGG11 mouse **(small arrows)**. Ubiquitin-stained intranuclear inclusions **(arrows, red fluorescence)** in Bergmann glia **(Fig. J and L, arrows)** and in a protoplasmic astroglia in the granule cell layer of the cerebellum **(Fig. 6K, arrow)** from a *Gfa2*-CGG99 mouse. Microglia immunolabeled with Iba1 **(red fluorescence)** did not show eGFP histofluorescence and did not have ubiquitin-stained intranuclear inclusions **(L, small arrow)**. Scale bars 10 µm. Figures **(A-C, E-L)**, immunostained ubiquitin visualized with Alexa 568 2o antibody (red). **Figure D**, immunostained ubiquitin visualized with Alexa 488 fluorescent 2o antibody (green), astrocytes immunostained for GFAP and visualized with Alexa 568 (red). **Figure E**, astrocyte immunostained for GFAP and visualized with Alexa 488 (green). **Figure L**, microglia immunostained for Iba1 and visualized with Alexa 568 (red). **Figures A-L**, nuclei stained with DAPI (blue).

Gfa2-CGG99 mice display nuclear pathology in astroglia

Although greater than 50% of astroglia in the *Gfa2*-CGG99 mice expressed eGFP, ubiquitin-positive inclusions were only observed in 0.1-0.5% of predominantly protoplasmic astroglia, depending on age and brain region examined. Astrocytes with inclusions, although low in number, were widely distributed throughout the brain including neocortex, cerebellum and occasionally in subcortical brain regions (*e.g.,* hypothalamus and some brain stem nuclei). Astroglia were visualized by eGFP histofluorescence (**Fig. 6C**) or co-labeled for the glial marker GFAP (**Fig. 6D**) with ubiquitin-positive intranuclear inclusions (arrows). The inclusions were spherical bodies averaging 1.82 ± 0.29 µm in diameter located within DAPI-stained nuclei of astroglia (**Fig. 6C-D**). No ubiquitin-positive intranuclear inclusions were found in astrocytes from WT mice (**Fig. 6E**) identified by anti-GFAP immunofluorescence, or in the *Gfa2*-CGG11 transgenic control mice (**Fig. 6F**). Examples of a *Gfa2*-CGG99 neocortical astrocyte lacking or harboring a ubiquitin-positive intranuclear inclusion are shown in **Figures 6G and 6H**, respectively. Interestingly, eGFP expression appeared to be lower in astrocytes from *Gfa2*-CGG99 mice that contained ubiquitin-positive intranuclear inclusions. For example, compare eGFP histofluorescence in an astrocyte without an inclusion in **Figure 6G** to an astrocyte with an inclusion in **Figure 6H**. Developmentally, intranuclear ubiquitin-positive inclusions in astroglia were first observed in neocortex at 4 months of age, but the number was low and only increased slightly at older age (greater than 10 months). We did not find evidence of increased astrocyte proliferation (*i.e.,* gliosis) in the *Gfa2*-CGG99 or *Gfa2*-CGG11 mice.

Gfa2-CGG99 mice exhibit intranuclear inclusions in Bergmann glia

Glia with characteristic Bergmann cell morphology [19, 21, 22, 31, 32] were observed by eGFP histofluorescence throughout the cerebellum in *Gfa2*-CGG99 and *Gfa2*-CGG11 mice. **Figure 6I** shows a representative example of a Bergmann glia cell from a *Gfa2*-CGG11 transgenic mouse which has the characteristic morphology of Bergmann glia (small arrows point to radial processes). No ubiquitin-positive inclusions were found in Bergmann glia from *Gfa2*-CGG11 mice. In contrast, ubiquitin-positive intranuclear inclusions averaging 1.88 ± 0.36µm in diameter were observed in somata of Bergmann glia from *Gfa2*-CGG99 mice (**Fig. 6J, K, L, arrows**). It is notable that ubiquitin-positive inclusions were more frequently found in Bergmann glia of the cerebellar lobuli 1, 2 and 10, and rarely in the other lobules. All of the ubiquitin-positive inclusions associated with Bergmann glia had defined spherical structures and were located within DAPI-positive nuclei. In addition to Bergmann glia, ubiquitin-positive inclusions were also seen in the velate protoplasmic astroglia of the granule layer, and in astroglia located within the molecular layer and white matter of the cerebellum (not shown). Ubiquitin-positive inclusions were not found in nuclei of Purkinje cells or other cerebellar neurons in *Gfa2*-CGG99 mice or from *Gfa2*-CGG11 control mice (**Fig. 6G**). We also did not observe a pattern of Purkinje cell loss in *Gfa2*-CGG99 mice resembling that reported earlier in transgenic mice expressing a similar, but

not identical construct [7]. Further, there were no ubiquitin-positive inclusions identified in selectively stained oligodendroglia (not shown) or in microglia (an Iba1-labeled red fluorescent microglia without an inclusion is shown in the bottom right panel of **Figure 6L**, small arrow; larger arrow points to an inclusion in an adjacent Bergmann glia).

Neuronal intranuclear inclusions were found in *Gfa2*-CGG99 mice

Neuronal intranuclear inclusions are key pathological features of CGG KI mice that appear as early as 3 months of age [19, 21, 22, 32]. We did not see and did not expect to see intranuclear inclusions in *Gfa2*-CGG11 control mice because we were using the *Gfa2*-specific promoter to limit expression to glia (**Fig. 7C**). Unexpectedly, all of the *Gfa2*-CGG99 mice studied exhibited some ubiquitin-positive inclusions in neuronal nuclei in distinct brain regions, particularly in the hypothalamus, including the paraventricular nucleus (**Fig. 7A**) and ventromedial (**Fig. 7B**) nuclei. In contrast to these regions, neuronal inclusions in *Gfa2*-CGG99 mice, although present, occurred less frequently in neocortex and cerebellum. Intranuclear inclusions were particularly large in periventricular nuclei (**Fig. 7A**). Neuronal intranuclear inclusions were also found in brainstem nuclei (*e.g.,* substantia nigra, reticular formation; data not shown). The appearance of neuronal inclusions in *Gfa2*-CGG99 mice was age-dependent, with 4-8 months old mice exhibiting only a few neuronal intranuclear inclusions, while older mice displayed higher numbers of inclusions in the brain regions described above. The presence of intranuclear ubiquitin-positive inclusions in neurons was further established by showing co-localization of the inclusions in cells that were identified as neurons by immunofluorescence for well-accepted neuronal markers, including NeuN (**Fig. 7D, E, arrowheads**), and showing localization within nuclei by DAPI staining. The inclusions showed a similar appearance to those previously described in neurons in the CGG KI mouse (**Fig. 7F**) [21].

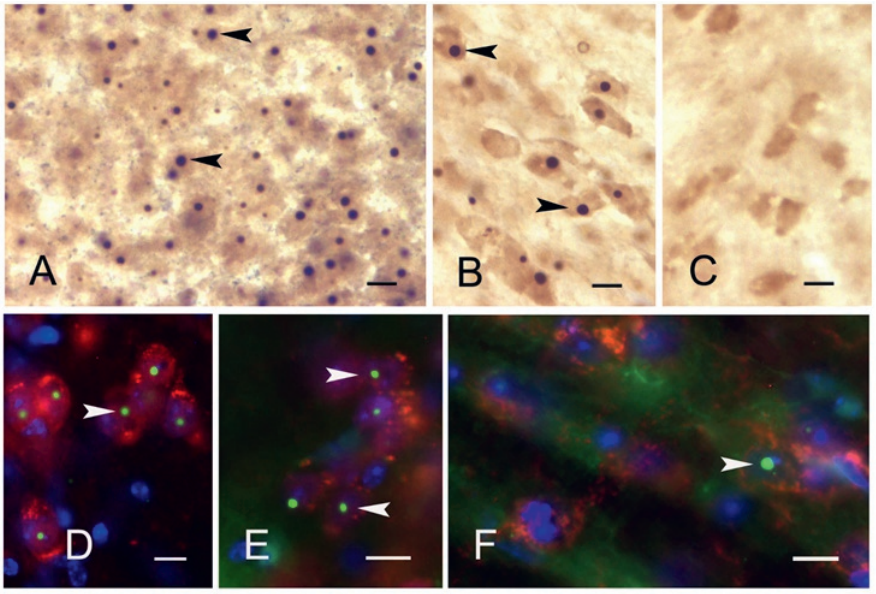

Figure 7 | Ubiquitin-positive neuronal intranuclear inclusions. (A-C) Ubiquitin-positive intranuclear inclusions were unexpectedly found in neurons. Neuronal intranuclear inclusions are shown for the paraventricular nucleus **(A)** of the hypothalamus (arrowheads in A; brown DAB reaction product) and **(B)** ventromedial hypothalamus (arrowheads in B). No inclusions were found in neurons in Gfa2-CGG11 control mice **(C)** or in WT mice. Scale bars: 5 µm. **(D-F)** Immunohistofluorescent staining for ubiquitin-positive intranuclear inclusions (arrowhead) in neurons in *Gfa2*-CGG99 mice **(D)** in the inferior olivary nucleus and **(E)** suprachiasmatic nucleus. **(F)** For comparison, these inclusions are similar to the inclusions found in neurons in the mammillary body of a CGG159 KI mouse. In **Figures D-F**, ubiquitin is immunofluorescently labeled green (Alexa 488, arrowheads) and neurons identified by immunostaining red for NeuN (Alexa 568). Scale bars: **Figure D**: 5 µm; **Figures E-F**: 10 µm.

In order to determine whether inclusion formation could be related to "leaky" expression in neurons of the astrocyte-specific *Gfa2* promoter in *Gfa2*-CGG99 mice, brain sections were immunoreacted using multiple antisera for NeuN, GFAP, and/or eGFP. These experiments revealed that (i) ubiquitin-positive inclusions were present in neurons, in addition to astroglia, in various brain regions; (ii) NeuN-positive cells (*i.e.,* neurons) did not show any detectable eGFP histofluorescence and/or GFAP immunoreactivity in the nucleus or cytoplasm; and (iii) only astroglia expressing eGFP (not neurons) were immuno-positive when reacted with antiserum against eGFP and GFAP.

Absence of eGFP expression in neurons with inclusions analyzed by single cell, laser-capture microdissection (LCM) PCR: Possible evidence for transfer of pathology from astrocytes to neurons.

The unexpected finding that neurons without eGFP histofluorescence had inclusions suggested the possibility of cell-to-cell transfer of pathology from astrocytes to neurons in *Gfa2*-CGG99-eGFP mice. However, it is also possible that eGFP expression in neurons was below the level of detection by histofluorescence. To test this possibility, PCR analysis of laser-capture microdissected cells (LCM) was used to detect possible eGFP mRNA expression in inclusion-bearing neurons in the ventromedial hypothalamus (VMH) of *Gfa2*-CGG99 mice, a region with numerous neuronal inclusions (**Fig. 7B**). Specifically, neurons in the VMH that lacked eGFP histofluorescence but contained ubiquitin-positive intranuclear inclusions were identified by immunofluoresent staining (**Fig. 8A1, 8A2**), isolated by LCM (**Fig. 8A3**) and combined for PCR analysis (**Fig. 8B, C**). Total RNA was isolated, quantified and linearly amplified using NuGEN SPIA technology (www.nugen.com). The resulting cDNA was processed for semi-quantitative real-time PCR with primers specific for EGFP and β-actin. As a positive control, RNA was also isolated from regions of neocortex that included astroglia that expressed eGFP (*i.e.,* GFA2-cortex). In addition, we isolated single cells with inclusions from the amygdala of a CGG168 KI mouse (*i.e.,* CGG KI Amygdala) that should not express eGFP. These neurons express an expanded CGG repeat under the control of an endogenous *Fmr1* promoter, develop neuronal intranuclear inclusions but do not express eGFP [21, 33, 34]. We did not observe expression of eGFP mRNA in VMH neurons with ubiquitin-positive intranuclear inclusions (*GFA2* LCM Neurons; **Fig. 8B**). Similarly, neurons isolated from the amygdala of a CGG168 KI mouse did not express eGFP (**Fig. 8B**). In contrast, larger cortical samples from *Gfa2*-CGG99 mice expressed high levels of eGFP mRNA (**Fig. 8B**) reflecting the presence of astroglia expressing the eGFP protein. The expected size and relative purity of PCR reactions were confirmed by gel electrophoresis (**Fig. 8C**).

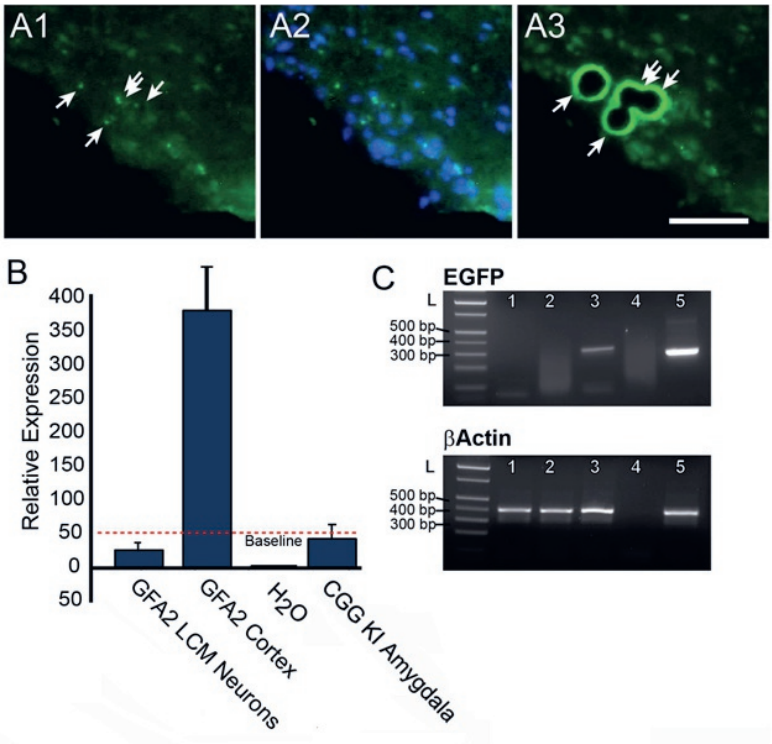

Figure 8 | Ventromedial hypothalamic neurons with inclusions from Gfa2-CGG99 mice do not express eGFP by qPCR analysis. (A1-3) (A1) Neurons in ventromedial hypothalamus (VMH) containing ubiquitin positive inclusions were visualized in 14 micron cryosections of brain by immunofluorescent labeling (green immunofluorescence). **(A2)** Same section with DAPI staining. **(A3)** Neurons with inclusions were collected by laser capture microdissection (LCM). Scale bar = 50 µm **(B)** Total RNA was extracted and amplified from LCM neurons and qPCR analysis was performed to detect expression of eGFP. VMH neurons from Gfa2-CGG99 mice with inclusions did how show detectable expression of eGFP (GFA2 LCM Neurons). In contrast, eGFP expression was readily detected in large LCM samples from cerebral cortex that included astrocytes with eGFP expression (GFA2 Cortex). No signal was detected in the water control (H_2O). As an additional tissue control, single neurons from the amygdala of a CGG KI mouse (168 CGG repeats) were isolated by LCM and analyzed for eGFP expression (CGG KI Amygdala), and as expected since these mice do not carry the eGFP reporter gene, no expression was detected. Red dashed line shows the detection threshold for qPCR analysis. **(C)** Analysis of qPCR samples by gel electrophoresis confirmed amplification of eGFP in cortical samples containing eGFP positive astrocytes, but not in samples of LCM-isolated hypothalamic neurons. L = DNA ladder; 1 = CGG KI amygdala; 2 = GFA2 LCM neurons; 3 = GFA2 cortex; 4 = water; 5 = eGFP and/βActin positive plasmid controls.

Intracytoplasmic inclusions in astroglia of *Gfa2*-CGG99 mice

Ubiquitin-positive inclusion bodies in *Gfa2*-CGG99 mice did not appear to be restricted to the nuclear compartment (**Fig. 9**). Initial observations in brain sections from *Gfa2*-CGG99 mice stained with neutral red and immunostained for ubiquitin revealed inclusion bodies that did not appear to be closely associated with somata of astrocytes or neurons. These ectopic

inclusion bodies shown in **Figure 9A** were prevalent across grey and white matter of all brain regions examined, but particularly frequent in upper neocortical layers, hippocampus, olfactory bulb and certain brain stem nuclei. These bodies (aggregates) were spherical and averaged 3.62±1.26 µm in diameter. In some regions (*e.g.,* ventromedial hypothalamus) they appeared to form larger clusters of several bodies. They were immunopositive for ubiquitin (dark-blue reaction product) using DAB peroxidase reaction (inset **Fig. 9a**), and/or exhibited ubiquitin immunofluorescence (**arrowheads, Fig. 9B-F**). Some appeared to be engulfed or surrounded by fine astroglial processes suggesting the inclusion bodies were intracytoplasmic in astroglia (**Fig. 9B-C, inset b; arrowheads**). Co-localization of inclusions with eGFP (**Fig. 9D, E**) and GFAP (**Fig. 9F**) confirmed the association of these inclusions with astrocytes. This observation was confirmed by electron microscopy (EM) as described below (**Fig. 11I & 11K**).

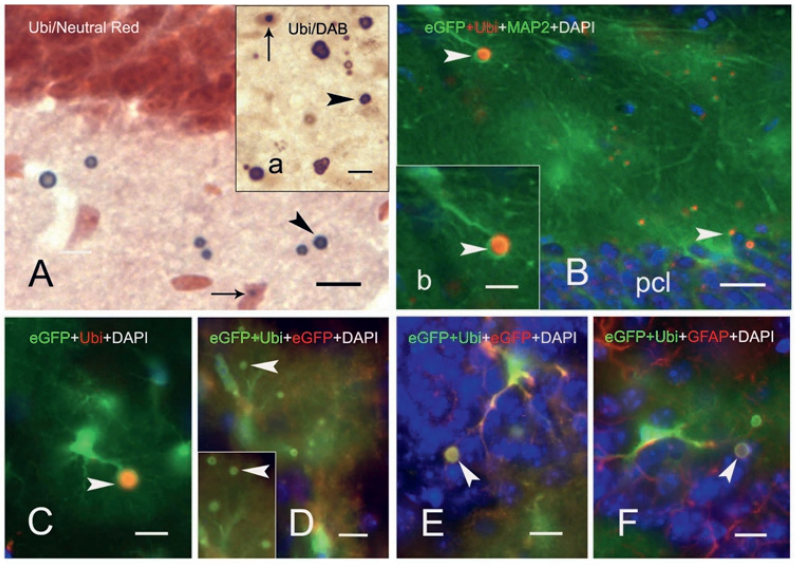

Figure 9 | Ectopic and intracytoplasmic ubiquitin-positive inclusions in Gfa2-CGG99-eGFP expressing astroglia. (A) Ubiquitin-positive astrocyte intranuclear inclusion (small arrow) and nearby inclusions that appear to be extracellular (arrowheads) in a neutral-red stained section of hilus from a *Gfa2*-CGG99 mouse. (Inset a) Intranuclear (small arrow) and extracellular (arrowhead) ubiquitin-positive inclusions. DAB immuno-peroxidase staining was used to label ubiquitin-positive inclusions in A and inset a. **(B)** Intracytoplasmic ubiquitin-positive inclusion (arrowhead) in an eGFP histofluorescent astrocyte in the stratum oriens of hippocampal CA1 region; pcl = pyramidal cell layer. (Inset b) shows higher magnification of the inclusion body (arrowhead). **(C)** An eGFP histofluorescent astrocyte from a *Gfa2*-CGG99 mouse with an intracytoplasmic ubiquitin-positive inclusion body (arrowhead) within the hippocampal CA1 stratum radiatum. **(D)** Ubiquitin-positive intracytoplasmic inclusion in astrocyte (arrowhead, yellowish-green fluorescence) that co-localizes with eGFP in the CA1 pyramidal cell layer. Inclusions were immunolabeled eGFP (red) and ubiquitin (green). Note that eGFP histofluorescence from expression of the eGFP reporter gene (green) is also present. Nuclei were labeled with DAPI. **Figures (E and F)** Co-localization of intracytoplasmic inclusions (arrowheads) in astrocytes. Immunofluorescent labeling with ubiquitin (green) and GFAP (red). eGFP histofluorescence from expression of the eGFP reporter gene (green) is also present. Nuclei were labeled with DAPI. Scale bars: **Figures A-F**: 10 µm.

The RAN translation product FMRpolyG is present in inclusions found in the *Gfa2*-CGG99 mice

Figure 10A shows an FMRpolyG-positive (red fluorescent) intranuclear inclusion in a GFAP-positive (green) neocortical astroglia from *Gfa2*-CGG99 mouse (arrow). This observation provides the first evidence for RAN translation in astroglia in a mouse model of the FXTAS. In addition, FMRpolyG immunostaining was also seen in an inclusion body in MAP2-positive (green) neuron in the hypothalamus (**arrow, Fig. 10B**). Arrowheads in **Figure 10A** and **Figure 10B**, show FMRpolyG-positive inclusions that are likely in an unlabeled neuron and an unlabeled astrocyte, respectively. Combined with the evidence against eGFP transgene expression in neurons (**Fig. 8**; laser-microdissection single-cell PCR for eGFP), the finding of FMRpolyG in neurons suggests that some form of cell-to-cell transfer of pathology, possibly involving FMRpolyG, may occur in *Gfa2*-CGG99 mouse brains. This could be similar to a recent report of cell-to-cell transfer of RAN translation peptides in other models of trinucleotide (or hexanucleotide) repeat disorders [35].

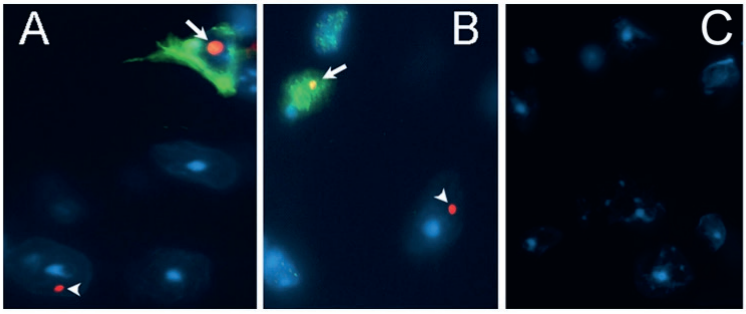

Figure 10 | Double immunofluorescent staining reveals FMRpolyG positive inclusion bodies in both astrocytes and neurons from *Gfa2*-CGG99 mice. (A) Photomicrograph showing FMRpolyG-positive inclusion bodies (red) located within GFAP positive astrocytes (green; arrow) as well as in a GFAP negative cell that is probably neuronal (arrow head). **(B)** Photomicrograph showing FMRpolyG-positive inclusion bodies (red) located within a MAP2 positive (green; arrow) neuron as well as in a MAP2 negative cell that is probably an astrocyte (arrow head). **(C)** Representative brain section from a *Gfa2*-CGG99 mouse processed for immunofluorescence but without 8FM mouse anti-FMRpolyG primary antibody.

Electron microscopy (EM) of inclusion bodies in astrocytes and neurons

Neurons and astroglia of CGG KI mice

Figures 11A and 11B (higher magnification) show electron micrographs of inclusions in the nucleus of neocortical pyramidal neurons from a CGG159 KI mouse. **Figures 11C and 11D** (higher magnification) show inclusions in the nucleus of an astroglia in the neocortex from the same KI mouse. Nuclei of these cells show characteristic ultrastructural features of a nucleolus (single asterisks) in which the partes granulosa and fibrosa appear as clearly separated regions and in which filaments and/or granules are dominant. In

contrast, inclusions in neurons (double asterisks) appear as compact, non-membrane bound arrangements of more loosely packed ribosome-like granules and fine filaments. Inclusions in CGG KI mice range between 1-2.5 µm diameter, similar to that reported earlier for immunostained neuronal intranuclear inclusions [21]. Intranuclear inclusions were mostly located closely to the nucleolus and varied in size. Occasionally some neurons contained 2 intranuclear inclusions.

Inclusions in astrocytes of Gfa2-CGG99 mice

As shown in **Figures 11E and 11F** (higher magnification), intranuclear ubiquitin-positive inclusions in astroglia appeared as a compact collection of densely packed granulo-filamentous material often closely localized to the marginal chromatin of the nucleus.

Inclusions in neurons of Gfa2-CGG99 mice

Figures 11G and 11H (higher magnification) show a representative example of a nucleolus (single asterisk) and proximal intranuclear inclusion (double asterisk) in a neuron in the posterior hypothalamus of a *Gfa2*-CGG99 mouse. The overall appearance of these inclusions was similar to that seen in the CGG KI mouse described above (**compare with Fig. 11A**). As shown at high magnification in **Figure 11H**, inclusions in neurons appeared as compact arrangements of non-membrane bound granulo-filamentous material consisting of densely-packed ribosome-like granules and filaments. Intranuclear inclusions were mostly located closely to the nucleolus and varied in size and shape.

Cytoplasmic inclusions in astrocytes

Electron microscopic examination revealed that these apparently non-membrane bound inclusion bodies are intracellular and surrounded by cytoplasm of astroglia processes containing mitochondria, ribosomes/polysomes and intermediate filaments, a characteristic feature of astroglia (**Fig. 11I, J and K, L**). Some cytoplasmic inclusion bodies contained an electron dense central region (core) exhibiting an amorphous to granular character. This core is surrounded by a less dense peripheral region (rim), in which predominantly loosely packed filaments are present, oriented in linear/radial direction. The adjacent cytoplasm often contained bundles of intermediate filaments and mitochondria. The size and morphology of these inclusions is similar in to the intranuclear neuronal inclusions of FXTAS patients observed by EM in human hippocampus [12] and in dorsal root ganglion cells [36].

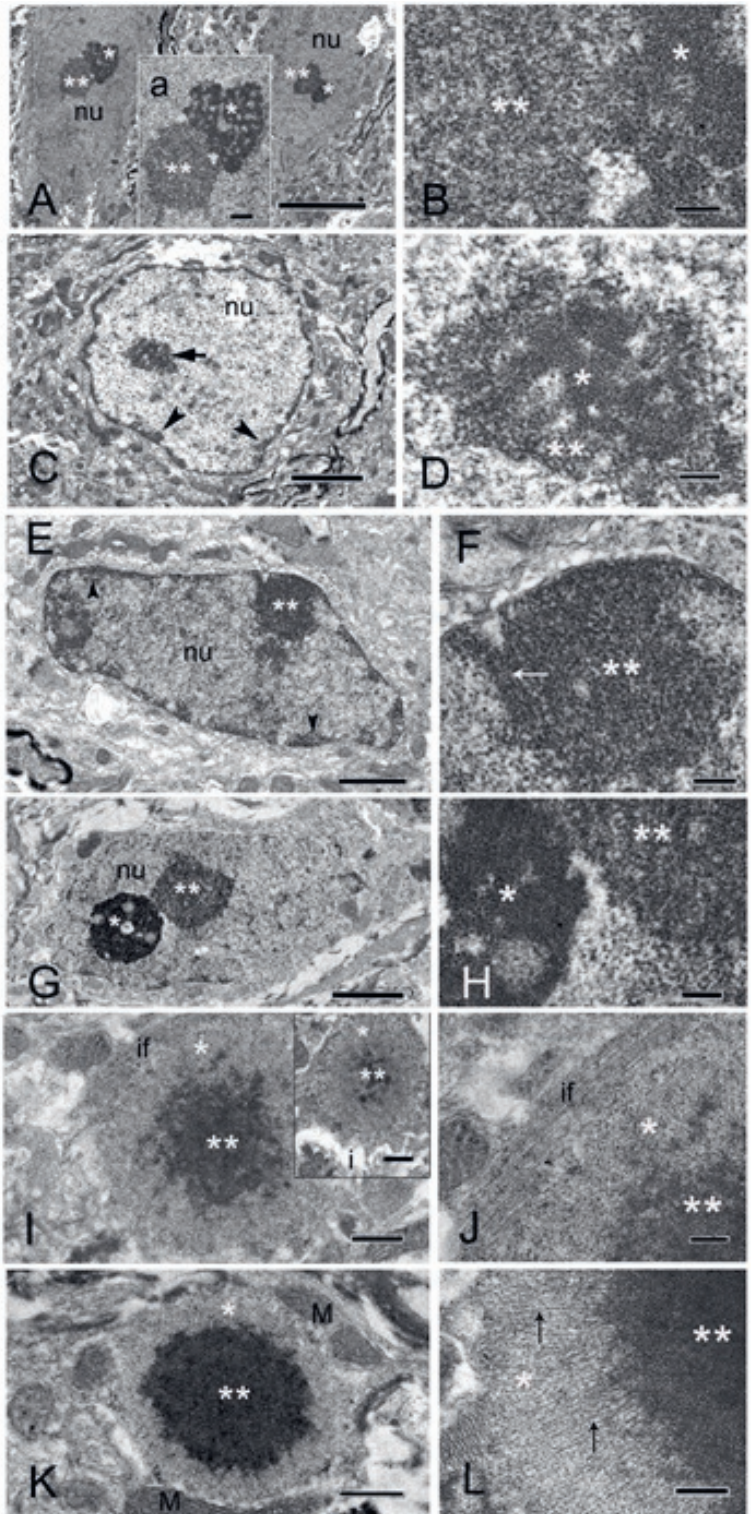
A
nu
a
nu
B
C
nu
D
E
nu
F
G
nu
H
I
if
i
J
if
K
M
M
L

Figure 11 | Electron microscopy of inclusion bodies in astrocytes and neurons. (A) Electron micrographs of two layer 3 pyramidal neurons in the neocortex from a 15.5 months old CGG159 KI mouse (159 repeats) showing the nucleoli (single asterisk) and intranuclear inclusions (double asterisks) in each of the nuclei (nu). **(Inset a)** shows the nucleolus (single asterisk) and a non-membrane bound electron-dense inclusion (double asterisks) of the left neuron. **(B)** Higher magnification of the adjacent region between the nucleolus (single asterisk) and intranuclear inclusion (double asterisks) from inset a. Note the granulo-filamentous ultrastructure of the inclusion material. **(C)** Electron micrograph of a protoplasmic astroglia in the neocortex of the same CGG KI mouse showing the marginal localization of the heterochromatin (arrowheads) and an intranuclear inclusion (arrow) within the nucleus (nu). **(D)** The inclusion in C shown at higher magnification consists of a predominantly granular material (double asterisks) surrounding some chromatin-like dense material (single asterisk) within the center. Scale bars: **Figure A**: 1 µm; **a**: 5 µm; **B, D**: 0.2 µm; **C**: 2 µm. **(E)** Electron micrograph of a fibrous astroglia in the posterior hypothalamus of a *Gfa2*-CGG99 mouse with an intranuclear inclusion (double asterisk) within the nucleus (nu). Note the marginal chromatin localization (arrowheads) in the nucleus. **(F)** Higher magnification of the intranuclear inclusion (double asterisk) reveals an electron-dense structure inclusion body made up of predominantly granular material and filaments (small arrow). Scale bars: **Figure E**: 1 µm; **F**: 0.2 µm. **(G)** Electron micrograph of a principal neuron in the posterior hypothalamus of a Gfa2-CGG99 mouse that shows the nucleolus (single asterisk) and an intranuclear inclusion (double asterisks) within the nucleus (nu). **(H)** Higher magnification of the adjacent regions of the nucleolus (single asterisk) and the intranuclear inclusion (double asterisk) in G which exhibit different ultrastructural features of the granular-filamentous material in the nucleolus versus the inclusion. Note the higher electron density of the nucleolus (pars granulosa and fibrosa) as compared with the more uniform appearing inclusion material. Scale bars: **Figure G**: 2 µm; **H**: 0.2 µm. **(I)** Electron micrographs of intracytoplasmic inclusion body located within astrocytic processes in the posterior hypothalamus of a *Gfa2*-CGG99 mouse. The inclusions display an electron-dense core (double asterisks) and a lighter rim (single asterisk) which varied in size between inclusions (compare with **inset i**). Note the intermediate filaments within the cytoplasm (if) near the inclusion. **(J)** Higher magnification of the inclusion body in I presents an amorphous to granular material within the core and a granular-filamentous material within the rim. Note the intermediate filaments (if) - a characteristic feature of the astrocytic cytoplasm. **(K)** Intracytoplasmic inclusion body in the posterior hypothalamus exhibits a large electron-dense core surrounded by a thinner and less dense rim region. Note the mitochondria **(M)** in the adjacent cytoplasm of the astrocytic process. **(L)** Higher magnification of a portion from the inclusion body shows a linear-oriented filamentous material in the rim (single asterisk) and a dense granular-filamentous material in the outer zone of the core (small arrows). Scale bars: **Figures I, i**: 1 µm; **K**: 1 µm; **J, L**: 0.2 µm.

Discussion

Solitary intranuclear ubiquitin-positive inclusions in neurons and astroglia are the hallmark neuropathology in FXTAS [11, 12]. CGG KI mice used to model FXTAS have similar intranuclear inclusions in both neurons and astroglia [20, 21, 33]. The present study focused on pathology in astroglia in a transgenic mouse model of FXTAS that selectively expressed a CGG99 trinucleotide repeat expansion fused to eGFP in astroglia and Bergmann glia (the *Gfa2*-CGG99 mouse). These investigations revealed that: *(1)* strong eGFP fluorescence in astrocytes and Bergmann glia was widespread throughout the brain with some glial cells exhibiting ubiquitin-positive inclusions; *(2)* subsets of neurons located within the brain and brainstem (*e.g.,* hypothalamus, reticular formation, olivary nuclei) also developed intranuclear ubiquitin-positive inclusions; *(3)* intracytoplasmic inclusion bodies were

observed, predominantly associated with astrocyte processes; *(4)* inclusion bodies in astrocytes and neurons immunolabeled for the RAN translation product FMRpolyG; and *(5) Gfa2*-CGG99 mice showed primarily a motor deficit phenotype. The rationale for developing transgenic *Gfa2*-CGG99-eGFP mice was to create a mouse model to determine the role of astroglia in overall FXTAS pathology. To this end, the *Gfa2*-CGG99 mice provide evidence that pathology mainly restricted to astrocytes can contribute to abnormal motor function, as seen on the ladder rung test, analysis of gait and rotarod performance compared to WT controls. However, the fact that intranuclear inclusions were also found in neurons in the *Gfa2*-CGG99 mice complicates attempts to attribute specific pathology to either astrocytes or neurons.

Behaviorally, the *Gfa2*-CGG99 mice displayed an abnormal, shortened gait and were impaired in their ability to skillfully walk along a horizontal ladder (*i.e.,* ladder rung task), slipping through the floor more often than WT mice. These findings of a primary motor phenotype in the *Gfa2*-CGG99 mice resemble the ataxia observed in FXTAS patients. Unexpectedly, *Gfa2*-CGG99 mice showed enhanced performance on the rotarod compared to WT littermates that did not appear to be due to differences in body weight. While superior rotarod performance could reflect better motor learning, it could also be due to use of an alternate strategy to stay on the rotarod such as flipping, which was prevalent in *Gfa2*-CGG99 mice. Enhanced performance on the rotarod by transgenic and KO mice has been reported. For example, neurexin-1α deletion [37], conditional knockout of PTEN in cortex and hippocampus [38], overexpression of human mutant α-Synuclein, SynA53T [39], and Neuroligin-3 R451C knock-in mice [40] show enhanced performance on the rotarod compared to WT mice. A recent study reported that neuroligin-3 mutations in mice increase repetitive behaviors through altered striatal circuitry, and that this may manifest as stereotyped behavior on the rotarod resulting in an apparent improvement in performance [41]. Therefore, it is possible that the superior rotarod performance in *Gfa2* mice is the result of both better motor learning and the adoption of repetitive behaviors on the rotarod such as flipping, and that abnormal motor functions are part of the phenotype of this novel *Gfa2*-CGG99 model of the Fragile X premutation.

Gfa2-CGG99 mice showed widespread expression of eGFP in more than 50% of all astroglia in the brain but less than 0.5% of astrocytes showing eGFP fluorescence had ubiquitin-positive inclusions. This is similar to the CGG KI mouse model of FXTAS where relatively few astrocytes develop ubiquitin-positive intranuclear inclusions [21]. In contrast, 10-20% of astrocytes in postmortem brain tissue from FXTAS patients contain intranuclear inclusions, and there are more inclusions in astrocytes than neurons in several brain region [11]. The reasons for these differences in the prevalence of inclusions in astrocytes and neurons, and between mouse models of FXTAS and FXTAS are unknown. One possibility may be differences in activity of the ubiquitin-proteasome system (UPS) leading to

the accumulation of aggregated proteins within the ubiquitin-positive intranuclear inclusions. The UPS is critical for intracellular protein degradation and turnover, including clearing cells of misfolded proteins. Moreover, UPS activity has been reported to be lower in neurons compared to astrocytes and to decrease with age [42]. It is also possible that inclusions form more slowly in astroglia than in neurons in mouse brain, when compared to human neurons and astrocytes.

Astroglia are known to play a major role in regulating neuronal growth and synaptic development [43-45], and also in the progression of neurodegenerative diseases and neurodevelopmental disorders [46-48]. In the present study, astroglia, including Bergmann glia, that contained intranuclear inclusions appeared to show lower levels of eGFP fluorescence in soma and often an absence of eGFP in astrocyte processes. This finding suggests eGFP expression may be reduced in astroglia bearing ubiquitin-positive inclusions. A possible link between translational efficiency and CGG repeat number in carriers of premutation alleles has been reported [49]. Specifically, *FMR1* mRNA translational efficiency was reduced in FXTAS patients with CGG repeat expansions in the range of 97-195 CGGs, with translational efficiency directly correlated CGG repeat length [49]. Therefore, it is possible that astroglia with inclusions in the *Gfa2*-CGG99 mouse brain may have reduced translational efficiency resulting in reduced expression of eGFP. Alternatively, eGFP mRNA or protein may be sequestered by the inclusions, thereby reducing eGFP fluorescence, similar to the sequestration of several other proteins found to be associated with inclusions in FXTAS [5, 50].

GFAP, the major intermediate filament protein, is almost exclusively expressed in astroglia, and is therefore the preferred astrocyte marker in clinical and basic research studies [51, 52]. Use of the GFAP promoter in the present study was therefore expected to limit transgene expression to astroglia. Previous reports have indicated that some portions of both the human and murine promoter may also direct expression of some genes in neurons, this occurred only in a few instances and not for green fluorescent protein (GFP) [53]. Because intranuclear inclusions were prevalent in distinct neuronal populations, particularly in the hypothalamus, we carried out a careful investigation of the specificity of eGFP/GFAP expression in neurons with intranuclear inclusions. Using LCM-PCR and immunofluorescent staining we failed to find any evidence for expression of eGFP or GFAP in neurons with inclusions. In addition, we did not find expression of eGFP in microglia or oligodendroglia, and this is consistent with a large number of studies using the GFAP promoter [53].

The finding that some neurons in *Gfa2*-CGG99 mice also develop intranuclear inclusions but do not express GFP opens the possibility that some form of cell-to-cell transfer of pathology from astrocytes to neurons may be occurring. One possibility is that either an

RNA transcript or a translational product (*e.g.,* FMRpolyG) is transferred from astrocytes to adjacent neurons. This could explain why inclusions in both astrocytes and neurons stain for FMRpolyG. We do not yet have direct evidence for such a mechanism in *Gfa2*-CGG99 mice or in carriers of the Fragile X Premutation or in FXTAS. However, cell-to-cell transmission of dipeptide repeat proteins linked to translation of hexanucleotide repeat expansions in ALS and FTD has been reported *in vitro* in several CNS cell types, including induced pluripotent stem cells from C9ORF72-ALS patients. Importantly, transmission was bidirectional, both from astrocytes to neurons and from neurons to astrocytes [35]. Cell-to-cell transfer processes have been reported in Alzheimer's pathology, Parkinson's disease, and polyglutamine diseases among others [35, 54-56].

Neurodegenerative diseases have been shown to exhibit various forms of glial-neuronal miscommunication in what has been called non-cell autonomous pathology [54]. While cell-to-cell transfer of pathology may itself be a form of non-cell autonomous pathology, it is also possible that some other process associated with such non-cell autonomous pathology may play a role in the development of neuronal inclusions that are both ubiquitin and FMRpolyG positive. For example, it is known that astrocytes play a critical role in regulating extracellular neurotransmitter levels in the central nervous system, including specific transport mechanisms for glutamate and metabolic pathways for GABA [57]. Non-cell autonomous pathology occurs in the polyglutamine repeat disease Spinocerebellar ataxia type 7 (SCA7), where extensive pathology in Bergmann glia that help maintain extracellular glutamate homeostasis results in glutamate toxicity and subsequent neurodegeneration of cerebellar Purkinje cells [58].

The finding that inclusions in both astrocytes and neurons showed immunofluorescent labeling for FMRpolyG supports the occurrence of repeat-associated non-ATG (RAN) translation in *Gfa2*-CGG99 mice. RAN translation of a potentially toxic polyglycine-containing peptide, FMRpolyG, has been previously reported in mouse models of the fragile X premutation and in FXTAS postmortem tissue [7, 25, 26]. This peptide is translated from the expanded CGG repeat initiated at a non-canonical ACG codon approximately 35 nucleotides upstream of the start of the expanded CGG repeat segment [7]. The mechanism of toxicity of FMRpolyG may involve disruption of the nuclear lamina of cells, and evidence suggests that it is the carboxy-terminus of FMRpolyG that mediates this toxicity [7]. RAN translation was originally described for CAG/CTG repeat expansions within the coding region of the *ATXN8/ATXN8PS* gene associated with the neurodegenerative disorder spinocerebellar ataxia type 8 (SCA8) [59]. RAN translation appears to be a pathological mechanism in the hexanucleotide repeat expansion disorder *C9ORF72*, the most common genetic mutation associated with ALS-FTD [35], and may also occur in the CAG repeat expansion disorder Huntington's disease [60]. Our results provide

the first evidence that RAN translation, and possible associated pathology, also occurs in astroglia and Bergmann glia.

We performed extensive ultrastructural analysis of the intranuclear inclusions found in astrocyte soma, neurons, and the cytoplasm of astrocytes. We found that the neuronal inclusions differ somewhat from those in astrocytes, appearing as compact collections of non-membrane bound granulo-filamentous material often closely localized to the marginal chromatin of the nucleus. Neuronal inclusions also appeared to be composed of granulo-filamentous material but tended to be located proximal to the nucleolus. In contrast, EM confirmed that intracytoplasmic inclusions were intracellular within astrocytic processes, with some having an electron dense central core with a less dense peripheral rim. These inclusions are similar to those described earlier in neurons of the human hippocampus in postmortem tissue from FXTAS patients [12], and in dorsal root ganglion cells [36]. Whether or not inclusions are toxic, or how they contribute to neuropathology is currently unknown, but their association with reduced eGFP expression in astrocytes and potential cell-to-cell spreading from astrocytes to neurons suggest a role in FXTAS disease pathogenesis.

Conclusions

Transgenic mice with high expression levels of an expanded CGG-99 trinucleotide repeat driven by a murine *Gfa2* promoter were developed to examine pathology in glia associated with the Fragile X premutation. Expression in glia was widespread throughout the brain, as visualized by the eGFP reporter expression within the *Gfa2*-CGG99-eGFP construct. eGFP fluorescence was limited to astroglia and Bergmann glia only, and a subset of these glia also developed ubiquitin-positive intranuclear inclusions between the ages of 4-16 months. Expression of eGFP was not observed in microglia immunolabeled with Iba1 or oligodendroglia immunolabeled with MBP, and intranuclear inclusions were never observed in these glial subtypes. Although we do not yet have direct evidence for cell-to-cell spread of pathology, the unexpected finding of intranuclear inclusions in NeuN-labelled neurons, particularly in the hypothalamus, opens the possibility for this type of transfer of pathology in our *Gfa2*-CGG99 mouse model of FXTAS. The presence of the RAN translation product FMRpolyG in the astrocyte inclusions indicates that this mechanism of pathology in trinucleotide repeat expansion disease may not be limited to neurons, and may occur in astrocytes in FXTAS patients, though this is yet to be documented. Taken together, our results highlight that FXTAS pathology is complex involving both astrocytes and neurons and their possible interactions. Our findings thus provide important new insights that should be considered when developing therapies for FXTAS in human patients.

Acknowledgements

We are grateful to s. Grete Adamson for excellent support in electron microscopy (Department of Medical Pathology and Laboratory Medicine, UC Davis). We thank Emily Doisy for her careful reading of drafts of this manuscript and many helpful suggestions. Supported by grants from the NIH (NINDS NS079775 and NINDS RL1 to R.F.B; NS062411; NIA RL1 AG032119 to P.J.H; AG033082 to A.R.L.S.), Roadmap Consortium NIDCR UL1 DE 19583, and NICHD U54D079125 to the UC Davis M.I.ND. Institute IDDRC.

Availability of Data and Materials

The datasets used and/or analyzed during the current study are available from the corresponding author on reasonable request.

Supplementary Figures

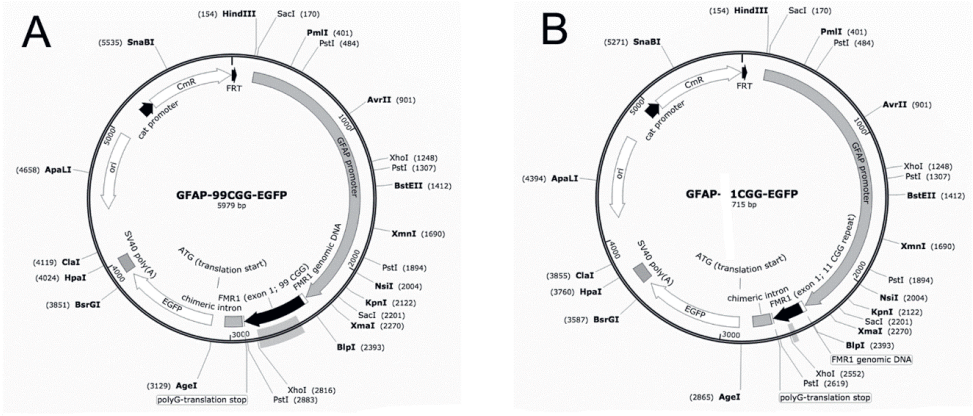

Figure S1 | Expression vector maps used to generate the (A) EGFP-CGG99-EGFP or (B) EGFP-CGG11-EGFP transgenic mouse lines.

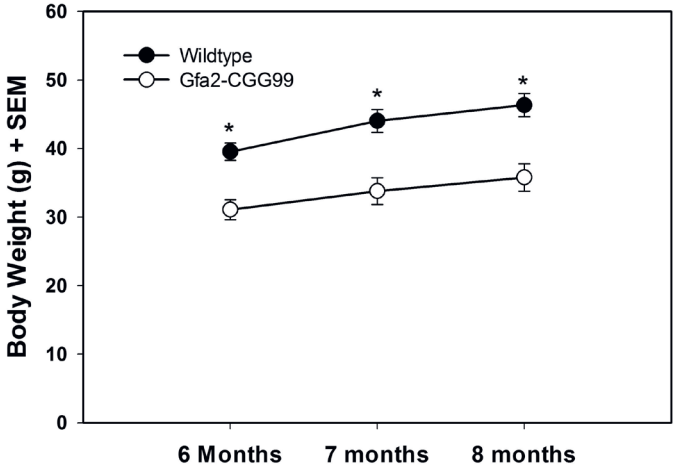

Figure S2 | Statistical results for behavioral experiments.

Body weight (Figure S2): *Gfa2*-CGG99 mice had lower body weights at 6 months of age when behavioral testing began, as well as at 7 and 8 months of age. A repeated measures ANOVA (genotype by age) showed the weight difference between genotypes to be significant [$F(_{1,18}) = 18.1$, $p<0.001$], that both groups gained weight over time [$F(_{2,56}) = 50.2$, $p<0.0010$], but that the genotype × age interaction was not significant [$F(_{2,56}) = 1.96$, $p=0.15$]. Therefore, body weight was used as a covariate in statistical analyses. Body length did not differ between *Gfa2*-CGG99 (93.6 ± 0.6mm) and WT mice (94.9 ± 0.5mm) [$t(28) = 1.76$, $p=0.09$] at the start of behavioral testing.

Rotarod (Figure 2 in manuscript): *Gfa2*-CGG99 mice stayed on the rotarod longer (*e.g.,* **A.** Time to Fall) and at a higher speed (**B.** Speed at Fall) compared to WT mice. A repeated measures ANOVA

for Time to Fall across trials (genotype X trial) revealed a significant difference between genotypes ($F_{(1,27)}$ = 6.35, p<0.05) and across trials ($F_{(8,216)}$ = 2.61, p<0.01). Planned comparisons of WT versus *Gfa2*-CGG99 across trials showed that differences were statistically significant on days 2, 3, 4, 6 & 9, but the difference the difference between groups on trial 1 was not statistically significant. A similar analysis for Speed at Fall showed a significant genotype × trial interaction ($F_{(8,21)}$ = 2.118, p<0.05), significant main effect for genotype ($F_{(1,27)}$ = 8.53, p<0.01) and for trials ($F_{(8,216)}$ = 2.269, p<0.05). Speed to Fall was significantly longer for *Gfa2* compared to WT on trials 2, 3, 4, & 9. In addition, numbers in parenthesis in Figure 2A show that Gfa2-CGG99 mice flipped (*i.e.,* clinging to the rotarod cylinder through complete 360 deg rotations) on 8 of 9 trials compared to only 3 of 9 trials for WT (χ 2(1) = 5.84, p<0.05). Eleven of 15 Gfa2 mice showed one or more episodes of flipping compared to 2 of 15 WT mice (χ 2(1) = 10.9, p<0.01).

Gait analysis (Figure 3): To determine whether *Gfa2*-CGG99 mice differed in basic gait parameters compared to wild-type controls, Treadscan data were analyzed for stance, swing and stride times, as well as for average running speed, right and left foot base and track width, coordination between feet, body rotation and range of motion for each foot (*i.e.,* longitudinal and lateral deviations). Analyses were carried out using a mixed-effect model with foot as within-subject and genotype as between-subject factors. For stance time, a measure of time each foot is in contact with the runway, a significant main effect was found for foot [$F_{(3, 84)}$ = 3.99, p<0.01] as well as a significant foot × genotype interaction [$F_{(3, 84)}$ = 3.16, p<0.05]. Post hoc analysis revealed *Gfa2*-CGG99 mice had shorter stance times for front-left [t(28) = 2.09, p<0.05] and rear-right [t(28) = 2.73, p<0.05] feet compared to WT controls. No significant differences were found for stride time or swing time between groups. For maximum longitudinal deviation which reflects range of motion, a significant main effect was found for genotype [$F_{(1,28)}$ = 7.94, p<0.01] as well as a significant foot × genotype interaction [$F_{(3,84)}$ = 3.18, p<0.05]. Individual comparisons for each foot showed that the maximum longitudinal deviation was significantly shorter in *Gfa2*-CGG99 mice for the front-left [t(28) = 3.42, p<0.01], front-right [t(28) = 2.33, p<0.05] and rear-right [t(28) = 2.66, p<0.05], indicating a shortened range of motion for the *Gfa2*-CGG99 versus WT mice. No other significant differences were found between genotypes for any other measures, including stride-time, stance-time, swing-time, overall stride-length, front or rear stance-width, running-speed and step-angle. When adjusted for body weight differences these gait effects were no longer statistically significant.

Ladder rung test (Figure 4): *Gfa2*-CGG99 mice made significantly more foot slips while crossing the ladder run apparatus compared to WT controls. A one way ANCOVA with body weight and locomotor activity as covariates showed that this difference between groups was statistically significant [$F_{(1,26)}$=27.6, p<0.001].

Elevated plus maze: For measures of anxiety, no differences were found for the number of entries [open arms: t(28) = 0.88; closed arms: t(28) = 0.70], latency to first enter [open arms: t(28) = 1.69; closed arms: t(28) = 1.20] or total time spent in the open [t(28) = 0.05] and closed [t(28) = 0.80] chambers of the elevated plus maze (p>0.05 for all measures). Similarly, in the open-field locomotor task, *Gfa2*-CGG99 mice did not differ from WT mice in the total time spent in the center [t(28) = 1.24], time spent in the margin [t(28) = 1.24] and total number of entries into the center [t(28) = 0.69, p>0.2 for all].

References

1. Hagerman, R.J. and P.J. Hagerman, *The fragile X premutation: into the phenotypic fold.* Curr Opin Genet Dev, 2002. **12**(3): p. 278-83.
2. Hagerman, R.J., et al., *Intention tremor, parkinsonism, and generalized brain atrophy in male carriers of fragile X.* Neurology, 2001. **57**(1): p. 127-30.
3. Jacquemont, S., et al., *Fragile X premutation tremor/ataxia syndrome: molecular, clinical, and neuroimaging correlates.* Am J Hum Genet, 2003. **72**(4): p. 869-78.
4. Hagerman, P.J. and R.J. Hagerman, *Fragile X-associated tremor/ataxia syndrome (FXTAS).* Ment Retard Dev Disabil Res Rev, 2004. **10**(1): p. 25-30.
5. Sellier, C., et al., *Sequestration of DROSHA and DGCR8 by expanded CGG RNA repeats alters microRNA processing in fragile X-associated tremor/ataxia syndrome.* Cell Rep, 2013. **3**(3): p. 869-80.
6. Kearse, M.G. and P.K. Todd, *Repeat-associated non-AUG translation and its impact in neurodegenerative disease.* Neurotherapeutics, 2014. **11**(4): p. 721-31.
7. Sellier, C., et al., *Translation of Expanded CGG Repeats into FMRpolyG Is Pathogenic and May Contribute to Fragile X Tremor Ataxia Syndrome.* Neuron, 2017. **93**(2): p. 331-347.
8. Berry-Kravis, E., et al., *Fragile X-associated tremor/ataxia syndrome: clinical features, genetics, and testing guidelines.* Mov Disord, 2007. **22**(14): p. 2018-30, quiz 2140.
9. Hagerman, R.J., et al., *Neuropathy as a presenting feature in fragile X-associated tremor/ataxia syndrome.* Am J Med Genet A, 2007. **143A**(19): p. 2256-60.
10. Brunberg, J.A., et al., *Fragile X premutation carriers: characteristic MR imaging findings of adult male patients with progressive cerebellar and cognitive dysfunction.* AJNR Am J Neuroradiol, 2002. **23**(10): p. 1757-66.
11. Greco, C.M., et al., *Neuropathology of fragile X-associated tremor/ataxia syndrome (FXTAS).* Brain, 2006. **129**(Pt 1): p. 243-55.
12. Greco, C.M., et al., *Neuronal intranuclear inclusions in a new cerebellar tremor/ataxia syndrome among fragile X carriers.* Brain, 2002. **125**(Pt 8): p. 1760-71.
13. Tassone, F., et al., *Intranuclear inclusions in neural cells with premutation alleles in fragile X associated tremor/ataxia syndrome.* J Med Genet, 2004. **41**(4): p. e43.
14. Foote, M.M., M. Careaga, and R.F. Berman, *What has been learned from mouse models of the Fragile X Premutation and Fragile X-associated tremor/ataxia syndrome?* Clin Neuropsychol, 2016. **30**(6): p. 960-72.
15. Hunsaker, M.R., et al., *Motor deficits on a ladder rung task in male and female adolescent and adult CGG knock-in mice.* Behav Brain Res, 2011. **222**(1): p. 117-21.
16. Van Dam, D., et al., *Cognitive decline, neuromotor and behavioural disturbances in a mouse model for fragile-X-associated tremor/ataxia syndrome (FXTAS).* Behav Brain Res, 2005. **162**(2): p. 233-9.
17. Castro, H., et al., *Selective rescue of heightened anxiety but not gait ataxia in a premutation 90CGG mouse model of Fragile X-associated tremor/ataxia syndrome.* Hum Mol Genet, 2017. **26**(11): p. 2133-2145.

18. Hunsaker, M.R., et al., *Temporal ordering deficits in female CGG KI mice heterozygous for the fragile X premutation.* Behav Brain Res, 2010. **213**(2): p. 263-8.
19. Hunsaker, M.R., et al., *Progressive spatial processing deficits in a mouse model of the fragile X premutation.* Behav Neurosci, 2009. **123**(6): p. 1315-24.
20. Brouwer, J.R., et al., *CGG-repeat length and neuropathological and molecular correlates in a mouse model for fragile X-associated tremor/ataxia syndrome.* J Neurochem, 2008. **107**(6): p. 1671-82.
21. Wenzel, H.J., et al., *Ubiquitin-positive intranuclear inclusions in neuronal and glial cells in a mouse model of the fragile X premutation.* Brain Res, 2010. **1318**: p. 155-66.
22. Willemsen, R., et al., *The FMR1 CGG repeat mouse displays ubiquitin-positive intranuclear neuronal inclusions; implications for the cerebellar tremor/ataxia syndrome.* Hum Mol Genet, 2003. **12**(9): p. 949-59.
23. Berman, R.F., et al., *Mouse models of the fragile X premutation and fragile X-associated tremor/ataxia syndrome.* J Neurodev Disord, 2014. **6**(1): p. 25.
24. Schluter, E.W., et al., *Distribution and frequency of intranuclear inclusions in female CGG KI mice modeling the fragile X premutation.* Brain Res, 2012. **1472**: p. 124-37.
25. Buijsen, R.A., et al., *FMRpolyG-positive inclusions in CNS and non-CNS organs of a fragile X premutation carrier with fragile X-associated tremor/ataxia syndrome.* Acta Neuropathol Commun, 2014. **2**: p. 162.
26. Todd, P.K., et al., *CGG repeat-associated translation mediates neurodegeneration in fragile X tremor ataxia syndrome.* Neuron, 2013. **78**(3): p. 440-55.
27. Brenner, M., et al., *GFAP promoter directs astrocyte-specific expression in transgenic mice.* J Neurosci, 1994. **14**(3 Pt 1): p. 1030-7.
28. Hua, Y., Sahashi, K., Rigo, F., Hung, G., Horev, G. Bennett, C.F. , *Peripheral SMN restoration is essential for long-term rescue of a severe SMA mouse model.* Nature, 2012. **478**(7367): p. 123-126.
29. Wenzel, H.J., C.T. Tamse, and P.A. Schwartzkroin, *Dentate development in organotypic hippocampal slice cultures from p35 knockout mice.* Dev Neurosci, 2007. **29**(1-2): p. 99-112.
30. Wenzel, H.J., et al., *Ultrastructural localization of zinc transporter-3 (ZnT-3) to synaptic vesicle membranes within mossy fiber boutons in the hippocampus of mouse and monkey.* Proc Natl Acad Sci U S A, 1997. **94**(23): p. 12676-81.
31. Palay, S.L. and V. Chan-Palay, *Cerebellar cortex: cytology and organization.* 1974, Berlin, Heidelberg, New York,: Springer. xii, 348 p.
32. Brouwer, J.R., et al., *Elevated Fmr1 mRNA levels and reduced protein expression in a mouse model with an unmethylated Fragile X full mutation.* Exp Cell Res, 2007. **313**(2): p. 244-53.
33. Berman, R.F. and R. Willemsen, *Mouse models of fragile x-associated tremor ataxia.* J Investig Med, 2009. **57**(8): p. 837-41.
34. Entezam, A., et al., *Regional FMRP deficits and large repeat expansions into the full mutation range in a new Fragile X premutation mouse model.* Gene, 2007. **395**(1-2): p. 125-34.
35. Westergard, T., et al., *Cell-to-Cell Transmission of Dipeptide Repeat Proteins Linked to C9orf72-ALS/FTD.* Cell Rep, 2016. **17**(3): p. 645-652.

36. Gokden, M., J.T. Al-Hinti, and S.I. Harik, *Peripheral nervous system pathology in fragile X tremor/ataxia syndrome (FXTAS).* Neuropathology, 2009. **29**(3): p. 280-4.
37. Etherton, M.R., et al., *Mouse neurexin-1alpha deletion causes correlated electrophysiological and behavioral changes consistent with cognitive impairments.* Proc Natl Acad Sci U S A, 2009. **106**(42): p. 17998-8003.
38. Kwon, C.H., et al., *Pten regulates neuronal arborization and social interaction in mice.* Neuron, 2006. **50**(3): p. 377-88.
39. Nakatani, J., et al., *Abnormal behavior in a chromosome-engineered mouse model for human 15q11-13 duplication seen in autism.* Cell, 2009. **137**(7): p. 1235-46.
40. Chadman, K.K., et al., Minimal aberrant behavioral phenotypes of neuroligin-3 R451C knockin mice. Autism Res, 2008. 1(3): p. 147-58.
41. Rothwell, P.E., et al., *Autism-associated neuroligin-3 mutations commonly impair striatal circuits to boost repetitive behaviors.* Cell, 2014. **158**(1): p. 198-212.
42. Tydlacka, S., et al., *Differential activities of the ubiquitin-proteasome system in neurons versus glia may account for the preferential accumulation of misfolded proteins in neurons.* J Neurosci, 2008. **28**(49): p. 13285-95.
43. Christopherson, K.S., et al., *Thrombospondins are astrocyte-secreted proteins that promote CNS synaptogenesis.* Cell, 2005. **120**(3): p. 421-33.
44. Chung, W.S., N.J. Allen, and C. Eroglu, *Astrocytes Control Synapse Formation, Function, and Elimination.* Cold Spring Harb Perspect Biol, 2015. **7**(9): p. a020370.
45. Risher, W.C., et al., *Astrocytes refine cortical connectivity at dendritic spines.* Elife, 2014. **3**.
46. Ilieva, H., M. Polymenidou, and D.W. Cleveland, *Non-cell autonomous toxicity in neurodegenerative disorders: ALS and beyond.* J Cell Biol, 2009. **187**(6): p. 761-72.
47. Lobsiger, C.S. and D.W. Cleveland, *Glial cells as intrinsic components of non-cell-autonomous neurodegenerative disease.* Nat Neurosci, 2007. **10**(11): p. 1355-60.
48. Sofroniew, M.V. and H.V. Vinters, *Astrocytes: biology and pathology.* Acta Neuropathol, 2010. **119**(1): p. 7-35.
49. Primerano, B., et al., *Reduced FMR1 mRNA translation efficiency in fragile X patients with premutations.* RNA, 2002. **8**(12): p. 1482-8.
50. Iwahashi, C.K., et al., *Protein composition of the intranuclear inclusions of FXTAS.* Brain, 2006. **129**(Pt 1): p. 256-71.
51. Eng, L.F. and R.S. Ghirnikar, *GFAP and astrogliosis.* Brain Pathol, 1994. **4**(3): p. 229-37.
52. McLendon, R.E. and D.D. Bigner, *Immunohistochemistry of the glial fibrillary acidic protein: basic and applied considerations.* Brain Pathol, 1994. **4**(3): p. 221-8.
53. Su, M., et al., *Expression specificity of GFAP transgenes.* Neurochem Res, 2004. **29**(11): p. 2075-93.
54. Garden, G.A. and A.R. La Spada, *Intercellular (mis)communication in neurodegenerative disease.* Neuron, 2012. **73**(5): p. 886-901.
55. Desplats, P., et al., *Inclusion formation and neuronal cell death through neuron-to-neuron transmission of alpha-synuclein.* Proc Natl Acad Sci U S A, 2009. **106**(31): p. 13010-5.

56. Loria, F., et al., *alpha-Synuclein transfer between neurons and astrocytes indicates that astrocytes play a role in degradation rather than in spreading.* Acta Neuropathol, 2017. **134**(5): p. 789-808.
57. Coulter, D.A. and T. Eid, *Astrocytic regulation of glutamate homeostasis in epilepsy.* Glia, 2012. **60**(8): p. 1215-26.
58. Custer, S.K., et al., *Bergmann glia expression of polyglutamine-expanded ataxin-7 produces neurodegeneration by impairing glutamate transport.* Nat Neurosci, 2006. **9**(10): p. 1302-11.
59. Zu, T., et al., *Non-ATG-initiated translation directed by microsatellite expansions.* Proc Natl Acad Sci U S A, 2011. **108**(1): p. 260-5.
60. Banez-Coronel, M., et al., *RAN Translation in Huntington Disease.* Neuron, 2015. **88**(4): p. 667-77.

CHAPTER 3

3

Lack of a clear behavioral phenotype in an inducible FXTAS mouse model despite the presence of neuronal FMRpolyG-positive aggregates

Saif N. Haify[1*], Ruchira S.D. Mankoe[1,2], Valerie Boumeester[1], Esmay C. van der Toorn[1], Rob F.M. Verhagen[1], Rob Willemsen[1], Renate K. Hukema[1,3], Laurens W.J. Bosman[2*]

[1] Department of Clinical Genetics, Erasmus MC, Rotterdam, Netherlands.
[2] Department of Neuroscience, Erasmus MC, Rotterdam, The Netherlands
[3] Department of Health Care Studies, Rotterdam University of Applied Sciences, Rotterdam, the Netherlands

[*] Corresponding authors: Saif N. Haify (s.haify@erasmusmc.nl) and Laurens W.J. Bosman (l.bosman@erasmusmc.nl)

Frontiers in Molecular Biosciences 2020 Dec 14;7:599101

Abstract

Fragile X-associated tremor and ataxia syndrome (FXTAS) is a rare neurodegenerative disorder caused by a 55 – 200 CGG repeat expansion in the 5' untranslated region of the *Fragile X mental retardation 1* (*FMR1*) gene. FXTAS is characterized by progressive cerebellar ataxia, Parkinsonism, intention tremors and cognitive decline. The main neuropathological hallmark of FXTAS is the presence of ubiquitin-positive intranuclear inclusions in neurons and astrocytes throughout the brain. The molecular pathology of FXTAS involves the presence of 2-8-fold elevated levels of *FMR1* mRNA, and of a repeat-associated non-AUG (RAN) translated polyglycine peptide (FMRpolyG). Increased levels of *FMR1* mRNA containing an expanded CGG repeat can result in cellular toxicity by an RNA gain-of-function mechanism. The increased levels of CGG repeat-expanded *FMR1* transcripts may create RNA foci that sequester important cellular proteins, including RNA-binding proteins and FMRpolyG, in intranuclear inclusions. To date, it is unclear whether the FMRpolyG-positive intranuclear inclusions are a cause or a consequence of FXTAS disease pathology. In this report we studied the relation between the presence of neuronal intranuclear inclusions and behavioral deficits using an inducible mouse model for FXTAS. Neuronal intranuclear inclusions were observed four weeks after dox-induction. After 12 weeks, high numbers of FMRpolyG-positive intranuclear inclusions could be detected in the hippocampus and striatum, but no clear signs of behavioral deficits related to these specific brain regions were found. In conclusion, the observations in our inducible mouse model for FXTAS suggest a lack of correlation between the presence of intranuclear FMRpolyG-positive aggregates in brain regions and specific behavioral phenotypes.

Keywords: FXTAS, nuclear inclusions, mouse behavior, *FMR1*, repeat expansion

Introduction

Fragile X-associated tremor and ataxia syndrome (FXTAS) is a late-onset neurodegenerative disease that is characterized mainly by essential tremor, cerebellar ataxia, Parkinsonism, peripheral neuropathy and cognitive decline [1-4]. FXTAS leads to cerebral and cerebellar atrophy, with increased T2 signal intensity in MRI images of the middle cerebellar peduncles as diagnostic hallmark [5]. Carriers of a premutation in the *FMR1* gene, consisting of a 55-200 CGG repeat expansion, are at risk of developing FXTAS. Such intermediate repeat expansions lead to elevated levels of *FMR1* mRNA [6-8]. In contrast, longer repeat expansions, more than 200 units, induce silencing of *FMR1* mRNA, which results in a lack of FMRP protein, causing the neurodevelopmental Fragile X syndrome [6, 9].

Several mechanisms by which the premutation and the consequential increase in *FMR1* mRNA levels may lead to the development of FXTAS have been proposed. Of these, arguably the most studied process is the formation of intranuclear inclusions that has been very well documented in patients as well as in animal models and their occurrence has been linked to alterations at the cellular level in neurons and astrocytes [10-14]. The intranuclear inclusions are mainly composed of proteins and to date more than 200 different proteins have been identified in nuclear inclusions [13, 15]. *FMR1* mRNA containing a CGG repeat expansion, although present itself only in relatively low concentrations in the nuclear inclusions, could act as a scaffold binding place for the other components [13, 16, 17]. The putative pathogenicity of these inclusions could be based on depleting essential molecules, including RNA-binding proteins [11, 18-20]. Another, not necessarily mutually exclusive, potential pathogenic mechanism is repeat-associated non-AUG (RAN) translation through which a toxic polyglycine (FMRpolyG) protein is produced from the elongated *FMR1* CGG repeat mRNA [21-23]. To date, the relative contributions of the RNA-based inclusions and the expression of toxic FMRpolyG to human pathology are still matter of debate. It has even been suggested that in early disease state the inclusions may serve a protective function by sequestering FMRpolyG [4, 24].

Our current clinical, molecular and histopathological understanding of FXTAS in patients is mostly derived from studies in mouse models. Several mouse models have been generated to study the (neuro)pathology and behavioral effects of FXTAS. Initially two knock-in (KI) mouse models were generated: the Dutch (CGG_{dut}) and the NIH (CGG_{nih}) KI mouse model. Both KI mouse models display FXTAS pathology at the genetic, molecular, histological and behavioral level with slight differences. Both show ubiquitin-positive intranuclear inclusions throughout the entire brain, but these inclusions are more common in the CGG_{dut} KI mice. Behavioral examination of both CGG KI mice revealed memory impairment [25], increased levels of anxiety in the CGG_{dut} KI mice while CGG_{nih} KI mice show decreased levels of anxiety. Also, assessment of motor function in the

CGG_{dut} KI mouse model showed impairment with increasing age of the mice [26]. This observed cognitive decline and motor function impairment in these mice may reflect the progressive cognitive decline and functionality impairment observed in FXTAS patients. Although both KI mouse models nicely recapitulate FXTAS disease pathology, the time to generate a phenotype is a major disadvantage. It takes roughly up to 52-72 weeks before any phenotype is observed in these mice. Therefore, several transgenic mouse models were developed to study specific research questions of FXTAS disease pathology such as RAN-translation, mRNA containing expanded CGG repeat and potential therapeutic interventions. We refer the reader to more advanced and detailed reviews covering all available mouse models for the premutation and FXTAS [10, 14]. All these mouse models show presence of ubiquitin-positive and FMRpolyG-positive inclusions in the central nervous system (CNS) organs in neurons and astrocytes as well as in non-CNS organs, thus display the most prominent neuropathological hallmark in FXTAS disease pathology, with the notable exception of the intention tremor.

We studied the occurrence of intranuclear inclusions in a novel inducible mouse model for FXTAS, and related these to quantitative alterations in mouse behavior. To avoid interactions during development, we induced – in adult mice – the expression of a randomly integrated 103x CGG repeat expansion in the mouse under control of the neuron-specific Ca^{2+}/calmodulin-dependent protein kinase II alpha (*CamKII-α*) promoter. The *CamKII-α* driver induces expression throughout the entire forebrain, but also in several other regions in the cerebrum such as the hippocampus and the basal ganglia, which are regions known to be involved in FXTAS disease pathology [27, 28]. In this report we mainly focused on the dentate gyrus (DG) and CA3 region of the hippocampus, and the striatum, being part of the basal ganglia. These regions are believed to contribute to several behavioral impairments in FXTAS such as in motor learning and coordination, and memory [2, 10, 29]. Also, cognitive decline based on performance in spatial learning, memory tasks, executive motor function impairments and anxiety associated disorders are observed in premutation carriers and FXTAS patients [30]. For a period of 3 months after induction, we quantified the formation of inclusions in the brain and characterized the behavioral performance. As expected, and in line with the expression pattern of the *CamKII-α* promoter [31], we found intranuclear inclusions in the hippocampus and the striatum, already appearing 4 weeks after dox-induction. To our surprise, however, virtually no impact on behavioral performance was detectable even after 3 months of dox-induction. We therefore propose based on this study that intranuclear inclusions do not have an immediate detrimental effect on neuronal function and this may point to a protective function of inclusion formation in the early-onset of disease-progression in FXTAS.

Materials and Methods

Mice

For this study, male and female *CamKII-α*-rtTA/TRE-103CGG-GFP-mice with a C57BL6/J background were used (**Fig. 1A**). This CamKII-α inducible mouse model was generated similarly to the ubiquitous inducible mouse model by random integration of the transgenes in the genome [32]. The TRE-103CGG-GFP mice were crossed with the *CamKII-α*-rtTA driver line to generate double transgenic mice using the Tet-On system. Dox-treatment was initiated at the age of 9 weeks in these mice. Dox drinking water contained 2 mg/ml doxycycline hyclate (Sigma) in 5% sucrose (Sigma) and was refreshed every 2–3 days. All experiments involving mice were performed according to Dutch law and following institutional guidelines (Erasmus MC, Rotterdam, The Netherlands) in confirmation with EU directive 2010/63. Prior to the start of the experiments, project licenses were obtained from the national authority (Centrale Commissie Dierproeven, The Hague, the Netherlands) after review by an independent ethical committee (DEC Consult, Soest, The Netherlands) and filed under numbers AVD101002015290 and AVD1010020197846.

Genotyping

For genotyping, toe clips from P5-7 mice and, after sacrificing, lung tissue, were incubated overnight in 300 µl tail digestion buffer (TDB; 50 mM KCl, 10 mM Tris-HCl pH 9, 0.1% Triton X-100 and 0.15 µg proteinase K (Roche)) at 55°C. The following day, samples were heat inactivated for 5' at 95°C and centrifuged to remove debris. Next, 1 µl of supernatant was used as template DNA in PCR. Templates were checked for presence of rtTA and/or TRE. The following PCR mix was used: 10x FastStart DNA Polymerase buffer with MgCl2 (Roche), 25 mM dNTPs, primers (10 mM), FastStart DNA polymerase (5 U/µl; Roche) and sterilized water. The PCR program consisted of 4' denaturation at 94°C, followed by 30 cycles of amplification through 30" at 94°C, 30" at 60°C, and 90" at 72°C, and ended with 5' at 72°C. PCR products were visualized by adding 10 µl 3x loading mix (30% Orange G (Sigma), 0.2% GelRed (Biotium) in H_2O) to 5 µl of PCR product and separating using gel electrophoresis on a 1.5% agarose gel. Gels were scanned using Gel Doc XR+ (Bio-Rad) Molecular Imager with Image Lab software. The TRE transgene was amplified using forward primer 5'-GCTTAGATCTCTCGAGTTTAC-3' and reverse primer 5'-ATGGAGGTCAAAACAGCGTG-3'. The rtTA transgene was amplified using forward primer 5'-CAGCAGGCAGCATATCAAGGT-3' and reverse primer 5'-GCCGTGGGCCACTTTACAC-3'.

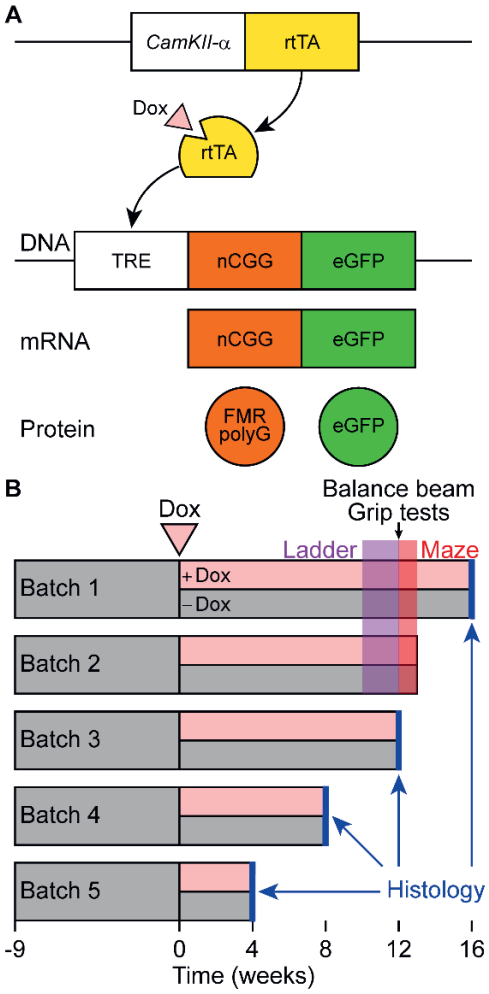

Figure 1 | Schematic representation of the Tet-On system and behavioral testing of a new brain-specific mouse model for FXTAS. (A) Brain-specific expression of the expanded CGG repeat RNA coupled to GFP was studied in the *CamKII-α*-rtTA/TRE-103CGG-GFP inducible mouse model with a C57BL6/J background. The Tet-On system was used to generate double transgenic mice expressing the expanded CGG repeat at the RNA level. Expression of the reverse tetracycline transactivator (rtTA) is controlled by the *CamKII-α* promoter on a separate transgene. Upon dox administration, rtTA will be activated and can bind the tet response element (TRE) on another transgene, which induces expression of the expanded CGG repeat at the RNA level and GFP at the protein level. As the transgene contains the 5'-UTR of the FMR1 gene with an expanded CGG repeat, the FMRpolyG polypeptide is produced from the expanded CGG repeat by RAN translation. **(B)** Schematic overview of the experimental schedule for histological analysis and behavioral testing. At around 9 weeks of age, dox-treatment started. Around 10 weeks later, ErasmusLadder tests were performed, followed by balance beam and grip tests. Finally, the mice were subjected to the Morris water maze test.

Repeat length PCR

Repeat length was determined according to an in-house PCR protocol. Brain tissue from mice having 11CGGs (positive control), wildtype mice (negative control) and TRE-103CGG-GFP 4 weeks old mice were incubated overnight in 300 µl tail mix buffer (50 mM Tris pH=7.5, 10 mM EDTA, 150 mM NaCl, 1% SDS and 20 µl proteinase K (10 mg/ml; Roche Cat. #3115852)) at 55°C. The next day, 100 µl 6M NaCl was added to the samples and samples were shaken very well to induce precipitation of cell debris. Samples were centrifuged (10.000g at RT for 10 minutes) to remove cell debris. The supernatant was transferred to a new tube and 1 ml 100% EtOH was added (shake very well). Tubes were centrifuged at 10.000g for 10 minutes to form DNA pellet. Next, the supernatant was discarded and DNA pellet was washed with 500 µl 70% EtOH. Samples were centrifuged at 10.000g for 5-10 minutes. The supernatant with EtOH was discarded and the DNA pellet was left to dry to the air for a couple of minutes. The DNA pellet was resuspended in 100 µl sterilized water. Next, 1 µl of supernatant was used as template DNA in the PCR reaction mix (total volume 21 µl). Following PCR mix was used: 10 µl Betaine (5 M), 4 µl 5x expand HF buffer without Mg, 1,5 µl $MgCl_2$ (25 mM) 1 µl forward primer (10 µM), 1 µl reverse primer (10 µM), 0,2 µl dNTP mix (100mM) (25mM each), 0,2 µl FastStart Taq DNA polymerase (5 U/µl; Roche) and 2,1 µl sterilized water. The PCR program consisted of 10' denaturation at 98°C, followed by 35 cycles of amplification through 35" at 98°C, 35" at 58°C and 3' at 72°C, and ended with a cooling step at 15°C. For quantification of the DNA size, 1 µl 1Kb Plus DNA ladder (ThermoFisher; Cat. # 10787018) was used with and without 0.2% GelRed (Biotium) in dH_2O. Staining with GelRed after electrophoresis run is necessary because GelRed interferes with the DNA and therefore influences CGG repeat measurement. To front track DNA separation during gel electrophoresis, 10 µl 30% Orange G (Sigma) loading dye was added to 5 µl of PCR product on the 1.5% agarose gel. After gel electrophoresis run, the agarose gel was stained for 30 minutes in 500 ml 1X TBE-buffer (1L 5X TBE-buffer: 54g Tris (CAS #77-86-1), 27.5g boric acid (CAS #10043-35-3) and 20 ml 0.5M EDTA pH=8.0 (CAS #60-00-4) + 50 µl 0.2% GelRed (Biotium). Gels were scanned using Gel Doc XR+ (Bio-Rad) Molecular Imager with Image Lab software. The CGG repeat was amplified using the following forward primer 5'-ATCCACGCTGTTTTGACCTC-3' and reverse primer 5'-CCAGTGCCTCACGACCAAC-3'.

RNA isolation and cDNA synthesis

RNA isolation was performed on dox and sucrose treated 16 weeks old *CamKII-α*-rtTA/TRE-103CGG-GFP mice. Per treatment group n=3 brains were used for RNA isolation. Prior to lysing, samples were thawed on ice and supplied with RIPA-buffer containing 0.05% protease inhibitors (Roche), 0.3% 1M DTT (Invitrogen) and 40U RNase Out (Roche). Samples were mechanically lysed, followed by 30 minutes of incubation on ice. After 30 minutes of incubation, mechanical lysing was repeated to ensure total homogenization. Homogenate was added to RNA Bee (Tel-Test) in a 1:10 (v/v) ratio and mixed thoroughly. Chloroform

(Millipore) was added to mixture in a 1:5 ratio (v/v), mixed thoroughly and incubated on ice for 15 minutes. After incubation the mixture was centrifuged for 15 minutes at 4°C and supernatant was collected and supplied with 0,6x (v/v) 100% 2-propanol (Honeywell). After 15 minutes centrifugation at 4°C, supernatant was discarded. Remaining pellet was washed with 80% EtOH (Honeywell) in duplicate with brief centrifugation at 4°C between washes. Following removal of residual supernatant, 50 µl dH_2O was added and concentration was determined using the Nanodrop 2000 (ThermoFisher).

Quantitative Real-Time PCR

Reverse transcriptase (RT) was performed using 1 µg of RNA with the iScript cDNA synthesis kit (Biorad) according to manufacturer's instructions. RNA was treated with DNase before cDNA synthesis. Q-PCR using iTaq Supermix (BioRad) was performed on 0.1 µl RT product. Cycling conditions were an initial denaturation of 3 minutes at 95°C, followed by 35 cycles of each 5 seconds at 95°C and 30 seconds at 60°C. As a reference gene GAPDH was used. For statistical analysis the two-sample unpaired t-test assuming equal variance was used.

Immunohistochemical staining

Tissues were fixed overnight in 4% paraformaldehyde (PFA) at 4°C and embedded in paraffin according to in-house protocols. Sections of 6 µm were cut and placed on silane coated slides (Klinipath). The sections were deparaffinized in decreasing concentrations of alcohol - starting with xylene and ending in demineralized H_2O - before performing antigen retrieval by microwave treatment in 0.01 M sodium citrate (pH=6). Endogenous peroxidase activity was blocked with 0.6% H_2O_2 in PBS. When staining for FMRpolyG an additional incubation with proteinase K (5 µg/ml) was performed for 20-30' at 37°C to ensure optimal antibody binding. Staining was performed overnight at 4°C with primary antibodies diluted in PBS/0.5% milk/0.15% glycine (PBS+). Staining with secondary antibodies was performed at RT for 60'. Antigen-antibody complexed were visualized using DAB-substrate (DAKO), after which slides were counterstained with haematoxylin for 5' and subsequently mounted with Entellan (Merck Milipore International). Antibodies used are listed in table 1 hereafter.

Table 1: Antibodies

Target	Dilution	Host	Source	Catalogue nr.
FMRpolyG (8FM)	1:10	Mouse	Gift from N. Charlet-Berguerand, IGBMC	X
GFP	1:2000	Mouse	Roche	11814460 001

Mouse specific anti-GFP and anti-FMRpolyG (8FM) antibodies were used to visualize GFP expression and the FMRpolyG protein aggregates in mouse brain respectively.

Behavioral testing

Muscle function was tested using a hanging wire test. A metal wire with a diameter of 2 mm was suspended around 20 cm above a cage. The mouse was brought to the wire so that he could grasp the wire with his front paws after which the latency to fall was recorded. The maximal trial duration was 60 s. In addition, we used the Bioseb grip strength test (Bioseb, Vitrolles, France). For this test, the mouse was placed on a metal grid and after he clamped to the grid with all four limbs, he was gently pulled down by the base of his tail. The maximal force was measured and the average of three consecutive trials was calculated.

The fine motor coordination of the mice was tested on the balance beam. During two consecutive days, the mice were habituated to the setup that consisted of a horizontal wooden beam with a diameter of 12 mm and a length of 100 cm located approximately 50 cm above a table. Each mouse was placed on one side of the beam and walked over the beam to a home cage at the other side of the beam. After two trials, the beam was replaced by one with a diameter of 8 mm and also on this beam two trials were performed. On the third day, the performance of the mice was quantified by counting the number foot slips and falls. Each mouse crossed each beam twice and the average time required to reach the other side of the beam was measured, taking only trials without falls into account.

Locomotor patterns were recorded on a horizontal ladder flanked by two plexiglass walls spaced 2 cm apart (ErasmusLadder, Noldus, Wageningen, The Netherlands) as described previously [33].

The ladder consisted of two rows of 37 rungs placed in an alternated high/low pattern. The rungs were spaced 15 mm apart and the height difference between high and low rungs was 9 mm. Each rung was connected to a pressure sensor recording rung touch. During a trial, the mouse had to walk from a shelter box on one side of the ladder to another on the other end. Trial start was indicated by lighting an LED in the shelter box followed three seconds later by a strong tail wind. Early escapes, thus before the LED was switched on, were discouraged as they triggered a strong head wind. In between trials, there was a resting period. Mice were first habituated to the setup by letting them freely explore the ladder for 15 min during which no light or air cues were given. On the next day, training started with 44 trials on each day. The initial training consisted of 6 daily sessions, after which the mice were measured once a week. Sensor touches were filtered to delete single backsteps or fake hind limb steps using the factory settings. For the further analysis, we used the touches of the front limbs with the first and the last step of each trial being deleted.

Using the water maze test, we quantified the spatial memory of the mice. Each mouse was placed on the border of a circular pool with a diameter of 120 cm filled with a mixture of water and non-toxic white paint kept constant at 26 °C. In the pool, a platform with a diameter of 11 cm diameter was hidden 1 cm below the water surface. The time to find the platform was recorded on two trials each day on five consecutive days. When the mouse did not find the platform within 60 s, the trial was stopped. On days 6 and 7, a probe trial was given. During the probe trials, the platform was absent and the mice were allowed to swim for 60 s while their trajectory was tracked (EthoVision XT11, Noldus, Wageningen, The Netherlands). The data of the probe trials were analyzed by subdividing the pool in four quadrants, with the original position of the platform in the middle of quadrant 3. We marked the original platform position as well as the same shape at the corresponding position in the other three quadrants and counted how often the mouse passed the borders of each of these positions per trial. We considered a crossing if it involved more than 50% of the body of the mouse. On top of that, we also quantified the time spent in each quadrant. The battery of behavioral tests is schematically represented in time in **Figure 1B**.

Statistics

Behavioral performance on each paradigm was compared between mice treated with and without doxycycline. The statistical tests used are mentioned in the Results section, whereby we used non-parametric tests for data that were not normally distributed. Throughout the manuscript, we considered a *p* value of 0.05 or less as indication for statistical significance.

Results

Expanded CGG expression results in inclusion formation in the hippocampus and basal ganglia

First of all, we studied the expression pattern of the FMRpolyG-GFP fusion protein in *CamKII-α*-rtTA/TRE-103CGG-GFP mice after induction of transgene expression by the addition of doxycycline (dox) to the drinking water. First, repeat length in the transgene was verified using an in-house PCR protocol. Repeat length PCR shows the repeat size of 103x CGGs at approximately 480 bp compared to the control 11x CGGs length at 290 bp (**Fig. S1A**). To verify whether dox treatment did not affect murine *Fmr1* mRNA expression, we performed quantitative real-time PCR on brain tissue of treated and control mice. The data show that dox treatment had no effect on *Fmr1* mRNA expression in the brain as tested in the hippocampus (**Fig. S1B**). Since the transgene expression was under the *CamKII-α* promoter, we expected the FMRpolyG protein to be present in neurons of, among other regions, the hippocampus, the neocortex, the basal ganglia, and in the

posterior part of the cerebellum, more specifically lobule X [27, 30]. In our hands, already after 4 weeks of dox treatment, GFP expression, indicative of FMRpolyG expression, was found in all aforementioned brain regions. After 12 weeks of dox treatment, the expanded CGG repeat was strongly expressed in the striatum of the basal ganglia, the hippocampus, the neocortex, and lobule X of the cerebellum (**Fig. 2A-B, D-E**). Low to modest expression of GFP was present at 12 weeks in the hypothalamus, the colliculus inferior and superior (**Fig. 2C-D**), and other sub-regions of the midbrain.

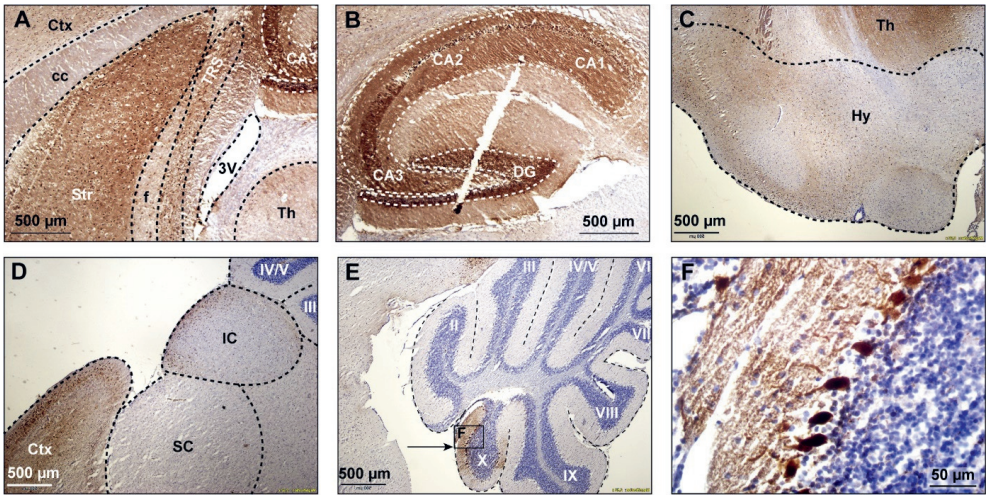

Figure 2 | GFP expression in multiple brain regions. GFP expression (brown staining) was visualized using immunohistochemical staining with a mouse specific anti-GFP antibody in sagittal brain sections at 12 weeks after onset of dox-treatment. Strong expression of GFP was present in the striatum **(A)**, the hippocampus **(B),** the hypothalamus **(C)** and the cerebral cortex **(D)**. Lower levels of expression were present in the superior and inferior colliculus **(D)**. In the cerebellum, GFP expression was only observed in vermal lobule X **(E**, indicated area amplified in **F)**. 3V = third ventricle; cc = corpus callosum, Ctx = cerebral cortex, DG = dentate gyrus, f = fornix, Hy = hypothalamus, IC = inferior colliculus, SC = superior colliculus, Str = striatum, Th = thalamus, TRS = triangular nucleus of the septum.

Next, we investigated whether FMRpolyG expression was associated with the formation of nuclear inclusions in the *CamKII-α*-rtTA/TRE-103CGG-GFP mice. To this end, we compared brain sections stained for FMRpolyG from mice that did receive dox with those from mice that did not. As expected, we could not detect any inclusions in the control mice. However, the mice treated with dox developed spherical FMRpolyG-positive inclusions in most of the brain regions in which GFP expression was observed. The highest density of inclusions was found in the striatum, the CA3 region of the hippocampus and the hypothalamus (**Fig. 3B-D**). Lower densities were present in the DG region of the hippocampus, as well as in the inferior and the superior colliculus (**Fig. 3A, E**). We did not observe a perfect correlation between GFP expression and the occurrence of inclusions: in lobule X of the

cerebellum, no inclusions were found despite the presence of GFP (**Fig. 2E-F**). In general, during 12 weeks of dox treatment, the number of inclusions increased over time with regional differences. Quantification of FMRpolyG-positive inclusions (**Fig. 3F**) was only done in the hippocampus and the striatum of the basal ganglia, since these regions are known to be involved in FXTAS disease pathology [28]. Irrespective of the brain region involved, most inclusions were located intranuclearly. Sometimes two or more smaller inclusions were located in the same nucleus. In summary, dox induced the production of CGG RNA in *CamKII-α*-rtTA/TRE-90CGG-GFP mice in several brain regions, which resulted in the formation of FMRpolyG-positive nuclear inclusions, predominantly in the striatum and the hippocampal CA3 region.

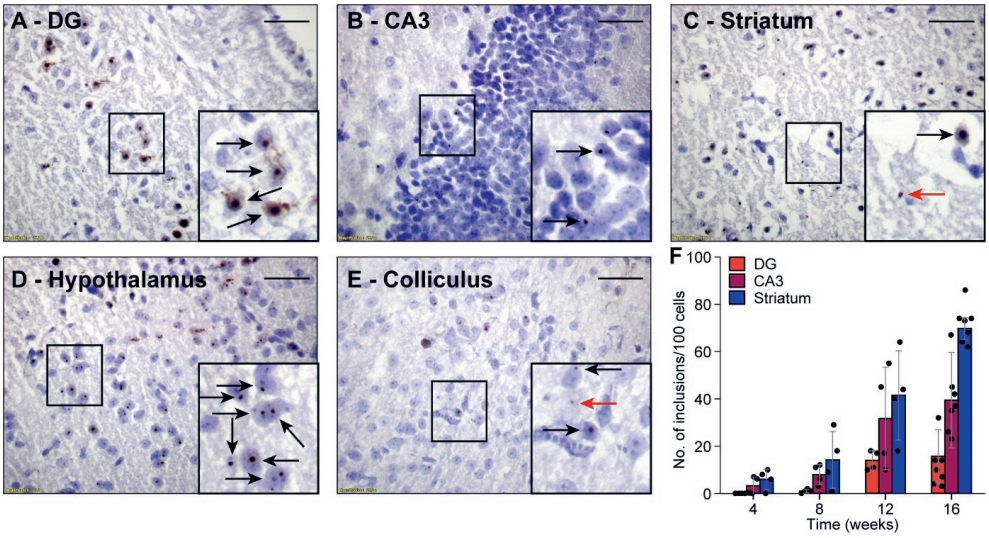

Figure 3 | FMRpolyG-positive inclusions are predominantly located in the nucleus. FMRpolyG-positive inclusions, visible as black dots, were stained using the mouse anti-FMRpolyG (8FM) antibody. Most often, the FMRpolyG-positive inclusions were observed in the nuclei (black arrows) but occasionally also outside the nuclei (red arrows). FMRpolyG-positive inclusions were found in the dentate gyrus **(DG, A)** and the CA3 region of the hippocampus **(B)**, the striatum **(C)**, the hypothalamus **(D)** and in the colliculi **(E)**. Rectangles indicate areas enlarged in insets. Scale bars = 50 µm. **(F)** The prevalence of FMRpolyG-positive inclusions increased over time after onset of dox treatment. Bars indicated average values and error bars the SD.

Absence of behavioral phenotype in mice expressing FMRpolyG-positive inclusions

To test whether the expression of the CGG repeat and the resulting nuclear inclusions had any impact on mouse behavior, we subjected the mice to a battery of behavioral tests. To control for possible confounding problems with the general condition of the mice, we first tested the muscle strength using the hanging wire and the Bioseb grip strength tests 12

weeks after the start of the dox treatment. The latency to fall was 22.0 ± 11.0 vs. 26.5 ± 10.2 s (control vs. dox mice, averages ± s.d., p=0.385, t = 0.944, df = 17, *t* test **Fig. 4A**) during the hanging wire test and the force was 1.79 ± 0.37 vs. 1.53 ± 0.39 N (control vs. dox mice, averages ± s.d., p=0.336, t = 0.991, df = 17, *t* test **Fig. 4B**) during the Bioseb grip strength test. We therefore conclude that there were no indications for changes in muscle strength due to the dox treatment.

Next, we tested the overall motor control and balance on the balance beam after 12 weeks of dox treatment. The numbers of hind foot slips per trial were comparable between control and dox mice (thick beam: 2.0 (inter-quartile range (IQR): 1.5) vs. 1.5 (IQR: 0.9), p=0.876, U = 47.5; thin beam: 1.0 (IQR: 1.4) vs. 2.5 (IQR: 2.5), p=0.220, U = 33.5, medians, Mann-Whitney tests, **Fig. 4C**). Also, the time required to cross the beam were not really different between control and dox mice (thick beam: 8.3 (IQR: 2.5) vs. 7.0 (IQR: 1.9) s, p=0.593, U = 42.5; thin beam: 9.8 (IQR: 8.6) vs. 12.5 (IQR: 9.1), p=0.820, U = 46.5, medians, Mann-Whitney tests, **Fig. 4C**). We take this as a sign that the treatment did not impair the overall motor control and ability to keep balance.

We continued by describing the behavior on the ErasmusLadder, which is a horizontal ladder consisting of two rows of rungs in an alternating high/low pattern spanning the space between two shelter boxes. After habituation and initial training, we measured the performance at 10, 11 and 12 weeks after the start of dox treatment. The start of each trial was indicated by switching on an LED in the start box and this was followed by a strong tail wind 3 s later. In roughly 75% of the trials, the mice waited until the tail wind started before leaving the start box. Leaving upon perception of the visual cue or even before that was observed less often. Changes in this pattern could be a sign of cognitive impairment [34], but these were not observed between control and dox mice (p=0.516, 3x2 Fisher's exact test, **Fig. 4D**).Next, we characterized the stepping pattern on the ErasmusLadder. Wild type C57BL/6J mice have a tendency to avoid the lower rungs and typically make steps from one high rung to the next or the second next high rung [33].

We considered these small and regular steps, respectively. Long steps, skipping at least two higher rungs, and lower rung steps occurred much less often, as did other irregular steps such as backwards walking. Thus, also regarding the stepping pattern, no impact of the dox treatment was observed (**Table 2, Fig. 4E-G**).

Table 2: Step size statistics for the ErasmusLadder

	Treatment	Median	IQR	*p*	F	df	Test
Step lengths [%}							
Short steps [step size = 2]	-Dox	6.4	15.8	0.687	0.168	1	Repeated measures ANOVA
	+Dox	7.1	22.8				
Regular steps [step size = 4]	-Dox	76.1	14.2	0.699	0.154	1	Repeated measures ANOVA
	+Dox	77.2	22.0				
Long steps [step size ≧ 6]	-Dox	3.4	7.9	0.688	0.166	1	Repeated measures ANOVA
	+Dox	5.1	4.1				
Lower rung steps	-Dox	1.7	0.9	0.153	2.226	1	Repeated measures ANOVA
	+Dox	2.3	0.8				
Backsteps	-Dox	1.3	1.0	0.629	0.241	1	Repeated measures ANOVA
	+Dox	2.1	1.8				
Step times [ms]							
Short steps [step size = 2]	-Dox	303	82	0.751	0.104	1	Repeated measures ANOVA
	+Dox	346	101				
Regular steps [step size = 4]	-Dox	251	59	0.588	0.304	1	Repeated measures ANOVA
	+Dox	261	75				

The percentages of steps to higher rungs, being either short, regular or long, as well as those to lower steps (irrespective of stride length), and backward steps were compared at 10, 11 and 12 weeks after onset of dox treatment. Note that the percentages do not add to 100% as some irregular types of steps were not considered here (in particular, steps starting from lower rungs). Of the two most frequent step categories, also the step times are indicated and compared. The values were first calculated per mouse, and then compared between the two groups (n=10 mice/group). The median and interquartile range (IQR) values in this table refer to the recording session at 12 weeks after onset of dox treatment. All values refer to front paw movements. *P* values reflect the between-subject comparisons of repeated measures ANOVAs. Since not a single *p* value was close to the threshold for significance, no correction for multiple comparisons was applied.

Finally, to test for putative defects in spatial memory formation, we subjected the mice to the Morris water maze test around 12 weeks after the start of the dox treatment. During five consecutive days, the mice were trained to find a hidden platform just below the surface of an opaque, circular pool. Over the sessions, both control and dox-treated mice managed to be faster in finding the hidden platform, with no statistically significant differences between the two groups (p=0.134, $F_{1,17}$ = 2.479, repeated measures ANOVA, **Fig. 4H**). On the next two days, the experiment was repeated – but without a hidden platform. On these probe trials we made video recordings of the mice (**Fig. 4I**). First, we counted how often the mice crossed location where the hidden platform had been during the training sessions and compared these with crosses of the analogous locations in the other three quadrants. During the first probe trial, both control and dox treated mice had a preference for the real location (in quadrant 3) over the other areas (control: 2.2 ± 1.5

crosses per trial of the real location vs. 1.0 ± 0.9 crosses of the other locations, p=0.021, U = 60.5, Mann-Whitney test, dox mice 2.0 ± 2.2 vs. 0.6 ± 0.7 crosses, averaged ± ss, p=0.107, U = 101.5, Mann-Whitney test, control vs. dox mice: p=0.813, χ^2 = 0.95, χ^2 test). During the second probe trial, the preference of the control mice for the real location was gone (1.8 ± 1.2 vs. 1.6 ± 1.3 crosses, p=0.624, U = 108.0, Mann-Whitney test), but remained present in the dox treated mice (3.3 ± 2.3 vs. 1.1 ± 1.1 crosses per trial, p=0.005, U = 63.0, Mann-Whitney test). This difference between control and dox mice was on the border of statistical significance (p=0.061, χ^2 = 7.36, χ^2 test, **Fig. 4J**). This might indicate that the dox-treated mice had more trouble understanding that the hidden platform was no longer in place. This, however, was not reflected in the relative dwell times per quadrant (p=1.00, $F_{1.17}$ = 0.000, repeated measures ANOVA), which leads us to conclude that also the Morris water maze did not reveal convincing differences in behavior due to activation of the premutation.

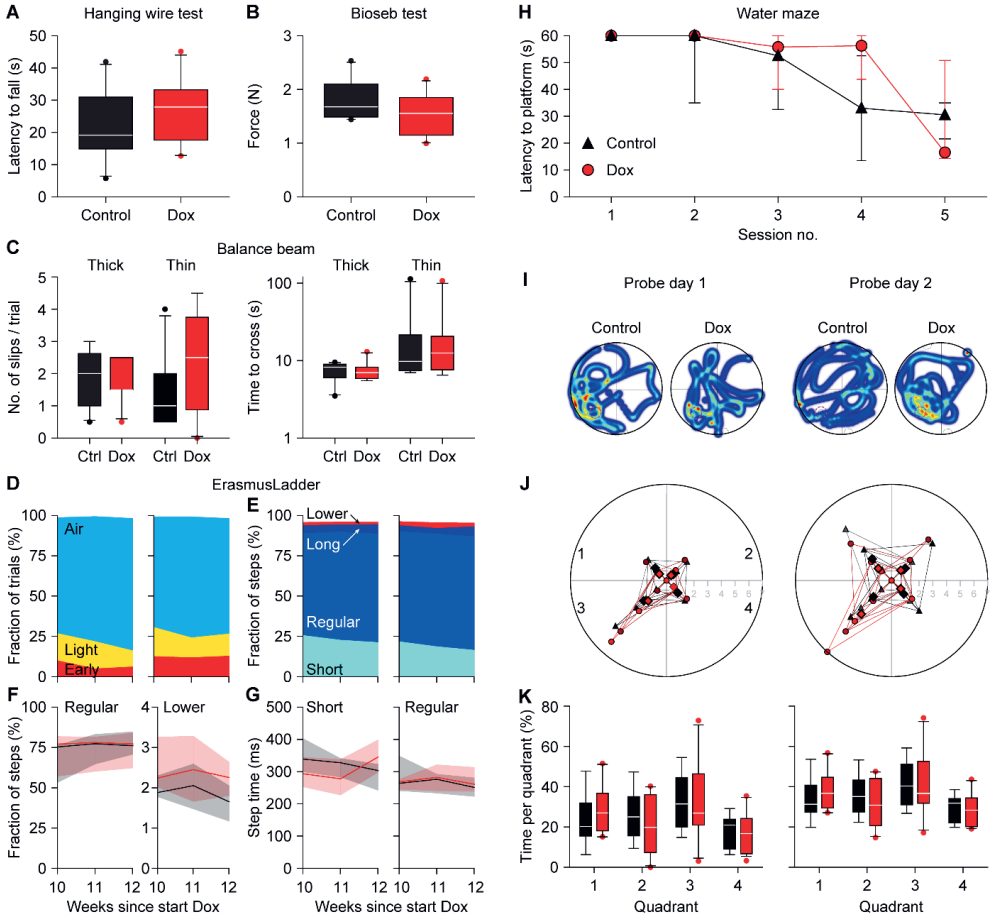

Figure 4 | Absence of a clear behavioral phenotype in dox-treated mice. Neither the hanging wire test **(A)** nor the Bioseb grip strength test **(B)** demonstrated an impact of dox-treatment on muscle strength. **(C)** Also, the balance beam test failed to find consistent differences in either the number of slips (left) or the time to cross (right). The tests were performed on a thick (12 mm diameter) and a thin (8 mm diameter) wooden beam. **(D)** On the ErasmusLadder, trial starts were indicated by lighting an LED in the start box, followed 3 s later by a strong tail wind. The fraction of trials with starts before the visual cue ("Early"), during the visual cue ("Light") or after the start of the tail wind ("Air") were comparable between control and dox-treated mice. Data recorded at 10, 11 and 12 weeks after the start of dox-treatment. **(E)** The ErasmusLadder consists of alternating high and low rungs. The fractions of short steps (from one high rung to the next), regular steps (from one high rung to the second high rung), long steps (from on high rung to another, skipping at least two) and lower rung touches were also similar for both groups, as further illustrated for the fraction of regular steps and lower rung touches **(F)** as well as for step times **(G)**. The data in **F**-**G** show the medians with the shades indicating the inter-quartile range. See Table 2 for a more extensive statistical analysis of the ErasmusLadder test. **(H)** In the water maze, the mice had to find a platform hidden just below the water surface. As the water was made opaque, the mice could not see the platform. During five consecutive training days, the latency to find the platform decreased both in control and dox-treated mice. **(I)** On the next two days, the hidden platform was removed (probe trials) and the trajectories of the mice were recorded. The heat maps indicate the time spent

per area of two exemplary mice. The original location of the hidden platform is indicated by a pink dashed circle in quadrant 3. **(J)** On the first probe day, the mice crossed the location where the hidden platform had been more often than the analogous regions of the other quadrants. On the second day, the control mice no longer searched more often in the area where the hidden platform had been (p=0.624, Mann-Whitney test), while the dox-treated mice kept searching specifically around the location where the hidden platform had been (p=0.005, Mann-Whitney test). **(K)** This retention, however, was not noticeable when comparing the times spent per quadrant. Unless indicated otherwise, behavioral tests were performed during the 12th week of dox-treatment. Group sizes were 10 mice.

Discussion

Wide-spread occurrence of nuclear inclusions is a major hallmark of FXTAS. To date, it is a matter of debate whether these inclusions contribute to cellular pathology in FXTAS, or – in contrast – slow down the disease process by sequestering toxic RNA and proteins. Such a protective function has been suggested for FXTAS [4, 24], but also for other protein-aggregation disorders, such as Huntington's disease and SCA1 [35-38]. To study the relation between the development of intranuclear inclusions and behavioral deficits, we used a novel, inducible and neuron-specific mouse model for FXTAS under the control of the *CamKII-α* promoter. Expression of an expanded 103CGG repeat RNA transgene is induced by dox and is under the control of the Tet-On system. This inducible mouse model shows no evidence of expression in the absence of dox (*i.e.,* no leakage of expression), and was induced after completion of normal development to avoid interaction with developmental processes. Within a month after transgene induction, FMRpolyG-positive nuclear inclusions were found in the striatum and the CA3 region of the hippocampus. Two months after the occurrence of the first nuclear inclusions, the inclusions were abundant in most brain areas in which the *CamKII-α* promoter is active such as the hippocampus, neocortex and the striatum. Yet, we could not identify a robust behavioral phenotype that could be caused by the inclusion pathology in these mice. Several mouse models have significantly contributed to our understanding of the molecular mechanisms underlying FXTAS and have characterized disease progression. Previously, we found in a different inducible mouse model for FXTAS, using the heterogeneous nuclear ribonucleoproteins (*hnRNP*) promoter, a rapid death after dox-induction. The neuronal level of transgene expression in these mice was low, and nuclear inclusions were sparse or even absent in the brain [32]. In contrast, in a third mouse line, under control of the brain-specific protease-resistant-protein (*PrP*) promoter, we observed both the formation of nuclear inclusions and behavioral deficits [39].

These mice developed only a deficit in the compensatory eye movement pathway after 20 weeks of treatment with dox. Although expression of the transgene containing the expanded CGG repeat mRNA was found in the hippocampus, lobule X of the cerebellum

and the striatum, these expression levels were low with the exception of lobule X of the cerebellum where expression was the most profound. Together, these results lead us to question whether the development of nuclear inclusions is indeed the cause of developing FXTAS symptoms. Therefore, we developed a new inducible transgenic mouse model under the control of the *CamKII-α* promoter expecting stronger expression in the brain.

In our *CamKII-α*-rtTA/TRE-103CGG-GFP mouse model, the expression of GFP followed that of the previously described distribution of the *CamKII-α* promoter [27]. Immunohistochemical staining shows the strongest GFP expression in the striatum, the CA3 region of the hippocampus and lobule X of the cerebellum. Moderate GFP expression was found in the neocortex, the dentate gyrus, the hypothalamus and several midbrain areas. In all of these regions, with the notable exception of the cerebellum, also nuclear inclusions were formed. If nuclear inclusions in these areas would result in functional deficits, a broad range of behavioral impairments is to be expected. As a consequence, typical cerebellar symptoms, although prominent in FXTAS patients [1-4], were not expected in our mouse model since the *CamKII-α* is only expressed in a very limited part of the cerebellum. We therefore focused on spatial learning, that has previously been shown to be affected in a knock-in mouse model ('the Dutch mouse') [25, 26], and striatal motor coordination functions, as they also occur as Parkinsonism in patients [1].

An intact hippocampus is essential for normal spatial learning in the water maze [40-42]. Our mice showed no, or only marginal, deficits at the water maze test, arguing against a severely impaired hippocampal function. The striatum is vital for motor control and striatal damage leads to impaired behavior on the balance beam [43, 44], which was not observed in our mice. This lack of an effect on motor coordination was further substantiated by equal performance of treated and control mice on the ErasmusLadder and the grip tests. Although we cannot exclude that there were subtle behavioral deficits that we did not observe, it is safe to state that there were no major changes in behavioral performance in spite of the abundance of nuclear inclusion in the dox treated mice.

The expanded CGG RNA and proteins can aggregate with many other molecules into nuclear inclusions [13]. The expanded CGG RNA on itself is not enough to induce toxicity and that the production of an out-of-frame FMRpolyG protein due to RAN translation is necessary for cellular toxicity [22, 45-47]. Our present results indicate that the development of FMRpolyG-positive nuclear inclusions themselves are probably not very detrimental to the function of neurons. It remains to be seen whether aggregation is an active process, aimed at sequestering toxic molecules and thereby slowing down the disease progression, or more an epiphenomenon that is a physical consequence of the molecular structure of the expanded CGG RNA and/or RAN translation protein FMRpolyG.

Contribution to the Field Statement

FXTAS is a neurodegenerative disorder that results in, among others, cerebellar ataxia, Parkinsonism and cognitive decline. A striking feature of FXTAS is the appearance of intranuclear inclusion in brain cells. FXTAS is caused by a moderately long repeat expansion in the *FMR1* gene. The resultant elongated mRNA and protein are present in the inclusions, where they form aggregates with many more molecules. It is as yet unclear whether these nuclear inclusions are cause of consequence of FXTAS. In our study, we employed a novel inducible mouse model for FXTAS that shows, after induction, a rapid occurrence of nuclear inclusions but even months later they did not display any obvious sign of behavioral deficits, even not after careful quantification. We conclude therefore that the formation of nuclear inclusions has no or limited acute impact on the functionality of neurons. The appearance of nuclear inclusions may therefore rather be a consequence than the cause of FXTAS.

Conflict of Interest

The authors declare that the research was conducted in the absence of any commercial or financial relationships that could be construed as a potential conflict of interest.

Author Contributions

S.N.H., R.K.H. and L.W.J.B. conceived the project. S.N.H., R.S.D.M., E.C.T., V.B., R.F.M.V. performed the experiments. S.N.H., R.S.D.M., R.W., R.K.H. and L.W.J.B. analyzed the data. S.N.H., R.W. and L.W.J.B. wrote the manuscript with input from all authors. R.W. contributed to funding by ZonMw grant the ANR-14-RARE-0003 E-RARE 'Drug_FXSPreMut'.

Acknowledgments

We thank Nicolas Charlet-Berguerand for the nCGG-GFP plasmids and the FMRpolyG 8FM mouse monoclonal antibody.

Supplementary Figures

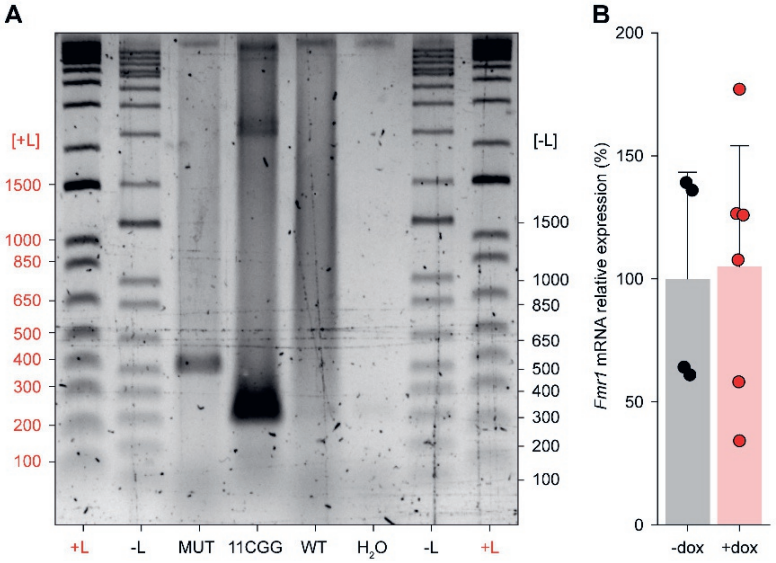

Figure S1 | CGG repeat length verification and *Fmr1* mRNA expression in dox-induced transgenic mice. (A) Gel electrophoresis analysis shows that the CGG repeat length in the *CamKII-α*-rtTA/TRE-103CGG-GFP transgenic mice is in the premutation range. Repeat length PCR shows the repeat size of 103x CGGs and 11x CGGs at approximately 480 bp and 290 bp, respectively. +L = Ladder with GelRed; -L = Ladder without GelRed; MUT = TRE-103CGG-GFP (mouse ID: 20464-1); 11CGG = normal repeat length (positive control); WT = wildtype (negative control); H_2O = water control. **(B)** Quantification of *Fmr1* mRNA expression in the hippocampus of dox-induced (n=3) and control (sucrose; n=2) mice 16 weeks after start of the dox treatment. Dox-induction does not affect *Fmr1* mRNA expression levels in these transgenic mice. Measurements were repeated twice with the same conditions using q-RT-PCR and normalized to the average level found in the control-dox mice.

References

1. Hagerman, R.J., et al., *Intention tremor, parkinsonism, and generalized brain atrophy in male carriers of fragile X.* Neurology, 2001. **57**(1): p. 127-30.
2. Hagerman, R. and P. Hagerman, *Advances in clinical and molecular understanding of the FMR1 premutation and fragile X-associated tremor/ataxia syndrome.* Lancet Neurol, 2013. **12**(8): p. 786-98.
3. Tassone, F., et al., *CGG repeat length correlates with age of onset of motor signs of the fragile X-associated tremor/ataxia syndrome (FXTAS).* Am J Med Genet B Neuropsychiatr Genet, 2007. **144B**(4): p. 566-9.
4. Hagerman, R.J. and P. Hagerman, *Fragile X-associated tremor/ataxia syndrome - features, mechanisms and management.* Nat Rev Neurol, 2016. **12**(7): p. 403-12.
5. Brown, S.S.G. and A.C. Stanfield, *Fragile X premutation carriers: A systematic review of neuroimaging findings.* J Neurol Sci, 2015. **352**(1-2): p. 19-28.
6. Salcedo-Arellano, M.J., et al., *Fragile X syndrome and associated disorders: Clinical aspects and pathology.* Neurobiol Dis, 2020. **136**: p. 104740.
7. Tassone, F., et al., *Elevated levels of FMR1 mRNA in carrier males: a new mechanism of involvement in the fragile-X syndrome.* Am J Hum Genet, 2000. **66**(1): p. 6-15.
8. Kenneson, A., et al., *Reduced FMRP and increased FMR1 transcription is proportionally associated with CGG repeat number in intermediate-length and premutation carriers.* Hum Mol Genet, 2001. **10**(14): p. 1449-54.
9. Bassell, G.J. and S.T. Warren, *Fragile X syndrome: loss of local mRNA regulation alters synaptic development and function.* Neuron, 2008. **60**(2): p. 201-14.
10. Haify, S.N., et al., In silico, *in vitro, and in vivo Approaches to Identify Molecular Players in Fragile X Tremor and Ataxia Syndrome.* Front Mol Biosci, 2020. **7**: p. 31.
11. Jin, P., et al., *Pur a binds to rCGG repeats and modulates repeat-mediated neurodegeneration in a Drosophila model of fragile X tremor/ataxia syndrome.* Neuron, 2007. **55**(4): p. 556-64.
12. Louis, E., et al., *Parkinsonism, dysautonomia, and intranuclear inclusions in a fragile X carrier: a clinical-pathological study.* Mov Disord, 2006. **21**(3): p. 420-5.
13. Ma, L., et al., *Composition of the Intranuclear Inclusions of Fragile X-associated Tremor/Ataxia Syndrome.* Acta Neuropathol Commun, 2019. **7**(1): p. 143.
14. Berman, R.F., et al., *Mouse models of the fragile X premutation and fragile X-associated tremor/ataxia syndrome.* J Neurodev Disord, 2014. **6**(1): p. 25.
15. Iwahashi, C.K., et al., *Protein composition of the intranuclear inclusions of FXTAS.* Brain, 2006. **129**(Pt 1): p. 256-71.
16. Cid-Samper, F., et al., *An Integrative Study of Protein-RNA Condensates Identifies Scaffolding RNAs and Reveals Players in Fragile X-Associated Tremor/Ataxia Syndrome.* Cell Rep, 2018. **25**(12): p. 3422-3434 e7.
17. Langdon, E.M., et al., *mRNA structure determines specificity of a polyQ-driven phase separation.* Science, 2018. **360**(6391): p. 922-927.

18. Qurashi, A., et al., *Nuclear accumulation of stress response mRNAs contributes to the neurodegeneration caused by Fragile X premutation rCGG repeats.* PLoS Genet, 2011. **7**(6): p. e1002102.
19. Sellier, C., et al., *Sequestration of DROSHA and DGCR8 by expanded CGG RNA repeats alters microRNA processing in fragile X-associated tremor/ataxia syndrome.* Cell Rep, 2013. **3**(3): p. 869-80.
20. Sofola, O.A., et al., *RNA-binding proteins hnRNP A2/B1 and CUGBP1 suppress fragile X CGG premutation repeat-induced neurodegeneration in a Drosophila model of FXTAS.* Neuron, 2007. **55**(4): p. 565-71.
21. Todd, P.K., et al., *CGG repeat-associated translation mediates neurodegeneration in fragile X tremor ataxia syndrome.* Neuron, 2013. **78**(3): p. 440-55.
22. Sellier, C., et al., *Translation of Expanded CGG Repeats into FMRpolyG Is Pathogenic and May Contribute to Fragile X Tremor Ataxia Syndrome.* Neuron, 2017. **93**(2): p. 331-347.
23. Krans, A., et al., *Neuropathology of RAN translation proteins in fragile X-associated tremor/ataxia syndrome.* Acta Neuropathol Commun, 2019. **7**(1): p. 152.
24. Greco, C.M., et al., *Neuropathology of fragile X-associated tremor/ataxia syndrome (FXTAS).* Brain, 2006. **129**(Pt 1): p. 243-55.
25. Hunsaker, M.R., et al., *Progressive spatial processing deficits in a mouse model of the fragile X premutation.* Behav Neurosci, 2009. **123**(6): p. 1315-24.
26. Van Dam, D., et al., *Cognitive decline, neuromotor and behavioural disturbances in a mouse model for fragile-X-associated tremor/ataxia syndrome (FXTAS).* Behav Brain Res, 2005. **162**(2): p. 233-9.
27. Wang, X., et al., *Distribution of CaMKIIalpha expression in the brain in vivo, studied by CaMKIIalpha-GFP mice.* Brain Res, 2013. **1518**: p. 9-25.
28. Greco, C.M., et al., *Neuronal intranuclear inclusions in a new cerebellar tremor/ataxia syndrome among fragile X carriers.* Brain, 2002. **125**(Pt 8): p. 1760-71.
29. Scaglione, C., et al., *MRI and SPECT of midbrain and striatal degeneration in fragile X-associated tremor/ataxia syndrome.* J Neurol, 2008. **255**(1): p. 144-6.
30. Hasegawa, S., et al., *Transgenic up-regulation of alpha-CaMKII in forebrain leads to increased anxiety-like behaviors and aggression.* Mol Brain, 2009. **2**: p. 6.
31. Burgin, K.E., et al., *In situ hybridization histochemistry of Ca2+/calmodulin-dependent protein kinase in developing rat brain.* J Neurosci, 1990. **10**(6): p. 1788-98.
32. Hukema, R.K., et al., *Induced expression of expanded CGG RNA causes mitochondrial dysfunction in vivo.* Cell Cycle, 2014. **13**(16): p. 2600-8.
33. Vinueza Veloz, M.F., et al., *Cerebellar control of gait and interlimb coordination.* Brain Struct Funct, 2015. **220**(6): p. 3513-36.
34. Vinueza Veloz, M.F., et al., *The effect of an mGluR5 inhibitor on procedural memory and avoidance discrimination impairments in Fmr1 KO mice.* Genes Brain Behav, 2012. **11**(3): p. 325-31.
35. Saudou, F., et al., *Huntingtin acts in the nucleus to induce apoptosis but death does not correlate with the formation of intranuclear inclusions.* Cell, 1998. **95**(1): p. 55-66.
36. Klement, I.A., et al., *Ataxin-1 nuclear localization and aggregation: role in polyglutamine-induced disease in SCA1 transgenic mice.* Cell, 1998. **95**(1): p. 41-53.

37. Cummings, C.J., et al., *Mutation of the E6-AP ubiquitin ligase reduces nuclear inclusion frequency while accelerating polyglutamine-induced pathology in SCA1 mice.* Neuron, 1999. **24**(4): p. 879-92.
38. Arrasate, M., et al., *Inclusion body formation reduces levels of mutant huntingtin and the risk of neuronal death.* Nature, 2004. **431**(7010): p. 805-10.
39. Hukema, R.K., et al., *Reversibility of neuropathology and motor deficits in an inducible mouse model for FXTAS.* Hum Mol Genet, 2015. **24**(17): p. 4948-57.
40. Okada, K. and H. Okaichi, *Functional differentiation and cooperation among the hippocampal subregions in rats to effect spatial memory processes.* Behav Brain Res, 2009. **200**(1): p. 181-91.
41. D'Hooge, R. and P.P. De Deyn, *Applications of the Morris water maze in the study of learning and memory.* Brain Res Brain Res Rev, 2001. **36**(1): p. 60-90.
42. Laeremans, A., et al., *Distinct and simultaneously active plasticity mechanisms in mouse hippocampus during different phases of Morris water maze training.* Brain Struct Funct, 2015. **220**(3): p. 1273-90.
43. Shear, D.A., et al., *Comparison of intrastriatal injections of quinolinic acid and 3-nitropropionic acid for use in animal models of Huntington's disease.* Prog Neuropsychopharmacol Biol Psychiatry, 1998. **22**(7): p. 1217-40.
44. Feng, Q., et al., *Specific reactions of different striatal neuron types in morphology induced by quinolinic acid in rats.* PLoS One, 2014. **9**(3): p. e91512.
45. Derbis, M., et al., *Quantitative Evaluation of Toxic Polyglycine Biosynthesis and Aggregation in Cell Models Expressing Expanded CGG Repeats.* Front Genet, 2018. **9**: p. 216.
46. Galloway, J.N. and D.L. Nelson, *Evidence for RNA-mediated toxicity in the fragile X-associated tremor/ataxia syndrome.* Future Neurol, 2009. **4**(6): p. 785.
47. Hashem, V., et al., *Ectopic expression of CGG containing mRNA is neurotoxic in mammals.* Hum Mol Genet, 2009. **18**(13): p. 2443-51.

CHAPTER 4

Small molecule *1a* reduces FMRpolyG-mediated toxicity in *in vitro* and *in vivo* models for *FMR1* premutation

Saif N. Haify[1*#], Ronald A.M. Buijsen[1,2#], Lucas Verwegen[1,3#], Lies-Anne W.F.M. Severijnen[1], Helen de Boer[1], Valerie Boumeester[1], Roos Monshouwer[1], Wong Y. Yang[4], Michael D. Cameron[4], Rob Willemsen[1], Matthew D. Disney[4], Renate K. Hukema[1,5]

[1] Department of Clinical Genetics, Erasmus MC, Rotterdam, the Netherlands
[2] Department of Human Genetics, LUMC, Leiden, the Netherlands
[3] Department of Cell Biology, Erasmus MC, Rotterdam, the Netherlands
[4] Department of Chemistry, Scripps Research Institute, Florida, the United States
[5] Department of Health Care Studies, Rotterdam University of Applied Sciences, Rotterdam, the Netherlands

[#] These authors contributed equally to this work
[*] Corresponding author: Saif N. Haify (s.haify@erasmusmc.nl)

Manuscript accepted for Human Molecular Genetics 2021

Abstract

Fragile X-associated tremor and ataxia syndrome (FXTAS) is a late-onset progressive neurodegenerative monogenetic disorder characterized by tremors, ataxia, and neuropsychological problems. This disease is quite common in the general population with approximately 20 million carriers worldwide. The chances of developing FXTAS increases dramatically with age, with about 45% of male carriers over the age of 50 being affected. FXTAS is caused by a CGG repeat expansion (CGG_{exp}) in the *FMR1* gene. CGG_{exp} RNA is translated into the FMRpolyG protein by a mechanism called RAN translation. Although both gene and pathogenic trigger are known, no therapeutic interventions are available at this moment. Here we present for the first time primary hippocampal neurons derived from the ubiquitous inducible mouse model used as a screening tool for targeted interventions. A promising candidate is the repeat binding, RAN translation blocking, small molecule *1a*. Small molecule *1a* shields the disease-causing CGG_{exp} from being translated into the toxic FMRpolyG protein. Primary hippocampal neurons formed FMRpolyG-positive inclusions, and upon treatment with *1a* the number of FMRpolyG-positive inclusions are reduced. We also describe for the first time the formation of FMRpolyG-positive inclusions in the liver of this mouse model. Treatment with *1a* reduced the insoluble FMRpolyG protein fraction in the liver but not the number of inclusions. Moreover, *1a* treatment had a reducing effect on the number of Rad23b-positive inclusions and insoluble Rad23b protein levels. These data suggest that targeted small molecule therapy is effective in a FXTAS mouse model and has potential to treat CGG_{exp}-mediated diseases, including FXTAS.

Keywords: *FMR1* premutation, Therapeutic intervention, Small molecule 1a, Primary neuron model, Inducible mouse model

Introduction

Fragile X-associated tremor and ataxia syndrome (FXTAS) is a late-onset neurodegenerative disorder. FXTAS was first described in 2001 and is clinically characterized by progressive intention tremors and cerebellar gait ataxia. More severe cases include progressive cognitive decline, Parkinsonism, autonomic dysfunction and a spectrum of neuropsychiatric disorders [1-4]. FXTAS neuropathology includes mild brain atrophy, loss of Purkinje neurons and Bergmann gliosis [4-6]. Life expectancy is estimated to be between 5 and 25 years after disease onset [7]. In post-mortem brain tissue from patients with FXTAS the major pathological hallmark is the presence of ubiquitin-positive intranuclear inclusions throughout the brain, in both neurons and astrocytes [7, 8]. Pathology is not only limited to the central nervous system, but intranuclear inclusions are also found in non-central nervous system organs [9-15]. FXTAS is caused by a trinucleotide expansion of the CGG repeat (CGG_{exp}) in the 5'-untranslated region (UTR) of the *Fragile X mental retardation 1* (*FMR1*) gene [1, 16]. Healthy individuals have repeat numbers ranging from 5 to 55 CGGs. The repeat can expand throughout generations due to its instable nature to lengths varying from 55 to 200 CGGs in number [17]. These individuals are often referred to as premutation (PM) carriers. PM carriers have 2- to 8-fold elevated levels of *FMR1* mRNA and paradoxically slightly decreased Fragile X Mental Retardation protein (FMRP) levels [18-20]. Approximately 40% of male PM carriers over the age of 50 will eventually develop FXTAS while between 8-16% of female PM carriers develop FXTAS and are also at risk of developing Fragile X-associated Primary Ovarian Insufficiency (FXPOI) [21, 22]. The partial protective influence of the second non-expanded allele in female carriers results in a lower penetrance.

Although the exact mechanism of FXTAS remains unclear, it is generally accepted that two mechanisms most likely contribute to FXTAS pathogenesis [23]. A first mechanism is the toxic RNA gain-of-function mechanism that is supported by elevated levels of *FMR1* mRNA bearing an CGG_{exp} that by itself is toxic to cells. In this mechanism, CG-rich expansion transcripts form secondary hairpin-like structures that can sequester RNA-binding proteins (RBPs) such as the Src-Associated substrate in Mitosis of 68 kDa (SAM68), DROSHA and DGCR8 and heterogeneous nuclear ribonucleoprotein (hnRNP) sequester in inclusions resulting in depletion of these proteins in the cell, disturbing critical processes causing aberrant miRNA processing, altered RNA splicing, integrated stress response and immune effects [24-27]. When analyzing post-mortem brain tissue of FXTAS patients, *FMR1* mRNA is found in intranuclear inclusions as well as in isolated nuclei [14, 24]. The second mechanism is a protein gain-of-function mechanism as a result of Repeat-Associated Non-AUG (RAN) translation, which was first described for FXTAS in 2013 [28-30]. The mechanistic understanding of RAN-translation and RAN-proteins in FXTAS has increased tremendously through the use of cell models and several animal models.

FMRpolyG RAN translation in FXTAS initiates in a cap-dependent manner at a non-AUG near cognate start-codon (ACG) located before the CGG_{exp} in the 5'-UTR region of the *FMR1* gene [29]. Initiation in the +0 frame (FMRpolyR) can occur at an ACG codon located upstream of the repeat insertion site. However, FMRpolyR production is less than 1% of FMRpolyG expression [31]. Initiation in the +2 reading frame occurs within the repeat itself and results in a FMRpolyA protein. More recently evidence was found suggesting that the integrated stress response (ISR) effectively inhibits global canonical translation and selectively up-regulates RAN-translation in repeat expansion diseases [32].

Several overexpressing animal models have shown that FMRpolyG can be toxic and result in FXTAS disease-like phenotypes. One example is a *Drosophila* over-expression model showing that increased production of the FMRpolyG protein results in toxicity through a rough eye phenotype [29]. To understand the contribution of repeat bearing RNA molecules and the FMRpolyG protein in FXTAS, we have generated different mouse models for FXTAS [33-35]. We refer the reader for a recently published advanced review summarizing to date all known mouse models for FXTAS [36]. In an inducible mouse model with ubiquitous expression, both ubiquitin- and FMRpolyG-positive intranuclear inclusions were found and their number increased over time. Furthermore, it has been shown that, by stopping mutant RNA expression in a brain specific inducible mouse model, we can halt further disease progression. Strikingly, stopping mutant RNA expression early in the disease process results in reversible neuropathology [34]. This suggests that early intervention might be beneficial for FXTAS patients and PM carriers. Sellier and colleagues generated a mouse model expressing high levels of RNA with and without FMRpolyG expression. Mice with FMRpolyG expression showed locomotor deficits, including decreased mobility and obesity, and died at 10 months of age suggesting a direct role for FMRpolyG in CGG-RNA repeat-associated toxicity [33]. In addition, the RNA-only mice showed no phenotype. Toxicity of the FMRpolyG protein has also been linked with impairment of the ubiquitination proteasome degradation system (UPS) [37]. Several studies have shown that the FMRpolyG protein together with other prominent proteins such as HSP40, Rad23b and the 20S subunit of the proteasome were found within intranuclear inclusions in several FXTAS animal models as well as patient brain tissue. Intranuclear inclusions containing different toxic polypeptides have been linked with neuronal degradation in other neurodegenerative diseases [10, 29, 33, 34, 36, 38-40]. In fact, for some neurodegenerative diseases RAD23B is proposed as a neuropathological hallmark like in Huntington's disease (HD), Parkinson's disease (PD) and several Spinocerebellar Ataxia's (SCA) like SCA3 and SCA7 [39]. It is yet unclear why these other proteins are also present in these inclusions. Even though we have a fair understanding of the pathological mechanisms underlying FXTAS, there is no current cure available to stop disease progression in FXTAS patients. However, there are symptomatic therapies available for FXTAS patients. Certain medications that are usually associated with other

diseases help slow down progression of several symptoms seen in FXTAS patients [2]. For example, FXTAS patients with severe intention tremors could respond well to β-blockers, primidone, and topiramate. Moreover, intention tremors are aggravated by anxiety and stress, which are also symptoms often seen in FXTAS patients. Benzodiazepines such as alprazolam may therefore in some cases of FXTAS also be effective treating anxiety and tremors [41].

Previously, we reported a small chemical compound, *1a*, targeting the mRNA containing the expanded CGG repeat (CGG_{exp}). Compound *1a* shields the CGG repeat by binding GG-mismatch binding spots preventing both the binding of RNA-binding proteins to the hairpin structure and RAN translation. The compound showed promising results *in vitro* in transfected COS7 cells by improving FXTAS-associated pre-mRNA splicing defects and reducing the size and number of protein aggregates in COS7 cells [42].

To test the potential of *1a* in more disease relevant neuronal cellular model, we generated primary hippocampal neuronal cultures originating from a FXTAS mouse model. Here, we show that treatment using compound *1a* partially prevents inclusion formation in these neuronal cells. Moreover, we showed the rapid formation of inclusions in the liver of FXTAS mice ubiquitously expressing FMRpolyG which makes this a useful model for quick testing for intervention methods [42-44]. Next, we tested the potential of compound *1a in vivo*. Our data shows a clear effect on FMRpolyG insoluble protein levels in these mice. These results will contribute to the general understanding of FMRpolyG toxicity and initiate first steps in developing a potential new therapy.

Materials and Methods

Mice

Transgenic mice used in this study were obtained from crossing TRE-90CGG-eGFP mice with hnRNP-rtTA driver mice [35]. The TRE-90CGG-eGFP mice express the enhanced green fluorescent protein (eGFP) under the control of a tetracycline responsive promoter element (TRE). Before the eGFP sequence, a human *FMR1* 5'UTR containing 90CGG repeats was placed. Normally, this transgene translates into eGFP, but RAN translation may result in the production of FMRpolyG. Therefore, mRNA of this transgene translates into either eGFP (canonical translation) or FMRpolyG (RAN translation), much like *FMR1* mRNA in FXTAS can translate into either FMRP or FMRpolyG. Over multiple generations we never observed any repeat instability in these mice. The hnRNP-rtTA driver mice express the reverse tetracycline transcriptional activator (rtTA) under the control of a ubiquitously expressed hnRNP promoter, able to activate the TRE in the presence of dox. Both transgenic mouse lines were generated in a C57BL/6JRj background. Heterozygous mice from both lines

were crossed to obtain double transgenic TRE-90CGG-eGFP/hnRNP-rtTA mice (hereafter referred to as double transgenic mice) as well as non-transgenic or single transgenic littermate controls (hereafter referred to as NT mice). Animals were treated with dox (2 mg/ml doxycycline hyclate (Sigma) and 5% sucrose (Sigma)) or only sucrose (5% sucrose) in their drinking water starting between the ages of P24-27. Drinking water was kept from light and refreshed every 2-3 days to guarantee the stability of dox. Mice treated with compound *1a* (6.6 mg/ml in DMSO) were given a single intra-peritoneal (IP) injection at a dose of 10 mg/kg simultaneous with dox-induction. Animals injected with vehicle (DMSO) were used as control for compound *1a*. Due to the toxic nature of DMSO, its concentration was kept low. Animals in experiment were sacrificed upon sudden weight loss, or 7 days after dox-induction. Mice were housed at the Erasmus MC animal facility (Rotterdam, The Netherlands), under standard housing and husbandry conditions. All experiments were approved by the local welfare committee under license number AVD10100201529 and protocol number 15-290-05.

Genotyping

For regular genotyping, toe clips from P5-7 mice were incubated overnight in 300 µl tail digestion buffer (TDB; 50 mM KCl, 10 mM Tris-HCl pH 9, 0.1% Triton X-100 and 0.15 µg proteinase K (Roche)) at 55°C. The following day samples were heat inactivated for 5' at 95°C and centrifuged to remove debris. Next, 1 µl of supernatant was used as template DNA in PCR. Templates were checked for presence of rtTA and/or TRE. Following PCR mix was used (10x FastStart DNA Polymerase buffer with $MgCl_2$ (Roche), 25 mM dNTPs, primers (10 mM), FastStart DNA polymerase (5 U/µl; Roche), sterilized water). The PCR program consisted of 4 min denaturation at 94°C, followed by amplification through 30 sec at 94°C, 30 sec at 60°C, and 90 sec at 72°C, and ended with 5 min at 72°C. PCR products were visualized by adding 10 µl 3x loading mix (30% Orange G (Sigma), 0.2% Gelred (Biotium) in H2O) to 5 µl of PCR product and separating is using gel electrophoresis on a 1.5% agarose gel. Gels were scanned using Gel Doc™ XR+ (Bio-Rad) Molecular Imager with Image Lab™ software.

For validating CGG repeat size, DNA was isolated from lung tissue as described in section 'DNA isolation'. The DNA isolates were submitted to a touchdown PCR with Betaine, to stretch the secondary structure formed within the expanded repeat and allow amplification across the CGG repeat (5 M Betaine, primers, 10 mM), 25 mM dNTPs, 10x FastStart DNA Polymerase buffer with MgCl2 (Roche), FastStart DNA polymerase (5 U/µl; Roche), sterilized water). The PCR program consisted of an initial denaturation of 10 min at 95°C, followed a touchdown of 70-55°C through 60 sec at 95°C, 30 sec at 70°C (-1°C/cycle), and 5 min at 72°C, after which DNA was amplified through 30 cycles of 60 sec at 95°C, 60 sec at 60°C, and 5 min at 72°C, finalized by 10 min at 72°C. PCR products were visualized as

described above and compared to a positive control of known repeat size. Primers used are listed in **Table S1A**.

DNA isolation

Lung tissue was dissected from mice and put in a 300 µl aliquot of tail mix (50 mM Tris-HCl pH 7.5, 10 mM EDTA, 150 mM NaCl, 1% SDS and 20 µg proteinase K). Tissue was incubated at 55°C overnight. The next day 100 µl of 6M NaCl was added. The sample was shaken and centrifuged at 13.000 rpm (Thermo Scientific; Heraeus Fresco 17 #75002420; Rotor #75003424) for 10 min, after which supernatant was transferred to a new recipient. A 1 ml aliquot of 100% EtOH (ethanol) was added to the supernatant to precipitate DNA and centrifuged again at 13.000 rpm (Thermo Scientific; Heraeus Fresco 17 #75002420; Rotor #75003424) for 10 min. Supernatant was discarded, and pellet was rinsed with 500 µl 70% EtOH. Afterwards, the DNA pellet was air-dried and dissolved in 100 µl sterilized water. The DNA concentration was measured on a NanoDrop™ 2000/2000c spectrophotometer (Thermo Scientific).

Primary hippocampal neuronal culture

Culturing of primary hippocampal neurons was done according the isolation and culturing procedure described in detail by Seibenhener and Wooten [45]. In summary, pregnancies were scheduled using C57Bl/6J mice that are heterozygous hnRNP-rtTA or heterozygous TRE-nCGG-eGFP. A pregnant mouse at 17-19 days post-fertilization was first shortly anesthetized using isoflurane and euthanized by cervical dislocation. Up to 10 E17-E19 double transgenic embryos for hnRNP-rtTA/TRE-nCGG-eGFP were removed from the uteri and decapitated under a dissecting microscope after which the hippocampi were carefully isolated and placed in a culture dish with neurobasal medium (Gibco) supplemented with 1% penicillin/streptomycin (Gibco), 1% glutamax (Gibco) and 2% B27-supplement (Gibco). This medium is further referred to as NBM+++. Brain tissue from multiple pups was combined. Hippocampi were dissociated using Trypsin/EDTA. Prior to the dissection procedure 30 mm glass coverslips were subsequently coated with poly-D-lysine (100 µg/ml; Sigma) overnight or one hour prior to procedure followed by laminin (50 µg/ml; Sigma) for at least 30 minutes. Cells were plated on coated coverslips and attached to the substrate in a droplet of NBM+++. After 90 min the volume was adjusted to 2 ml per coverslip in a 6-well plate and the plates were stored at 37°C and 5% CO_2. To induce and maintain stable expression of 90CGG RNA in the primary hippocampal neurons, two µl dox (0.5 mM) was administered to the cultures on a regular daily bases for up to 21 days in culture. Daily administration is necessary to ensure stable induction of the transgene in the primary hippocampal neurons. Since dox is sensitive for light, working solutions of 0.5 mM were prepared and stored at 4°C in tinted bottles [46].

Compound *1a* treatment *in vitro*

Analyte *1a*, specifically 9-hydroxy-5,11-dimethyl-2-(2-(piperidin-1-yl)ethyl)-6H-pyrido[4,3-b]carbazol-2-ium, is a designer bioactive small molecule RNA binding probe that shields the expanded CGG repeats by binding the internal GG-mismatches preventing RAN-translation and the sequestration of proteins to the secondary hairpin-like structure formed by the repeat [42, 44]. For *in vitro* treatment compound *1a* was dissolved in DMSO at a final stock concentration of 2 µM. Each primary hippocampal culture was treated once with compound *1a*. One µl of compound *1a* was added to 2 ml NBM+++ culture medium the same day dox administration started or one week after dox-induction. Half-life of compound *1a* was determined in the liver and plasma using HPLC and LC-MS/MS analysis.

Tissue homogenization

Tissues were homogenized in 500 µl RIPA buffer (20 mM Tris-HCl, pH 7.5, 150 mM NaCl, 1% IGEPAL®, 0.01% sodium dodecyl sulphate (SDS), 1% sodium deoxycholate), containing complete protease inhibitor (Roche), 40 mM beta-mercaptoethanol, and 1 µl RNAse OUT (40 U/µl; Invitrogen). Homogenates were incubated for 30 min' on ice, of which 100 µl was added to 1 ml of TRIzol® reagent (Life technologies) for RNA isolation and the remainder was used for protein isolation.

RNA isolation

Tissue homogenates were made as described in section '*Tissue homogenization*'. 100 µl of homogenate was added to 1 ml of TRIzol™ reagent (Life technologies) and mixed thoroughly before adding 200 µl of chloroform, after which the mix was incubated on ice for 15 min'. Samples were spun down at 4°C, 13.000 rpm (Thermo Scientific; Heraeus Fresco 17 #75002420; Rotor #75003424) for 10 min and the aqueous phase of the mix - containing the RNA - was taken and put in a new recipient. To this aqueous phase 1 volume of isopropanol was added to precipitate RNA and mixed thoroughly before spinning down again under the same conditions. Pellets were rinsed twice with 80% EtOH and air-dried. Eventually the RNA pellets were dissolved in RNAse free water and RNA concentration was measured on a NanoDrop™ 2000/2000c spectrophotometer (Thermo Scientific).

Reverse Transcriptase (RT) Quantitative PCR

To measure relative mRNA levels in our samples we performed reverse transcriptase (RT) quantitative (q) PCR. The RT reaction was performed on 1 µg of RNA using the iScript cDNA synthesis kit (Bio-Rad) according to the manufacturer's instructions. Prior to the RT reaction, a DNAse treatment was performed on the samples to remove residual genomic DNA. The qPCR was performed on 0.7 µl of RT product using iTaq™ Universal SYBR® Green Supermix (Ratio 1:1.5; Bio-Rad) using the CFX96 Touch™ Real-Time PCR Detection System (Bio-Rad). GAPDH2 was used as a reference gene. The PCR program consisted of initial denaturation through 3 min at 95°C, amplification and readout through 40 cycles of 5 sec

at 95°C, 30 sec at 60°C, and plate reading, finalized by a melt curve. Primers are listed in **Table S1A**.

Protein isolation

Tissue homogenates were centrifuged at 4°C, 13.000 rpm (Thermo Scientific; Heraeus Fresco 17 #75002420; Rotor #75003424) for 20 min, after which a soluble and insoluble fraction were obtained. Of the soluble fraction of the homogenate the protein concentration was determined with a Pierce™ BCA Protein Assay Kit (Thermo Scientific). Homogenates were diluted to a concentration of 500 µg protein/µl and sample loading mix (0.25 M Tris-HCl pH 6.8, 8% SDS, 20% glycerol, 0.008% Bromophenol Blue, 3M beta-mercaptoethanol) was added to the isolates in a 1:4 ratio and mixes were heated at 95°C for 5 min. From there on samples were directly used for further analysis or stored at -80°C. For FMRpolyG and Rad23b analyses, sample loading mix was immediately added to the soluble fractions after which they were heated and stored for further analyses. Here the insoluble fraction was also saved and stored at -80°C to determine the amount of these proteins.

Western blot

Western blot analysis was performed to visualize protein and quantify their relative expression in our samples. Protein was isolated, sample loading mix was added, and samples were heated as described in section '*Protein isolation*'. Samples and a protein marker (Precision Plus Protein™ All Blue Standards; Bio-Rad) were run on a 16.5% Criterion pre-cast Tris-Tricine Peptide gel (Bio-Rad) using Tris/Tricine/SDS (TTS) running buffer (Bio-Rad) at 100-150 volts. Next, protein was transferred to a 0.2 µm nitrocellulose trans-blot membrane (Bio-Rad) using a Trans-Blot Turbo Transfer System (Bio-Rad). After transfer the blot was washed briefly with 0.1% Tween 20 in PBS (PBST) and then blocked for 30' with 5% milk (Protifar, Nutricia) in PBST. The blot was incubated with primary antibodies diluted in 5% milk/PBST overnight at 4°C. The next day the blot was rinsed with PBST before incubation with the secondary antibodies. Secondary antibodies were diluted in PBST and incubated for 60 min at RT. Next, the blot was rinsed with PBST and placed in dH_2O. Blots were scanned using a LI-COR Odyssey Imaging System and analysis was performed using LI-COR Odyssey 3.0 software. Antibodies used are listed in **Table S1B**.

Dot blot

To visualize and quantify proteins that are not found in the soluble fraction of tissue/cell lysates (*i.e.,* proteins in aggregates), we made use of dot blotting. Protein was isolated as described in section '*Protein isolation*' and insoluble fractions were obtained. The insoluble fractions were resuspended in 50-200 µl 20% SDS and incubated at 95°C for 160 min, after which the samples were diluted 3x with 2% SDS. Next, the insoluble fractions were run through a Bio-Dot Microfiltration Apparatus (Bio-Rad) using an Amersham Protran

0.2 µm nitrocellulose membrane (GE Life Sciences). Prior to loading the samples, the membrane was washed with 20% and 2% SDS respectively, and once more with 2% SDS after running the samples. Afterwards the blot was blocked in 5% milk/PBS for 30 min and incubated with a primary antibody diluted in 5% milk/PBS overnight at 4°C. The following day the blot was rinsed with PBS and incubated with a secondary antibody diluted in PBS at RT for 60 min. Next, the blot was rinsed again with PBS and placed in dH_2O. Blots were scanned using a LI-COR Odyssey Imaging System and analysis was performed using LI-COR Odyssey 3.0 software. To normalize for the amount of input on the dot blot, the soluble fractions accompanying the insoluble fractions used were processed for Western blot analysis as described in section '*Western blot*' and stained against a loading control (cofilin). Antibodies used are listed in **Table S1B**.

Determination of *1a* concentration in liver samples

Tissue samples were flash-frozen, shipped on dry ice, and stored at -80°C until analyzed. Samples were thawed on ice and homogenized in 3-times w:v water. Liver homogenate was mixed 1:3 with acetonitrile containing 100 nM carbamazepine as an internal standard. The sample was allowed to sit on ice for thirty minutes to precipitate proteins prior to filtration using a MultiScreen Solvinert 0.45 µm low-binding hydrophilic PTFE plate (Millipore). The filtrate was directly analyzed by LC–MS/MS using a Thermo BetaSil column, 2.1x50 mm, 5 µm. The analyte *1a* was detected on a Sciex 5500 mass spectrometer following mass transition Q1 = 375.1 AMU and Q2 = 84.2 AMU. Samples were compared to freshly prepared standards prepared in blank mouse liver homogenates. Concentration was determined as ng analyte per mg liver tissue. Density = 1 was assumed to convert to molarity (1 mg = 1 µl). Half-life of compound *1a* was determined in the liver and plasma using HPLC and LC-MS/MS analysis.

Immunological staining

Tissues were fixed overnight in 4% paraformaldehyde (PFA) at 4°C and embedded in paraffin according to in-house protocols. Sections of 6 µm were cut and placed on silane coated slides (Klinipath). The sections were deparaffinized in decreasing concentrations of alcohol, starting with xylene and ending in dH_2O, before performing antigen retrieval by microwave treatment in 0.01 M sodium citrate (pH 6). For immunohistochemical staining using DAB, endogenous peroxidase activity was blocked with 0.6% H_2O_2 in PBS. For fluorescent staining, sections were blocked in Sudan Black. When staining for FMRpolyG an additional incubation step with proteinase K (5 µg/ml) was performed for 20-30 min at 37°C. Immunostaining was performed overnight at 4°C with primary FMRpolyG antibodies diluted in PBS/0.5% milk/0.15% glycine (PBS+). Staining with secondary antibodies was performed at RT for 60 min. For immunohistochemical staining using DAB, antigen-antibody complexes were visualized using DAB-substrate (DAKO), after which slides were counterstained with haematoxylin for 5 min and subsequently mounted with Entellan

(Merck Milipore International). Fluorescent stained slides were mounted using ProLong™ Gold with DAPI (Invitrogen). Antibodies used are listed in **Table S1B**.

Fluorescence microscopy

All fluorescent imaging presented in this study was performed using a Leica TCS SP5 confocal microscope with a 20x lens. Filters used: 405 nm (Hoechst/DAPI), 488 nm argon laser (Alexa 488/GFP), 561 nm (Cy3), and 633 nm (Cy5). ImageJ image analysis software was used to process the images.

Quantification of inclusions

Inclusions were quantified by first counting approximately 100 GFP-positive cells and then by counting the number of FMRpolyG- and ubiquitin-positive intranuclear inclusions in these GFP-positive cells from different aged dox treated primary hippocampal neuronal cultures using a Leica confocal microscope and LAS AF software. After administration of compound *1a* the same measurement principle was applied only this time mainly focusing on FMRpolyG-positive intranuclear inclusions.

The number and size of inclusions in liver tissue was determined using an Olympus BX40 microscope and CellSens Dimension software. Inclusions were quantified by counting liver cells at a 40x magnification in 5 randomly selected areas per liver slice. FMRpolyG-positive or inclusions were quantified using a counting frame. Per mouse two liver slices were counted and then the average of both counts was used. Researchers were blinded for experimental groups. The same quantification procedure was also applied for Rad23b-positive inclusions.

Statistical analysis

Statistical analysis was performed using GraphPad Prism software version 8 [47]. Statistical test used for *in vitro* experiments is one-way ANOVA multiple comparison test. For statistical analysis between the *in vivo* experimental groups one-way ANOVA test followed by Tukey's posthoc correction test was used. A value of $p<0.05$ was considered significant.

Results

Intranuclear inclusions in an inducible neuronal cell model for FXTAS

Previously, we showed that the formation of intranuclear inclusions in an inducible mouse model of FXTAS was reversible by stopping expression of RNA containing the expanded CGG repeat [34]. After this proof-of-principle, the next challenge was to find a therapeutic intervention targeting the pathogenic trigger for FXTAS, the *FMR1* RNA containing an CGG_{exp}. To test potential therapeutic interventions, we generated inducible hippocampal

neuronal cultures derived from inducible double transgenic TRE-nCGG-eGFP/hnRNP-rtTA mice. In these cells, either the RNA bearing the 5'UTR of the *FMR1* gene with a control size repeat of 11CGGs or RNA containing the 5'UTR of the *FMR1* gene with a PM size of 90CGGs was coupled to eGFP. These cultures were derived from E17-19 embryos from timed breedings with heterozygous transgenic mice. This resulted in a mixed population of nCGG-GFP RNA positive and negative cells. Indeed, administration of dox to the culture medium resulted in GFP-positive and GFP-negative cells in cultures originating from both 11CGG and 90CGG repeat containing mice (**Fig. 1A, A-F**). There were no GFP-positive cells in cultures originating from double transgenic mice without addition of dox to the culture medium (**Fig. 1A, G-L**) or in control cultures containing only one of the two transgenes (not shown).

To confirm whether intranuclear inclusions could be formed in these primary hippocampal neuronal cell cultures, we performed immunofluorescence (IF) staining for ubiquitin. Ubiquitin-positive inclusions were observed in GFP-positive cells in TRE-90CGG-eGFP/hnRNP-rtTA cultures after 10 days of dox-induction. The number of ubiquitin-positive intranuclear inclusions increased significantly in time up to 37% of the GFP positive cells at 24 days of dox-induction (**Fig. 1B and 1C**). In addition, previous work demonstrated that ubiquitin and FMRpolyG co-localize in inclusions in transfected cells, brain tissue of mouse models and post-mortem brain tissue from FXTAS patients [10, 29, 34]. Immunofluorescence double staining confirm that in inducible hippocampal mouse neurons ubiquitin and FMRpolyG co-localize within approximately 90% of all intranuclear inclusions (**Fig. 1D**).

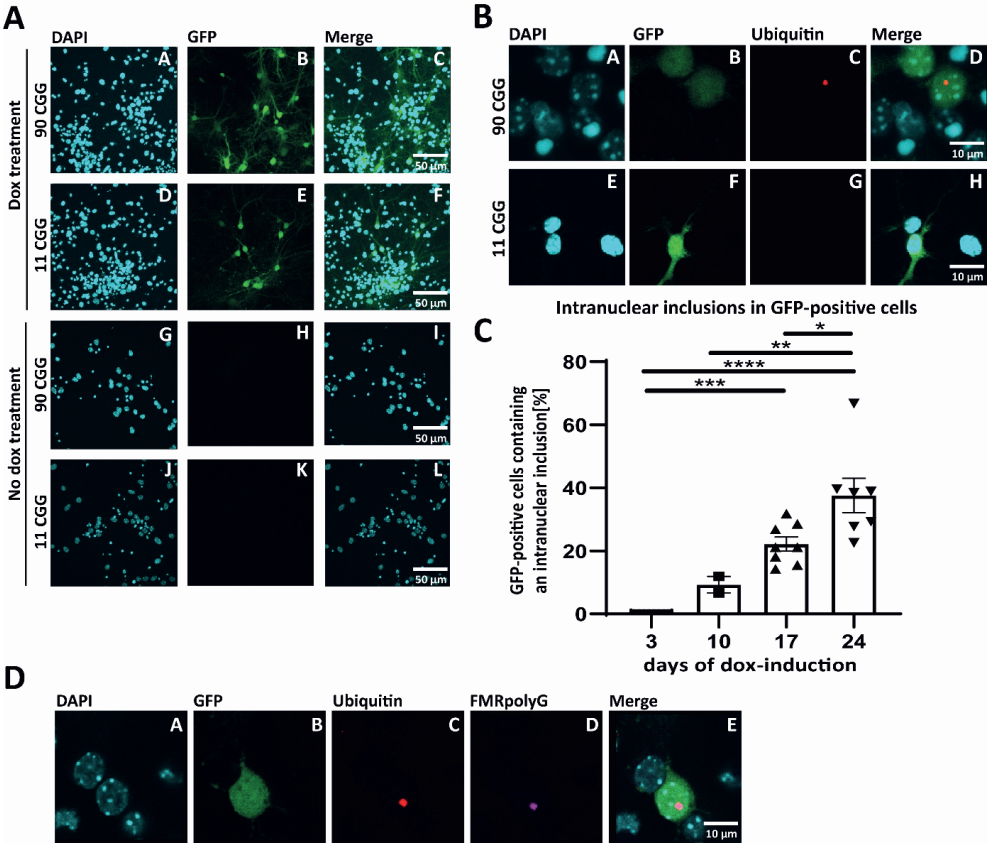

Figure 1 | FMRpolyG-positive inclusions form in GFP-positive primary hippocampal neurons. **(A)** eGFP expression (green) after dox-induction of 11CGG and 90CGG double transgenic (DT) TRE-nCGG-eGFP/hnRNP-rtTA primary hippocampal neurons. No eGFP expression is observed in DT neuronal cultures without dox. **(B)** Ubiquitin-positive intranuclear inclusions (red) are found in GFP-positive TRE-90CGG-eGFP/hnRNP-rtTA cells, but not in GFP-positive TRE-11CGG-eGFP/hnRNP cells or GFP-negative cells. **(C)** Quantification of intranuclear inclusions in GFP-positive cells. The percentage of GFP-positive nuclei containing GFP-positive inclusions after 0 (*n=8*), 10 (*n=2*), 17 (*n=8*) and 24 (*n=7*) days dox-treatment. Per isolation and per timepoint 100 GFP-positive cells were counted. For statistical analysis the One-Way ANOVA test with multiple comparison was used. Error bars represent standard error of the mean (SEM). Asterisks indicate different levels of significance (* = $p \leq 0.05$, ** = $p \leq 0.01$, *** = $p \leq 0.001$ and **** = $p < 0.0001$). **(D)** Co-localization of ubiquitin (red) with FMRpolyG (purple) in intranuclear inclusions. Approximately 90% of ubiquitin-positive and FMRpolyG-positive intranuclear inclusions co-localize.

To study which cell types are present in the neuronal culture, we performed immunofluorescence double staining in the primary hippocampal cell cultures. We found that both neurons and astrocytes are present in the primary hippocampal cultures using the neuronal marker microtubule-associated protein 2 (MAP2), and the astrocytic marker glial fibrillary acidic protein (GFAP), respectively (**Fig. 2A and 2B**). More specifically,

antibodies against Ca^{2+}/calmodulin-dependent protein kinase II (CamKII) and gamma-aminobutyric acid (GABA) for different types of neurons showed that both excitatory and inhibitory neurons can be found in these primary hippocampal cultures (**Fig 2C and 2D**). Intranuclear inclusions were only found in GFP-positive neurons but not in astrocytes (**Fig. 2A, 2C and 2D**). In short, these data confirm that we generated an *in vitro* neuronal culture with multiple cell types, and that these primary hippocampal neurons are capable of forming ubiquitin-positive and FMRpolyG-positive intranuclear inclusions, which is the major neuropathological hallmark for FXTAS.

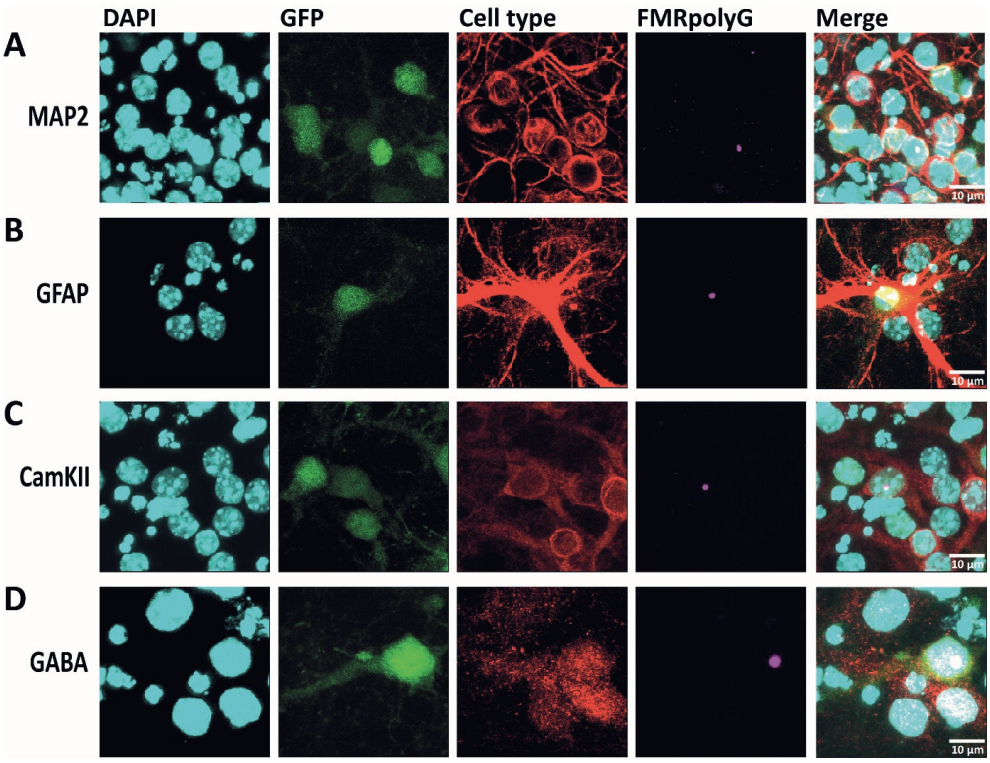

Figure 2 | Multiple relevant cell types formed in an *in vitro* neuronal model for FXTAS. Immunofluorescent staining using the **(A)** neuronal microtubule-associated protein 2 (MAP2) and **(B)** astrocytic glial fibrillary acidic protein (GFAP) markers show that these *in vitro* cultures are heterogenous. More specifically immunofluorescent staining shows that both **(C)** inhibitory and **(D)** excitatory neurons are present in the cultures and in both types of neurons FMRpolyG-positive intranuclear inclusions are formed. FMRpolyG-positive intranuclear inclusions were not present in astrocytes. Scale bars represent 10 µm.

Compound *1a* can reduce number of FMRpolyG-positive inclusions in primary neurons

Since the primary hippocampal cultures showed one of the main hallmarks of the disease, we could use the model to test therapeutic interventions that may halt or reduce the formation of FMRpolyG-positive inclusions. Several small chemical compounds that target CGG_{exp} were developed of which compound *1a* was a promising candidate (**Fig. 3A**). It can bind to the internal GG-loop of the expanded CGG repeat shielding the RNA and thus prevent its translation [42]. For several repeat associated disorders several promising compounds have been described (reviewed in [43]).

Compound *1a* was first tested for toxicity. Titration experiments showed that using concentrations of 1 nM and 10 nM of compound *1a* did not result in abnormal cell death and that compound *1a* did not result in adverse effects in the culture up to 24 days after compound administration. Also, using HPLC and LC-MS/MS analysis we calculated the half-life of compound *1a* in blank NBM+++ to be 9 hours. Next, we performed immunofluorescence staining and the number of FMRpolyG-positive intranuclear inclusions was quantified. **Figure 3B** represents a schematic overview of dox and compound *1a* treatment. We added compound *1a* one day prior to the start of dox-induction followed by 17 days of dox treatment. Upon quantification significantly less intranuclear inclusions were observed with both 1 and 10 nM concentrations of compound *1a* (**Fig. 3C**). The addition of compound *1a* one week after start of dox-induction resulted also in a significant reduction of the number of intranuclear inclusions compared with untreated cultures (**Fig. 3D**). There was no significant difference in number of inclusions between cultures that received *1a* prior to the dox-induction and one week after dox-induction. In summary, these data show that compound *1a* is capable of reducing the number of FMRpolyG-positive intranuclear inclusions in primary hippocampal neuronal cultures when applied as a preventative treatment and when administered after CGG repeat RNA expression is induced in these primary neurons.

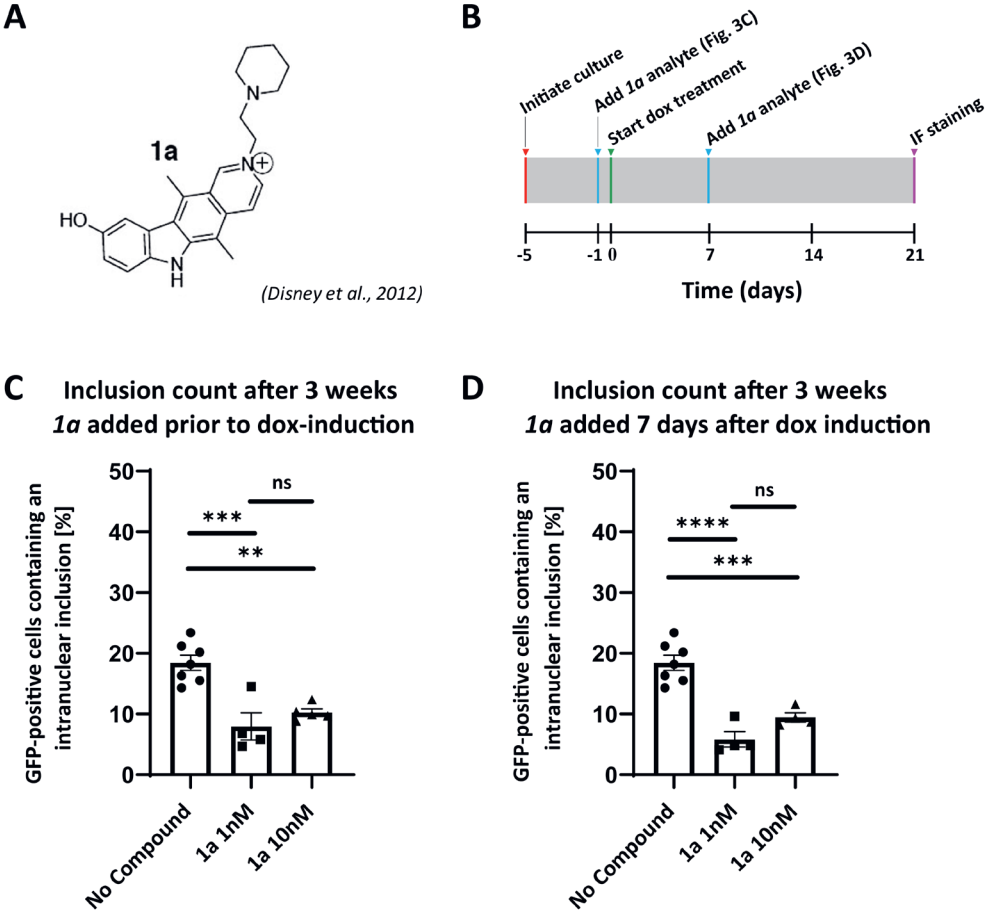

Figure 3 | Less FMRpolyG-positive intranuclear inclusions *in vitro* after treatment with *1a*. (A) Chemical structure of compound *1a*. **(B)** Schematic overview of doxycycline and compound *1a* treatment. Compound *1a* was added 1 day prior to the start of doxycycline induction followed by **(C)** 21 days of doxycycline treatment. Significantly less intranuclear inclusions were observed with a concentration of both 1nM (*n=4*; $p \leq 0.001$) and 10nM (*n=5*; $p \leq 0.01$) of compound *1a* both compared to no compound treatment (*n=7*). No significant difference was found between the concentrations 1nM and 10nM used for compound *1a*. **(D)** Addition of compound *1a* 7 days after start of doxycycline induction resulted also in a reduction of the number of intranuclear inclusions for 1nM (*n=4*; $p < 0.0001$) and 10nM (*n=4*; $p \leq 0.001$) of compound *1a* compared with untreated cultures (*n=7*). No significant difference was found between the concentrations 1nM and 10nM used for compound *1a*. No significant difference was observed in number of intranuclear inclusions between cultures that received compound *1a* (both 1nM and 10nM) prior to the doxycycline induction and cultures that received compound *1a* after 7 days of dox-induction. For statistical analysis the One-Way ANOVA test with multiple comparison was used. Asterisks in the figures indicate different levels of significance (** = $p \leq 0.01$, *** = $p \leq 0.001$ and **** = $p < 0.0001$). Error bars represent standard error of the mean (SEM).

Inducible ubiquitous expression of expanded CCG RNA in mice

To confirm the results from the *in vitro* study in an animal model we injected compound *1a* in this inducible mouse model [35]. These mice show ubiquitous expression of an CGG_{exp} resulting in rapid formation of inclusions in the liver but not in the brain.

To induce transgene expression in double transgenic mice, we provided them with dox or sucrose water from the age of P24-27. Mice were then split into 5 experimental groups, as shown in **Figure 4A**. All mice were double transgenic mice except for group 3, which had only one of the two transgenes. Group 1 is the negative control group in which mice were left untreated for both dox and compound *1a*. Group 2 is the compound control group where mice only received a single intra-peritoneal (IP) injection of compound *1a* to account for the effects compound *1a* has on these mice. Group 3 were single transgenic mice having only the hnRNP-rtTA transgene. These mice were provided with only dox to account for any leakage of the promoter. Group 4 was the positive control and were administered dox to induce expression of the transgene but were not treated with compound *1a*. Finally, group 5 is the treatment group. These mice were provided with dox in their drinking water followed by a single IP injection of compound *1a*. After 5 days, all mice showed a normal increase in body weight (**Fig. S1A**) and expression of the transgene was confirmed for dox-induced double transgenic mice through quantitative RT-PCR of the expanded CGG mRNA (**Fig. 4B**) and immunohistochemical staining for GFP (**Fig. 4C**) on liver tissue. Sucrose-water and single transgenic control mice showed no expression of the expanded CGG mRNA and no staining of GFP in liver tissue (**Fig. 4B**) Western blot analysis further confirmed expression of GFP-protein in the liver (**Fig. 4D; Full blots in Fig. S2**). Expression of expanded CGG mRNA and GFP-protein was limited to transgenic mice induced with dox and absent in non-double transgenic and negative control mice. No significant differences were observed in these levels between mice treated with compound *1a* or vehicle (DMSO) (**Fig. 4B and 4D**). After weighing the mice daily and sacrificing the mice and macroscopically observing the liver, severe liver toxicity was absent in these experiments (**Fig. S1A-B**). To confirm there was no liver toxicity present, we performed quantitative RT-PCR on mRNA from livers of positive (untreated and treated double transgenic mice) and negative control mice for glutathione peroxidase-1 (GPX-1) and cytochrome C (CytC) which are indicative for mitochondrial stress when elevated in the liver (**Fig. S1C-D**). Indeed, both GPX-1 and CytC mRNA levels were similar in dox-induced and control mice confirming absence of severe liver toxicity in these double transgenic mice. In summary these data show that we successfully induced expression of the transgene at mRNA and protein level without any severe toxicity after 5 days.

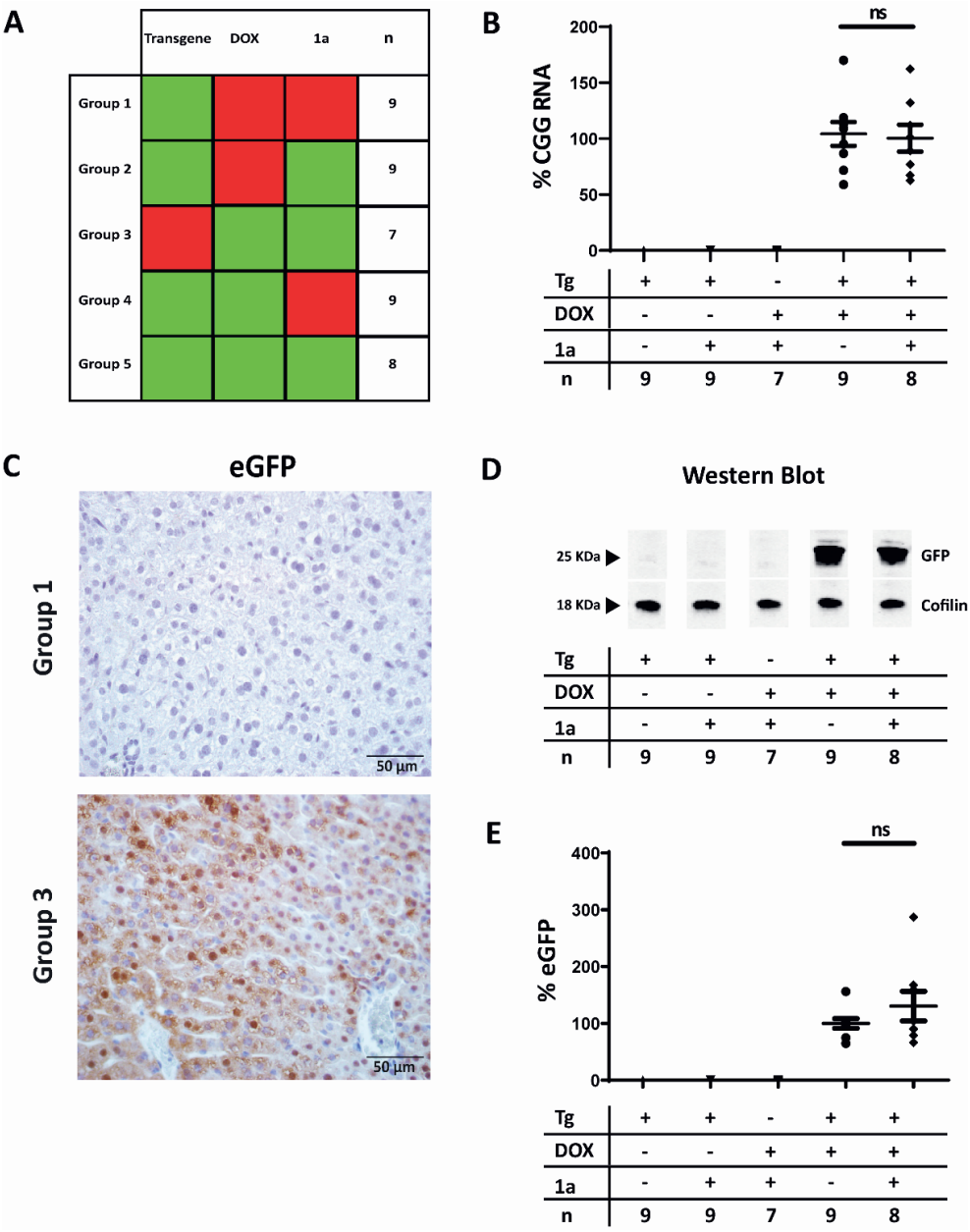

Figure 4 | *In vivo* induction of expanded CGG repeat expression in double transgenic mice. (A) Schematic overview of experimental mouse groups in regards to transgenic status, doxycycline administration, compound *1a* administration, and group size (*n*). Red squares mean 'not present or no' and green squares mean 'present or yes'. **(B)** Relative expression level of 90CGG mRNA analyzed through quantitative RT-PCR. Only the dox-induced double transgenic (DT) mice express the expanded repeat mRNA. Values are shown as percentage relative to the positive control group (group 4). No significant difference in 90CGG mRNA expression between the compound *1a* untreated DT and treated DT group was found (One-way ANOVA *post-hoc* Tukey's). Error bars

represent standard deviation (SD). **(C)** Immunohistological staining against eGFP in liver tissue of group 1 (negative control; upper panel) and group 4 (positive control; lower panel) mice. 40x magnification. Scale bars represent 50 µm. Group 1 shows no staining whereas group 4 shows a strong staining throughout the tissue. **(D)** Western blot analysis of eGFP protein expression across experimental groups. Upper lane shows eGFP at 25KDa. Lower lane shows loading control cofilin at 18 KDa. Only the dox-induced double transgenic mice express GFP protein. Full Western blot in supplements (**Fig. S2**). **(E)** Relative expression of eGFP protein analyzed through Western blot. Values are shown as percentage relative to the positive control group (group 4). There is no significant difference in eGFP protein expression between the compound *1a* untreated and treated double transgenic mice (One-way ANOVA *post-hoc* Tukey's). Error bars represent standard error of the mean (SEM).

Double transgenic mice produce FMRpolyG-positive protein inclusions

Having confirmed expression of the transgene in these mice, the next step was to see whether expression leads to the formation of intranuclear inclusions, which is the pathological hallmark for FXTAS. For the first time we could show through immunohistochemistry staining in liver sections for FMRpolyG the presence of FMRpolyG-positive inclusions in dox-induced double transgenic mice, but not in the sucrose-water or single transgenic control groups (**Fig. 5A**). FMRpolyG-positive inclusions were located both in the cytoplasm and in the nucleus, as opposed to FXTAS-patient brain tissue where the inclusions are primarily intranuclear [7, 8]. In addition to FMRpolyG-positive inclusions, we also confirmed the presence of ubiquitin-positive inclusions in liver tissue from dox-induced double transgenic mice (**Fig. 5B**). Co-localization of both ubiquitin and FMRpolyG within the inclusions was confirmed through immunofluorescence double labelling of the liver sections (**Fig. 5C**).

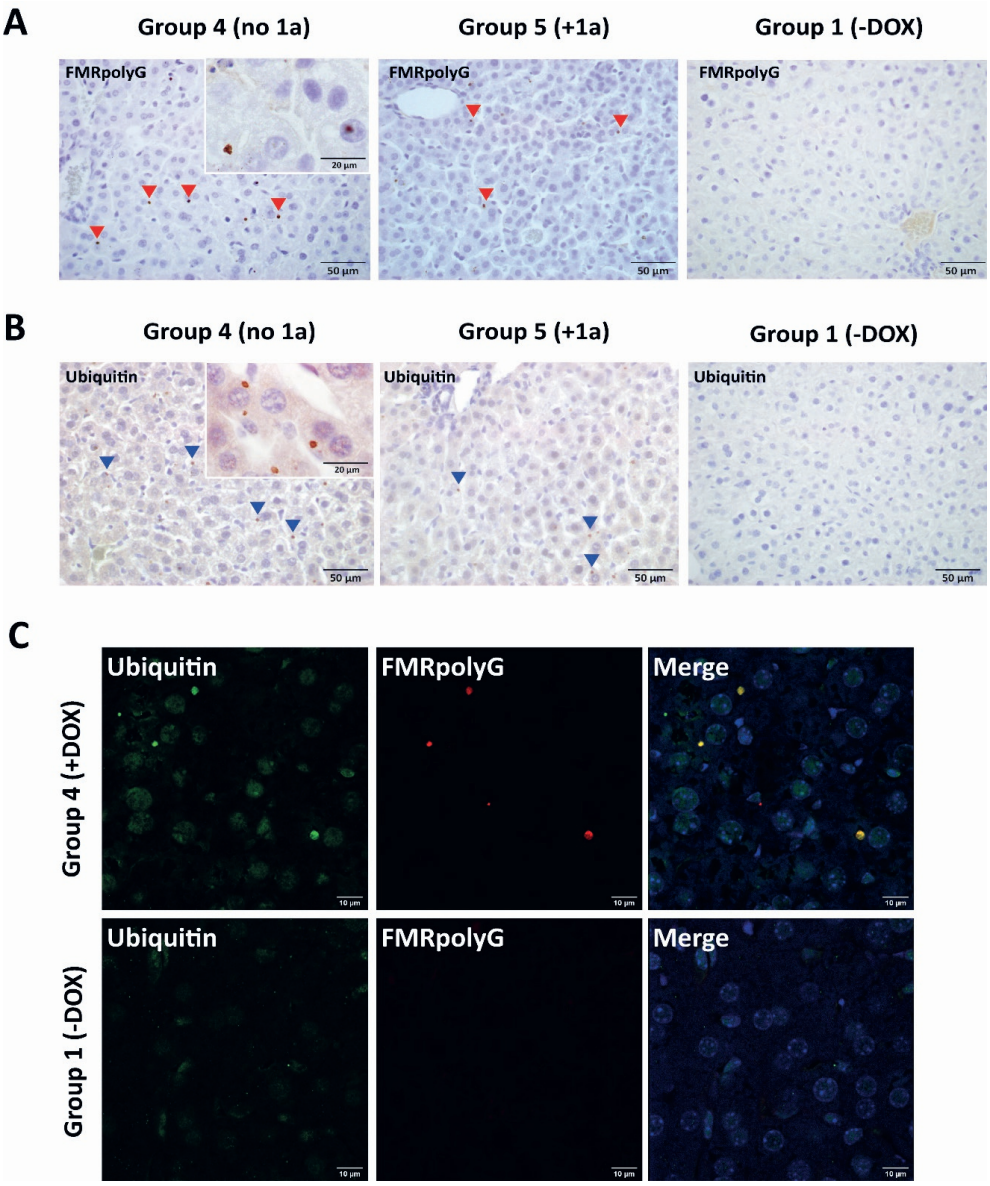

Figure 5 | Formation of FMRpolyG-positive inclusions and co-localization with ubiquitin-positive inclusions after dox-induction in double transgenic mice. (A) Immunohistological staining of liver tissue belonging to respectively compound *1a* untreated double transgenic (group 4), treated double transgenic (group 5), and negative control mice (group 1) for FMRpolyG. Magnifications used are 40x and 100x for inset. Scale bars represent 50 µm and 20 µm for inset. Red arrowheads show FMRpolyG-positive inclusions. **(B)** Immunohistological staining of liver tissue belonging to respectively compound *1a* untreated double transgenic (group 4), treated double transgenic (group 5), and negative control (group 1) mice for ubiquitin. Magnifications used are 40x and 100x for inset. Scale bars represent 50 µm and 20 µm for inset. Blue arrowheads show ubiquitin-positive inclusions. **(C)** Immunofluorescent double staining of liver tissue of compound *1a* untreated

double transgenic (group 4) and negative control (group 1) mice for FMRpolyG (red) and ubiquitin (green). Magnification used is 100x. Scale bars represent 10 µm. Merged panels show co-localization of FMRpolyG and ubiquitin within inclusions.

Another protein commonly observed to be present within inclusions in brain tissue from FXTAS patients is RAD23B, a protein involved in the ubiquitin-mediated proteasomal degradation pathway [34, 39, 48]. Indeed, Rad23b-positive inclusions could be detected in the dox-induced double transgenic mice as well (**Fig. 6A**). Notably, in sucrose-water control mice Rad23b was localized only in the cytoplasm without formation of aggregates. Immunofluorescence staining confirmed co-localization of Rad23b-positive and FMRpolyG-positive inclusions both in the cytoplasm and nucleus (**Fig. 6B**). All together these data show that expression of CGG_{exp} mRNA resulted in the formation of FMRpolyG-positive inclusions intranuclearly as well as cytoplasmic. We could also confirm the presence of Rad23b-positive intranuclear and cytoplasmic inclusions. Rad23b co-localized in the vast majority of inclusions nicely with FMRpolyG. The presence of Rad23b in these inclusions suggests a role for the proteasome degradation pathway in inclusion formation.

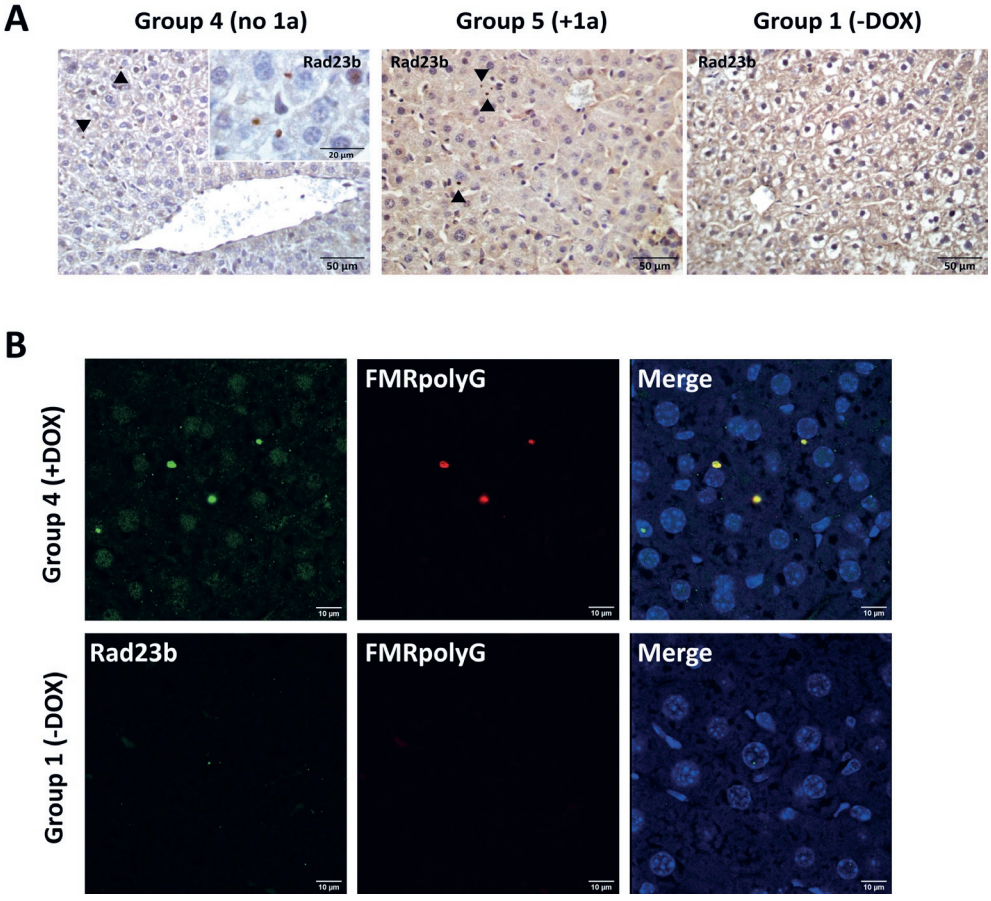

Figure 6 | Formation of Rad23b-positive inclusions and co-localization with FMRpolyG-positive inclusions after dox-induction in double transgenic mice. (A) Immunohistological staining of liver tissue belonging to respectively compound *1a* untreated double transgenic (group 4), treated double transgenic (group 5), and negative control mice (group 1) for Rad23b. Magnifications used are 40x and 100x for inset. Scale bars represent 50 µm and 20 µm for inset. Black arrowheads show protein inclusions. **(B)** Immunofluorescent double staining of liver tissue belonging to compound *1a* untreated double transgenic (group 4) and negative control (group 1) mice against FMRpolyG (red) and Rad23b (green). Magnification used is 100x. Scale bars represent 10 µm. Merged panels show co-localization of FMRpolyG and Rad23b within inclusions.

Compound *1a* reduces the amount of FMRpolyG *in vivo*

Having confirmed the expression of the transgene and the presence of FMRpolyG-positive inclusions, we next tested whether treatment with compound *1a* could reduce the number of FMRpolyG-positive inclusions and FMRpolyG levels *in vivo*. Before onset of the study, we determined the half-life of compound *1a* in the liver and plasma at 32 hours and 5 hours, respectively. This is important to understand the effectiveness of compound *1a* after a

single IP dosing regimen. First, we quantified the number of FMRpolyG-positive inclusions in all the experimental groups after treatment with compound *1a* (Quantification method is discussed in 'Quantification of inclusions'). We did not find a significant decrease for the number of FMRpolyG-positive inclusions between the dox-induced positive control and *1a*-treated double transgenic mice (**Fig. 7A**; p=0.1407). To have a more accurate measure of the amount of FMRpolyG protein present in the tissue of these mice, we used the dot blot technique to visualize the amount of FMRpolyG within the insoluble fractions of protein lysates taken from the liver tissues. Due to the localization of FMRpolyG within aggregates it is unfortunately not possible to detect the protein in the soluble fractions on a Western blot. Using the dot blot technique to visualize FMRpolyG protein levels within the insoluble fractions of protein lysates, we observed a significant decrease of FMRpolyG-protein levels after treatment with compound *1a* (**Fig. 7C**; p<0.001; full blots shown in **Fig. S3**). Similarly, we quantified the number of Rad23b-positive inclusions and aggregated protein levels. Interestingly, dox-induced double transgenic mice treated with compound *1a* showed less Rad23b-positive inclusions compared to control dox-induced double transgenic mice (**Fig. 7B**; p<0.01). Also, Rad23b protein level from the insoluble protein fractions was significantly decreased in double transgenic mice treated with compound *1a* (**Fig. 7D**; p<0.01; full blots shown in **Fig. S4**).

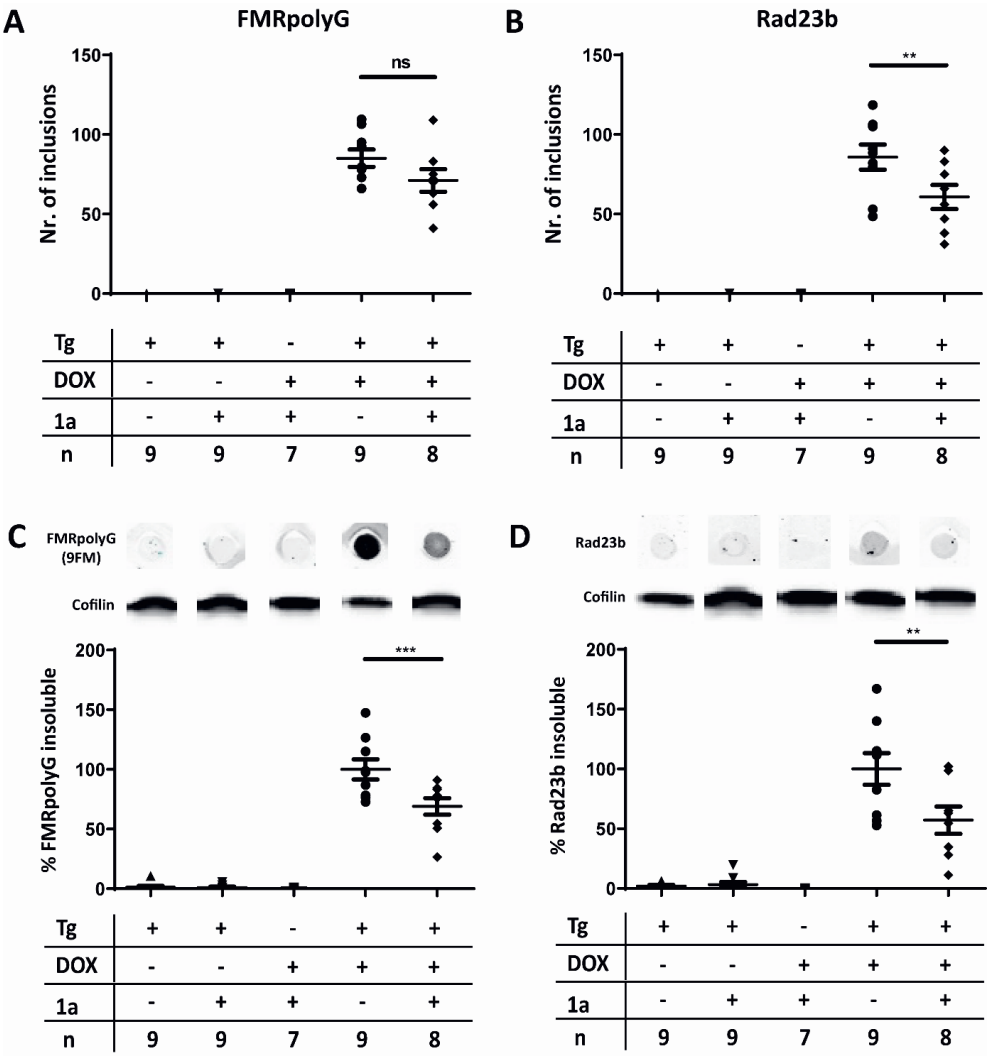

Figure 7 | Depletion of protein inclusions and insoluble protein levels upon treatment of double transgenic mice with compound *1a*. (A) Quantification of number of FMRpolyG-positive inclusions found in liver tissue. There is no significant decrease in inclusion count upon treatment with compound *1a* (One-way ANOVA *post-hoc* Tukey's). **(B)** Quantification of number of Rad23b-positive inclusions found in liver tissue. There is a significant decrease in inclusion count upon treatment with compound *1a* (One-way ANOVA *post-hoc* Tukey's; $p<0.01$). **(C)** Dot blot analysis of insoluble FMRpolyG present in liver tissue. Cofilin analyzed through Western blot is depicted as a loading control. Full blots in supplements **(Fig. S3)**. Insoluble FMRpolyG (9FM) signal was calculated using the cofilin signal as loading control. There is a significant decrease of insoluble FMRpolyG upon treatment with compound *1a* (One-way ANOVA *post-hoc* Tukey's; $p<0.001$). **(D)** Dot blot analysis of insoluble Rad23b present in liver tissue. Cofilin analyzed through Western blot is depicted as a loading control. Full blots in supplements **(Fig. S4)**. Insoluble Rad23b signal was calculated using the cofilin signal as loading control. There is a significant decrease of insoluble FMRpolyG upon treatment with compound *1a* (One-way ANOVA *post-hoc* Tukey's; $p<0.01$). Error bars in this

figure represent standard error of the mean (SEM). Asterisks indicate different levels of significance (** = $p \leq 0.01$ and *** = $p \leq 0.001$).

Discussion

This study shows the strength of the ubiquitous expression inducible model in the rapid screening of potential therapeutic interventions targeting cellular toxicity. The *in vitro* primary hippocampal neuronal culture serves as a primary screening to identify promising therapeutics in a relevant cell type. The *in vivo* mouse model confirms the potential therapeutic effect of compound *1a* on FMRpolyG-positive inclusions and FMRpolyG protein level in liver tissue. Although liver tissue is not affected in FXTAS we believe the *in vivo* model can serve as a quick *in vivo* screening method to study therapeutic strategies to prevent cellular toxicity. In contrast to other FXTAS mouse models this mouse model shows early manifestations including FMRpolyG-positive inclusions. To our knowledge, we are here first to report the use of a small chemical compound, specifically compound *1a*, in a ubiquitous inducible mouse model. We were able to induce FMRpolyG inclusion formation in the primary hippocampal neuronal cultures and upon treatment with compound *1a* significantly decrease the number of FMRpolyG-positive inclusions *in vitro*. Additionally, we have successfully induced formation of FMRpolyG-positive inclusions in liver tissue of the inducible mouse model. Unfortunately, we were not able to reduce FMRpolyG-positive inclusions in liver tissue but we showed that compound *1a* could reduce insoluble FMRpolyG protein levels by targeting CGG_{exp} mRNA in the ubiquitous inducible mice. We successfully generated a relevant primary neuronal cell culture model derived from the inducible mouse model displaying FXTAS-related neuropathology in all cells allowing rapid screening of future targeted interventions *in vitro* and to confirm their potential *in vivo*.

Cellular and animal models have significantly contributed to the understanding of the underlying molecular mechanisms of FXTAS. Recently, our group demonstrated that reversibility of both neuropathology and functional deficits in an inducible FXTAS mouse model could be achieved [34]. With this work we demonstrated that effective targeted treatment for patients with FXTAS might be possible.

The challenge in the search for therapeutic interventions is to develop a rapid and reliable drug screening model. In the present study we present a relevant cellular model and *in vivo* mouse model for rapid testing of potential therapeutic interventions [35]. We were able to successfully induce formation of FMRpolyG-positive inclusions in these *in vitro* and *in vivo* models, and subsequently significantly reduce FMRpolyG-positive inclusions *in vitro* and FMRpolyG protein levels *in vivo* through targeting the CGG_{exp} using small

molecule, *1a*. Because of the rapid development of relevant pathologies, in contrast to other premutation mouse models where FXTAS-related pathologies develop only after months, both *in vitro* and *in vivo* models are suitable for rapid determining the therapeutic potential of targeted interventions against the CGG_{exp}.

In vitro we were able to show that dox induces expression of GFP and thus CGG_{exp} mRNA in primary hippocampal neuronal cultures, without any leakage of the Tet-On system. Heterozygous hnRNP-rtTA mice were crossed with heterozygous TRE-nCGG-eGFP mice resulting in 25% of the offspring having both transgenes. After administration of dox to the culture medium approximately 25% of the neurons show GFP expression, as expected by Mendelian inheritance. Primary neuronal cell cultures from the hnRNP-rtTA/TRE-90CGG-eGFP mice show the presence of characteristic intranuclear inclusions in both neurons (excitatory and inhibitory) and astrocytes illustrating similarities between this model and post-mortem brain tissue from FXTAS patients [8]. Interesting to note is that primary neurons cultured from the Dutch KI mouse model showed no inclusion phenotype at all. This is presumably due to the fact that this mouse model uses an endogenous *FMR1* promoter resulting in lower expression (data not shown). Since FXTAS is a late onset disorder, the process of inclusion formation needs time. Therefore, to study the potential of therapeutic interventions such as *1a* on inhibiting inclusion formation, an overexpression *in vitro* model is necessary. We also generated cultures of FXTAS patient fibroblasts and mouse embryonic fibroblasts (MEFs) from the inducible mice. In both models we also could not observe inclusion formation in time (data not shown).

Ubiquitin-positive intranuclear inclusions in neurons and astrocytes are the neuropathological hallmark of FXTAS. The formation of inclusions staining positive for both ubiquitin and FMRpolyG, together with the presence of these inclusions in both neurons and astrocytes, like in post-mortem brain from patients with FXTAS, points towards an appropriate *in vitro* model to further test possible therapeutic interventions for FXTAS.

From previous work we know that these mice exposed to dox may experience quick deterioration of their condition due to liver toxicity and die after 5 days [35]. Therefore, these mice form a useful model for quick testing of general cellular toxicity. Although the brain is the organ of interest in FXTAS, in this model the study of inclusion formation seems not to be possible in the brain since the expression of the CGG_{exp} RNA can never be long enough because the mice die after only 4 days of dox treatment. Other pathogenic triggers such as deficient mitochondrial signaling, may also contribute to the dramatic cellular toxicity observed that the mice die before any formation of inclusions in the brain or any other organ. Another possible explanation why these mice don't have expression in the brain is that dox may need more time to reach the brain and induce transgene

expression in the brain. Because of this previously observed phenotype in the liver, we chose to use liver tissue for further analyses.

Although the primary scope of this study was the effect of compound *1a* on the production of FMRpolyG and the formation of inclusions, the role of these inclusions should not be left undiscussed. The presence of significant numbers of inclusions in several brain regions in both neurons and astrocytes, suggests that such inclusions are a common neuropathological correlate of the tremor and ataxia phenotype seen in FXTAS patients and PM carriers [8]. In analogy with FXTAS patients, ubiquitin-positive intranuclear inclusions can also be detected in the brains of the Dutch CGG-KI mice [38]. Cognitive and behavioral deficits in these mice correlate nicely with the increased number of intranuclear inclusions found in both neurons and astrocytes [49]. Recently we published about a new *Gfa2* mouse model with astroglial-specific expression of the CGG_{exp} RNA throughout the entire brain including cerebellar Bergmann glia. We could show that astrocyte-specific expression of the CGG_{exp} RNA is sufficient to induce key features of FXTAS pathology, including RAN-translation of the FMRpolyG protein, the formation of ubiquitin-positive and FMRpolyG-positive inclusions accompanied with impaired motor performance [50]. These data suggest a disease-causing role for astroglia in FXTAS. Although all this data presented suggest a disease-causing role for inclusions in neurons and astrocytes, the presence of inclusions might not be related or even protective, as has already been described in patients with hereditary ataxia and polyglutamine diseases [51, 52]. To date, the role of inclusions in both neurons and astrocytes in the pathogenesis of FXTAS is not clear and needs further research.

The use of small molecules that shield the CGG repeat RNA (reviewed in [43]) has great potential to ameliorate FXTAS. The advantage of therapeutic interventions targeting CGG RNA is that the RNA folds into diverse structures with repeating motifs allowing small chemical compounds to bind these repeating motifs in the RNA repeating transcripts [53]. It has been shown that RNA containing an expanded CGG repeat forms hairpin structures with periodically repeating internal GG-loops. Several RNA binding small molecule compounds targeting the internal GG-loop of the expanded CGG repeat were developed [42, 54-56]. One potential liability of small chemical compounds, despite their improved affinities, selectivity, and potency, is their high molecular weights, which could decrease cellular and tissue permeability. To overcome this problem, favorable properties of monomeric ligands can be incorporated in the compound to enhance its permeability. Studies using transfected COS7 cells that transiently overexpressed RNA containing an expanded CGG repeat showed that compound *1a* can improve FXTAS-associated pre-mRNA splicing defects and reduce the size and number of nuclear RNA foci. Furthermore, the binding of compound *1a* does not affect translation of the downstream open reading frame (ORF) [42, 57, 58]. The advantage of this approach is that it prevents RNA-binding

proteins from binding to the hairpin structure and additionally the small molecules will block RAN translation, without having an effect on the translation of *FMR1* mRNA. In the inducible neuronal cultures, the number of intranuclear inclusions is significantly reduced by adding compound *1a* to the culture medium. This suggests that the use of compound *1a* is a promising intervention strategy and it is crucial to test these compounds *in vivo*. Both the ubiquitous expressing and the brain specific inducible mouse models are excellent models, using survival, liver pathology, neuropathology and animal behavior as outcome measures. A similar approach has been used for C9FTD/ALS. Small molecule compounds targeting RNA containing the expanded GGGGCC repeat were designed and found to significantly inhibit RAN translation and foci formation in cultured cells expressing mutant RNA in neurons transdifferentiated from fibroblasts of repeat expansion carriers [56]. Given the structural similarity between CGG repeat and GGGGCC repeat, it was expected that compound *1a* might bind the GGGGCC repeat sequence in C9ALS/FTD [43]. Recognition and binding of GG-motifs by compound *1a* in CG-rich sequences could form a liability for further development of compound *1a* since the effect on CG-rich coding regions is not known. The short CGG repeats in the other genes are less likely to be affected by *1a*. Compound *1a* can bind to the long CGG repeats of *FMR1* in FXTAS selectively due to the greater structural stability and the larger abundance of the 1x1 GG internal loops in the long CGG repeats [56]. The fact that *1a* is not restricted to FXTAS only suggests it could be further developed as a multi-disease drug making it more attractive for big pharmaceutical companies to invest in the future development and improvement of compound *1a*.

Next, we exposed these ubiquitous inducible mice to compound *1a*. Similar to the *in vitro* model the inducible mouse model shows expression of GFP and CGG_{exp} mRNA after induction with dox. Surprisingly, these mice did not suffer from liver toxicity as was published before by our lab in 2014 [35]. First, we speculated that the age of the mice at experimental onset might explain the absence of the liver toxicity but after inducing expression with dox in younger mice we did not see any signs for liver toxicity. Current hypothesis is that the change in phenotype is due to the background the mice were bred in. Initially these mice were bred in the C57BL/6 background but overtime we maintained these mice by crossing them with a mouse line having a C57BL/6JRj background. It is known from literature that different mouse strains respond differently to treatments [59]. Even though we do not understand in which way the background could have influenced the phenotype and therefore loss of initial functional read-out, we still could show that these mice express the transgene with qRT-PCR, Western blot and dot blot. Since these mice lived longer, we hypothesized next that that these mice should be able to develop inclusions in the liver. Indeed, when we sacrificed the mice and examined for the presence of inclusions, we could already detect FMRpolyG-positive inclusions throughout the entire liver within 5 days after dox-induction. Using double staining for ubiquitin and Rad23b,

we also found both proteins being present in these FMRpolyG-positive inclusions. In addition, we were also able to detect both FMRpolyG and Rad23b in the insoluble protein fractions at the molecular level. Taken together, these mice have developed a protein aggregation liver pathology without dying, allowing us to rapidly test potential therapeutic interventions.

We could show that upon treatment of the mice with compound *1a*, FMRpolyG levels together with Rad23b levels could be reduced. A striking difference in results between the *in vitro* and *in vivo* model is that we did not see a significant decrease of FMRpolyG-positive inclusions in this mouse model. We hypothesize that while there may not be a decrease in number of inclusions, the inclusions could have decreased in size. The significant decrease in aggregated FMRpolyG protein level we present in this study supports this hypothesis. In addition, it may be that a second IP injection is necessary to halt the formation of inclusions. Nevertheless, further optimization of compound *1a* is warranted. Importantly, we could reduce the protein levels of FMRpolyG in these mice using a single IP injection. In previous studies the presence of FMRpolyG-positive inclusions showed a clear effect on behavior and locomotor function [33]. Unfortunately, we were not able to show effect of the compound on motor- and cognitive function. To see whether reduction of FMRpolyG levels can also rescue motor- and cognitive phenotypes associated with FXTAS, a brain-specific inducible mouse model can be treated with compound *1a*. Further research involving mouse models with brain-specific CGG_{exp} expression that allow for functional analyses on *i.e.,* the compensatory eye movement – of which we observed a phenotype in earlier studies [34] – could be performed as follow-up studies.

While both *in vitro* and *in vivo* models used in this study involve the same inducible mouse models there are notable differences between the models such as the speed at which the models develop FMRpolyG-positive inclusions. Inclusions in the *in vivo* model are formed within 5 days after dox induction whereas in the primary hippocampal neuronal cultures this process needs approximately 10 days. It is hard to compare protein inclusion formation in both systems and make conclusive remarks on both models since we are comparing two totally different tissue types. Whole liver metabolism and gene expression patterns in a living organism could have accelerating effects on the protein aggregation process. Neurons are regulating cells with a limited capacity for cell renewal while the liver has a more robust renewal capability and is highly involved in the metabolic processes. Second, in line with the high metabolic activity in the liver, is the effect of dox on neurons and hepatocytes. Dox is an antibiotic derived from the tetracycline family known for its anti-oxidant and anti-inflammatory effects. Even though this is the case for neurons where dox has a more protective and anti-inflammatory role in the brain, in the liver it mitigates hepatic injury after 1 to 2 weeks of administration [60, 61]. Although these mice were sacrificed before any hepatic injury could be detected macroscopically, at the molecular

level dox could have already had its effects inducing stress in the hepatocytes. It's known for *C9ORF72*-linkedALS/FTD and FXTAS that the integrated stress response stimulates the production of RAN-translation proteins like FMRpolyG in FXTAS [32].

In addition to the speed at which the inclusions form, the localization of them also differs between the *in vitro* and *in vivo* model. Ubiquitin-positive intranuclear inclusions in neurons and astrocytes are the neuropathological hallmark of FXTAS. In the primary neuronal cell culture model we show the presence of characteristic intranuclear inclusions in both neurons (excitatory and inhibitory) and astrocytes illustrating similarities between this model and post-mortem brain tissue from FXTAS patients [8]. However, the inclusions in the *in vivo* model are generally located in the cytoplasm. The speed at which the inclusions form most likely plays a role. Because in our *in vivo* model the inclusions form within 5 days, we hypothesize that upon sacrificing the mice the aggregates formed were not able to relocate to the nucleus yet [33].

In this present study we found that *in vivo* Rad23b co-localizes with FMRpolyG in these inclusions. It is an interesting question to ask whether FMRpolyG recruits for example Rad23b to the inclusions, or that FMRpolyG is sequestered into these inclusions because it is toxic to the cells and aggregation is a way to prevent cellular toxicity and Rad23b is recruited to assist in the protein degradation of FMRpolyG. Previously many other molecular chaperones like HSP40 and the 20S catalytic core complex of the proteasome were found to also accumulate in these inclusions in mice [38]. It is not entirely clear why Rad23b is present in these inclusions. Accumulation of Rad23b in the inclusions can be an effect of a cellular state or serve a more functional role in the cause of these inclusions. It is known that Rad23b interacts with the 26S proteasome for degradation of ubiquitinated proteins [39]. Ubiquitylation is a general protein modification process involved in the degradation of misfolded or toxic proteins via sequential process by the ubiquitin-activating enzyme (E1) a ubiquitin-conjugating enzyme (E2) and a specific ubiquitin ligase (E3). Through a ubiquitin-associated domain (UBA) ubiquitinated proteins are recognized and send to the 26S proteasome for degradation. Although Rad23b has two of these UBA domains it is protected by an intrinsic stabilization signal [62] making it an ideal candidate to serve for the shuttling of misfolded proteins to be degraded by the 26S proteasome [63, 64] possibly explaining the presence of Rad23b in these inclusions. Another possible hypothesis as why Rad23b co-localizes with FMRpolyG and ubiquitin in these inclusions is because Rad23b has two UBA domains that are capable of binding ubiquitinated proteins that are present in these inclusions. In this *in vivo* inducible mouse model inclusions where predominantly present in the cytoplasm. Although we do not know the origin or the function of Rad23b in these cytoplasmic inclusions, it might be that Rad23b is also a prelude in the formation of intranuclear inclusions. Overexpression of Rad23b in living cells is known to inhibit 26S proteasome degradation potential [65,

66]. It is also known that RAN translation of the CGG_{exp} in FXTAS causes impairment in the UPS [37]. Despite the fact that no correlation between Rad23b protein levels and proteasome activity *in vivo* has been made in the present study, this may suggest that the UPS is impaired. Impairment in protein degradation by the UPS is directly or indirectly involved in many neurodegenerative disorders but whether it is a cause or consequence needs further research [67].

Interesting to note is that while *in vivo* treatment with compound *1a* resulted in less Rad23b in the inclusions, there was no significant effect on the number of FMRpolyG-positive inclusions. Although there are several hypotheses about why Rad23b is present in the inclusions, it remains fascinating why compound *1a* affects Rad23b presence in the inclusions but not the FMRpolyG protein. Although the definitive reason remains unclear based on what is aforementioned, we like to hypothesize that upon treatment with compound *1a* RAN-translation is inhibited. This inhibition results in less production of FMRpolyG and potentially stimulate the UPS. Stimulation of the UPS could result in the need for Rad23b to shuttle misfolded and toxic ubiquitinated proteins to the 26S proteasome for degradation resulting in less Rad23b capture in inclusions. This supports our initial hypothesis that FMRpolyG-positive inclusions may have decreased in size and not in number, and also explain the decreased levels of FMRpolyG.

Acknowledgements

The authors wish to acknowledge the contribution of Mirjam Schoof to this work during her internship and thank Nicolas Charlet-Berguerand for the nCGG-GFP plasmids and the FMRpolyG mouse monoclonal antibodies. This work was funded by the Dutch Brain Foundation (project number F2012(1)-101) including project 1-R35-NS116846-01 from the US National Institutes of Health (to MDD).

Conflict of Interest Statement

The authors declare that they have no conflicts of interest.

Supplementary Tables and Figures

Table S1A: Primers

Target	Forward (5'à 3')	Reverse (5'à 3')	Application
TRE	GCTTAGATCTCTCGAGTTTAC	ATGGAGGTCAAAACAGCGTG	Genotyping
rtTA	CAGCAGGCAGCATATCAAGGT	GCCGTGGGCCACTTTACAC	Genotyping
90CGG	CGGGTCCAGTAGGCGTGTAC	CCAGTGCCTCACGACCAAC	Genotyping
Gapdh2	TCAAGAAGGTGGTGAAGCAGG	GCCCAAGATGCCCTTCAGT	RT-PCR
90CGG	GAGGCACTGGGCAGGTGT	GGTACCGTCGACTGCAGAAT	RT-PCR
Gpx-1	CAATGTAAAATTGGGCTCGAA	GTTTCCCGTGCAATCAGTTC	RT-PCR
CytC	TGGGCACACTTCTGAACAAA	GGACGTCTGTCTTCGAGTCC	RT-PCR

Table S1B: Antibodies

Target	Application	Dilution	Host	Manufacturer	Catalogue nr.
FMRpolyG (9FM)	WB; DB	1:100 (WB/ DB)	Mouse	Gift from N. Charlet-Berguerand, IGBMC	X
FMRpolyG (8FM)	IHC; IF	1:10 (IHC/IF)	Mouse	Gift from N. Charlet-Berguerand, IGBMC	X
Cofilin	WB	1:10000 (WB)	Rabbit	Abcam	ab11062
hHR23b (RAD23B)	WB; DB; IHC; IF	1:1000 (WB/ DB); 1:100 (IHC/IF)	Rabbit	Abcam	ab86781
Ubiquitin	IHC; IF	1:100 (IHC/IF)	Rabbit	Invitrogen	PA1-10023
GFP	WB	1:20000 (WB)	Rabbit	Abcam	AB 290
GFP	IHC	1:2000 (IHC)	Mouse	Roche	11814460 001
Anti-mouse-680LT	WB	1:10000 (WB)	Goat	LI-COR	926-68020
Anti-mouse-800CW	WB	1:10000 (WB)	Goat	LI-COR	926-32210
Anti-rabbit-680LT	WB	1:10000 (WB)	Goat	LI-COR	926-68021
Anti-rabbit-800CW	WB	1:10000 (WB)	Goat	LI-COR	926-32211
Anti-mouse-Cy3	IF	1:200 (IF)	Donkey	Jackson Immunoresearch	715-165-150
Anti-rabbit-Cy2	IF	1:200 (IF)	Donkey	Jackson Immunoresearch	711-225-152
Poly-HRP-anti mouse/rabbit	IHC	Ready-to-use	Goat	ImmunoLogic	VWRKDPVO55HRP

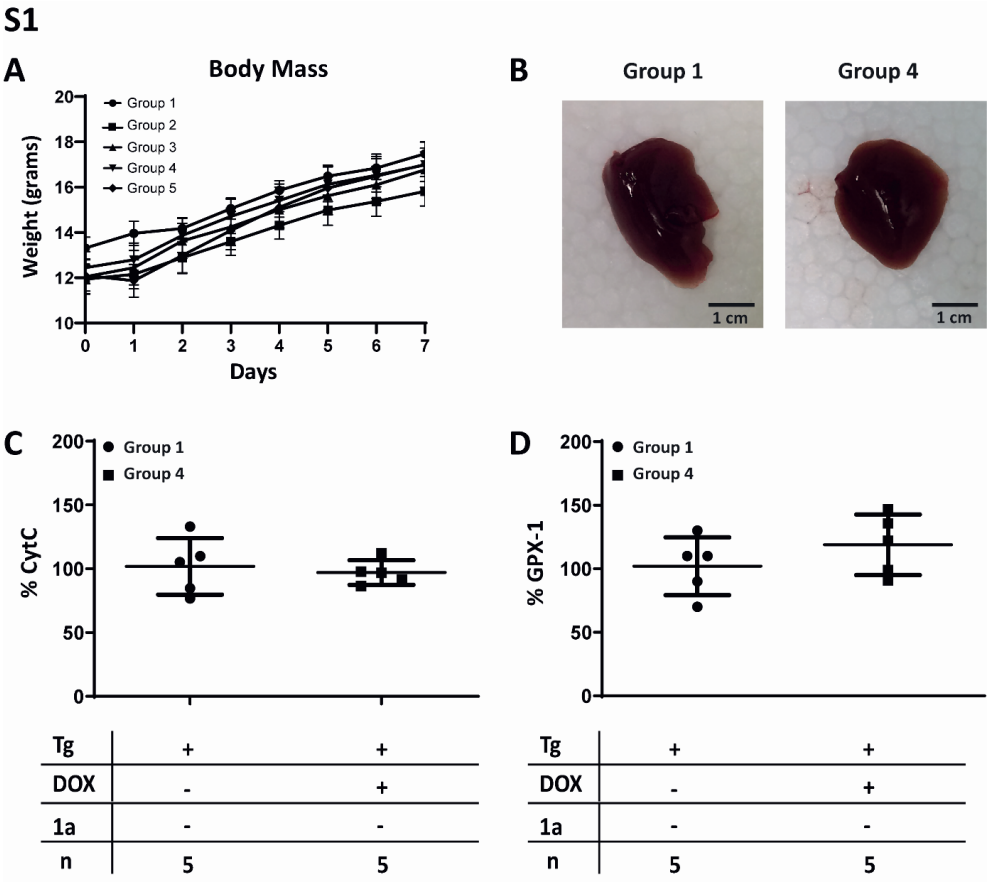

Figure S1 | Total body mass and expression levels of oxidative stress markers in transgenic mice. (A) Total body weight increased during the experiment. All mice showed an increase in their total body weight without significant differences between groups (Two-way ANOVA). **(B)** Representative images of dissected livers from negative control (group 1) and compound *1a* untreated bouble transgenic mice (group 4). No morphological differences between the groups could be observed. **(C)** Expression level of *Cytochrome C (CytC)* mRNA analyzed through quantitative RT-PCR. No significant difference in *CytC* mRNA expression between the negative control (group 1) (*n=5*) and compound *1a* untreated double transgenic (group 4) group (*n=5*) was found (One-way ANOVA *post-hoc* Tukey's). Values are shown as percentage relative to the negative control group (group 1). **(D)** Expression level of *glutathione peroxidase-1 (GPX-1)* mRNA analyzed through quantitative RT-PCR. No significant difference in *GPX-1* mRNA expression between the negative control (group 1) (*n=5*) and compound *1a* untreated double transgenic (group 4) group (*n=5*) was found (One-way ANOVA *post-hoc* Tukey's). Values are shown as percentage relative to the negative control group (group 1). Error bars in this figure represent standard deviation (SD).

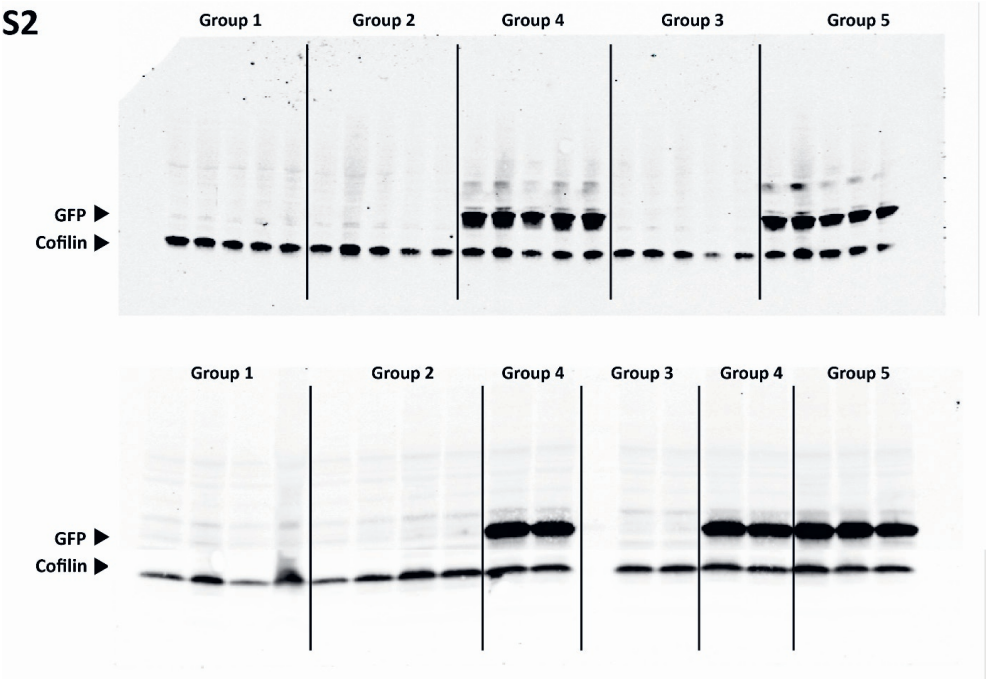

Figure S2 | Uncut Western blot membranes stained for GFP (25 KDa bands) together with the loading control cofilin (18 KDa bands) for all experimental groups (Group 1 (*n=9*), Group 2 (*n=9*), Group 3 (*n=7*), Group 4 (*n=9*), and Group 5 (*n=8*)).

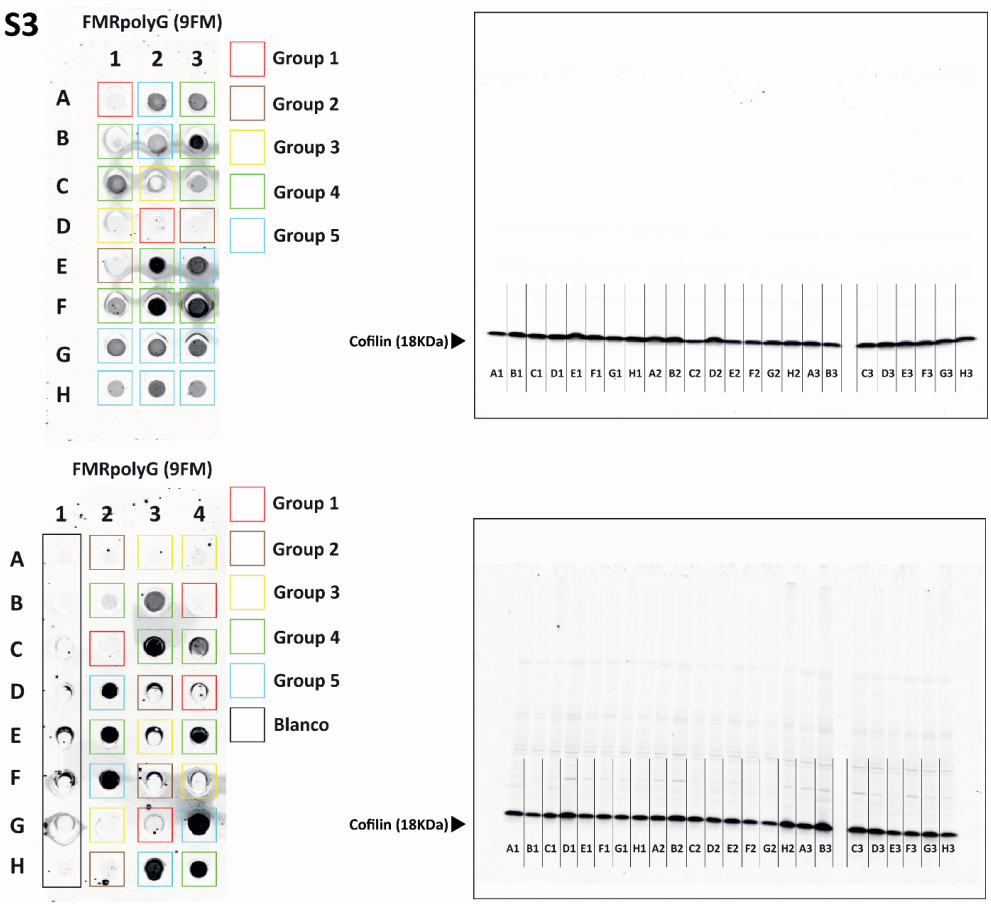

Figure S3 | Uncut dot blot membranes stained for FMRpolyG (9FM) together with the uncut Western blot membrane with matching samples for the loading control cofilin (18 KDa bands). All experimental groups are indicated with different colors. Group 1 (red; *n=6*), Group 2 (brown; *n=6*), Group 3 (yellow; *n=7*), Group 4 (green; *n=15*) and Group 5 (blue; *n=13*). Blanco controls are indicated with black (*n=8*). Insoluble FMRpolyG (9FM) signal was calculated using the cofilin signal as loading control.

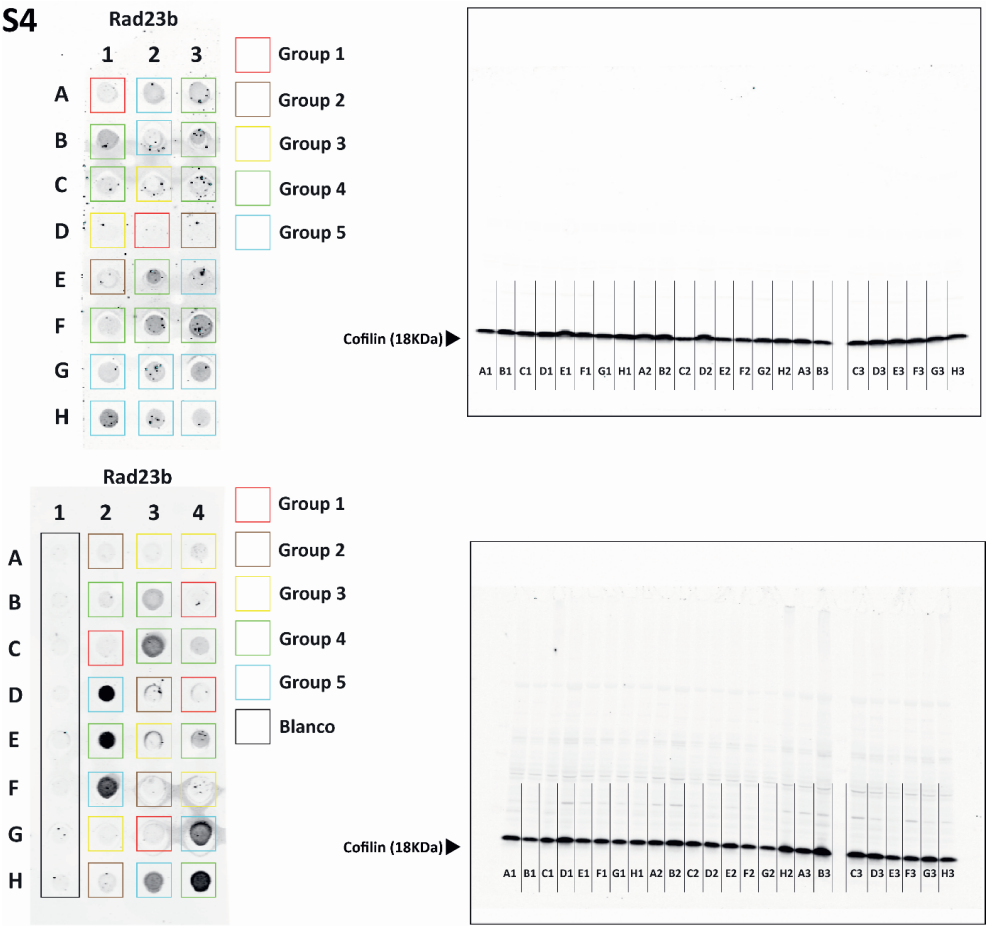

Figure S4 | Uncut dot blot membranes stained for Rad23b together with the uncut Western blot membrane with matching samples for the loading control cofilin (18 KDa bands). All experimental groups are indicated with different colors. Group 1 (red; *n=6*), Group 2 (brown; *n=6*), Group 3 (yellow; *n=7*), Group 4 (green; *n=15*) and Group 5 (blue; *n=13*). Blanco controls are indicated with black (*n=8*). Insoluble Rad23b signal was calculated using the cofilin signal as loading control.

References

1. Hagerman, R.J., et al., *Intention tremor, parkinsonism, and generalized brain atrophy in male carriers of fragile X.* Neurology, 2001. **57**(1): p. 127-30.
2. Leehey, M.A., *Fragile X-associated tremor/ataxia syndrome: clinical phenotype, diagnosis, and treatment.* J Investig Med, 2009. **57**(8): p. 830-6.
3. Grigsby, J., et al., *FXTAS: Neuropsychological/Neuropsychiatric Phenotypes*, in *The Fragile X-Associated Tremor Ataxia Syndrome (FXTAS)*, F. Tassone and E.M. Berry-Kravis, Editors. 2010, Springer New York: New York, NY. p. 31-53.
4. Jacquemont, S., et al., *Fragile X premutation tremor/ataxia syndrome: molecular, clinical, and neuroimaging correlates.* Am J Hum Genet, 2003. **72**(4): p. 869-78.
5. Hall, D.A., et al., *Emerging topics in FXTAS.* J Neurodev Disord, 2014. **6**(1): p. 31.
6. Brunberg, J.A., et al., *Fragile X premutation carriers: characteristic MR imaging findings of adult male patients with progressive cerebellar and cognitive dysfunction.* AJNR Am J Neuroradiol, 2002. **23**(10): p. 1757-66.
7. Greco, C.M., et al., *Neuropathology of fragile X-associated tremor/ataxia syndrome (FXTAS).* Brain, 2006. **129**(Pt 1): p. 243-55.
8. Greco, C.M., et al., *Neuronal intranuclear inclusions in a new cerebellar tremor/ataxia syndrome among fragile X carriers.* Brain, 2002. **125**(Pt 8): p. 1760-71.
9. Hunsaker, M.R., et al., *Widespread non-central nervous system organ pathology in fragile X premutation carriers with fragile X-associated tremor/ataxia syndrome and CGG knock-in mice.* Acta Neuropathol, 2011. **122**(4): p. 467-79.
10. Buijsen, R.A., et al., *FMRpolyG-positive inclusions in CNS and non-CNS organs of a fragile X premutation carrier with fragile X-associated tremor/ataxia syndrome.* Acta Neuropathol Commun, 2014. **2**: p. 162.
11. Greco, C.M., et al., *Testicular and pituitary inclusion formation in fragile X associated tremor/ataxia syndrome.* J Urol, 2007. **177**(4): p. 1434-7.
12. Gokden, M., J.T. Al-Hinti, and S.I. Harik, *Peripheral nervous system pathology in fragile X tremor/ataxia syndrome (FXTAS).* Neuropathology, 2009. **29**(3): p. 280-4.
13. Louis, E., et al., *Parkinsonism, dysautonomia, and intranuclear inclusions in a fragile X carrier: a clinical-pathological study.* Mov Disord, 2006. **21**(3): p. 420-5.
14. Tassone, F., et al., *Intranuclear inclusions in neural cells with premutation alleles in fragile X associated tremor/ataxia syndrome.* J Med Genet, 2004. **41**(4): p. e43.
15. Buijsen, R.A., et al., *Presence of inclusions positive for polyglycine containing protein, FMRpolyG, indicates that repeat-associated non-AUG translation plays a role in fragile X-associated primary ovarian insufficiency.* Hum Reprod, 2016. **31**(1): p. 158-68.
16. Boivin, M., et al., *Potential pathogenic mechanisms underlying Fragile X Tremor Ataxia Syndrome: RAN translation and/or RNA gain-of-function?* Eur J Med Genet, 2018. **61**(11): p. 674-679.
17. Yu, S., et al., *Fragile X genotype characterized by an unstable region of DNA.* Science, 1991. **252**(5009): p. 1179-81.

18. Peprah, E., et al., *Examination of FMR1 transcript and protein levels among 74 premutation carriers.* J Hum Genet, 2010. **55**(1): p. 66-8.
19. Kenneson, A., et al., *Reduced FMRP and increased FMR1 transcription is proportionally associated with CGG repeat number in intermediate-length and premutation carriers.* Hum Mol Genet, 2001. **10**(14): p. 1449-54.
20. Tassone, F., et al., *Elevated levels of FMR1 mRNA in carrier males: a new mechanism of involvement in the fragile-X syndrome.* Am J Hum Genet, 2000. **66**(1): p. 6-15.
21. Jacquemont, S., et al., *Penetrance of the fragile X-associated tremor/ataxia syndrome in a premutation carrier population.* JAMA, 2004. **291**(4): p. 460-9.
22. Rodriguez-Revenga, L., et al., *Penetrance of FMR1 premutation associated pathologies in fragile X syndrome families.* Eur J Hum Genet, 2009. **17**(10): p. 1359-62.
23. Sellier, C., et al., *The multiple molecular facets of fragile X-associated tremor/ataxia syndrome.* J Neurodev Disord, 2014. **6**(1): p. 23.
24. Sellier, C., et al., *Sam68 sequestration and partial loss of function are associated with splicing alterations in FXTAS patients.* EMBO J, 2010. **29**(7): p. 1248-61.
25. Sellier, C., et al., *Sequestration of DROSHA and DGCR8 by expanded CGG RNA repeats alters microRNA processing in fragile X-associated tremor/ataxia syndrome.* Cell Rep, 2013. **3**(3): p. 869-80.
26. Jin, P., et al., *Pur alpha binds to rCGG repeats and modulates repeat-mediated neurodegeneration in a Drosophila model of fragile X tremor/ataxia syndrome.* Neuron, 2007. **55**(4): p. 556-64.
27. Sofola, O.A., et al., *RNA-binding proteins hnRNP A2/B1 and CUGBP1 suppress fragile X CGG premutation repeat-induced neurodegeneration in a Drosophila model of FXTAS.* Neuron, 2007. **55**(4): p. 565-71.
28. Zu, T., et al., *Non-ATG-initiated translation directed by microsatellite expansions.* Proc Natl Acad Sci U S A, 2011. **108**(1): p. 260-5.
29. Todd, P.K., et al., *CGG repeat-associated translation mediates neurodegeneration in fragile X tremor ataxia syndrome.* Neuron, 2013. **78**(3): p. 440-55.
30. Nguyen, L., J.D. Cleary, and L.P.W. Ranum, *Repeat-Associated Non-ATG Translation: Molecular Mechanisms and Contribution to Neurological Disease.* Annu Rev Neurosci, 2019. **42**: p. 227-247.
31. Kearse, M.G., et al., *CGG Repeat-Associated Non-AUG Translation Utilizes a Cap-Dependent Scanning Mechanism of Initiation to Produce Toxic Proteins.* Mol Cell, 2016. **62**(2): p. 314-322.
32. Green, K.M., et al., *RAN translation at C9orf72-associated repeat expansions is selectively enhanced by the integrated stress response.* Nat Commun, 2017. **8**(1): p. 2005.
33. Sellier, C., et al., *Translation of Expanded CGG Repeats into FMRpolyG Is Pathogenic and May Contribute to Fragile X Tremor Ataxia Syndrome.* Neuron, 2017. **93**(2): p. 331-347.
34. Hukema, R.K., et al., *Reversibility of neuropathology and motor deficits in an inducible mouse model for FXTAS.* Hum Mol Genet, 2015. **24**(17): p. 4948-57.
35. Hukema, R.K., et al., *Induced expression of expanded CGG RNA causes mitochondrial dysfunction in vivo.* Cell Cycle, 2014. **13**(16): p. 2600-8.
36. Haify, S.N., et al., *In silico, in vitro, and in vivo Approaches to Identify Molecular Players in Fragile X Tremor and Ataxia Syndrome.* Front Mol Biosci, 2020. **7**: p. 31.

37. Oh, S.Y., et al., *RAN translation at CGG repeats induces ubiquitin proteasome system impairment in models of fragile X-associated tremor ataxia syndrome.* Hum Mol Genet, 2015. **24**(15): p. 4317-26.
38. Willemsen, R., et al., *The FMR1 CGG repeat mouse displays ubiquitin-positive intranuclear neuronal inclusions; implications for the cerebellar tremor/ataxia syndrome.* Hum Mol Genet, 2003. **12**(9): p. 949-59.
39. Bergink, S., et al., *The DNA repair-ubiquitin-associated HR23 proteins are constituents of neuronal inclusions in specific neurodegenerative disorders without hampering DNA repair.* Neurobiol Dis, 2006. **23**(3): p. 708-16.
40. Hashem, V., et al., *Ectopic expression of CGG containing mRNA is neurotoxic in mammals.* Hum Mol Genet, 2009. **18**(13): p. 2443-51.
41. Gunal, D.I., et al., *New alternative agents in essential tremor therapy: double-blind placebo-controlled study of alprazolam and acetazolamide.* Neurol Sci, 2000. **21**(5): p. 315-7.
42. Disney, M.D., et al., *A small molecule that targets r(CGG)(exp) and improves defects in fragile X-associated tremor ataxia syndrome.* ACS Chem Biol, 2012. **7**(10): p. 1711-8.
43. Childs-Disney, J.L. and M.D. Disney, *Approaches to Validate and Manipulate RNA Targets with Small Molecules in Cells.* Annu Rev Pharmacol Toxicol, 2016. **56**: p. 123-40.
44. Yang, W.Y., et al., *Small Molecule Recognition and Tools to Study Modulation of r(CGG)(exp) in Fragile X-Associated Tremor Ataxia Syndrome.* ACS Chem Biol, 2016. **11**(9): p. 2456-65.
45. Seibenhener, M.L. and M.W. Wooten, *Isolation and culture of hippocampal neurons from prenatal mice.* J Vis Exp, 2012(65).
46. Zakeri, B. and G.D. Wright, *Chemical biology of tetracycline antibiotics.* Biochem Cell Biol, 2008. **86**(2): p. 124-36.
47. Motulsky, H.J. *Graphpad Statistics Guide*. [cited 2020; Available from: http://www.graphpad.com/guides/prism/7/statistics/index.htm.
48. Iwahashi, C.K., et al., *Protein composition of the intranuclear inclusions of FXTAS.* Brain, 2006. **129**(Pt 1): p. 256-71.
49. Van Dam, D., et al., *Cognitive decline, neuromotor and behavioural disturbances in a mouse model for fragile-X-associated tremor/ataxia syndrome (FXTAS).* Behav Brain Res, 2005. **162**(2): p. 233-9.
50. Wenzel, H.J., et al., *Ubiquitin-positive intranuclear inclusions in neuronal and glial cells in a mouse model of the fragile X premutation.* Brain Res, 2010. **1318**: p. 155-66.
51. Zoghbi, H.Y. and J. Botas, *Mouse and fly models of neurodegeneration.* Trends Genet, 2002. **18**(9): p. 463-71.
52. Saudou, F., et al., *Huntingtin acts in the nucleus to induce apoptosis but death does not correlate with the formation of intranuclear inclusions.* Cell, 1998. **95**(1): p. 55-66.
53. Swayze, E.E., Bhat B., *The Medicinal Chemistry of Oligonucleotides*, in *Antisense Drug Technology: Principles, Strategies, and Applications, Second Edition*, S.T. Crooke, Editor. 2007, Taylor & Francis. p. 143-182.
54. Parkesh, R., et al., *Design of a bioactive small molecule that targets the myotonic dystrophy type 1 RNA via an RNA motif-ligand database and chemical similarity searching.* J Am Chem Soc, 2012. **134**(10): p. 4731-42.

55. Lee, M.M., A. Pushechnikov, and M.D. Disney, *Rational and modular design of potent ligands targeting the RNA that causes myotonic dystrophy 2.* ACS Chem Biol, 2009. **4**(5): p. 345-55.
56. Su, Z., et al., *Discovery of a biomarker and lead small molecules to target r(GGGGCC)-associated defects in c9FTD/ALS.* Neuron, 2014. **83**(5): p. 1043-50.
57. Tran, T., et al., *Targeting the r(CGG) repeats that cause FXTAS with modularly assembled small molecules and oligonucleotides.* ACS Chem Biol, 2014. **9**(4): p. 904-12.
58. Yang, W.Y., et al., *Inhibition of Non-ATG Translational Events in Cells via Covalent Small Molecules Targeting RNA.* J Am Chem Soc, 2015. **137**(16): p. 5336-45.
59. Yoshiki, A. and K. Moriwaki, *Mouse phenome research: implications of genetic background.* ILAR J, 2006. **47**(2): p. 94-102.
60. Meli, D.N., et al., *Doxycycline reduces mortality and injury to the brain and cochlea in experimental pneumococcal meningitis.* Infect Immun, 2006. **74**(7): p. 3890-6.
61. *LiverTox: Clinical and Research Information on Drug-Induced Liver Injury.* 2012.
62. Heessen, S., M.G. Masucci, and N.P. Dantuma, *The UBA2 domain functions as an intrinsic stabilization signal that protects Rad23 from proteasomal degradation.* Mol Cell, 2005. **18**(2): p. 225-35.
63. Varadan, R., et al., *Structural determinants for selective recognition of a Lys48-linked polyubiquitin chain by a UBA domain.* Mol Cell, 2005. **18**(6): p. 687-98.
64. Verma, R., et al., *Multiubiquitin chain receptors define a layer of substrate selectivity in the ubiquitin-proteasome system.* Cell, 2004. **118**(1): p. 99-110.
65. Ortolan, T.G., et al., *The DNA repair protein rad23 is a negative regulator of multi-ubiquitin chain assembly.* Nat Cell Biol, 2000. **2**(9): p. 601-8.
66. Raasi, S. and C.M. Pickart, *Rad23 ubiquitin-associated domains (UBA) inhibit 26 S proteasome-catalyzed proteolysis by sequestering lysine 48-linked polyubiquitin chains.* J Biol Chem, 2003. **278**(11): p. 8951-9.
67. Glickman, M.H. and A. Ciechanover, *The ubiquitin-proteasome proteolytic pathway: destruction for the sake of construction.* Physiol Rev, 2002. **82**(2): p. 373-428.

CHAPTER 5

5

Neuropathology of *FMR1*-premutation carriers presenting with dementia and neuropsychiatric symptoms

Anke A. Dijkstra[1*], Saif N. Haify[2], Niek A. Verwey[3], Niels D. Prins[4,5], Esmay C. van der Toorn[2], Annemieke. J.M. Rozemuller[1], Marianna Bugiani[1], Wilfred F.A. den Dunnen[6], Peter K. Todd[7,8], Nicolas Charlet-Berguerand[9], Rob Willemsen[2], Renate K. Hukema[2,10], Jeroen J.M. Hoozemans[1]

[1] Department of Pathology, Amsterdam Neuroscience, Amsterdam University Medical Centre, location VUmc, Amsterdam, The Netherlands.
[2] Department of Clinical Genetics, Erasmus MC, Rotterdam, the Netherlands.
[3] Department of Neurology, Medisch Centrum Leeuwarden, Leeuwarden, The Netherlands
[4] Alzheimer Center, Department of Neurology, VU University Medical Center, Amsterdam Neuroscience, Netherlands.
[5] Brain Research Center, Amsterdam, The Netherlands.
[6] Department of Pathology and Medical Biology, University Medical Center Groningen, Groningen, The Netherlands.
[7] Department of Neurology, University of Michigan, Ann Arbor, MI, 48109 USA
[8] Department of Veterans Affairs Ann Arbor Healthcare System, Ann Arbor, MI USA
[9] Institut de Génétique et de Biologie Moléculaire et Cellulaire (IGBMC), INSERM U964, CNRS UMR7104, University of Strasbourg, 67400 Illkirch, France
[10] Rotterdam University of Applied Sciences, Department of Health Care Studies, Rotterdam, The Netherlands

[*] Corresponding author: Anke A. Dijkstra (a.dijkstra@amsterdamumc.nl)

Brain Communications, 2021 Jan 27; Volume 3, Issue 1, fcab007

Abstract

CGG repeat expansions within the premutation range (55-200) of the *FMR1* gene can lead to Fragile-X associated tremor and ataxia syndrome (FXTAS) and Fragile-X associated neuropsychiatric disorders (FXAND). These CGG repeats are translated into a toxic polyglycine-containing protein, FMRpolyG. Pathology of FXTAS and FXAND comprise FMRpolyG- and p62-positive intranuclear inclusions. Diagnosing a *FMR1*-premutation carrier remains challenging, as the clinical features overlap with other neurodegenerative diseases. Here, we describe two male cases with FXAND symptoms and mild movement disturbances and novel pathological features that can attribute to the variable phenotype. Macroscopically, both donors did not show FXTAS-characteristic white matter lesions on MRI, however, vascular infarcts in cortical- and subcortical regions were identified. Immunohistochemistry analyses revealed a high number of FMRpolyG intranuclear inclusions throughout the brain, which were also positive for p62. Importantly, we identified a novel pathological vascular phenotype with inclusions present in pericytes and endothelial cells. Although these results need to be confirmed in more cases, we propose that these vascular lesions in the brain could contribute to the complex symptomology of *FMR1*-premutation carriers. Overall, our report suggests that FXTAS and FXAND may present diverse clinical involvements resembling other types of dementia, and in the absence of genetic testing, FMRpolyG can be used post-mortem to identify premutation carriers.

Keywords: neuropathology, trinucleotide repeat diseases, inclusion diseases, small vessel disease, genetics, dementia

Introduction

The *Fragile X mental retardation 1 (FMR1)* gene contains a CGG dynamic trinucleotide repeat sequence. Within the general population, this number of CGG repeats is present under 55 repeats [1]. Expansions of the repeat sequence to more than 200 CGG repeats result in the absence of the *FMR1* protein, and in the fragile X syndrome [2]. Smaller expansions, from 55 to 200 CGG repeats, are in the premutation range [3] and can lead to Fragile-X associated diseases, including the neurodegenerative diseases Fragile X-associated tremor and ataxia syndrome (FXTAS) [4], and the Fragile X-associated neuropsychiatric disorders (FXAND) [5]. CGG-repeats in the premutation range are transcribed and translated into a toxic polyglycine-containing protein, named FMRpolyG protein [6]. FMRpolyG is considered to play a major role in the pathogenesis of FXTAS [7, 8].

The FXTAS phenotype is found in 30% of male carriers and 11-18% of female carriers of the *FMR1*-premutation and is characterized primarily by intention tremors and cerebellar gait ataxia, and in severe cases accompanied by executive function, memory deficits, and Parkinsonism [9-11]. The onset of the motor symptoms may present after 50 years of age, with longer expansions correlating with an earlier onset and more severe disease [12]. However, additional clinical features have been recently described in premutation carriers that include anxiety and depression, which has led to the recent identification of FXAND, encompassing a large group of premutation carriers presented with neuropsychiatric symptoms [5]. Consequently, diagnosing a *FMR1*-premutation carrier remains challenging, as the clinical features may overlap with other neurodegenerative diseases [13, 14]. A genetic screening for CGG expansion can provide the conclusive answer, especially when a grandchild or child is diagnosed with a full mutation leading to the Fragile X syndrome [15].

The pathology of an *FMR1*-premutation includes p62-positive and mostly solitary, spherical intranuclear inclusions, present in both neurons and astrocytes and found in broad distribution throughout the brain and brainstem [16, 17]. Post-mortem studies in FXTAS donors also revealed cerebellar and cerebral white matter abnormalities with inclusions in astrocytes, particularly evident in sub-cortical cerebral white matter [17]. This is consistent with MRI studies that reveal global brain atrophy and white matter signal changes with characteristic feature middle cerebral peduncle (MCP) presents in about 40% of the FXTAS patients [18]. Here, we describe novel pathological features of two cases with a *FMR1*-premutation and a clinical profile of FXAND with mild movement impairments. Our study supports recent studies showing that testing for FMRpolyG immunoreactivity can confirm presence of the *FMR1*-premutation [6, 19].

Materials and methods

Magnetic Resonance Imaging

Donors were scanned on a 3T whole-body magnetic resonance system (General Electric, Milwaukee, WI). The protocol included a 3D T1-weighted fast spoiled gradient echo sequence for volumetric measurements and for donor two, a 3D T2-weighted fluid-attenuated inversion recovery (FLAIR) sequence for white matter lesion segmentation.

Post-mortem tissue

Post-mortem tissue was obtained through the Netherlands Brain Bank (NBB) and the department of Pathology, University Medical Center Groningen, The Netherlands. Tissue of a spinocerebellar ataxia donor type 3 (SCA3) was obtained through the NBB and used as a negative control for FMRpolyG. Tissue was fixed in 4% PFA for 4 weeks and dissected in 24 diagnostic regions. Sections of 8 µm of each region were cut and stained using Hematoxylin and Eosin (H&E) and Perls staining for iron deposits. Donors were routinely immunostained for amyloid-beta (1:800; mouse, clone IC16 kind gift of Prof Dr Korth, Heinrich Heine University, Düsseldorf, Germany), tau (1:800; mouse, clone AT8, Thermo Fisher Scientific, MA, USA), alpha-synuclein (1:1000; mouse, Zymed; Thermo Fisher Scientific, Bleiswijk, The Netherlands), TDP-43 (pTDP43, 1:8000; mouse, clone 11-9, Cosmo Bio, Japan) and polyQ (1:800; mouse, clone 5TF1-1C2, Merck Millipore, Burlington, USA).

Immunohistochemical procedures

Sections were deparaffinized and then incubated in 0.3% H_2O_2 in phosphate buffer saline (PBS; pH 7.4) for 30 minutes. Sections were then washed with PBS (3x5 minutes) and antigen retrieval was performed in citrate buffer (pH 6.0) using an autoclave (121°C for 5 minutes). After washing, sections were incubated in primary antibody (p62, 1:1000; mouse, clone 3/P62 lck ligand, BD Transduction Laboratories, San Jose, CA, USA) FMRpolyG (NTF1), 1:200; Rabbit, antibody developed by Peter Todd; FMRpolyG (1C5), 1:500; mouse developed by Nicolas Charlet-Berguerand) for 1 hour at room temperature. After washing, sections were incubated with HRP-labelled Envision (K5007; DAKO, Glostrup, Denmark), washed and visualization of immunostaining was seen with chromogen 3,3'-diaminobenzidine (DAB; K5007; DAKO). Finally, sections were counterstained with hematoxylin, dehydrated, and cover slipped with Quick-D (Klinipath, Duiven, The Netherlands). Negative controls were included by omitting the primary antibody and showed no immunoreactivity.

Double-labelling immunofluorescence

For double-immunofluorescence, sections were incubated for one hour with a combination of primary antibodies; p62 (1:1000) and FMRpolyG (NTF1) (1:200). Subsequently sections were incubated with fluorescent probed secondary antibodies 1:250 (1 hour); Goat Anti-Rabbit-594 (Invitrogen, Carlsbad, CA, USA), and Goat Anti-Mouse 488 (Life Technologies,

Carlsbad, CA, USA). Auto-fluorescence was blocked with 0.2% Sudan Black for 5 minutes at room temperature and mounted with DAPI Fluoromount G (Southern Biotech, AL, USA).

Statistical Analysis
No analyses were performed.

Data availability
Data are available upon request.

Results

Clinical profile
Donor one: At age 57, the patient complained about pain in his legs and subsequently polyneuropathy was diagnosed. At 59, he was seen again at the neurological outpatient clinic due to a minor stroke. Besides the sub-acute stroke related neurological signs, the patient complained about progressive cognitive problems (memory and slowness). Additionally, behavioral changes (apathic and passive) were mentioned. The patient spent whole days just listening to music and was easily agitated and not cooperative. Neurological examination showed several signs of Parkinsonism. Initially, Vascular Dementia/Parkinsonism (VAD) or Parkinson's Disease (PD) were mentioned as diagnosis. The MRI showed mild vascular changes, and VAD seemed unlikely. As disease progressed, other symptoms became more apparent such as executive problems, increased cognitive decline but also significant bradyphrenia. Clinically, the patient was demented and atypical Alzheimer's disease (AD) and fronto-temporal dementia (FTD) were added to the differential diagnosis. Biomarkers did not provide any indication for AD. Additionally, an FDG-PET scan was performed showing a pattern which partially suited corticobasal degeneration (CBD) or less likely progressive supranuclear palsy. However, CBD or PSP were clinically less evident, since dementia with significant frontal characteristics was pronounced. The patient showed increased psychiatric problems, including aggressiveness towards partner, apathy, and compulsive behavior. Due to an acute unsustainable situation at home, the patient was taken into a psychiatric hospital where he committed suicide at age 62. After autopsy, the donor presented intranuclear inclusion pathology. FMRpolyG immunohistochemistry was positive and subsequent genetic testing revealed a 107 CGG repeat within the *FMR1* gene.

Donor two: At age 43, this patient came to the memory clinic with memory problems and aphasia, while his partner noted that he became aggressive towards her. He showed signs of social anxiety and suffered from chronic depression. He was initially diagnosed with Korsakoff's syndrome based on earlier excessive alcohol consumption and the early onset

of the symptoms. At age 51, he complained of memory loss and concentration problems and character changes. At age 53 he suffered from cardiac palpitations and cramps in his fingers, but no cause was found. He had visual hallucinations, in which he saw persons and felt drawn towards the cemetery. A year later he experienced a change in gait, and dragged his feet. At age 55, he had a major stroke in the right occipital region, reporting loss of strength and coordination in his left arm and leg, followed by a spontaneous recovery. A year later he suffered from falling and increased bradykinesia. He had a light tremor in both hands, started snoring and developed sleep apnea. Around this time, his grandchildren were born and diagnosed with Fragile X syndrome. Genetic testing revealed a 77 CGG repeat in the *FMR1* gene, and his initial diagnosis of Korsakov's syndrome was retracted. Neuropsychological tests showed cognition disorders concerning short- and long-term memory, feelings of depression, fear, paranoia and anger, agitation, loss of concentration and initiative, and difficulties with divided attention. Over the years, his symptoms worsened, with increasing cognitive problems, ataxia, tremor, hallucinations and dependency on others for his personal care and hygiene. He was well aware of his deterioration and started a euthanasia trajectory and passed away at age 65. The disease course of both donors is summarized in **Figure 1A**.

MRI findings

Both donors showed general atrophy throughout the cortex (**Fig. 1B, C, F, G**) and dilation of ventricles (**Fig. 1C, E, G**). White matter intensity changes were observed around the ventricles, and small lesions were observed (**Fig. 1B, C, D, E, M**) Donor 1 (**Fig. 1E**) and Donor 2 (**Fig. 1K**). While donor two suffered from a stroke 10 years prior to his passing, a susceptibility weighted imaging (SWI) for donor 2 revealed no large vascular damage (**Fig. 1L**). No obvious thinning of the corpus callosum was seen (**Fig. 1M**). Overall, both donors revealed mild abnormalities on MRI including periventricular white matter intensities and mild global atrophy fitting with several neurodegenerative diseases.

P62-Inclusion pathology

Intranuclear p62-positive inclusions were found in all brain structures, similar as reported before for FXTAS [17]. Cortical structures such as the frontal cortex showed inclusions in neurons and astrocytes in grey and white matter (**Fig. 2A-D**). Hippocampus showed many inclusions in CA and dentate gyrus granular cells (**Fig. 2E, F**). In the cerebellum, inclusions were observed in the white matter and granular cell layer, and in most of the Bergmann glia but not in the Purkinje cells (**Fig. 2G, H**). The substantia nigra (SN) showed inclusions in astrocytes and dopaminergic neurons (**Fig. 2I**). Similar to earlier reported findings in FXTAS, inclusions were also found in the ependymal layer (**Fig. 2J**) and choroid plexus (**Fig. 2K**). Additional findings include the presence of inclusions in the extra-axial part of nerve 3, but not intra-axial (**Fig. 2L**).

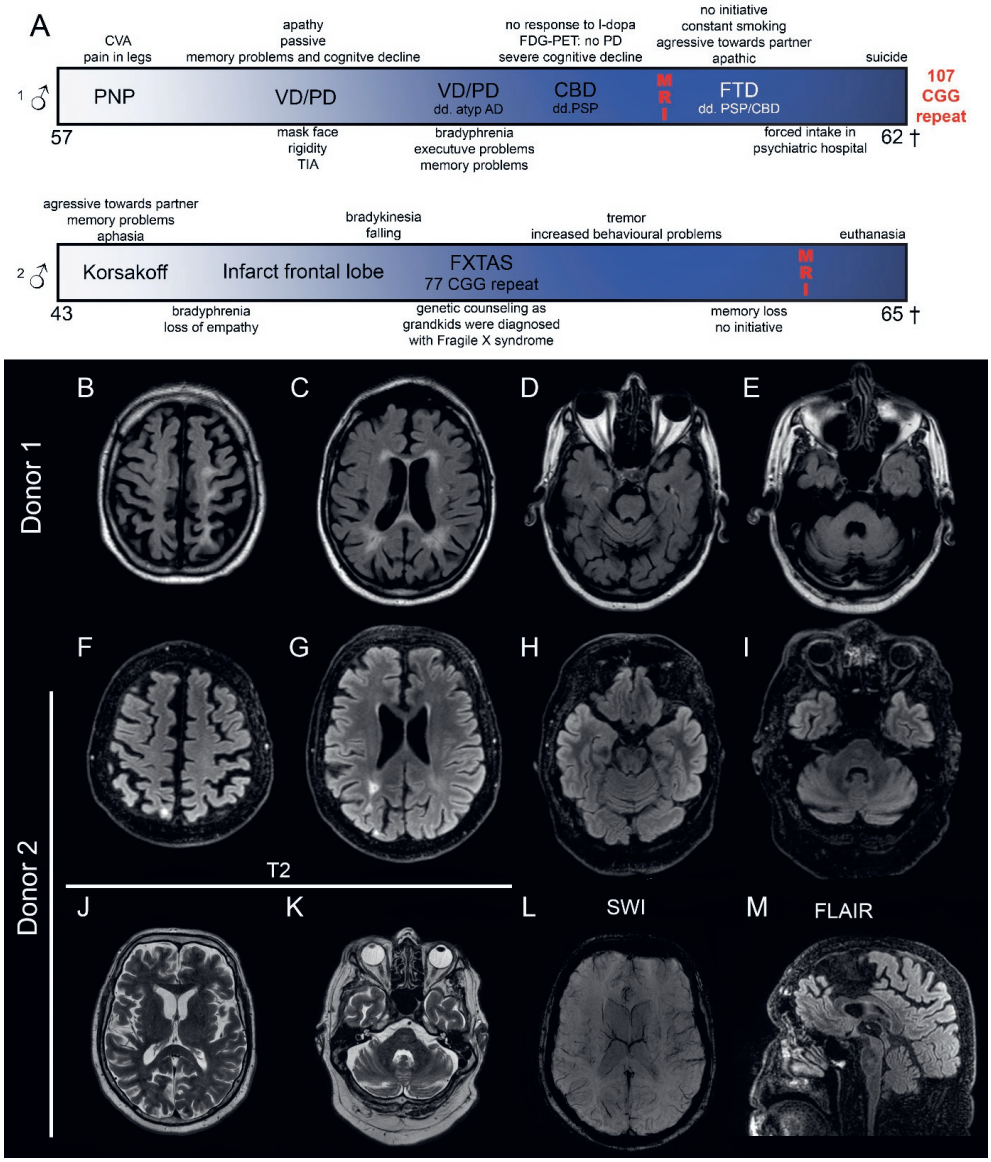

Figure 1 | Clinical course and imaging results of Donors 1 and 2. Clinical course **(A)** shows moment in time of MRI. General mild atrophy is observed **(B, F)**. Ventricles are slightly dilated and donor one shows periventricular white matter lesions **(C)**, donor two shows an increased signal due to an infarct **(G)**. Slight cerebellar atrophy can be seen in both donors **(D, E, H, I)**. Enlargement of the fourth ventricle, but no FXTAS-characteristic MCP sign can be seen. T2-FLAIR of donor two does not show increased insular and MCP signal intensities **(J, K)**, no abnormalities in vasculature **(K)**, and no thinning of the corpus callosum **(M)**. CVA: cerebrovascular accident; PNP: polyneuropathy; VD: vascular dementia; PD: Parkinson's disease: AD: Alzheimer's disease: CBD: corticobasal degeneration: FTD: frontotemporal dementia; PSP: progressive supranuclear palsy.

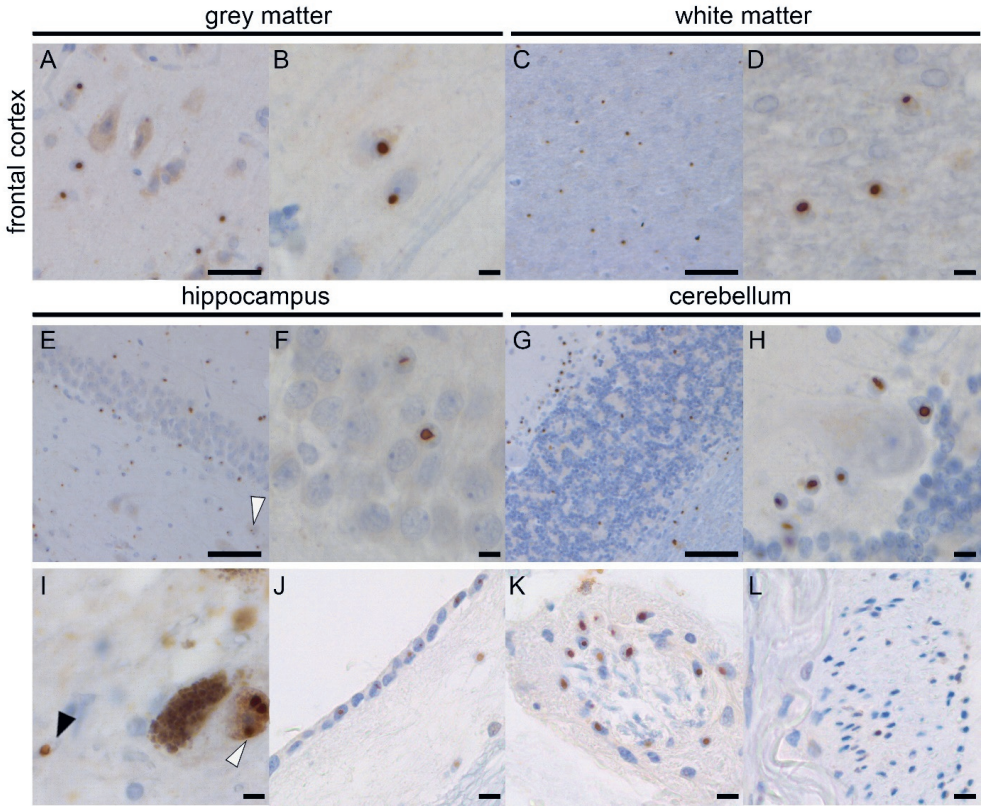

Figure 2 | p62-Pathology in Donor 2. Abundant p62-positive nuclear inclusions in the frontal cortex grey matter **(A, B)** and white matter **(C, D)**. The hippocampus shows nuclear inclusions in the CA4 neuron **(white arrowhead)** and the dentate gyrus **(E, F)**. In the cerebellum, inclusions are seen in the white matter and granular layer **(G, H)**. No inclusions were seen in the Purkinje cells, whereas most Bergmann glia showed inclusions **(H)**. Pathology was also seen in the dopaminergic neurons (white arrowhead) and astrocytes **(black arrowhead)** in the substantia nigra **(I)**, ependymal **(J)**, extra-axial cells of the 3rd nerve **(K)**, and choroid plexus cells **(L)**. Scale bar **A** is 50 µm, scale bar **B, D, F, H, I-L** is 10 µm, scale bar **C, E, G** is 100 µm.

Vascular pathology

Both donors showed vascular lesions such as lacunae and strokes throughout the brain. In the H&E staining, brown iron deposits were appreciated (**Fig. 3A, E**). Perls staining showed that the disrupted vasculature resulted in iron deposits, found throughout the cortex and hippocampus in normal age-related amounts (**Fig. 3B, F**), and an abnormal increased amount of iron deposits in the ventral region of the SN (**Fig. 3C, G**). Small p62-positive intranuclear inclusions were observed in the endothelial cells of the blood vessels, as well as in the pericytes (**Fig. 3D, H**). An overview of p62-inclusions in different cell types and iron deposits visualized by Perls staining is provided per region in **Table 1**.

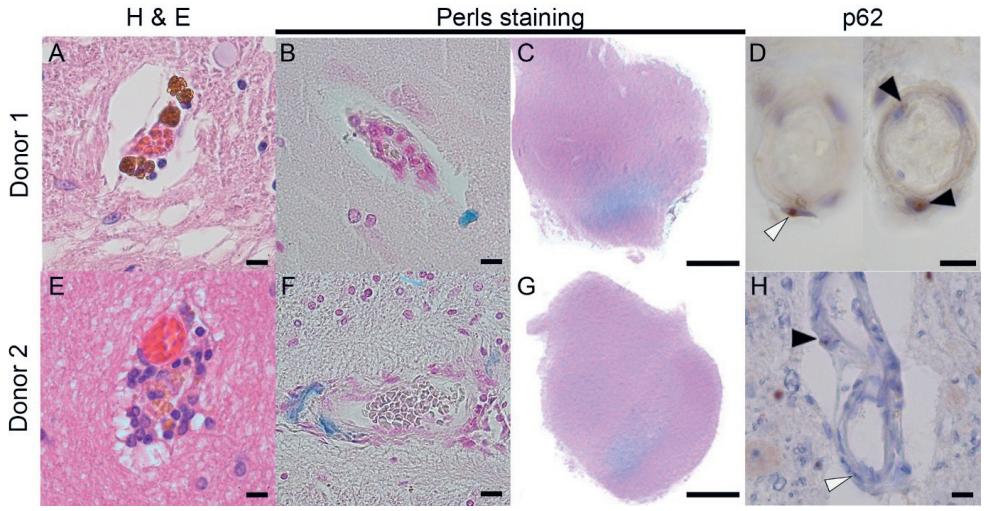

Figure 3 | Vascular pathology of Donors 1 and 2. Brown iron-like deposits are seen in both donors **(A, E)**, which stain blue in a Perls staining **(B, F)**. Both donors showed abnormal increased iron deposits in the ventral part of the substantia nigra **(C, G)**. Throughout the brain, inclusions were seen in the endothelial cells **(black arrowhead)** and the pericytes **(white arrowhead) (D, H)**. Scale bar **A, B, D, E, F, H** is 10 µm, scale bar **C, G** is 0.5 cm.

Table 1 | Distribution and burden of inclusion pathology and iron deposits throughout the brain of donor 1 and 2.

		Donor 1 p62				Donor 2 p62			
Area	**Region**	**neuron**	**astrocytes**	**vessel**	**Perls**	**neuron**	**astrocytes**	**vessel**	**Perls**
Cortex	Frontal cortex	•••	•••	••	•	•••	•••	•••	••
	Temporal cortex	•••	•••	••	•	•••	•••	••	••
	Parietal	••	••	•	•	•••	•••	••	•
	Occipital cortex	••	••	•	•	••	•••	••	•
	Insular cortex	••	•••	•	•	••	•••	•	•
Limbic	Amygdala	••	••	•	-	••	•••	-	-
	Hippocampus	•••	•••	••	-	•••	•••	•••	-
	Entorhinal cortex	•	••	•	•	••	•••	•	-
Subcortical	Putamen	•••	•••	•••	•••	••	••	•	•••
	Globus Pallidus	•••	•••	•••	•••	•	••	•	•••
	Caudatus	•••	•••	••	•••	••	•••	••	•••
	Thalamus	••	••	•	••	••	••	•	•
Cerebellum	Dentate nucleus	•	••	•	-	•	•••	•	-
	Folia	-	•••	•	-	-	•••	-	-
Brainstem	Substantia Nigra	••	••	•••	••	•••	•••	•••	•••
	Locus ceruleus	•••	•••	•	-	•••	•••	-	-

p62: -, not present; •, few inclusions present; ••, moderate amount of inclusions present; •••, abundant amount of inclusion present. Perls: -, not present; •, few iron deposits; ••, moderate amount of iron deposits; •••, abundant amount of iron deposits.

FMRpolyG pathology

FMRpolyG was detected in all regions of the brain. FMRpolyG intranuclear inclusions are shown in the frontal cortex (**Fig. 4A**), the hippocampus (**Fig. 4B**), the astrocytes in SN (**Fig. 4C**) and in the Bergmann glia in the cerebellum (**Fig. 4D**). FMRpolyG positivity was also observed in the vasculature. Double-immunofluorescence for FMRpolyG and p62 showed that FMRpolyG protein co-localizes with p62 inclusions in the cerebellum (**Fig. 4E-H**), where an occasional p62-inclusion did not show FMRpolyG positivity. As a negative control, no immunoreactivity of FMRpolyG was observed in a case of spinocerebellar ataxia 3 (SCA3) (**Fig. 4I-L**), confirming the specificity of our antibodies for the *FMR1*-premutation translated product, FMRpolyG.

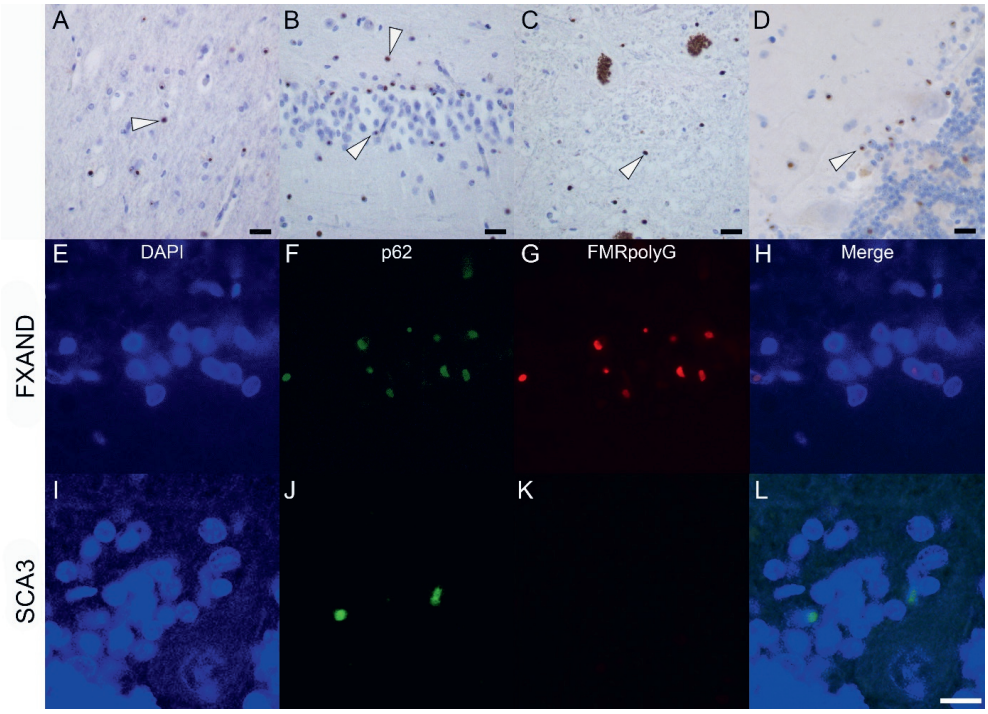

Figure 4 | FMRpolyG staining in Donor 2. FMRpolyG (1C5) positive-inclusions are seen in the frontal cortex **(A)**, hippocampus **(B)**, substantia nigra **(C)**, and cerebellum **(D)**. Inclusions are indicated with white arrowheads. Co-localization of p62 and FMRpolyG (NTF1) immunopositivity in the Bergmann glia of the cerebellum in donor two and spinocerebellar ataxia 3 (SCA3) donor. Bergmann glia shown with DAPI **(E, I)** showed inclusions with p62 **(F, J)**, and FMRpolyG **(G, K)**. Co-localization of the immunopositivity shows overlap in FXAND **(H)** and not in SCA3 **(L)**. Scale bars are 10 µm.

Discussion

Here, we report two cases with dementia and psychiatric symptoms that were diagnosed as *FMR1*-premutation carriers either post-mortem or in advanced disease state. While initial symptoms suggested dementia, both donors showed mild movement disturbances during the progression of the disease. MRI did not reveal the characteristic FXTAS-related imaging profile, which, in combination with the symptoms, posed a challenge for the attending clinicians to diagnose the patients as potential FMR1-premutation carriers. Interestingly, both donors experienced cerebrovascular accidents which could be explained by the post-mortem findings of FMRpolyG inclusions in the endothelial cells and pericytes. We propose that these brain vascular lesions may contribute to the complex symptomology of *FMR1*-premutation carriers.

Clinical findings

The clinical phenotype for FXTAS has been described in detail, where movement symptoms are the most prominent features of the disease [9, 10, 20]. However, the two *FMR1*-premutation individuals described here exhibited only mild movement symptoms such as rigidity and bradykinesia, and showed predominantly psychiatric problems, matching the recent description of FXAND [5]. Interestingly, donor one experienced polyneuropathy as one of the first symptoms, which can be a prevalent sign in FMR1-premutation carriers with FXTAS presentation [21, 22]. Of clinical importance, the two donors did not show the typical MCP imaging feature of FXTAS, however, they did show mild atrophy, similar to other dementias. This work highlights the challenge for clinicians to diagnose *FMR1*-premutation carriers, and stresses the importance of genetic screening for CGG repeats within *FMR1* for suspected dementia with behavioral features.

Inclusion pathology

The p62-inclusion pathology of the two cases described here show a similar distribution pattern as described in FXTAS [17, 23]. However, we describe here an additional feature with inclusions present in the endothelial cells and pericytes that can compromise vascular function. As both donors also suffered from multiple vascular incidents in the brain, this suggests that apart from cellular dysfunction, problems in the brain vasculature can contribute to the *FMR1*-premutation phenotype where infarcts or transient ischemic attacks can disrupt blood supply. Consistent with our hypothesis, a high incidence of cardiac abnormalities and cerebrovascular disease have been observed in FXTAS donors [24, 25], which could be linked to a decline in vascular integrity due to inclusion pathology. In addition, inclusions have been observed in cardiomyocytes [26], suggesting that the peripheral vasculature could also be compromised. Furthermore, inclusions were found in the extra-axial part of the nerve sheet, it is possible that the neuropathy can be explained by nerve involvement in the sensory nerves, which has to be studied in future autopsies of carriers.

Our work also confirms that the inclusion pathology in carriers of the *FMR1* premutation can be visualized with antibodies directed against FMRpolyG [19], with almost all p62-positive inclusions also positive for FMRpolyG. However, we noted that the dopaminergic neurons of the SN showed multiple p62-positive inclusions in one cell that were not positive for FMRpolyG. These inclusions are most likely Marinesco bodies [27], which are age-related nuclear inclusions restricted to the SN. FMRpolyG labeling is specific to the protein translated from the *FMR1*-premutation, and is not present in the polyQ aggregates found in SCA3. Importantly, we propose that FMRpolyG antibodies can be used as diagnostic tools to identify *FMR1*-premutation carriers post-mortem, notably in large retrospective brain bank cohorts.

Conclusion

Our study also confirms that the inclusion pathology in carriers of the *FMR1* premutation can be visualized with antibodies directed against FMRpolyG [19], with almost all p62-positive inclusions also positive for FMRpolyG. However, we noted that the dopaminergic neurons of the SN showed multiple p62-positive inclusions in one cell that were not positive for FMRpolyG. These inclusions are most likely Marinesco bodies [27], which are age-related nuclear inclusions restricted to the SN. FMRpolyG labelling is specific to the protein translated from the *FMR1*-premutation, and it is not present in the polyQ aggregates found in SCA3. Importantly, we propose that FMRpolyG antibodies can be used as diagnostic tools to identify *FMR1*-premutation carriers post-mortem, notably in large retrospective brain bank cohorts.

Acknowledgements

The authors thank the Netherlands Brain Bank for providing tissue and Irene van Dijken for her input on the immunofluorescence experiments.

Funding

This study was funded by Memorabel Zorgonderzoek Nederland, gebied Medische wetenschappen (733050507). Peter Todd was supported by the National Institutions of Health (R01NS086810, R01NS099280) and the Veterans affairs (BLRD BX004842).

Competing interests

The authors report no competing interests.

References

1. Hagerman, P.J. and R.J. Hagerman, *Fragile X-associated tremor/ataxia syndrome.* Ann N Y Acad Sci, 2015. **1338**: p. 58-70.
2. Murray, J., et al., *Screening for fragile X syndrome: information needs for health planners.* J Med Screen, 1997. **4**(2): p. 60-94.
3. Brouwer, J.R., R. Willemsen, and B.A. Oostra, *The FMR1 gene and fragile X-associated tremor/ataxia syndrome.* Am J Med Genet B Neuropsychiatr Genet, 2009. **150B**: p. 782-798.
4. Berry-Kravis, E., et al., *Fragile X-associated tremor/ataxia syndrome: Clinical features, genetics, and testing guidelines.* Movement Disorders, 2007. **22**(14): p. 2018-2030.
5. Hagerman, R.J., et al., *Fragile X-Associated Neuropsychiatric Disorders (FXAND).* Front Psychiatry, 2018. **9**: p. 564.
6. Todd, P.K., et al., *CGG repeat-associated translation mediates neurodegeneration in fragile X tremor ataxia syndrome.* Neuron, 2013. **78**(3): p. 440-55.
7. Sellier, C., et al., *Translation of Expanded CGG Repeats into FMRpolyG Is Pathogenic and May Contribute to Fragile X Tremor Ataxia Syndrome.* Neuron, 2017. **93**(2): p. 331-347.
8. Boivin, M., et al., *Potential pathogenic mechanisms underlying Fragile X Tremor Ataxia Syndrome: RAN translation and/or RNA gain-of-function?* Eur J Med Genet, 2018. **61**(11): p. 674-679.
9. Leehey, M.A., et al., *Clinical Neurological Phenotype of FXTAS, in FXTAS, FXPOI, and Other Premutation Disorders, F. Tassone and D.A. Hall, Editors.* 2016, Springer International Publishing: Cham. p. 1-24.
10. Robertson, E.E., et al., *Fragile X-associated tremor/ataxia syndrome: phenotypic comparisons with other movement disorders.* Clin Neuropsychol, 2016. **30**(6): p. 849-900.
11. Jacquemont, S., et al., *Penetrance of the fragile X-associated tremor/ataxia syndrome in a premutation carrier population.* JAMA, 2004. **291**(4): p. 460-9.
12. Tassone, F., et al., *CGG repeat length correlates with age of onset of motor signs of the fragile X-associated tremor/ataxia syndrome (FXTAS).* Am J Med Genet, 2007. **144B**: p. 566-569.
13. Seritan, A.L., et al., *Dementia in fragile X-associated tremor/ataxia syndrome (FXTAS): Comparison with Alzheimer's disease.* Am J Med Genet B Neuropsychiatr Genet, 2008. **147B**: p. 1138-1144.
14. Grigsby, J., et al., *Impairment of executive cognitive functioning in males with fragile X-associated tremor/ataxia syndrome.* Movement Disorders, 2007. **22**(5): p. 645-650.
15. Young, I.D., *Diagnosing Fragile-X Syndrome.* Lancet, 1993. **342**(8878): p. 1004-1005.
16. Tassone, F., et al., *Neuropathological, clinical and molecular pathology in female fragile X premutation carriers with and without FXTAS.* Genes Brain Behav, 2012. **11**(5): p. 577-85.
17. Greco, C.M., et al., *Neuropathology of fragile X-associated tremor/ataxia syndrome (FXTAS).* Brain, 2006. **129**(Pt 1): p. 243-55.
18. Famula, J.L., et al., *Presence of Middle Cerebellar Peduncle Sign in FMR1 Premutation Carriers Without Tremor and Ataxia.* Front Neurol, 2018. **9**: p. 695.
19. Krans, A., et al., *Neuropathology of RAN translation proteins in fragile X-associated tremor/ataxia syndrome.* Acta Neuropathol Commun, 2019. **7**(1): p. 152.

20. Hagerman, P., *Fragile X-associated tremor/ataxia syndrome (FXTAS): pathology and mechanisms.* Acta Neuropathol, 2013. **126**(1): p. 1-19.
21. Hagerman, R.J., et al., *Neuropathy as a presenting feature in fragile X-associated tremor/ataxia syndrome.* Am J Med Genet A, 2007. **143A**: p. 2256-2260.
22. Berry-Kravis, E., et al., *Neuropathic features in fragile X premutation carriers.* American Journal of Medical Genetics Part A, 2007. **143A**(1): p. 19-26.
23. Tassone, F., et al., *Intranuclear inclusions in neural cells with premutation alleles in fragile X associated tremor/ataxia syndrome.* J Med Genet, 2004. **41**(4): p. E43.
24. Hamlin, A.A., et al., *Hypertension in FMR1 premutation males with and without fragile X-associated tremor/ataxia syndrome (FXTAS).* Am J Med Genet A, 2012. **158A**(6): p. 1304-9.
25. Hall, D.A., et al., *Initial diagnoses given to persons with the fragile X associated tremor/ataxia syndrome (FXTAS).* Neurology, 2005. **65**(2): p. 299-301.
26. Hunsaker, M.R., et al., *Widespread non-central nervous system organ pathology in fragile X premutation carriers with fragile X-associated tremor/ataxia syndrome and CGG knock-in mice.* Acta Neuropathol, 2011. **122**(4): p. 467-79.
27. Beach, T.G., et al., *Substantia nigra Marinesco bodies are associated with decreased striatal expression of dopaminergic markers.* J Neuropathol Exp Neurol, 2004. **63**(4): p. 329-37.

CHAPTER 6

6

An Enzyme-Linked Immunosorbent Assay (ELISA) to detect FMRpolyG levels in post-mortem brain tissue from FXTAS patients

Saif N. Haify[1*], Rob F.M. Verhagen[1], Esmay C. van der Toorn[1], Renate K. Hukema[1,2], Nicolas Charlet-Berguerand[3] and Rob Willemsen[1*]

[1] Department of Clinical Genetics, Erasmus MC, Rotterdam, Netherlands.
[2] Department of Health Care Studies, Rotterdam University of Applied Sciences, Rotterdam, Netherlands
[3] Institut de Génétique et de Biologie Moléculaire et Cellulaire (IGBMC), INSERM U964, CNRS UMR7104, University of Strasbourg, 67400 Illkirch, France

[*] Corresponding authors: Saif N. Haify (s.haify@erasmusmc.nl) and Rob Willemsen (r.willemsen@erasmusmc.nl)

Manuscript in preparation

Abstract

Fragile X-associated tremor and ataxia syndrome (FXTAS) is a neurodegenerative disorder associated with a premutation repeat expansion (55-200 CGG repeats) in the 5' noncoding region of the *FMR1* gene. Carriers of the PM with FXTAS are clinically characterized with severe intention tremors and cerebellar gait ataxia. In addition, patients with FXTAS may develop cognitive defects, Parkinsonism and dementia. Ubiquitin-positive intranuclear inclusions in neurons and astrocytes throughout the brain is a major neuropathological hallmark of FXTAS. It is hypothesized that the disease is caused by the expression and accumulation of a toxic polyglycine peptide (FMRpolyG) through a mechanism called repeat associated non-AUG (RAN) translation. To date, our understanding how FMRpolyG and inclusion formation contribute to onset and progression of this devastating disease and how FMRpolyG-induced neurodegeneration, especially in the context of its soluble and insoluble form, occurs is still elusive. Nevertheless, FMRpolyG could play an important role as a potential biomarker for predicting disease progression and could serve as pharmacodynamic marker in disease-modifying treatments for FXTAS. In this report, we demonstrate successful isolation of soluble FMRpolyG fractions from transfected COS7 cells and insoluble FMRpolyG fractions from post-mortem brain tissue of a female FXTAS patient using a newly developed urea-specific protein isolation protocol. Next, FMRpolyG levels were determined using a new FMRpolyG-specific sandwich enzyme-linked immunosorbent assay (ELISA). Although this proof-of-principle ELISA is promising, further validation of this ELISA is necessary before further implementation in biomedical research can be established, including detection of FMRpolyG levels in PBMCs, blood plasma and/or CSF. If successful, FMRpolyG could be used as a potential biomarker in monitoring disease progression and also assist in the search for targeted therapeutic interventions for FXTAS.

Keywords: FXTAS, FMRpolyG, biomarker, ELISA, COS7 cells, patient brain tissue

Introduction

Fragile X-associated tremor and ataxia syndrome (FXTAS) is a late-onset progressive neurodegenerative disorder that is clinically mainly characterized by tremors and cerebellar gait ataxia [1]. FXTAS is also associated with multisystem atrophy, Parkinsonism, dysautonomia, neuropathy, and dementia [1-4]. The *Fragile X mental retardation 1* (*FMR1*) gene is located on the X-chromosome and is responsible for the production of the fragile X mental retardation protein (FMRP). FXTAS patients are molecularly characterized by 2- to 8-fold increase in *FMR1* mRNA and modest reduction of the FMRP protein [5]. FMRP is necessary for normal brain development and neuronal plasticity. Healthy individuals have less than 50 CGG-repeats in their 5′ untranslated region (5′-UTR) of the *FMR1* gene. The CGG-repeat can expand to lengths between 50-200 CGGs throughout generations due to its instability. These individuals with the expanded CGG-repeat (55-200) are referred to as premutation (PM) carriers and have an increased risk of developing FXTAS. It is estimated that in the general population 1:250 females and 1:850 males are PM carriers [6-8]. Interestingly, not all PM carriers develop FXTAS due to incomplete penetrance. About 30% of male carriers and 16% of female carriers over the age of 50 develop FXTAS [8, 9].

A major hallmark of the disease is the presence of ubiquitin-positive intranuclear inclusions in neurons and astrocytes throughout the brain of FXTAS patients [10, 11]. Two disease mechanisms have been proposed to cause FXTAS. First, is an RNA gain-of-function toxicity and sequestration mechanism that is directly linked to the elevated *FMR1* mRNA levels observed in FXTAS patients [1, 5, 12]. Increased levels of *FMR1* mRNA containing an expanded CGG-repeat induce the formation of aggregates and are known to result in neuronal death [13-16]. *FMR1* mRNA containing an expanded CGG-repeat can sequester key cellular RNA-binding proteins (RBPs) and prevent these proteins from their normal function [16-18]. Recently, a second mechanism was proposed which results in the toxic aggregation of a repeat-associated non-AUG (RAN) translated polyglycine peptide called FMRpolyG [19]. FMRpolyG co-localizes with ubiquitin in intranuclear inclusions together with other proteins, including HNRNP A2/B1, SAM68, DGCR8 and DROSHA, all involved in pre-mRNA alternative splicing processes and mRNA transport [17, 18, 20, 21]. FMRpolyG-positive intranuclear inclusions have been reported in cellular models as well as in many different animal models including the *Drosophila* and mice [19, 22-24]. Moreover, FMRpolyG has been shown to induce a toxic eye phenotype in *Drosophila* and has been reported to be the pathogenic factor in mice [19, 25]. FMRpolyG-positive intranuclear inclusions have also been reported in post-mortem FXTAS brain tissue in neurons and astrocytes, and in systemic organs including the kidneys, heart, adrenal gland and the thyroid [26]. FMRpolyG-positive inclusions were also reported to be present in ovaries of PM carriers [27]. Interestingly, FMRpolyG-positive intranuclear inclusions were recently reported in mural granulosa cells of PM carriers before disease onset [28]. All these

observations indicate that FMRpolyG is an important factor in FXTAS pathogenesis and may be interesting to target when developing therapeutic interventions.

Currently, treatment of FXTAS patients is symptomatic as there is no targeted therapy available yet. One possible method of targeted treatment would be the use of antisense oligonucleotides (AONs). AONs are short single-stranded (ss)RNA molecules that specifically bind complementary mRNA sequences. AONs can block the ssRNA and prevent translation of the disease-causing mRNA or upon binding form RNA:DNA duplexes that recruit the RNase H enzyme and degrade the disease-causing mRNA [29]. Another more promising strategy is the use of small chemical compounds. Small synthetic compounds are specifically designed to bind and shield a specific microsatellite repeat sequence to prevent protein sequestration and RAN translation while leaving canonical translation unharmed. For FXTAS a small molecule, *1a*, was designed that binds GG-mismatches in the expanded CGG-repeat that could prevent aberrant splicing effects in the cell [30]. These strategies are promising in inhibiting progression of the disease but more ideally would be to therapeutically intervene before the onset of FXTAS disease. We have previously reported that early intervention in mice results in reversibility of neuropathology and late intervention can halt but not reverse the disease progression in these mice [31]. Unfortunately, we are not able yet to accurately predict when PM carriers will develop FXTAS. Currently T2-weighted magnetic resonance imaging (MRI) and fluid-attenuated inversion recovery (FLAIR) images of the middle cerebellar peduncles (MCP sign) and corpus callosum splenium (CCS) are used as MRI biomarkers for FXTAS [32-34]. Complementary to MRI, plasma metabolic concentrations can be measured to determine brain pathophysiology in symptomatic and asymptomatic PM carriers [35-37]. However, both MCP sign and CCS hyperintensity are not exclusively seen in FXTAS [38, 39]. In addition, plasma metabolic ratios can easily be influenced by supplement (ab)use including vitamins, alcohol and medication. Therefore, there is an immediate need for accurate and disease specific prognostic biomarkers. FMRpolyG may be such a candidate biomarker if FMRpolyG can be detected accurately in blood plasma or serum, or in cerebrospinal fluid (CSF). Moreover, since we know that early intervention in mice can reverse neuropathology and halt disease progression, FMRpolyG may also be an interesting pharmacodynamic biomarker for successful implementation of an early targeted therapeutic intervention.

To date, absolute measurement of total FMRpolyG concentrations in any type of tissue has been very difficult. Western blot analysis allows for quantification of FMRpolyG in the soluble fraction of transfected cells and mouse tissue. Unfortunately, the insoluble protein fraction of FMRpolyG in cellular, animal and human tissue could not be detected using Western blot, not even with high concentrations of SDS and urea. This may be due to the insoluble character of FMRpolyG in the intranuclear inclusions. One way to overcome this

issue is by measuring insoluble FMRpolyG fraction with the dot blot technique. We have generated an in-house protocol that allows us to analyze insoluble FMRpolyG fractions in *in vitro* models and in mouse models using high concentrations of SDS. Unfortunately, the dot blot technique is a semi-quantitative method. Also, the accuracy of quantification with the Western blot and dot blot technique is limited. The need for more accurate absolute quantitative methods remains. In this report, we developed an enzyme-linked immunosorbent assay (ELISA) that allows measurement of both FMRpolyG soluble and insoluble protein levels.

Method

Transfection of COS7 cells

COS7 cells were cultured in Dulbecco's modified Eagle's medium (DMEM, Gibco) supplemented with 10% Fetal Calf Serum (FCS), 1% Penicillin/Streptomycin (P/S) and 1% Non-Essential Amino Acids (NEAA, Lonza). Cells were kept at 37°C in 5% CO_2 humidified incubator. For protein isolation and ELISA, COS7 cells were plated at 200.000 cells/well in 6-well plates without coverslips and transfected with a 1µg/µl solution of linear 25kDa PolyEthyleneimine (PEI, Polysciences cat# 23966-2). COS7 cells used for immunofluorescent staining were plated on 24 mm coverslips (Thermo Scientific). The COS7 cells were left to acclimatize for at least 4 hours in the incubator and are washed with PBS to remove cell secreted material that could interfere with PEI reagent. COS7 cells are replenished with fresh pre-heated 2ml of supplemented DMEM medium. Next, 400µl transfection mix is prepared containing 1.5µg of the ATG-mediated 99xCGG-repeat-GFP plasmid DNA (plasmid: ATG-99CGG-GFP) and PEI reagent in a PEI:DNA volume ratio of 2.5:1. The transfection mix was vortexed shortly and left to incubate for 15 minutes at RT. After 15 minutes, add transfection mix evenly to the well and incubate COS7 cells for 48-72h at 37°C in 5% CO_2 humidified incubator.

Immunohistochemistry on paraffin brain sections

FXTAS and non-demented (ND) control post-mortem brain sections were obtained via the Netherlands Brain Bank (NBB). Brain sections of 6 µm were cut and placed on silane coated slides (Klinipath). The brain sections were deparaffinized in decreasing concentrations of alcohol, starting with 100% xylene and ending in dH_2O. Antigen retrieval was performed by pressure cooker treatment in 0.01 M sodium citrate (pH 6). Endogenous peroxidase activity was blocked with 0.6% H_2O_2 in 0.1M PBS. For staining FMRpolyG an additional incubation step with proteinase K (5 µg/ml) was performed for 20-30 min at 37°C. Immunostaining was performed overnight at 4°C with primary FMRpolyG antibodies (1C5) diluted 1:5000 in 0.1M PBS/0.5% protifar (Nutricia; cat# 032018)/0.15% glycine (Sigma-Aldrich, cat# G7126-1KG) (PBS+). Staining with secondary antibodies was performed

at RT for 60 min. Antigen-antibody complexes were visualized using DAB-substrate (Sigma-Aldrich), followed by counterstaining with Mayer's haematoxylin for 5 min and subsequently mounted with Entellan (Merck Milipore International). Images were taken using an Olympus BX40 microscope (Olympus).

Immunofluorescence staining cells and paraffin brain tissue

Coverslips with transfected COS7 cells were rinsed twice with 0.1M PBS to remove residual medium. Cells were fixed with 4% paraformaldehyde (PFA) for 15 minutes and rinsed three times with 0.1M PBS. Following fixation, the cells were permeabilized with 0.5% Triton X-100 in 0.1M PBS for 10 minutes and rinsed three times with 0.1M PBS. Immunostaining was performed overnight at 4°C with primary FMRpolyG antibodies (1C5) diluted 1:5000 in PBS block buffer containing 0.1M PBS/0.5% protifar (Nutricia; cat# 032018)/0.15% glycine (Sigma-Aldrich, cat# G7126-1KG) (PBS+). The next day, cells were rinsed three times with PBS+ before incubation with anti-mouse secondary antibodies conjugated with Cyanine 3 (1:500, ThermoFisher) in PBS+ at room temperature for 60 min. After incubation with secondary antibodies, cells were rinsed three times with 0.1M PBS and shortly incubated with Hoechst 33342 (1:15.000, Invitrogen) in 0.1M PBS (1:15.000) for 5 min to visualize nuclei. Following Hoechst incubation, cells were rinsed twice with 0.1M PBS before mounting in Pro-Long Gold media (Invitrogen). Slides were examined using the Leica TCS SP5 confocal microscope.

Brain sections were treated similarly as to immunohistochemistry treatment described in 'immunohistochemistry on paraffin brain sections' except for the endogenous peroxidase blocking step. After incubation with primary antibodies, brain sections were rinsed in PBS+ and incubated with secondary anti-mouse antibodies conjugated with Cyanine 3 (1:500, ThermoFisher). To minimize autofluorescence signal, sections were incubated with Whatman filtered Sudan Black B solution (Sigma 0.1g in 100ml 70% EtOH) for 4-6 minutes followed by rinsing three times with PBS+. Sections were mounted with Pro-Long Gold media (Invitrogen) containing DAPI to stain for the nuclei. Sections were kept at 4°C until imaging with a Zeiss LSM700 confocal microscope.

Protein isolation cells and brain sections

Prior to mechanical lysing, either COS7 cells or brain sections were supplied with 1% CHAPS buffer containing 0.05% protease inhibitors (Roche) and 0.3% 1M DTT (Invitrogen). After 30 min incubation on ice, mechanical lysing was repeated and samples were centrifuged for 15 min at 4°C, followed by 3x 1 min sonication. After sonication, samples were centrifuged for 20 min at 4°C and supernatant was collected. Residual pelleted material was treated with 4M urea for 20 min in a shaking heat block (VWR International) at 500rpm and 30°C. After urea treatment the samples were centrifuged for 10 min at 6800g. Urea fraction was

collected in separate tube. Whole protein content was determined in the soluble protein fractions using the BCA assay (Thermo Fisher Scientific).

Sandwich Enzyme-Linked Immunosorbent Assay (ELISA)

FMRpolyG Sandwich ELISA study was performed on COS7 cells, FXTAS hippocampal (*n=1*) and non-demented frontal cortex (*n=1*) cryosection material (*n=6* cryosections per region, 20µm/section). MaxiSorp 96 well F-bottom plates (ThermoFisher) were coated for 120 min with 2.0 µg/ml monoclonal anti-FMRpolyG antibody (9FM) followed by overnight blocking with 1% BSA in 0.1M PBS-Tween (0.05% Tween-20) at 4°C. After washing, samples were added at 300 µg total protein. Standard curve was added in duplo. For supernatant fraction, samples were 2-fold serial diluted in 0.1M PBS. For urea fraction, samples were 2-fold serial diluted in 4M urea. For either matrix a standard curve, using a synthesized PolyG peptide (IGBMC), was diluted in 0.1M PBS or 4M urea respectively. All contents were incubated for 60 min. After washing, all samples were incubated for 60 min with biotinylated monoclonal anti-FMRpolyG antibody (9FM-Bio) at a final concentration of 0.125 µg/ml in 0.1M PBS-Tween/1% BSA. After washing, samples were incubated for 20 min with Streptavidin-HRP conjugate (R&D Sciences) diluted 1:200 in 0.1M PBS-Tween/1% BSA. Following extensive washing, samples were incubated with substrate reaction mix (R&D Sciences) for 15 min and stopped using 2N H_2SO_4. Read-out was carried out using a plate reader (Varioskan) at 450nm and 570nm.

Statistical analysis

Statistical analysis was performed using GraphPad Prism software version 8. Statistical test used for COS7 cell experiments is the unpaired *t*-test with Welch's correction. A value of $p \leq 0.05$ was considered significant.

Results

Clinical profile FXTAS donor

Donor was reported for the first time with FXTAS symptoms at the age of 60 years. She suffered from dysarthria and apraxia of speech. Her mouth was asymmetric and perception was variably disturbed. Patient suffered from absences, occasionally multiple times a day. She had mild walking problems, sometimes temporarily losing control over her legs and used a walking aid. At the age of 82 years, she fell down the stairs probably after a TIA and lost consciousness. Examination in the hospital showed a CVA. This accident resulted in worsening of the aphasia and wordfinding problems as well as walking and increased risk of falling. After this accident her short-term memory declined quickly. At the age of 84 she was found unconscious in her garden with a severe head trauma due to presumably a partial epileptic seizure. Patient's condition deteriorated quickly with moderate dementia,

unable to walk, communication was no longer possible and she refused food and drinks. Palliative sedation was started which eventually led to euthanasia. A few years before she passed away, she was diagnosed with FXTAS and a positive family history for the syndrome. Upon autopsy, the diagnosis of FXTAS was confirmed with neuropathological examination showing a globally smaller brain with many white matter abnormalities. Microscopic examination confirmed the presence of numerous p62 (ubiquitin)-positive intranuclear inclusions throughout the entire brain. Ubiquitin-positive inclusions were dispersed in the temporal cortex. In the frontal and occipital cortex more inclusions were found in small rounded-off neurons, presumably oligodendrocytes and hardly any were found in the pyramidal cells. In the hippocampus ubiquitin-positive inclusions were mostly found in the pyramidal cells of the cornus ammonis (CA) regions 1 to 4 and only a few inclusions were found in the small neurons of the granular layer. The basal ganglia nuclei, the thalamus and the amygdala showed a similar pattern with a large number of ubiquitin-positive inclusions found in small rounded-off neurons and only a few were found in the bigger pyramidal neurons. The substantia nigra showed an overall image of few dispersed nuclear ubiquitin-positive inclusions. In the underlying grey matter, a large number of small neurons stained positive for ubiquitin in nuclear inclusions. The midbrain and the pons showed relatively few ubiquitin-positive nuclear inclusions while the cervical spinal cord showed more nuclear inclusions. The locus coeruleus and the tegmentum showed a moderate number of nuclear inclusions. The cerebellum showed a wide-spread presence of nuclear inclusions in oligodendrocytes and the Bergmann glia. The dentate nucleus and the Purkinje cells showed only a few nuclear inclusions.

FMRpolyG-positive inclusions in COS7 cells and post-mortem FXTAS hippocampus

We transfected COS7 cells with an ATG-99xCGG-GFP expression plasmid under the control of the cytomegalovirus (CMV) promoter and in frame with the green fluorescent protein (GFP), and performed immunofluorescence (IF) staining. Immunofluorescent imaging shows that transfected COS7 cells nicely express the GFP-marker protein and form intranuclear GFP-positive inclusions (**Fig. 1**). Since the expanded 99xCGG-repeat is in frame with the GFP-marker protein, the GFP-positive inclusions also should contain the RAN translated FMRpolyG. IF double staining with the anti-FMRpolyG antibody confirmed that approximately 90% of the FMRpolyG-positive inclusions co-localized with the GFP-positive inclusions (**Fig. 1**).

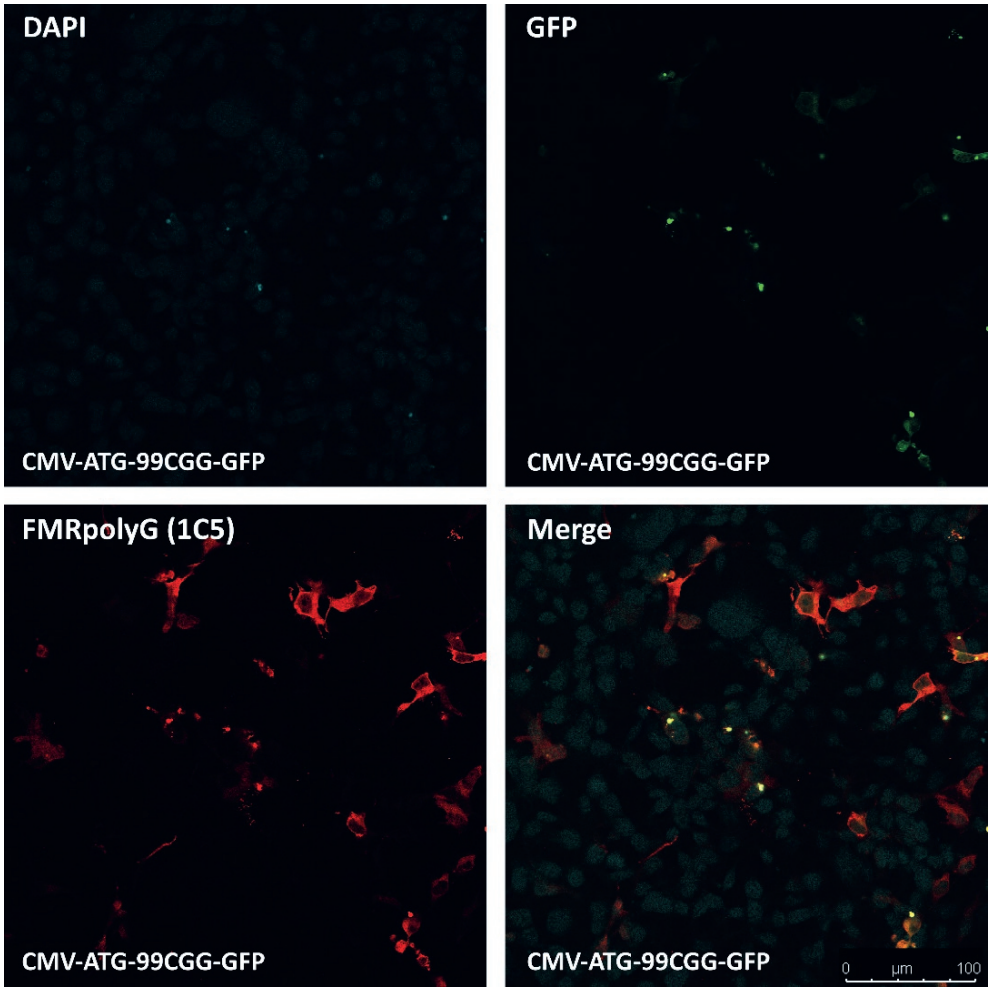

Figure 1 | The 1C5 anti-FMRpolyG antibody specifically stains FMRpolyG in transfected COS7 cells. Transfected COS7 cells clearly express GFP (green) throughout the entire cell and form GFP-positive inclusions. Immunofluorescent staining using the 1C5 anti-FMRpolyG antibody shows that FMRpolyG (red) co-localizes with the GFP-positive inclusions. FMRpolyG is also expressed in the cytoplasm after transfection. Immunofluorescent staining of CMV-ATG-GFP transfection COS7 cells controls never showed FMRpolyG-positive inclusions. Scale bar = 100 µm.

Next, we performed IF labeling of hippocampal post-mortem brain sections from the female FXTAS donor and *C9ORF72*-linked ALS/FTD hippocampal control tissue (*n=1*) (**Fig. 2**). This staining shows that FMRpolyG-positive inclusions were present in the hippocampus from the patient with FXTAS but not in the control hippocampus from the *C9ORF72*-linked ALS/FTD patient. We also performed immunohistochemistry labeling of post-mortem brain tissue from the female FXTAS patient and post-mortem brain tissue

from one non-demented (ND) control patient (*n=1*) (data not shown). We found that FMRpolyG-positive intranuclear inclusions were abundantly present in the hippocampus in post-mortem brain tissue from the FXTAS patient while no FMRpolyG-positive inclusions could be detected in the brain tissue from the ND control patient.

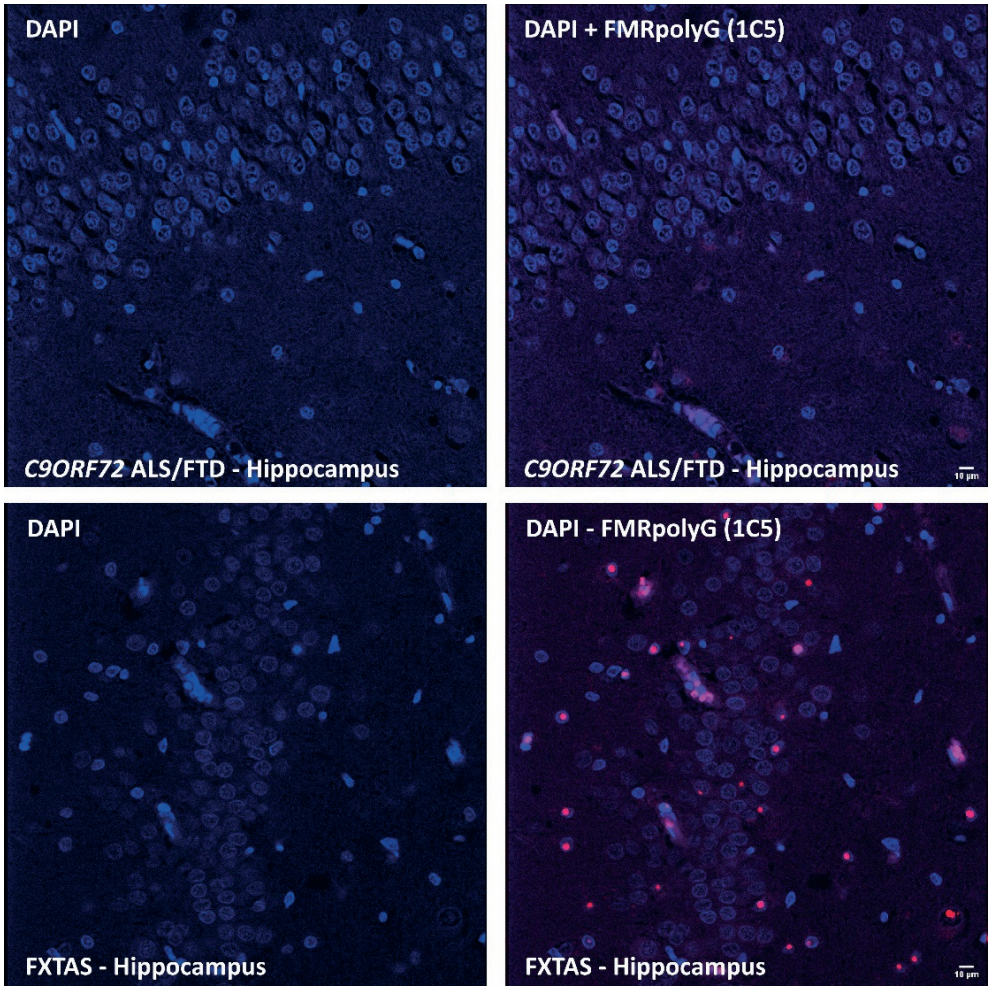

Figure 2 | FMRpolyG-positive intranuclear inclusions in the hippocampus from patient with FXTAS. Immunofluorescent staining with the 1C5 antibody shows FMRpolyG-positive intranuclear inclusions (in red) present in post-mortem FXTAS hippocampus while no staining is visible in control *C9ORF72*-linked ALS/FTD hippocampal tissue. Nuclei are visualized using DAPI (in blue). Scale bars = 10 µm.

FMRpolyG protein can be detected with the sandwich-ELISA

After confirming the presence of FMRpolyG-positive inclusions in both transfected COS7 cells and in FXTAS post-mortem brain tissue, the next step was to develop a sandwich-ELISA that allowed us to measure both soluble and insoluble FMRpolyG fractions (**Fig. 3**). First, we used a synthetic polyglycine (polyG, 12xGly) response peptide (LifeTein) to generate a positive signal in the sandwich-ELISA. We analyzed the signal in the sandwich-ELISA for both the soluble treatment in PBS matrix and the insoluble (*i.e.,* inclusions) treatment in urea matrix. The sandwich-ELISA nicely detects the synthetic polyG peptide in both matrices while no signal is present in the blank samples (**Fig. 3A**). Next, we generated a dose-response curve for the synthetic polyG peptide in both PBS and urea matrices. The detection range of the ELISA is between 0.39-25 ng peptide per ml (**Fig. 3B**). Signal development from 25 ng upwards shows a non-linear OD development. To further validate the sandwich-ELISA, we isolated FMRpolyG from the ATG-99xCGG-GFP and CMV-ATG-GFP transfected COS7 cells, and measured FMRpolyG levels in the soluble and insoluble fractions. Surprisingly, FMRpolyG levels could only be detected in the soluble fraction from the ATG-99CGG-GFP transfected COS7 cells. In contrast, in the insoluble fraction of the ATG-99xCGG-GFP transfected COS7 cells, we could not detect FMRpolyG levels. No FMRpolyG could be detect in the soluble and insoluble protein fractions in CMV-ATG-GFP transfection control COS7 cells (**Fig. 3C**). The calculated amount of soluble FMRpolyG in COS7 cells transfected with ATG-99xCGG-GFP plasmid DNA was on average 32 pg per µg total protein load in the sandwich-ELISA. FMRpolyG levels in the insoluble protein fraction as well as FMRpolyG levels in the controls were below the detection limit of the sandwich-ELISA. Next, we measured FMRpolyG levels in the hippocampus of the FXTAS donor and the frontal cortex of ND controls (**Fig. 3D**). We could demonstrate 9 pg FMRpolyG per µg total protein load in the insoluble protein fraction, while FMRpolyG levels in the soluble fraction were similar to background levels in the ND controls.

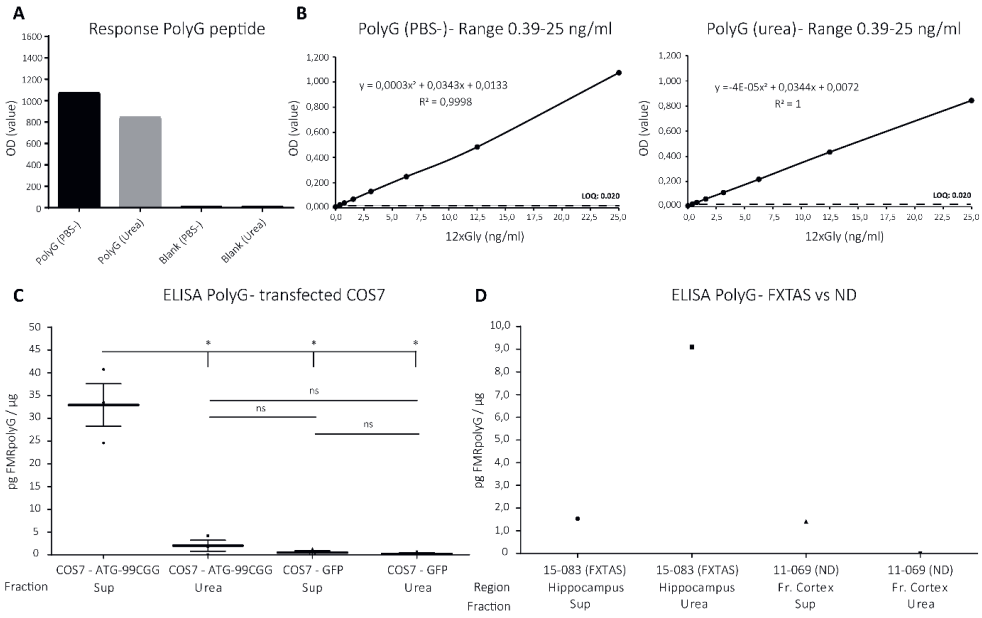

Figure 3 | ELISA detection of FMRpolyG in soluble and insoluble protein fractions from transfected COS7 cells and post-mortem FXTAS brain. (A) The ELISA shows a positive OD value for the synthetic polyG peptide in both the soluble (PBS) and insoluble (urea) fractions. Both PBS matrix blank and urea matrix blank show no OD value. **(B)** Dose-response curve for the synthetic polyG peptide in PBS and urea matrices. The limit of quantification in both matrices is 0.020 OD value. This OD value corresponds with 0.39 ng/ml. **(C)** Quantification of soluble (supernatant; sup) and insoluble (urea) FMRpolyG protein fractions in CMV-ATG-99xCGG-GFP (*n=3*) and CMV-ATG-GFP (*n=3*) transfected COS7 cells. FMRpolyG protein levels were significantly ($p \leq 0.05$) higher in the soluble protein fraction in CMV-ATG-99xCGG-GFP transfected COS7 cells compared to the urea protein fraction in CMV-ATG-99xCGG-GFP transfected COS7 cells ($p=0.0169$; statistical test unpaired *t*-test with Welch's correction was applied). Also, the soluble FMRpolyG protein level in CMV-ATG-99xCGG-GFP transfected COS7 cells was significantly higher compared to the soluble and insoluble protein fractions from CMV-ATG-GFP transfected control COS7 cells ($p=0.0196$). In the CMV-ATG-GFP soluble and urea protein fraction no significant FMRpolyG protein levels could be detected. **(D)** Measurement of FMRpolyG protein in post-mortem hippocampus brain tissue (*n=1*) and frontal cortex from non-demented (ND) control (*n=1*). In the urea protein fraction of FXTAS hippocampus 9 pg FMRpolyG per µg total protein could be detected in the sandwich-ELISA. Soluble FMRpolyG protein fraction from FXTAS hippocampus was 1.5 pg, which is similar to the background FMRpolyG protein levels measured in the soluble protein fraction from the ND control. No FMRpolyG protein could be detected in the urea protein fraction in the frontal cortex of the ND control patient.

Discussion

In this study we show that COS7 cells transfected with the ATG-99xCGG-GFP expression plasmid produce the RAN-translated FMRpolyG fused with GFP and form FMRpolyG-positive intranuclear inclusions. FMRpolyG-positive inclusions are abundantly observed

in our donor FXTAS brain tissue in neurons and astrocytes, as described in literature [19, 22, 23, 25, 26, 40]. Ubiquitin-positive intranuclear inclusions are currently the major neuropathological hallmark in FXTAS. In the vast majority of post-mortem FXTAS brain tissue FMRpolyG co-localizes with ubiquitin in intranuclear inclusions. More importantly, FMRpolyG is unique for FXTAS while intranuclear inclusions containing ubiquitin are also observed in other neurodegenerative disorders [41]. Moreover, we have previously reported that FMRpolyG-positive intranuclear inclusions are not only abundantly present in post-mortem CNS tissue but also in non-CNS tissue of PM carriers with FXTAS including the thyroid, adrenal gland, heart, kidney, pituitary gland and ovaries [26, 27]. In this report we showed that FMRpolyG-positive inclusions could exclusively be detected in post-mortem hippocampal brain tissue from one FXTAS patient while in *C9ORF72*-linked ALS/FTD hippocampal control brain tissue no FMRpolyG-positive inclusions were present. In *C9ORF72*-linked ALS/FTD patients RAN translation of the G_4C_2-repeat can generate five different dipeptides that also form intranuclear inclusions and induce cellular toxicity [42-44]. However, it is clear that our anti-FMRpolyG antibody specifically targets FMRpolyG. We also found that FMRpolyG-positive inclusions were not present in post-mortem ND-control brain tissue (data not shown). Therefore, based on previous and current findings we propose FMRpolyG-positive intranuclear inclusions as neuropathological hallmark for FXTAS as FMRpolyG-positive intranuclear inclusions are exclusively found in FXTAS patients.

Isolation of aggregated FMRpolyG from animal tissue as well as post-mortem FXTAS patient tissue has been challenging. One recent proteomics study using autofluorescence-based FACS and liquid chromatography - tandem mass spectrometry (LC-MS/MS) found very low concentrations of FMRpolyG in the inclusions indicating the importance of proper protein isolation protocols for aggregated FMRpolyG [45]. Aggregated FMRpolyG in inclusions is highly insoluble and different tissues may require a different approach to solubilize and detect FMRpolyG. Isolation methods may vary and some are not able to properly dissolve FMRpolyG, which may explain some negative results. We have generated a proof-of-principle protein isolation protocol for the isolation of the soluble and insoluble protein fractions of FMRpolyG from both cell culture and FXTAS patient post-mortem brain tissue. Subsequent to the protein isolation procedure, we were able to detect FMRpolyG levels in the soluble and insoluble fractions using the new developed sandwich-ELISA. We found that high concentrations of urea are needed to dissolve FMRpolyG from the aggregates in post-mortem FXTAS brain tissue, more specifically the hippocampus. We were able to detect soluble FMRpolyG fractions in transfected COS7 cells using the 9FM monoclonal antibody against FMRpolyG. Unfortunately, FMRpolyG levels in the insoluble protein fraction from transfected COS7 cells were below the detection limit of the sandwich-ELISA. There are several explanations for this observation. First, low insoluble FMRpolyG levels may be due to the relatively short transfection period (48 hours). Perhaps soluble

FMRpolyG concentrations in the cell are just enough to start the formation of inclusions after 48 hours of transfection. Second, the transfection period in COS7 cells may be long enough for the immunodetection of FMRpolyG-positive inclusions but the COS7 cells do not produce enough FMRpolyG to be quantitatively measured using the sandwich-ELISA. Third, inclusions in transfected COS7 cells may have a different protein composition compared to inclusions in human tissue. One or more components of the aggregates in transfected COS7 cells may hinder the urea from fully dissolving the protein inclusion bodies containing FMRpolyG. Finally, overexpression of the expanded CGG-repeat RNA in this cellular system may result in protein aggregates containing FMRpolyG that are toxic for the cell. FMRpolyG induced toxicity may therefore result in more cell death, and consequently result in more accessible soluble FMRpolyG. However, since we are still able to detect FMRpolyG-positive inclusions in the transfected COS7 cells it is more probably that a combination of events could explain our observations.

Interestingly, using this new protein isolation protocol in FXTAS post-mortem brain tissue, we were able for the first time to (partially) isolate aggregated FMRpolyG fraction from FXTAS post-mortem hippocampal brain tissue and detect FMRpolyG levels using the newly developed sandwich-ELISA approach. Although there are similarities between protein aggregate composition in *in vitro*, *in vivo* and human tissues [11, 17, 18, 21, 26, 27, 31, 45-47], the fact that we are able to (partially) dissolve FMRpolyG from FXTAS brain tissue may also argument for discrepancies in protein aggregate composition between cellular models and FXTAS brain tissue. How these discrepancies may influence the solubility of aggregated FMRpolyG is yet unknown. In post-mortem FXTAS brain tissue FMRpolyG-positive protein aggregates are abundantly present, also in our FXTAS donor. However, we only measure low concentrations of insoluble FMRpolyG. Recently, hydrophobic pattern analysis revealed that the C-terminal region of FMRpolyG had high hydrophobicity potentially reducing the solubility of FMRpolyG [47]. In addition, the polyglycine stretch (*i.e.,* the amino acid sequence) within FMRpolyG contains low-complexity disordered domains that drive aggregate formation in the cell [47]. Disordered proteins are reported to be less soluble which may strongly explain the low solubility of FMRpolyG [48]. The expanded CGG-repeat RNA quadruplex structures present in inclusions prefers interaction with these disordered domains further promoting aggregation and decreasing solubility of FMRpolyG [47]. All these observations suggest a low solubility of FMRpolyG and may explain why even high concentrations of urea may not be able to dissolve all FMRpolyG from protein aggregates. Additional factors may also contribute to the low solubility of FMRpolyG, including intramolecular interactions and kinetics of the aggregation process [49]. Although in the past 15 years our understanding of FMRpolyG, RAN translation and protein aggregates has advanced, the detailed mechanism of the protein aggregation process is yet unknown. Interestingly, recent reports show that Porphyrin protoporphyrin IX (PpIX), which is an organic precursor for hemoglobin, can interact with the expanded

CGG-repeat RNA quadruplex structure, reduce FMRpolyG binding to the CGG-repeat RNA and prevent FMRpolyG aggregation [47]. Thus, treatment of the insoluble FMRpolyG containing isolates with PpIX may improve solubility without interfering with the signal in the sandwich-ELISA.

The presence of numerous FMRpolyG-positive inclusions in post-mortem FXTAS brain and mouse models, raises the question whether FMRpolyG could be a useful prognostic biomarker in blood or CSF to monitor onset of disease and progression in PM carriers. The FMRpolyG protein may also be suitable as a pharmacodynamic biomarker for targeted therapeutic engagement and measurement of biochemical responses after therapeutic intervention. For example, poly-GP dipeptide protein levels in *C9ORF72*-linked ALS/FTD patients are reported to remain fairly stable over time supporting that RAN peptides may function as pharmacodynamic biomarkers [50]. Moreover, AONs that specifically target the G_4C_2 expanded repeat in *C9ORF72*-linked ALS/FTD in human cell models and mouse models, show that AON treatment can reduce extracellular poly-GP protein levels in human cell models and reduce poly-GP protein levels in the CSF [51, 52]. We reported here that we are able to measure FMRpolyG protein levels in transfected COS7 cells and FXTAS brain tissue. The next step would be to collect peripheral blood mononuclear cell (PBMC) fractions or blood plasma from PM carriers with and without FXTAS which are relatively easy to obtain, and to test whether it is possible to detect FMRpolyG levels in these tissues using our sandwich-ELISA. In *C9ORF72*-linked ALS/FTD, toxic RAN-proteins are reported in PBMC and CSF [53]. FMRpolyG might also be present in CSF, but a lumbar puncture procedure is more invasive for patients. All possibilities need further research to explore the potential role of FMRpolyG as a fluid prognostic and/or pharmacodynamic biomarker. In other neurodegenerative disorders like Alzheimer's disease and *C9ORF72*-linked ALS/FTD, fluid biomarkers have proven to be essential in monitoring disease progression and for successful assessment of future clinical trials [54-56].

In conclusion, ELISA technology is already widely implemented as a diagnostic tool in several neurodegenerative disorders like Alzheimer's disease and Parkinson's disease [39, 40]. It requires relatively small samples to detect very low protein concentrations in the picogram range. High concentrations of urea seem to efficiently dissolve FMRpolyG containing aggregates without interfering with our ELISA signaling. Further optimization of this sandwich-ELISA could be the first step towards a prognostic tool for PM carriers and assist in the future development of therapeutic interventions for FXTAS.

Acknowledgements

The authors would like to thank Sanne Thewessen for her contribution to this work by assisting in the optimization of the protein isolation protocol and the sandwich-ELISA setup during her internship at our lab.

References

1. Hagerman, R.J. and P. Hagerman, *Fragile X-associated tremor/ataxia syndrome - features, mechanisms and management.* Nat Rev Neurol, 2016. **12**(7): p. 403-12.
2. Hagerman, R.J., et al., *Intention tremor, parkinsonism, and generalized brain atrophy in male carriers of fragile X.* Neurology, 2001. **57**(1): p. 127-30.
3. Berry-Kravis, E., et al., *Fragile X-associated tremor/ataxia syndrome: clinical features, genetics, and testing guidelines.* Mov Disord, 2007. **22**(14): p. 2018-30, quiz 2140.
4. Hagerman, R. and P. Hagerman, *Advances in clinical and molecular understanding of the FMR1 premutation and fragile X-associated tremor/ataxia syndrome.* Lancet Neurol, 2013. **12**(8): p. 786-98.
5. Hagerman, P., *Fragile X-associated tremor/ataxia syndrome (FXTAS): pathology and mechanisms.* Acta Neuropathol, 2013. **126**(1): p. 1-19.
6. Hunter, J., et al., *Epidemiology of fragile X syndrome: a systematic review and meta-analysis.* Am J Med Genet A, 2014. **164A**(7): p. 1648-58.
7. Hantash, F.M., et al., *FMR1 premutation carrier frequency in patients undergoing routine population-based carrier screening: insights into the prevalence of fragile X syndrome, fragile X-associated tremor/ataxia syndrome, and fragile X-associated primary ovarian insufficiency in the United States.* Genet Med, 2011. **13**(1): p. 39-45.
8. Jacquemont, S., et al., *Penetrance of the fragile X-associated tremor/ataxia syndrome in a premutation carrier population.* JAMA, 2004. **291**(4): p. 460-9.
9. Rodriguez-Revenga, L., et al., *Penetrance of FMR1 premutation associated pathologies in fragile X syndrome families.* Eur J Hum Genet, 2009. **17**(10): p. 1359-62.
10. Greco, C.M., et al., *Neuropathology of fragile X-associated tremor/ataxia syndrome (FXTAS).* Brain, 2006. **129**(Pt 1): p. 243-55.
11. Greco, C.M., et al., *Neuronal intranuclear inclusions in a new cerebellar tremor/ataxia syndrome among fragile X carriers.* Brain, 2002. **125**(Pt 8): p. 1760-71.
12. Tassone, F., et al., *Elevated levels of FMR1 mRNA in carrier males: a new mechanism of involvement in the fragile-X syndrome.* Am J Hum Genet, 2000. **66**(1): p. 6-15.
13. Hashem, V., et al., *Ectopic expression of CGG containing mRNA is neurotoxic in mammals.* Hum Mol Genet, 2009. **18**(13): p. 2443-51.
14. Hoem, G., et al., *CGG-repeat length threshold for FMR1 RNA pathogenesis in a cellular model for FXTAS.* Hum Mol Genet, 2011. **20**(11): p. 2161-70.
15. Arocena, D.G., et al., *Induction of inclusion formation and disruption of lamin A/C structure by premutation CGG-repeat RNA in human cultured neural cells.* Human Molecular Genetics, 2005. **14**(23): p. 3661-3671.
16. Tassone, F., C. Iwahashi, and P.J. Hagerman, *FMR1 RNA within the intranuclear inclusions of fragile X-associated tremor/ataxia syndrome (FXTAS).* RNA Biol, 2004. **1**(2): p. 103-5.
17. Sellier, C., et al., *Sequestration of DROSHA and DGCR8 by expanded CGG RNA repeats alters microRNA processing in fragile X-associated tremor/ataxia syndrome.* Cell Rep, 2013. **3**(3): p. 869-80.

18. Sellier, C., et al., *Sam68 sequestration and partial loss of function are associated with splicing alterations in FXTAS patients.* EMBO J, 2010. **29**(7): p. 1248-61.
19. Todd, P.K., et al., *CGG repeat-associated translation mediates neurodegeneration in fragile X tremor ataxia syndrome.* Neuron, 2013. **78**(3): p. 440-55.
20. Iwahashi, C. and P.J. Hagerman, *Isolation of pathology-associated intranuclear inclusions.* Methods Mol Biol, 2008. **463**: p. 181-90.
21. Iwahashi, C.K., et al., *Protein composition of the intranuclear inclusions of FXTAS.* Brain, 2006. **129**(Pt 1): p. 256-71.
22. Haify, S.N., et al., *In silico, in vitro, and in vivo Approaches to Identify Molecular Players in Fragile X Tremor and Ataxia Syndrome.* Front Mol Biosci, 2020. **7**: p. 31.
23. Wenzel, H.J., et al., *Astroglial-targeted expression of the fragile X CGG repeat premutation in mice yields RAN translation, motor deficits and possible evidence for cell-to-cell propagation of FXTAS pathology.* Acta Neuropathol Commun, 2019. **7**(1): p. 27.
24. Haify, S.N., et al., *Lack of a Clear Behavioral Phenotype in an Inducible FXTAS Mouse Model Despite the Presence of Neuronal FMRpolyG-Positive Aggregates.* Front Mol Biosci, 2020. **7**: p. 599101.
25. Sellier, C., et al., *Translation of Expanded CGG Repeats into FMRpolyG Is Pathogenic and May Contribute to Fragile X Tremor Ataxia Syndrome.* Neuron, 2017. **93**(2): p. 331-347.
26. Buijsen, R.A.M., et al., *FMRpolyG-positive inclusions in CNS and non-CNS organs of a fragile X premutation carrier with fragile X-associated tremor/ataxia syndrome.* Acta Neuropathologica Communications, 2014. **2**(1): p. 162.
27. Buijsen, R.A., et al., *Presence of inclusions positive for polyglycine containing protein, FMRpolyG, indicates that repeat-associated non-AUG translation plays a role in fragile X-associated primary ovarian insufficiency.* Hum Reprod, 2016. **31**(1): p. 158-68.
28. Friedman-Gohas, M., et al., *FMRpolyG accumulates in FMR1 premutation granulosa cells.* J Ovarian Res, 2020. **13**(1): p. 22.
29. Stenvang, J. and S. Kauppinen, *MicroRNAs as targets for antisense-based therapeutics.* Expert Opinion on Biological Therapy, 2008. **8**(1): p. 59-81.
30. Disney, M.D., et al., *A small molecule that targets r(CGG)(exp) and improves defects in fragile X-associated tremor ataxia syndrome.* ACS Chem Biol, 2012. **7**(10): p. 1711-8.
31. Hukema, R.K., et al., *Reversibility of neuropathology and motor deficits in an inducible mouse model for FXTAS.* Hum Mol Genet, 2015. **24**(17): p. 4948-57.
32. Jacquemont, S., et al., *Fragile X premutation tremor/ataxia syndrome: molecular, clinical, and neuroimaging correlates.* Am J Hum Genet, 2003. **72**(4): p. 869-78.
33. Famula, J.L., et al., *Presence of Middle Cerebellar Peduncle Sign in FMR1 Premutation Carriers Without Tremor and Ataxia.* Front Neurol, 2018. **9**: p. 695.
34. Shelton, A.L., et al., *Middle Cerebellar Peduncle Width-A Novel MRI Biomarker for FXTAS?* Front Neurosci, 2018. **12**: p. 379.
35. Giulivi, C., et al., *Plasma Biomarkers for Monitoring Brain Pathophysiology in FMR1 Premutation Carriers.* Front Mol Neurosci, 2016. **9**: p. 71.

36. Giulivi, C., et al., *Plasma metabolic profile delineates roles for neurodegeneration, pro-inflammatory damage and mitochondrial dysfunction in the FMR1 premutation.* Biochem J, 2016. **473**(21): p. 3871-3888.
37. Zafarullah, M., et al., *Metabolic profiling reveals dysregulated lipid metabolism and potential biomarkers associated with the development and progression of Fragile X-Associated Tremor/Ataxia Syndrome (FXTAS).* FASEB J, 2020. **34**(12): p. 16676-16692.
38. Brunberg, J.A., et al., *Fragile X premutation carriers: characteristic MR imaging findings of adult male patients with progressive cerebellar and cognitive dysfunction.* AJNR Am J Neuroradiol, 2002. **23**(10): p. 1757-66.
39. Quattrone, A., et al., *MR parkinsonism index predicts vertical supranuclear gaze palsy in patients with PSP-parkinsonism.* Neurology, 2016. **87**(12): p. 1266-73.
40. Krans, A., et al., *Neuropathology of RAN translation proteins in fragile X-associated tremor/ataxia syndrome.* Acta Neuropathol Commun, 2019. **7**(1): p. 152.
41. Atkin, G. and H. Paulson, *Ubiquitin pathways in neurodegenerative disease.* Front Mol Neurosci, 2014. **7**: p. 63.
42. Lee, K.H., et al., *C9ORF72-linked Dipeptide Repeats Impair the Assembly, Dynamics, and Function of Membrane-Less Organelles.* Cell, 2016. **167**(3): p. 774-788 e17.
43. Mori, K., et al., *The C9ORF72-linked GGGGCC repeat is translated into aggregating dipeptide-repeat proteins in FTLD/ALS.* Science, 2013. **339**(6125): p. 1335-8.
44. Swaminathan, A., et al., *Expression of C9ORF72-linked-related dipeptides impairs motor function in a vertebrate model.* Hum Mol Genet, 2018. **27**(10): p. 1754-1762.
45. Ma, L., et al., *Composition of the Intranuclear Inclusions of Fragile X-associated Tremor/Ataxia Syndrome.* Acta Neuropathol Commun, 2019. **7**(1): p. 143.
46. Wenzel, H.J., et al., *Ubiquitin-positive intranuclear inclusions in neuronal and glial cells in a mouse model of the fragile X premutation.* Brain Res, 2010. **1318**: p. 155-66.
47. Asamitsu, S., et al., *CGG repeat RNA G-quadruplexes interact with FMRpolyG to cause neuronal dysfunction in fragile X-related tremor/ataxia syndrome.* Sci Adv, 2021. **7**(3).
48. Churion, K.A. and S.E. Bondos, *Identifying solubility-promoting buffers for intrinsically disordered proteins prior to purification.* Methods Mol Biol, 2012. **896**: p. 415-27.
49. Fink, A.L., *Protein aggregation: folding aggregates, inclusion bodies and amyloid.* Folding and Design, 1998. **3**(1): p. R9-R23.
50. Gendron, T.F., et al., *Poly(GP) proteins are a useful pharmacodynamic marker for C9ORF72-LINKED-associated amyotrophic lateral sclerosis.* Sci Transl Med, 2017. **9**(383).
51. Jiang, J., et al., *Gain of Toxicity from ALS/FTD-Linked Repeat Expansions in C9ORF72-LINKED Is Alleviated by Antisense Oligonucleotides Targeting GGGGCC-Containing RNAs.* Neuron, 2016. **90**(3): p. 535-50.
52. Su, Z., et al., *Discovery of a biomarker and lead small molecules to target r(GGGGCC)-associated defects in c9FTD/ALS.* Neuron, 2014. **83**(5): p. 1043-50.

53. Herranz-Martin, S., et al., *Viral delivery of C9ORF72-linked hexanucleotide repeat expansions in mice leads to repeat-length-dependent neuropathology and behavioural deficits.* Dis Model Mech, 2017. **10**(7): p. 859-868.
54. Lewczuk, P., et al., *Clinical significance of fluid biomarkers in Alzheimer's Disease.* Pharmacol Rep, 2020. **72**(3): p. 528-542.
55. Meeter, L.H., et al., *Imaging and fluid biomarkers in frontotemporal dementia.* Nat Rev Neurol, 2017. **13**(7): p. 406-419.
56. Balendra, R., T.G. Moens, and A.M. Isaacs, *Specific biomarkers for C9ORF72-linked FTD/ALS could expedite the journey towards effective therapies.* EMBO Mol Med, 2017. **9**(7): p. 853-855.

CHAPTER 7

7

General discussion and conclusion

Fragile X-associated tremor and ataxia syndrome (FXTAS) is a late-onset neurodegenerative disorder caused by an expanded CGG-repeat in the 5' untranslated region (UTR) of the *FMR1* gene in premutation (PM) carriers. FXTAS is one of the many microsatellite trinucleotides repeat expansion disorders [1] that have been described over the past decades, including spinocerebellar ataxias (SCA) [2], myotonic dystrophy type 1 and 2 (DM1; DM2) [3-5], *C9ORF72*-linked amyotrophic lateral sclerosis / frontotemporal dementia (ALS/FTD) [6] and Huntington disease (HD) [7]. Microsatellite repeat expansions can be present in coding regions of a gene, as is the case in HD, resulting in a toxic or mutant Huntingtin protein or in non-coding intronic regions [7, 8]. Repeat expansions in introns can affect gene transcription, mRNA splicing and nucleocytoplasmic transport of mRNAs [9]. Microsatellite repeats are also found in promoter and regulatory flanking regions (*i.e.,* UTR regions) of genes as is the case in FXTAS [1, 9]. It is thought that microsatellite repeat expansions in regulatory regions do not affect the primary protein product of the gene but rather affect chromosome stability, induce gene silencing via methylation, and modulate transcription and translation processes in the cell [1].

Based on what has been reported in the literature, there is no doubt that the expanded CGG-repeat in the 5'-UTR region of the *FMR1* gene contributes to a RNA gain-of-function disease mechanism in FXTAS [10-12]. In PM carriers the expanded CGG-repeat can lead to clinical features, including intention tremors and cerebellar gait ataxia but also more generic disease-associated phenotypes involving mental health problems [13-15]. PM carriers with and without FXTAS express increased levels of *FMR1* mRNA containing an expanded CGG-repeat [10]. These elevated *FMR1* mRNA levels in PM carriers with and without FXTAS may sequester important proteins in the cell and disrupt cellular processes. Other less profound effects caused by the elevated *FMR1* mRNA levels containing an expanded CGG-repeat are reported, including mitochondrial dysfunction [16-18], autophagy [19] and excessive R-loop formation and DNA damage repair mechanisms [20]. Interestingly, non-canonical repeat-associated non-AUG (RAN) translation of the *FMR1* mRNA containing an expanded CGG-repeat can also result in disease-causing events through the production of a toxic polyglycine peptide called FMRpolyG (protein gain-of-function disease mechanism) [21]. FMRpolyG can interact with the nuclear lamina and the expanded CGG-repeat inducing cellular toxicity and intranuclear inclusion formation driving FXTAS pathogenesis. In addition, RAN translation of the expanded CGG-repeat can also generate other potentially toxic polypeptides and affect the canonical translation of the *FMR1* mRNA open-reading frame (ORF) [21, 22].

It has been shown that the expanded CGG-repeat RNA alone cannot explain all cellular and behavioral defects observed in *in vitro* and *in vivo* models for FXTAS [21, 23, 24]. A synergistic effect of both RNA gain-of-function and protein gain-of-function disease mechanisms is in my opinion the most plausible explanation for FXTAS pathogenesis

and has been proposed in literature as well [23]. To better understand the role of RAN translation in PM carriers with and without FXTAS, and to define whether RAN translation is truly the bad boy in FXTAS pathogenesis, a new mouse model expressing alternative codon sequences in the PM range coding for the FMRpolyG peptide should be generated in the future. Molecular and histopathological data, together with behavioral studies in this mouse model, could give more insight in the leading role of RAN translation and FMRpolyG in FXTAS pathogenesis. So far, the mechanistic link between the *FMR1* mRNA containing an expanded CGG-repeat, RAN translation and FMRpolyG production and disease manifestations is still not entirely clarified. The main focus of this thesis is to understand the role of RAN translation and the formation of FMRpolyG-positive inclusions in the cell as well as the effects of the presence of inclusions on behavior in two new FXTAS mouse models. In addition, this thesis will focus on a potential new therapeutic intervention using a small molecule and a role for FMRpolyG as biomarker.

RNA gain-of-function

PM carriers express 2- to 8-fold elevated *FMR1* mRNA levels in blood while the expression of the protein encoded by the *FMR1* gene, FMRP, remains unaffected or is slightly reduced [10, 25]. Elevated *FMR1* RNA levels correlate nicely with the size of the CGG-repeat [10, 25]. Post-mortem examination of FXTAS brains and/or isolated nuclei showed eosinophilic intranuclear inclusions containing *FMR1* mRNA, but also many other components, including ubiquitin [11, 26-29]. Ubiquitin-positive intranuclear inclusions is considered a neuropathological hallmark for FXTAS [28, 29]. Based on these molecular and histopathological observations, a pathogenic RNA gain-of-function mechanism has been proposed for FXTAS [30, 31]. Expression of the abnormal *FMR1* mRNA containing an expanded CGG-repeat in cellular and animal models is toxic [32-34]. The expanded CGG-repeats in *FMR1* mRNA alter the secondary structure of *FMR1* mRNA forming hairpin-like structures and/or G-quadruplex structures that can sequester essential proteins in the cell, leading to cellular dysfunction and neurodegeneration [35-37]. Re-locating the expanded CGG-repeat from the 5'-UTR region to the 3'-UTR region preludes toxicity (*i.e.,* rough-eye phenotype) in *Drosophila* FXTAS models suggesting that the altered secondary structure containing the expanded CGG-repeat *per se* is not toxic but rather the expanded CGG-repeat RNA [21]. *In vitro* and *in vivo* identification of the molecular players involved in important cellular pathways is essential for understanding the mechanistic link between *FMR1* mRNA containing an expanded CGG-repeats and disease features of FXTAS (reviewed in **chapter 1**; adapted from [38]).

Mass spectrometry studies in post-mortem brain tissue from FXTAS patients and FXTAS animal models like the mouse and *Drosophila*, identified an extensive list of RNA-binding proteins (RBPs) including HNRNP A2/B1, Pur-α, DGCR8 and SAM68 to be present in the intranuclear inclusions [27, 35, 36, 39, 40]. In the *Drosophila* model for FXTAS, HNRNP A2/

B1 can alter RNA metabolism through direct interaction with the CGG-repeat or indirect interaction after binding CUGBP1 or TDP-43 [39, 41]. Interaction between CUGBP1 and HNRNP A2/B1 results in neurotoxicity due to loss of the pre-mRNA alternative splicing function and the mistrafficking of important mRNAs [39, 42]. TDP-43 interacts with two HNRNP A2/B1 homologues in the *Drosophila* and acts as a suppressor of CGG-repeat induced toxicity [41]. The rescue of CGG-repeat RNA induced toxicity appears to be specific for the expression of TDP-43, since co-expression of other RBPs aggravated the toxic effects induced by CGG-repeat RNA [41]. Pur-α interacts with the expanded CGG-repeat RNA in the *Drosophila* FXTAS model and sequesters Rm62, a *Drosophila* ortholog of p68 RNA helicase, which results in nuclear accumulation of specific RNAs involved in stress and immune responses [43]. Additionally, Sellier *et al.,* reported that CGG-repeat RNA within the inclusions can bind DGCR8 and SAM68, which are both involved in micro-RNA processing. The binding of DGCR8 and SAM68 to CGG-repeat RNA leads to decreased mature microRNAs, disruption of cellular homeostasis and consequently increased cell death [35, 36].

RAN translation and protein-gain-of-function

Although strong evidence for the RNA gain-of-function mechanism in FXTAS exists, a second rather uncommon phenomenon was first proposed in 2011 after Laura Ranum and colleagues described a non-canonical protein translation mechanism of microsatellite repeat expansions in DM1, called RAN translation [44]. Short after this discovery, Todd and colleagues were the first to show that RAN translation also initiates in *FMR1* mRNA containing an expanded CGG-repeat from a non-canonical ACG start-codon upstream of the expanded CGG-repeat. This results in the production of a cytotoxic polyglycine peptide, called FMRpolyG (+1 reading frame) [21]. The presence of FMRpolyG was confirmed by Western blot and tandem mass spectrometry (MS-MS) in cerebellar lysates in post-mortem FXTAS brain tissue and *Drosophila* lysates, respectively [21]. FMRpolyG could also be detected in intranuclear inclusions in post-mortem FXTAS brain tissue and co-localizes with ubiquitin [21]. In addition to the production of FMRpolyG, which is the best studied RAN protein, RAN translation of the CGG-repeat can also generate other polypeptides, namely the polyalanine (FMRpolyA, +2 reading frame) protein and the polyarginine (FMRpolyR, +0 reading frame) protein [21, 45]. In transfected COS7 cells and SY5Y neuroblastoma cells overexpressing the *FMR1* mRNA containing an expanded 88xCGG-repeat, only FMRpolyA could be detected in intranuclear inclusions [21]. Interestingly, in post-mortem FXTAS brain tissue or mouse brain sections, FMRpolyA could not be detected [23, 45]. FMRpolyA translation is probably less efficient compared to FMRpolyG which could explain why FMRpolyA could not be detected [21, 46]. Interestingly, *in vitro* expression plasmids could also produce FMRpolyA even when a stop codon was placed directly upstream of the expanded CGG-repeat, suggesting that translation initiation in this reading frame also occurs within the repeat itself independent of a non-canonical start-codon [21, 46]. The

FMRpolyR protein could not be observed in transfected cells or *in vivo* which could be explained by its extreme low translation efficiency with increasing CGG-repeat size in contrast to the other two polypeptides [21]. In PM carriers antisense (AS) transcription of the *FMR1* mRNA is also possible. In PM carriers 2- to 3-fold *ASFMR1* mRNA levels have been reported [47]. AS transcription and non-canonical translation of the *ASFMR1* mRNA in PM carriers result in a N-truncated polyproline peptide (ASFMRpolyP), an ASFMRpolyR peptide and an ASFMRpolyA peptide [47, 48]. Similarly, antisense transcription mechanisms have been described in DM1 and SCA8 [49, 50]. The exact role of these ASFMR-polypeptides in FXTAS disease pathogenesis is yet unclear. ASFMRpolyP and ASFMRpolyA have been observed in intranuclear inclusions in post-mortem FXTAS brain tissue while ASFMRpolyR could not be detected due to low antibody specificity in validation assays [48]. Notably, RAN translation of all ASFMR-polypeptides increases with increased CGG-repeat size [48]. In transfected COS7 cells, increased CGG-repeat size causes ASFMRpolyR to re-localize to the nucleolus, and ASFMRpolyA to re-localize from the cytoplasm to the nucleus [48]. It is unclear whether these ASFMR-polypeptides have either toxic or protective effects in the cell.

Toxic polypeptides containing proline (P), arginine (R) and/or alanine (A) have been reported for multiple microsatellite expansion neurodegenerative disorders, including oculopharyngeal muscular dystrophy (OPMD), HD, *C9ORF72*-linked ALS/FTD and more. Expression of poly-A peptides causes OPMD [51, 52]. Aggregates containing poly-A were shown to recruit and alter proteasomal components, including ubiquitin and heat shock proteins (HSPs) in OPMD [51, 52]. In *C9ORF72*-linked ALS/FTD, two RAN translated arginine-rich dipeptides, poly-PR and poly-GR, are proposed to have toxic effects in the cell [53, 54]. Transfecting different cell lines with overexpression constructs encoding for poly-PR and poly-GR show extreme toxicity in the cell [55-58]. When expressed in the *Drosophila* disease models, these dipeptides reduce survival of the flies and induce a severe rough-eye phenotype [53, 55, 59-62]. Augmenting for the findings in the *Drosophila*, expression of the poly-GR dipeptide in the zebrafish also reduced survival of the fish and induced developmental abnormalities [63]. More recently, poly-GR has been shown to induce oxidative stress by binding mitochondrial ribosomal proteins, and poly-PR has been reported to inhibit the proteasome and also bind to the nuclear pore disrupting normal nuclear transport [64-66]. Interestingly, while dipeptides containing arginine seem to induce toxicity, polypeptides containing only arginine seem to have some neuroprotective properties in *in vitro* stroke disease models [67]. Consistent with this observation, polypeptides containing only proline prevent the aggregation of polyglutamine-containing Huntingtin in HD [68, 69]. While both amino acids seem to have some neuroprotective properties, it seems that when proline and arginine come together in for example the poly-PR peptide, they lose this property and become toxic to cell. It is necessary to be careful when interpreting these toxic effects as these studies

often use overexpression systems which do not reflect the endogenous expression of these polypeptides in cells from patients. All these findings in literature show that many contradictions exist regarding these polypeptides and the amino acids they hold. Further research is necessary to understand their cellular role in FXTAS pathology.

Nuclear inclusion pathology in FXTAS

Meanwhile, extensive research in FXTAS has focused on CGG-repeat mediated RAN translation and FMRpolyG-induced toxicity. Many studies show that FMRpolyG is indeed a key player in FXTAS pathogenesis and neurodegeneration. FMRpolyG, which is a relatively small protein, is the best characterized RAN translation product in FXTAS pathogenesis. FMRpolyG-positive and ubiquitin-positive intranuclear inclusions in neurons and astrocytes are the neuropathological hallmark for FXTAS [28, 29, 70, 71]. Several groups, including our lab, have shown that FMRpolyG accumulates in intranuclear inclusions in neurons and astrocytes in post-mortem brain tissue of FXTAS patients (**chapter 5**, [21, 28, 29, 45, 72]). Many cellular and animal models have been generated, including the *Drosophila* and the mouse, to study FMRpolyG and inclusion formation as well as its impact on behavior and motor function (**chapter 2 and 3**, [21, 23, 33]). Recently, researchers reported in cellular models that the expanded CGG-repeat RNA G-quadruplex structure propagates protein aggregation formation upon interaction with the polyglycine stretch of FMRpolyG [12]. Interestingly, FMRpolyG was found to aggregate in exosomes. Electrophysiological analysis in cultures of primary hippocampal neurons of the Dutch CGG KI mouse treated with FMRpolyG containing exosomes revealed neuronal changes indicative of neuronal dysfunction in the primary neurons [12]. Previous work in our lab showed that FMRpolyG-positive intranuclear inclusions are not restricted to neurons and astrocytes in brain tissue but could also form in several systemic organs in mice and FXTAS patients [73, 74]. In both studies, the majority of FMRpolyG-positive intranuclear inclusions co-localized with ubiquitin-positive intranuclear inclusions. The formation of toxic FMRpolyG-positive and ubiquitin-positive intranuclear inclusions in several systemic organs may in some cases explain the overlap between the FMRpolyG induced inclusion pathology and multiple system atrophy (MSA) that is observed in FXTAS patients [75, 76]. Although intranuclear inclusions are found in neurons and astrocytes in FXTAS, the primary focus in research studies has always been on neurons and how the hypothesized disease mechanisms contribute to the neurodegeneration in FXTAS. The role of astroglia in FXTAS is often not discussed while astroglia have a detrimental disease-causing role in many other neurodegenerative disorders including Alzheimer's disease (AD) [77-79], HD [80-82], Parkinson's disease (PD) (reviewed in [83]) and ALS [84-86]. Astrocytes play a critical role in the viability and function of the brain as they are involved in the formation, maintenance, and elimination of synapses during development and disease (reviewed in [87]). Astroglia are required for neuronal survival [88], and the loss of normal astroglia function can be a primary contributor to neurodegeneration [89-91]. In fact, for some

neurodegenerative disorders intranuclear protein inclusions in astrocytes are the primary cause of disease rather than neuronal dysfunction [89-91].

To understand the role of astroglia, we generated a transgenic mouse model expressing the expanded CGG-repeat RNA in astrocytes and Bergmann glia, providing the first evidence for RAN translation in these cells, and a potential disease-causing role for astroglia in mice and in FXTAS patients (**chapter 2**). Studies in FXTAS generally describe RAN translation and inclusion formation in neurons, but none of the studies investigate the role of astroglia in FXTAS pathology, even though Greco *et al.,* found that 20-30% of astrocytes in post-mortem FXTAS brain sections contain intranuclear inclusions [28, 29]. Interestingly, researchers found that more inclusions were present in astrocytes than in neurons in several brain regions in FXTAS brain [27-29]. Our transgenic mice expressing an expanded CGG-repeat in astroglia showed ubiquitin-positive inclusions in approximately 0.5% of the astroglia [92]. This finding is similar to what has been observed in the Dutch CGG KI mouse model of FXTAS where relatively few astrocytes developed ubiquitin-positive intranuclear inclusions [93]. Reasons for the observed differences in the prevalence of intranuclear inclusion formation between mice and post-mortem FXTAS brain tissue are yet unknown. A possible explanation for this discrepancy could be that inclusion formation is slower in astroglia in mouse brain, when compared to inclusion formation in neurons and astrocytes in human brain. It is important to mention that we are comparing 24-weeks old astroglia-specific mice expressing the expanded CGG-repeat and 72-weeks old Dutch CGG KI mice with end stage human post-mortem FXTAS brain tissue. It is possible that follow-up of these mice to their end stage (2 years), we may find more astrocytes with intranuclear inclusions.

The ubiquitin proteasome system (UPS) may also play a leading role in the accumulation of aggregated proteins within the ubiquitin-positive intranuclear inclusions. The UPS is critical for intracellular protein degradation and turnover, including clearing intracellular misfolded proteins. Moreover, UPS activity has been reported to be lower in neurons compared to astrocytes and to decrease with aging [94]. Also, components of the UPS such as ubiquitin and HSPs are observed in intranuclear inclusions in post-mortem FXTAS brain [27]. In addition, in mice several other UPS components were found in inclusions, including Rad23b and the 20S subunit of the proteasome [33, 95-97]. We showed in our inducible mouse model with ubiquitous expression of the expanded CGG-repeat RNA, that Rad23b co-localized with FMRpolyG in intranuclear inclusions upon dox-induction (**chapter 4**). Treatment with a small chemical compound resulted in a reduction of Rad23b protein levels and evidently restored the cytoplasmic distribution of the Rad23b protein in the cell (**chapter 4**). Rad23b (*i.e.,* HR23B in humans) pathology has been described in several neurodegenerative disorders including HD, *C9ORF72*-linked ALS/FTD, SCA type 3 and 7, FXTAS and PD [96, 98]. Rad23b can bind ubiquitin via ubiquitin-associated motifs

[99, 100] and shuttle toxic and misfolded proteins as well as undesired transcription factors into the proteasome, and promote their turnover [101-103]. Misregulation of protein degradation due to the capture of the Rad23b protein in inclusions may directly or indirectly be involved in FXTAS pathology [104]. Our brain-specific inducible mouse models may provide new insights in the role of Rad23b in FXTAS pathology. Moreover, Rad23b plays a crucial role in the regulation of the global genome nucleotide excision repair (NER) mechanism by protecting other important NER proteins from being degraded by the proteasomal pathway [105]. If Rad23b is captured in inclusions it is possible that NER proteins are degraded which enhances the formation of R-loops and DNA damage [20]. R-loop formation and deficits in DNA damage repair mechanisms have been reported in FXTAS [18, 106]. Interestingly, a recent protein composition study showed six new proteins that are involved in DNA damage repair pathways to be present in intranuclear inclusions [107]. It may be interesting to investigate the presence of Rad23b in intranuclear inclusions in our transgenic mice expressing the expanded CGG-repeat RNA in astroglia. Moreover, Rad23b rescue experiments in transgenic brain-specific mouse models would give more insight into the role of Rad23b on behavior. These experiments would allow us to further understand the role and contribution of Rad23b, additional disease mechanisms including the UPS in astroglia but also in overall FXTAS neuropathology. Importantly, the toxic FMRpolyG protein also co-localized with ubiquitin-positive intranuclear inclusions in the astroglia and Bergmann glia in our transgenic mice expressing the expanded CGG-repeat (**chapter 2**). Notably, inclusions were never observed in microglia and oligodendrocytes. The presence of toxic FMRpolyG in the astroglia could also contribute to the disease pathology in these mice.

The role of FMRpolyG in expanded CGG-repeat associated cellular toxicity is well studied in cellular and animal models. Transgenic mice expressing the expanded CGG-repeat in astroglia show behavioral deficits in motor function and performance on the ladder-rung test and impaired gait of the hind limbs (**chapter 2**, [92]). A number of factors may argue for the toxic effects of FMRpolyG in astroglia cells. First, the presence of the amino acid C-terminal region of FMRpolyG may interact with lamin-associated proteins [23]. Protein interaction studies in transfected Neuro2A cells revealed that FMRpolyG containing the C-terminal region interacts with LAP2β [23]. LAP2β assists in the organization of lamin proteins near the nuclear inner membrane. In FXTAS, also other lamin-associated proteins have been found within inclusions, including lamin A/C isoform 1 and vimentin [27]. Alterations of LAP2β, and perhaps also other lamin-associated proteins, result in disorganization of the nuclear lamina architecture causing cellular toxicity [108]. Similar findings were observed in other microsatellite repeat expansion disorders, including *C9ORF72*-linked ALS/FTD and HD in which RAN-translated pathogenic proteins disrupt the nuclear architecture and nucleocytoplasmic transport in the cell [109, 110]. Sellier and colleagues also showed that FMRpolyG containing the C-terminal region results

in increased cell death in mouse cortical neurons compared to FMRpolyG without the C-terminal region [23]. Expression of FMRpolyG containing the C-terminal region in *Drosophila* also induced a more severe eye phenotype confirming the increased toxicity due to the presence of the C-terminal region [23]. It may be possible that FMRpolyG-positive intranuclear inclusions in astroglia induce increased toxicity in astroglia and consequently contribute to neuronal degeneration as astroglia are necessary for the maintenance of neurons [284]. As an indirect consequence of the astroglia cell dropout, subsequent neuronal degeneration can cause the behavioral deficits we reported in our transgenic mice (**chapter 2**). Secondly, FMRpolyG may also induce cellular toxicity by accumulating misfolded proteins and proteasomal components in intranuclear inclusions in astroglia through alterations of the UPS system [21, 24]. Accumulation of misfolded proteins in the astroglia may induce cellular stress. Cellular stress has been reported to enhance RAN-translation in *C9ORF72*-linked ALS/FTD disease models, creating a feed-forward loop that potentially drives excess production of FMRpolyG in FXTAS and thus enhancing neurodegeneration [22].

Surprisingly, the transgenic mice expressing an expanded CGG-repeat in astroglia performed better on the rotarod assay. There are several explanations for this observation. First, we believe that mice in general tend to use an alternative strategy to stay on the rotarod called flipping (*i.e.,* mice cling on the rotarod bar rotating 360 degrees without falling). This "flipping" behavior was prevalent in our transgenic astroglia-specific mice, however we do not have a clear explanation for this behavior. It could be that these mice learn by trial and error that clinging on the rotarod prevents falling from the rotarod. Second, enhanced performance on the rotarod assay has been reported in several mouse models including neuroxin-1α KO mice [111], conditional *PTEN* KO mice [112] and autism spectrum disorder mouse models, including mice with overexpression of human α-synuclein, SynA53T [113], and neuroligin-3 R451C KI mice [114, 115]. Although most researchers only mention the observed enhanced rotarod performance in these mice without any clear clarification, one study reported that mutations in neuroligin-3 protein may alter the striatal circuitry, improve spatial learning and increase repetitive behavioral learning in mice [116]. This behavioral phenotype may manifest as a consequence of improved motor learning and adoption of stereotyped behavior on the rotarod assay resulting in an apparent improvement in motor performance compensating for any (minor) motor function deficit in our transgenic mice expressing an expanded CGG-repeat in astroglia. However, the fact that intranuclear inclusions were also found in neurons in the astroglia-specific expression mice complicated attempts to truly attribute specific pathology to the astroglia. Important to mention is that the number of neuronal intranuclear inclusions in these mice was very low but nevertheless, their contribution to the motor deficits cannot be left unmentioned (**chapter 2**).

Evidence for cell-to-cell transfer of FMRpolyG

The fact that we found FMRpolyG-positive and ubiquitin-positive intranuclear inclusions in neurons in various brain regions while expression of the expanded CGG-repeat RNA was restricted to astroglia was unexpected (**chapter 2**). One study reported that both the human and murine astroglia promoter may also direct expression of some genes in neurons depending on the nature of the expressed sequence and/or the transgene insertion site, however this occurred only in a few examples [117]. One possible explanation for this aberrant expression pattern could be leaky expression of the *Gfa2* promoter in neurons, but this is very unlikely since neurons in our mice did not show any detectable GFP fluorescent signal or glial fibrillary acidic protein (GFAP) immunoreactivity in the nucleus or cytoplasm. Astroglia expressing GFP were immuno-positive when reacted with antiserum against GFP and GFAP while neurons were not (**chapter 2**). GFAP is almost exclusively expressed in astroglia, and is therefore the preferred astrocyte marker in clinical and basic research studies [118, 119]. However, during early development in mice, the *Gfa2* promoter is shortly expressed in neuronal progenitor cells [120] which may give rise to neurons expressing the expanded CGG-repeat RNA for a short period of time. Several studies using different experimental approaches like time-lapse video analysis [121, 122], flowcytometry [123, 124] and Cre/LoxP fate-mapping [124, 125] of progenitor cells have shown that GFAP-positive progenitor cells in mice could indeed give rise to specific populations of neurons during development which may explain the observation in our mice [120, 126]. However, it is more likely that cell-to-cell transfer of pathology from astrocytes to neurons may occur in our mice. Cell-to-cell transmission of toxic dipeptide proteins linked to translation of the G_4C_2-repeat expansions in *C9ORF72*-linked ALS/FTD has been reported *in vitro* in several CNS cell types, including induced pluripotent stem cells from *C9ORF72*-ALS patients [127]. Importantly, transmission was bidirectional, both from astrocytes to neurons and from neurons to astrocytes [127]. Cell-to-cell pathology has been reported for disease-relevant proteins in AD, PD, and polyQ diseases, including HD [128-139]. Several mechanisms of transmission have been reported including secretion of exosomes, tunneling nanotubes, hemichannels between cells, exocytosis and endocytosis of proteins, and phagocytosis of infected cells or cell debris that contains the disease-relevant proteins [135, 140-142]. We do not yet have direct evidence for such mechanisms in our astroglia-specific mice or any reports of cell-to-cell transfer in PM carriers with and/or without FXTAS. Recently, researchers reported that FMRpolyG can interact with exosomal proteins and that FMRpolyG was present in exosomes isolated from neurons of the Dutch CGG KI mice [12]. Cell-to-cell transmission of neurotoxic proteins including Tau, α-synuclein and TDP-43 via exosomes is common in neurodegenerative disorders [133]. Exocytosis and endocytosis may also be one of the transmission mechanisms in PM carriers with or without FXTAS. We used COS7 cells to test this hypothesis since COS7 cells are robust and easy to handle. More importantly, COS7 cells are reported to have exocytosis and endocytosis capabilities [143, 144]. We

were able to generate a proof-of-principle transmission experiment in which donor COS7 cells were transfected for 48 hours with an expanded CGG-repeat fused with GFP RNA expression construct and receiver non-transfected COS7 cells. Receiver cells could take up FMRpolyG and form FMRpolyG-positive intranuclear inclusions (*unpublished data*). Another explanation could be that not the cell type is important in the prion-like disease mechanism but the disease-relevant protein. Interestingly, researchers recently found that the polyglycine stretch of FMRpolyG propagates cell-to-cell transfer through the presence of a prion-like amino acid composition domain in FMRpolyG [12]. When we transfer cell culture medium of COS7 cells transfected with a construct expressing the expanded CGG-repeat fused to GFP RNA to non-transfected receiver COS7 cells, we could observe minimal diffuse GFP fluorescence in these non-transfected receiver cells and occasionally FMRpolyG-positive inclusions could be detected (*unpublished data*). All together, these findings may suggest that FMRpolyG holds prion-like properties. The next step would be to transfect relevant cell types including neurons and astrocytes and study cell-to-cell transmission of FMRpolyG in these cells. Further research is necessary to understand the exact mechanism behind cell-to-cell transfer, which proteins and/or mechanisms may facilitate transmission and its contribution in FXTAS pathogenesis [12].

Potential protective role for inclusion bodies

Compelling evidence has been presented in cellular and animal models augmenting for the disease-causing role of toxic FMRpolyG [23, 97, 145, 146]. Wide-spread occurrence of nuclear inclusions, containing ubiquitin and FMRpolyG is a major hallmark of FXTAS [13, 28]. However, independent of the presence of FMRpolyG, the process of inclusion formation in the neurons and astrocytes might be also detrimental to the cells. We and others have shown that in mice inclusion formation follows expression of the expanded CGG-repeat RNA and is associated with behavioral impairments in these mice [33, 147, 148]. We have also shown that behavioral impairments could be halted at later age in our brain-specific inducible mouse model upon early intervention in the process of inclusion formation. This resulted in a decreased number and size of inclusions in the brain [33]. Nevertheless, there is some debate in the field whether inclusion bodies contribute to the cellular pathology in FXTAS, or — in contrast — slow down the disease process by sequestering toxic expanded CGG-repeat RNA and potential toxic proteins, including FMRpolyG. If the latter would be the case, this would argue for a more protective function for inclusion bodies in FXTAS. In other neurodegenerative disorders researchers found that SCA1 transgenic mice displayed disease-related neurological defects in the absence of protein containing inclusion bodies [149] and in cellular models for HD researchers found that the Huntingtin protein induced apoptosis and cell death without the formation of inclusion bodies in the cell [150, 151]. These reported findings suggest that inclusion bodies are not necessarily disease-causing. Interestingly, protective properties of inclusions have been proposed for FXTAS as well [15, 21].

To investigate this hypothesis for the PM, we generated a novel transgenic brain-specific inducible mouse model under the control of the *CamKII-α* promoter (**chapter 3**). The *CamKII-α* driver results in higher expression of the expanded CGG-repeat RNA compared to our previously published PrP-driven brain-specific inducible mouse model. The *CamKII-α* promoter drives expression throughout the entire forebrain, but also in regions of the cerebrum including the hippocampus and the basal ganglia. These brain regions are known to be involved in FXTAS disease pathology [29, 152]. Within a month upon transgene dox-induction, the first FMRpolyG-positive intranuclear inclusions were found in the striatum and the CA3 region of the hippocampus. After two months, these inclusions were abundant in the hippocampus, striatum and neocortex. If inclusions are indeed solely disease-causing, we would expect that inclusion formation in these brain regions is accompanied by a broad range of behavioral impairments associated with these brain regions in our inducible mice. Exposing these mice to a battery of motor function and cognitive assays did not result in a clear behavioral phenotype even after 16 weeks of transgene induction (**chapter 3**). This may be explained by the fact that intranuclear inclusions are not toxic and that the formation of nuclear inclusions is just a physical epiphenomenon that occurs in the cell simultaneously with the primary pathogenic process. Transfection of cellular models including HeLa, COS7 cells, and neuronal SH-SY5Y cells with a construct that generates FMRpolyG independent of the presence of the expanded CGG-repeat RNA resulted in the formation of inclusions [145]. This suggests that FMRpolyG has either the capabilities or an amino acid domain that may be needed to induce protein aggregate formation. Interestingly, recent *in vitro* experiments found such an amino acid composition domain in the polyglycine stretch [12]. Fluorescence recovery after photobleaching (FRAP) experiments showed that the expanded CGG-repeat RNA quadruplex structure can accelerate protein aggregation formation upon interaction with this domain in the polyglycine stretch in FMRpolyG [12]. The soluble FMRpolyG protein may be toxic for the cell but secondary interactions may mitigate this toxicity by inducing inclusion body formation. Inclusion bodies in HD have been reported to reduce levels of polyQ containing mutant Huntingtin and the risk for neuronal cell death in primary striatal neurons [151]. In a mouse model for SCA1, researchers have demonstrated that overexpression of mutant ataxin-1 protein in cerebellar Purkinje cells resulted in ataxia with the formation of nuclear inclusions [153]. Preventing nuclear inclusion formation in these mice had no phenotypical effects while only preventing mutant ataxin-1 expression mitigated the Purkinje cell pathology and the SCA1 phenotype in these mice [149]. Inclusions observed in FXTAS closely resemble neuronal intranuclear inclusions seen in polyQ diseases and other protein-mediated neurodegenerative disorders therefore allowing careful comparison between findings [154].

These arguments suggest that nuclear inclusions *per se* are not pathogenic. A protective function for the formation of intranuclear inclusions has been proposed.Ubiquitin and

FMRpolyG are known to co-localize in neurons in post-mortem brain tissue of FXTAS patients [21, 73]. A similar observation has been found in our FXTAS mouse models (**chapter 2 and 4,** [23, 33]) and in transfected cells [21, 45]. Previous studies in FXTAS, using *in vitro* and *in vivo* disease model systems, showed that inhibiting the UPS leads to increased neurodegeneration without a clear correlation between neurodegeneration and inclusion formation [24]. Saudou *et al.,* demonstrated that inhibiting ubiquitination of mutant Huntingtin fragments suppressed nuclear inclusion formation but also worsened cellular toxicity [150]. Similarly, in SCA1 mice lacking ubiquitin ligase E6-AP expression resulted in suppression of inclusion formation but enhanced neurodegeneration, arguing a potential guardian role for ubiquitin in the cell [155]. One study reported that the surface coating of nuclear inclusions mainly contains mono-ubiquitin and not poly-ubiquitin which is required for proteasomal degradation by the UPS [156]. Moreover, they showed that mono-ubiquitin is capable of preluding the growth of nuclear inclusions and preventing interactions between toxic proteins in the nuclear inclusions and the cell [156]. Alltogether, these studies suggest that ubiquitin as a component of nuclear inclusions may have protective capacities within nuclear inclusions by concealing the toxic contents of the inclusions and preventing them from interacting and disrupting important cellular mechanisms. Inclusion formation may well be an early active process that continues in the cell aiming to sequester toxic proteins and prevent cell damage. In polyQ mouse models, an inverse correlation has been demonstrated between the formation of inclusions and cellular degeneration or dysfunction [157-160]. In an *in vitro* polyQ model, Arrasate *et al.* demonstrated that neurons that failed to develop inclusions showed an increased risk of death whereas those that developed inclusions survived [151]. Moreover, inclusion formation correlated with a reduction of diffuse mutant Huntingtin in the remainder of the cell, providing a possible mechanistic explanation for enhanced survival of neurons with inclusions. Finally, compelling evidence showed that isolated polyQ fragments, but not isolated inclusions, are capable of inhibiting proteasomal function, further attesting to the protective role of inclusions [275]. We have to be careful with this observation, since often there is a lack of correlation between the neuronal degeneration observed in FXTAS brain and the location of the nuclear inclusions in the brain. For example, in FXTAS, nuclear inclusions are rarely observed in cerebellar Purkinje cells but there is often a substantial drop-out of these cells observed in post-mortem brain tissue from FXTAS patients [28]. It is practically impossible to determine whether neurons that have degenerated formed nuclear inclusions compared with those that survived did not form inclusions. It is important to remember in this context that neuronal degeneration does not necessarily correspond with neuronal dysfunction and that nuclear inclusions are primarily disrupting neuronal function without necessarily causing cell death.

Potential fluid biomarkers for FXTAS

On average, 25-30% of all PM carriers develop FXTAS [161-163]. However, due to the lack of a prognostic biomarker it is currently still unknown if and when a PM carrier will develop FXTAS. Clinical assessments fail to identify which PM carriers are at risk of developing FXTAS before any significant neurological symptoms are presented. The ideal prognostic biomarker should be reliable (*i.e.,* precise), reproducible, detect one major pathological feature and preferably discriminate between different symptomatic condition stages [164]. In addition, the procedure to measure the biomarker should be simple and non-invasive, and be validated in confirmed FXTAS cases [164]. Radiological features of FXTAS include decreased brain volume and bilateral white matter degeneration [165-167]. Neuroimaging using magnetic resonance imaging (MRI) to measure middle cerebellar peduncle (MCP) width or corpus callosum splenium (CCS) hyperintensity on T2-weighted images are proposed as MRI biomarkers for FXTAS [167-173]. Both measurements are observed in approximately 60% of all PM carriers with FXTAS. Unfortunately, both MCP sign and CCS sign are not specific for FXTAS and are seen in other disorders, including sporadic olivopontocerebellar atrophy and SCA [165, 174], and thus cannot be used as reliable prognostic biomarkers for FXTAS. Researchers have reported plasma metabolites and their ratios in serum of PM carriers with and without FXTAS as potential prediction biomarkers [175, 176]. The plasma metabolic ratios of oleamide and isocitrate seemed to discriminate PM carriers with FXTAS from those that do not show FXTAS symptoms [175]. However, plasma metabolites are very sensitive to secondary manipulation of supplement (ab)use including vitamins, minerals, alcohol but also medications that are often prescribed to PM carriers. Thus, plasma metabolites are not very reliable as prognostic biomarkers for FXTAS as well. Therefore, an immediate need for early molecular prediction biomarkers for FXTAS is warranted.

Proteins found within intranuclear inclusions may serve as prognostic and/or diagnostic biomarkers for FXTAS. FMRpolyG-positive intranuclear inclusions contain intermediate filament proteins such as lamin A/C, internexin neuronal intermediate filament protein and the neurofilament (NF) protein encoded by the *NEFL* gene [28]. Neurofilament proteins are part of the neuroaxonal cytoskeleton and play an important role in axonal transport and in the synapses [177]. Increased levels of NF proteins are associated with axonal damage. Neurofilament staining in the granular layer of the cerebellum in post-mortem FXTAS brain tissue showed swollen Purkinje axons (*i.e.,* Purkinje cell axonal torpedoes) [28, 29, 70]. In FXTAS, but also other neurodegenerative disorders [29, 178], neurofilament proteins are proposed to be involved in the regulation of RNA synthesis and processing [179, 180]. Soluble NF proteins are abundantly present in the blood and CSF. Mouse models of neurodegeneration that exhibit tau-, Aβ- or α-synuclein pathology showed increased levels of neurofilament light chain (NfL) protein in their blood and CSF, and coincide with the onset of pathology and progression in the brain [181]. In blood and CSF of FTD patients,

NfL protein levels were increased when compared with healthy control individuals [182-188]. Elevated NfL protein levels correlated with disease severity and progression, survival and cerebellar atrophy in FTD patients [182-188]. In other neurodegenerative disorders including ALS, AD and vascular dementia, similar correlations between the NfL protein and disease progression and onset have been reported [184, 186, 189-192]. These findings for neurofilament proteins in neurodegenerative disorders may suggest that NfL or other neurofilament proteins are potential prognostic biomarkers in FXTAS. In addition, also other proteins involved in FXTAS pathology present within intranuclear inclusions, may serve as potential biomarkers for FXTAS disease onset and/or progression. FMRpolyG and HSP70 were reported to form intracellular complexes *ex vivo* in fibroblasts obtained from one FXTAS patient [193]. HSPs have been found in intranuclear inclusions in FXTAS brain, and overexpression of HSP70 in *Drosophila* resulted in protection from toxicity induced by the expanded CGG-repeat [21, 24]. Elevated HSP70 protein levels have been suggested as marker for cellular defense mechanisms against increased levels of toxic proteins, including FMRpolyG [27]. In this FXTAS patient, researchers reported that the elevated HSP70 levels resulted in complex formation with the toxic FMRpolyG [194]. This observation suggests that HSP70 may be used as biochemical prognostic markers for FXTAS. However, this needs to be validated in more FXTAS patients before any diagnostic and/or prognostic value can be given for the formation of FMRpolyG-HSP70 protein complexes. Longitudinal studies in PM carriers with and without FXTAS are necessary to confirm if neurofilament and HSP70 protein levels correlate with age of onset in FXTAS, disease severity and progression as well as initial symptom development in PM carriers with and without FXTAS.

FMRpolyG is considered as a neuropathological hallmark of FXTAS. Moreover, (over) expression of FMRpolyG in cellular and primary neuron models (**chapter 4**, [21]), *Drosophila* [21] and many mouse models (**chapter 2 and 4**, [23, 33, 38, 92] is reported to be pathogenic and induce cell death. In addition, the presence of FMRpolyG is associated with motor function deficits in mice [23, 147]. FMRpolyG-positive intranuclear inclusions are abundantly present in *in vitro* and *in vivo* disease models as well as in CNS and systemic post-mortem tissue of PM carriers with FXTAS [73]. Also, the number and size of FMRpolyG-positive inclusions in mice increase over time (**chapter 4**, [33]). This suggests a steady expression of FMRpolyG over time and that once FMRpolyG production in the cell exceeds the clearance capacity, FMRpolyG starts to accumulate in inclusions. All these observations propose a potential role for FMRpolyG as biomarker for FXTAS. In *C9ORF72*-linked ALS/FTD, RAN translation of the G_4C_2 expanded repeat results in toxic dipeptides. These dipeptides play a key role in the *C9ORF72*-linked ALS/FTD pathology. One of these dipeptides, the poly-GP dipeptide, is found in peripheral blood mononuclear cells (PBMCs) and cerebrospinal fluid (CSF) of *C9ORF72*-linked ALS/FTD patients as well as in asymptomatic G_4C_2 carriers [195, 196]. These findings suggest a potential role as

biomarker for poly-GP in *C9ORF72*-linked ALS/FTD as well as for other RAN translated proteins in neurodegenerative disorders, including FXTAS [195-197]. However, in FXTAS accurate quantification of FMRpolyG levels is necessary before such a statement can be made. This has not yet been established for FMRpolyG. With the Western blot technique, we are able to quantify soluble FMRpolyG fractions using transfected COS7 cells expressing the expanded CGG-repeat and from mouse brain and liver tissue. Unfortunately, we were not able to quantify soluble FMRpolyG from post-mortem FXTAS brain tissue. Recently, we developed a protein isolation protocol for the dot blot technique that allowed us to quantify both the soluble and insoluble FMRpolyG fraction from in *in vitro* and *in vivo* samples (**chapter 4**), as well as post-mortem FXTAS brain tissue (data not published). Absolute quantification of the soluble and insoluble FMRpolyG protein fraction using the dot blot technique is not possible. The dot blot technique only allows semi-quantification of FMRpolyG. Also, the dot blot technique is not sensitive enough to measure very low protein concentrations, which is necessary before a technique can be used as a potential biomarker in the clinic. Alternatively, an Enzyme-Linked Immunosorbent Assay (ELISA) could be an option to quantify FMRpolyG levels. ELISA is already widely implemented as a diagnostic tool for several neurodegenerative disorders like AD and PD [198, 199]. Relatively small samples are required to detect very low protein concentrations up to the picogram range. We were able to isolate FMRpolyG from transfected COS7 cells expressing the expanded CGG-repeat. We could also isolate FMRpolyG from post-mortem FXTAS brain tissue using high concentrations of urea and subsequent quantification of soluble and insoluble FMRpolyG fractions using our newly developed sandwich-ELISA (**chapter 6**). In the transfected COS7 cells, high concentrations of the soluble FMRpolyG fraction could be detected while relatively low concentrations of the insoluble protein fraction could be measured. Although the COS7 cells were transfected with constructs overexpressing an expanded CGG-repeat, the relative short transfection period in our COS7 cells may explain low insoluble FMRpolyG fractions. In addition, the protein inclusion composition in the cells may contain components that hinder the urea from dissolving the aggregates properly in this specific cellular model. In post-mortem FXTAS brain tissue we observed opposite findings. We were able to measure insoluble FMRpolyG fraction in post-mortem FXTAS brain tissue but no difference could be observed between the soluble protein fraction in our FXTAS patient sample and non-demented control sample (**chapter 6**). An explanation could be that the soluble FMRpolyG fraction in the tissue has been degraded between death and the obduction procedure. Although many FMRpolyG-positive inclusions were immunodetected in FXTAS brain tissue, only low concentrations of insoluble FMRpolyG were detected in post-mortem FXTAS brain tissue using the sandwich-ELISA. Perhaps the concentration of FMRpolyG in inclusions is low. Another explanation could be that the concentration of urea used in the protein isolation procedure may not be strong enough to solubilize the entire inclusion and only affects the outer layer resulting in a fraction of insoluble FMRpolyG becoming available for detection. Also, FMRpolyG co-localizes

with many different proteins in inclusions that could prevent the urea from interacting with FMRpolyG. Importantly, the FXTAS post-mortem brain tissue used in the sandwich-ELISA measurements was obtained from a female donor. Since FXTAS is an X-linked disorder, perhaps the protective effect of the normal *FMR1* allele may reduce FMRpolyG levels in this patient. Immunohistochemical analysis in this patient showed abundant presence of FMRpolyG-positive inclusions, although when compared to male FXTAS post-mortem brain tissue the number of FMRpolyG-positive inclusions was clearly less. To date, we were only able to quantify FMRpolyG levels in one FXTAS patient, however validation in more post-mortem FXTAS brain tissue samples is necessary to confirm our findings. Unfortunately, post-mortem FXTAS brain tissue is very scarce and alternatives should be explored including PBMCs, blood plasma and serum and/or CSF. Non-invasive bio-fluids including PBMCs and blood plasma or serum samples are relatively easy to obtain from PM carriers with and without FXTAS. FMRpolyG might also be present in CSF, but a lumbar puncture procedure is more invasive for patients and should only be considered if FMRpolyG cannot be detected in PBMC or blood plasma/serum samples. Since we are able to measure FMRpolyG levels in very low concentrations in FXTAS patient material, the next step would be to collect PBMC and blood plasma/serum from PM carriers with and without FXTAS and measure FMRpolyG levels. If FMRpolyG can be detected in these samples, this would allow us to further optimize the sandwich-ELISA, as further optimization could be the first step towards a prognostic tool for PM carriers. If we could demonstrate that FMRpolyG levels correlate with age of onset and FXTAS disease progression, and/or with onset of symptoms in PM carriers with FXTAS, FMRpolyG would be an ideal prognostic biomarker for FXTAS. However, we know from *C9ORF72*-linked ALS/FTD that the poly-GP dipeptide does not show any of these correlations [195-197]. In contrast, poly-GP protein levels remain stable in these patients over time, suggesting a potential role as pharmacodynamic biomarker in therapeutic target engagement [195]. Further validation of our sandwich-ELISA may answer the question whether FMRpolyG has potential as prognostic and/or pharmacodynamic biomarker in FXTAS. In addition, the sandwich-ELISA will offer new possibilities in the future development of targeted therapeutic interventions for FXTAS.

Therapeutic interventions

Targeted strategies

As described in this thesis, cellular and animal models (reviewed in **chapter 1**) have contributed significantly to our current understanding of the underlying disease mechanisms for FXTAS. The toxic role of expanded CGG-repeat RNA, RAN translation and subsequent expression of FMRpolyG or a combination of both is undoubtedly contributing to FXTAS pathology. Reliable and fast *in vitro* and *in vivo* drug screening tools

are warranted in the search for targeted therapeutic interventions. We showed for the first time that one of our inducible mouse models can be used as an *in vivo* screening tool for promising expanded CGG-repeat RNA targeting interventions (**chapter 4**). Several strategies to develop a targeted therapeutic intervention can be applied based on our current knowledge of the FXTAS disease mechanisms including: ***i)*** small chemical molecules designed to prevent RAN translation and FMRpolyG expression; ***ii)*** protein replacement therapy compensating for essential proteins found in the inclusions; ***iii)*** targeting the expanded CGG-RNA for degradation and disrupting interactions with RBPs using antisense oligonucleotides (AONs), and; ***iv)*** removing the genomic expanded CGG-repeat using CRISPR-Cas9 technology.

i) Small chemical molecules targeting the expanded CGG-repeat RNA have great potential in ameliorating FXTAS pathology (reviewed in [200]). Microsatellite repeat expansions, including expanded CGG-repeat RNA have the tendency to form hairpin-like and G-quadruplex structures [12, 201-203]. The Matthew Disney lab have developed a small chemical molecule called *1a* that shields the expanded CGG-repeat hairpin by binding the internal GG-mismatches that are formed instead of the entire complementary CGG-repeat sequence [204]. Small molecule *1a* prevents expanded CGG-repeat RNA mediated RAN translation and thus production of FMRpolyG, while leaving *FMR1* mRNA and the downstream translation of the normal ORF unaffected [204]. In *in vitro* experiments, small molecule *1a* can bind to the expanded CGG-repeat motif, disrupted CGG-repeat mediated RAN translation, improved pre-mRNA splicing defects and reduced the size and number of nuclear foci formed containing the expanded CGG-repeat RNA [204]. This rationale has also been shown to work for the G_4C_2 repeat in *C9ORF72*-linked ALS/FTD inhibiting RAN translation and *foci* formation in the cell [197]. Other researchers have obtained similar results targeting the CGG-repeat in FXTAS cellular models [197, 205, 206]. In **chapter 4**, we showed for the first time that treatment with the small chemical molecule *1a* is capable of reducing the number of FMRpolyG-positive inclusions in primary hippocampal cultures. In addition, FMRpolyG levels were reduced both *in vitro* and *in vivo*. Interestingly, *1a* treatment also significantly decreased the number of Rad23b-positive inclusions and Rad23b levels in the mice expressing the expanded CGG-repeat RNA ubiquitously. While the CGG-repeat is prevalent in our genome, most CGG repetitions are in the normal range [207]. Normal range CGG-repeats are less likely to form hairpin or G-quadruplex structures, and consequently have no GG-mismatches. This minimizes the probability of small chemical molecule *1a* binding these genome wide-spread CGG-repeats, potentially resulting in off-target effects. Unfortunately, no behavioral assessment could be made in the hnRNP-driven inducible mouse model because the expression of the transgene is extremely low in the brain. The impact of compound *1a* on behavior should be examined in a brain-specific inducible FXTAS mouse model (**chapter 3**, [33]). Recently, Todd and colleagues published a high-throughput screen [208] to yield new potential small chemical

molecules for the expanded CGG-repeat that we may test *in vivo* using our PM screening mouse models. Altogether, this strategy seems very promising for developing targeted therapeutic interventions in the near future, taking into consideration that toxicity and specificity of these small chemical compounds need to be improved before they can be used in clinical trials.

ii) RNA *foci* and protein aggregates in the cell sequester critical proteins important for normal functional processes in the cell. To date, over thirty proteins have been reported to be present in the intranuclear inclusions [26, 27, 35, 36]. Rescue of the functional protein levels of these target proteins, trapped in these aggregates including Pur-α, DGCR8 and Lap2β, is another potential therapeutic strategy (reviewed in **chapter 1**; [35, 36, 40]). Although overexpression of one of these entrapped proteins seems to reverse toxicity and pathological events in neuronal cultures and animal models, it is highly unlikely that restoring functional protein levels of just one of these proteins in FXTAS patients is sufficient to halt or even reverse the (neuro)pathology. In addition, evidence to restore (neuro)pathology is currently limited to neurons but, for example, we and others showed that FMRpolyG-positive intranuclear inclusions are also present in astroglia and that astroglia may also contribute to motor function pathology (**chapter 2**) [92]. For FXTAS, it is likely that the entrapped proteins of interest have a different basal protein level in different cells and therefore different protein levels may be required in different cell types making implementation of protein replacement therapy extremely complicated. Moreover, to date, there is no safe delivery method for proteins to all required target cells but if this method is established in the future, protein replacement therapy would require lifelong repeated administration with probably very expensive costs.

iii) A more effective approach may be the use of targeted AONs. AONs can be divided in two major categories: RNase H competent AONs and steric blockers, similar to what small chemical molecules do. To ensure medical use, both categories include phosphorothioate (PS) backbone modifications [209]. Modified PS-AONs displayed better binding affinity to the target RNAs. Moreover, PS-modified AONs showed better pharmacological properties, including stability, distribution and tissue delivery, cellular uptake, intracellular trafficking, potency and toxicity (reviewed in [210, 211]). The first category of PS-AONs utilized the RNase H endonuclease, which is an enzyme that recognizes RNA–DNA heteroduplexes that are formed when DNA-based AONs bind to the target mutant RNA transcripts. In normal biology these RNA-DNA heteroduplexes cannot exist and therefore are immediately degraded. This approach has been widely used as a means of downregulating disease-causing or disease-modifying genes [211]. Current RNase H competent AONs follow the 'gapmer' design. A 'gapmer' contains a central block of deoxynucleotides sufficient to recruit RNase H endonuclease and induce cleavage of the mutant RNA:DNA heteroduplex while being flanked by blocks of 2'-*O*-methyl modified ribonucleotides that protect the

internal block from nuclease degradation [212, 213]. Modifications at the 2' position of the sugars enhanced the potency and pharmacokinetic properties of AONs [211]. RNase H-mediated degradation of Huntingtin mRNA in symptomatic HD mouse models delayed disease progression and also mediated sustained reversal of disease phenotype [214]. In a transgenic mouse model for DM1 antisense silencing by the RNase H degradation caused a rapid knockdown of CUG-repeat RNA in skeletal muscle, correcting features of the disease at the physiological, histopathologic and transcriptomic level [215]. In a rat model for ALS caused by a mutation in the *SOD1* gene, researchers have shown that the SOD1 protein can be downregulated using RNase H mediated AONs [216, 217]. Not long after this publication the first phase 1 randomized clinical trial in humans was conducted using an AON specifically targeting the *SOD1* mutation [218]. For SCA two 'gapmer' AONs are currently in pre-clinical development [219, 220]. To date, many RNase H AONs have received regulatory approval by the FDA including Fomivirsen (*i.e.,* targeting the CMV UL123 protein), Mipomersen (*i.e.,* targeting the *APOB* gene) and Inotersen (*i.e.,* targeting the *TTR* gene).

The second strategy uses steric block AONs that are designed to bind to target RNA with high affinity but do not induce target degradation as they lack RNase H endonuclease competence. Steric blocking AONs can mask specific sequences within a target sequence and consequently interfere with RNA–RNA and/or RNA–protein interactions. The most widely used application for blocking AONs is to modulate alternative splicing. Expanded CGG-repeat RNA blocking AONs have shown that it is possible to partially reverse FXTAS-associated splicing defects and also reduce FMRpolyG levels in transfected cells [205, 206]. However, these blocking AONs also block the downstream canonical translation of the ORF of the *FMR1* gene when they bind with the expanded CGG-repeat. This results in lower levels of FMRP; and lack of FMRP is associated with the mental retardation observed in FXS patients (**chapter 1**; [221]). A few examples of steric blocking AONs that are approved by the FDA are Eteplirsen (*i.e.,* blocking *DMD* exon 51), Golodirsen (*i.e.,* blocking *DMD* exon 53) and Nusinersen (*i.e.,* blocking *SMN2* exon 7). One disadvantage of blocking AONs is their specificity for the target sequence. Our genome contains several CGG-rich domains across all chromosomes and in multiple genes, predominantly located near or in promoter and regulatory regions [8, 202, 207]. It is expected that CGG-repeat RNA blocking AONs will target these domains as well, resulting in off-target effects such as inhibiting the downstream translation of the ORF [205]. Moreover, since the expanded CGG-repeat forms stable secondary hairpin and/or G-quadruplex structures, complementary blocking AONs are less likely to efficiently bind these secondary structures [205]. This problem can be circumvented by additional AON modifications such as the 2'-O-methyl (2-OMe)-PS or locked nucleic acids (LNA) modification that improve the thermodynamics and potency of AONs [205, 222]. Another issue concerning all AONs developed to target neurodegenerative disorders is that they cannot cross the blood-brain-barrier (BBB)

and therefore need direct delivery to the CNS. This can be achieved via delivery into the CSF through intracerebroventricular (ICV) or intrathecal (IT) injection or infusion using a compartment that is connected to the ventricles in the brain or spinal cord but these methods are very invasive. Studies have shown that AONs administered via IT injection, the AON is distributed broadly in the CNS and is taken up by the majority of neurons and astrocytes [214, 223-225]. Less invasive methods can be used such as systemic delivery and intranasal administration. Unfortunately, this method of delivery does not result in efficient transfer across the BBB. Although many modified AONs have been proposed to cross the BBB after systemic delivery, including morpholino AONs conjugated with cell penetrating peptides [226, 227], tricyclic modified AONs [228] and nanoparticle delivery of AONs [229], most have shown limited success. Systemic delivery of AONs to the CNS remains a challenge that is largely unresolved [230].

iv) Finally, a promising strategy to overcome the disease-causing effects of the expanded CGG repeat RNA and FMRpolyG, is removal of the expanded CGG-repeat using the genome editing tool named clustered regularly interspaced short palindromic repeat (CRISPR) [231]. CRISPR-associated RNA-guided endonucleases like the CRISPR-associated protein 9 (Cas9) and its variants enable diverse manipulations of genome function [232-234]. The CRISPR-Cas9 system has been used *in vitro* and *in vivo* to correct disease-causing mutations [235-240]. A similar approach has been used in iPSC-derived neurons of FXS patients to reactivate the *FMR1* gene by shortening the expanded CGG-repeat at the 5'-UTR region, partially restoring *FMR1* expression in these neurons [241-243]. Recently, researchers showed that CRISPR-Cas9 treatment of FXS iPSC-derived neurons could restore the electrophysiological abnormalities and that this rescue could be maintained after engraftment of the iPSC-derived neurons into the mouse brain [243]. Although in theory removing the expanded CGG-repeat in cells from PM carrier prevents the formation of the hairpin structure, the sequestration of essential proteins in the cell, RAN translation and the expression of toxic FMRpolyG, this approach is also very controversial in society. It allows researchers and medical doctors not only to cure diseases but also create "perfect organisms". In 2014, the first genetically modified cynomolgus monkey was generated by co-injection of Cas9 mRNA and sgRNAs into one-cell-stage embryos [244]. The first very controversial human study was performed in 2015 using human tripronuclear (3PN) zygotes [245]. The authors claimed they effectively could cleave the endogenous hemoglobin beta (*HBB*) gene but they also reported off-target effects of the Cas9 protein which resulted in unwanted mutations. In 2017, researchers co-injected Cas9 mRNA, gRNAs, and donor DNA into early human 3PN embryos successfully introducing the normal *CCR5*Δ32 allele [246] and in 2018 dr. He Jiankui shocked the world with his claim that he managed to disable the CCR5 gene that enables the HIV infection in two baby twin girls [247, 248]. However, so far, he still did not present complete evidence of this achievement nor is his work independently confirmed or reviewed by other scientists.

The work of He Jiankui raised a public debate regarding whether his study was good or dangerous. Personally, I find it very difficult to judge his work. It could be that He Jiankui just found a way to cure HIV, world's number one infectious disease. But at the same time his work is a precedent for others to alter the genetic profile of human beings with all the known and unknown downsides. I believe that the CRISPR-Cas9 technology should be further optimized in cellular and animal models for efficacy and safety allowing us to better understand its mechanism and capabilities, but at the same time we need strict, clear international regulations and trustworthy controlling authorities. CRISPR-Cas9 as gene-editing tool has already had an impact on medical biology but will definitely change human biology.

Clinical trials

Currently, treatment of FXTAS patients is limited to symptomatic intervention improving the two major clinical symptoms, intention tremors and cerebellar gait ataxia [249-251]. A variety of existing drugs or treatments are currently used to treat FXTAS patients and in a small percentage of patients these treatments show beneficial effects. For example, deep brain stimulation as well as beta-blockers and anti-epileptic drugs like primidone can reduce tremors [13, 71, 252, 253]. Cerebellar gait ataxia can be treated with a variety of drugs, including the most described amantadine [162, 251, 254]. Selective serotonin re-uptake inhibitors can be used to treat depression and/or anxiety, and can stimulate neurogenesis in the aging brain and may therefore be neuroprotective for cognitive decline related to aging [255, 256]. Various other FDA-approved drugs have shown promising results for the minor clinical features in these patients [249, 250, 257]. Although these drugs offer relief for a small number of patients, the need for a targeted treatment is high. The first randomized double-blind placebo-controlled trial for FXTAS in thirty-four FXTAS patients was conducted using memantine [258]. Memantine, a non-competitive N-methyl-D-aspartate (NMDA) receptor antagonist approved by the FDA, has been investigated extensively in animal studies, and its efficacy and safety has been confirmed by clinical trials in humans. Memantine is considered to be a promising neuroprotective drug for the treatment of dementia, especially for AD, since no neuroprotective therapy is currently available for this devasting disease [259]. In addition, memantine is believed to slow down neurodegeneration which can be beneficial for FXTAS patients [259]. Unfortunately, memantine showed no benefits with respect to the selected primary outcome measures (*i.e.,* intention tremor severity and behavioral dyscontrol scale (BDS)) for individuals with FXTAS compared to the placebo treatment group [258]. Also, no improvement could be observed evaluating secondary outcome measures, including postural and writing tremor severity, hand and finger tapping frequency, tests of declarative learning, working memory and executive function [258]. Furthermore, evaluation of participants in the placebo group showed overall low rates of placebo response [260]. Notably, the placebo response (*i.e.,* at least 50% improvement in motor function) is often used for PD where

robust and long-lasting placebo effects are frequently observed [261, 262]. Although the neuropsychiatric profiles in both diseases are different, it may be interesting to include the placebo response measurement for FXTAS patients as well [263].

Two open-label intervention studies showed that weekly treatment with allopregnanolone significantly improved GABAergic-metabolism, oxidative stress and mitochondrial function in PM carriers with FXTAS as well as some clinical features [264-266]. One patient reported improved balance and walking after treatment with allopregnanolone. Also, executive function and episodic memory and learning improved in these patients. Altered GABAergic metabolism has been reported in PM carriers with FXTAS [175, 176, 267] as well as in FXTAS murine models [268]. Improved GABA transmission in the brain could well explain the cognitive improvements seen in these patients when compared to GABA transmission studies performed in mice [269, 270]. Allopregnanolone is a natural neurosteroid that is synthesized from the hormone progesterone [271]. Allopregnanolone may improve cell proliferation and myelination processes in the cell [264]. In addition, reports show that allopregnanolone may exert neuroprotective properties during normal brain development [264, 272] and under pathological conditions as well [273-277]. Allopregnanolone may prevent neuronal degeneration and apoptosis by inhibiting excessive caspase-3 protein expression in neurons [278]. Interestingly, we have observed caspase-3 induced apoptosis in the livers of our hnRNP-driven inducible mice [74]. Surprisingly, in a more recent study using the same inducible mouse model these effects were absent (discussed in **chapter 4**). When interpreting these outcomes, we must be careful before drawing conclusions as this is an open-label study, placebo effects cannot be ruled out. Also, allopregnanolone was not tested on healthy subjects in both open-label studies. Pharmacokinetic effects and clinical adverse events may be ruled out as allopregnanolone is reported to be well tolerated in healthy female individuals however all participants in both studies were male PM carriers with FXTAS [279]. Nevertheless, the outcomes from both open-label studies are promising enough to introduce allopregnanolone for the symptomatic treatment of FXTAS. However, it is advised to first test allopregnanolone in a large cohort of PM carriers with FXTAS in a randomized controlled trial setting with healthy non-PM subjects.

More recently, an open-label pilot clinical trial was conducted using citicoline [280]. Citicoline is an endogenous nucleotide and intermediate in the biosynthesis of structural membrane phospholipids known to inhibit phospholipase A_2. Positive effects from citicoline have been shown in an FXTAS *Drosophila* model [281]. Also, citicoline has shown positive effects in a double-blind placebo-controlled trial for AD where citicoline improved cognition in these participants [282]. In the open-label pilot study citicoline did not improve motor function although worsening is generally expected in these patients. Although a significant improvement in two secondary outcome measures has been observed, *i.e.,* the Beck anxiety inventory (BAI) scores as well as in the Stroop color-word

(SCW) scores, it is complicated how these cognitive improvements should be translated to FXTAS patients. Patients that are recruited for these types of studies may be very nervous and have higher anxiety baselines. Decrease in anxiety can then be explained by the fact that patients over-time became more used to the study settings and increased executive function could be due to a learning effect during the study. A deficit in the Stroop CW test has been shown in male PM carriers without FXTAS [283], however the exact impact of this observation in these patients is yet unclear. Nevertheless, the call for targeted therapeutic interventions rather than symptomatic therapies for FXTAS is absolutely necessary.

Conclusion

FXTAS is a devastating disease caused by an expanded CGG-repeat in the 5'-UTR of the *FMR1* gene. Research described in this thesis shows that RAN translation not only occurs in neurons but also in astroglia, including Bergmann glia. Expression of expanded CGG-repeat RNA in astroglia-specific mouse model results in the formation of FMRpolyG-positive intranuclear inclusions accompanied with motor function impairment (**chapter 2**). Interestingly, in our transgenic mice expressing an expanded CGG-repeat in astroglia, FMRpolyG-positive intranuclear inclusions were also present in neurons providing possible evidence for cell-to-cell propagation of FXTAS neuropathology. In contrast to the disease-causing role of FMRpolyG expression and the presence within intranuclear inclusions, we found that intranuclear inclusions in our brain-specific inducible mouse model might also harbor an early protective function in the cell suggesting prolonged expression is necessary to induce (neuro)pathology in these mice (**chapter 3**). The *CamKII-α* driven brain-specific inducible mice formed FMRpolyG-positive intranuclear inclusions in the hippocampus and striatum but did not show any clear behavioral phenotype associated with these brain regions. More research using cellular and animal models is necessary to better understand the toxic or protective role of FMRpolyG expression and the formation of intranuclear inclusions in the brain. More mechanistic insight in the underlying disease mechanisms is necessary to develop potential targets for future therapeutic interventions and to identify new candidate biomarkers. Here we show that the small chemical molecule *1a* is a promising therapeutic strategy to tackle RAN translation and consequently reduce the number of FMRpolyG-positive inclusions and FMRpolyG protein levels in the cells (**chapter 4**). FMRpolyG-positive inclusions in post-mortem brain tissue can be used to identify unidentified FXTAS cases as we propose in **chapter 5**. Moreover, we developed a sandwich-ELISA that allows us to detect low concentrations of soluble and insoluble FMRpolyG fractions in transfected COS7 cells and post-mortem brain tissue of FXTAS patients (**chapter 6**). Although this proof-of-principle study shows great potential, the next steps would be to measure FMRpolyG levels in PBMCs, blood plasma and/or CSF samples. If this is successful, FMRpolyG may be a potential candidate biomarker to predict

disease onset, monitor disease progression and assess the efficacy of new targeted therapeutic interventions in PM carriers.

References

1. Usdin, K., *The biological effects of simple tandem repeats: lessons from the repeat expansion diseases.* Genome Res, 2008. **18**(7): p. 1011-9.
2. Martindale, J.E., *Diagnosis of Spinocerebellar Ataxias Caused by Trinucleotide Repeat Expansions.* Curr Protoc Hum Genet, 2017. **92**: p. 9 30 1-9 30 22.
3. Brook, J.D., et al., *Molecular basis of myotonic dystrophy: expansion of a trinucleotide (CTG) repeat at the 3' end of a transcript encoding a protein kinase family member.* Cell, 1992. **68**(4): p. 799-808.
4. Mahadevan, M., et al., *Myotonic dystrophy mutation: an unstable CTG repeat in the 3' untranslated region of the gene.* Science, 1992. **255**(5049): p. 1253-5.
5. Liquori, C.L., et al., *Myotonic dystrophy type 2 caused by a CCTG expansion in intron 1 of ZNF9.* Science, 2001. **293**(5531): p. 864-7.
6. DeJesus-Hernandez, M., et al., *Expanded GGGGCC hexanucleotide repeat in noncoding region of C9ORF72 causes chromosome 9p-linked FTD and ALS.* Neuron, 2011. **72**(2): p. 245-56.
7. *A novel gene containing a trinucleotide repeat that is expanded and unstable on Huntington's disease chromosomes. The Huntington's Disease Collaborative Research Group.* Cell, 1993. **72**(6): p. 971-83.
8. Subramanian, S., R.K. Mishra, and L. Singh, *Genome-wide analysis of microsatellite repeats in humans: their abundance and density in specific genomic regions.* Genome Biol, 2003. **4**(2): p. R13.
9. Li, Y.-C., et al., *Microsatellites Within Genes: Structure, Function, and Evolution.* Molecular Biology and Evolution, 2004. **21**(6): p. 991-1007.
10. Tassone, F., et al., *Elevated levels of FMR1 mRNA in carrier males: a new mechanism of involvement in the fragile-X syndrome.* Am J Hum Genet, 2000. **66**(1): p. 6-15.
11. Tassone, F., C. Iwahashi, and P.J. Hagerman, *FMR1 RNA within the intranuclear inclusions of fragile X-associated tremor/ataxia syndrome (FXTAS).* RNA Biol, 2004. **1**(2): p. 103-5.
12. Asamitsu, S., et al., *CGG repeat RNA G-quadruplexes interact with FMRpolyG to cause neuronal dysfunction in fragile X-related tremor/ataxia syndrome.* Sci Adv, 2021. **7**(3).
13. Hagerman, R.J. and P. Hagerman, *Fragile X-associated tremor/ataxia syndrome - features, mechanisms and management.* Nat Rev Neurol, 2016. **12**(7): p. 403-12.
14. Hagerman, R.J., et al., *Intention tremor, parkinsonism, and generalized brain atrophy in male carriers of fragile X.* Neurology, 2001. **57**(1): p. 127-30.
15. Hagerman, R.J., et al., *Fragile X-Associated Neuropsychiatric Disorders (FXAND).* Front Psychiatry, 2018. **9**: p. 564.
16. Ross-Inta, C., et al., *Evidence of mitochondrial dysfunction in fragile X-associated tremor/ataxia syndrome.* Biochem J, 2010. **429**(3): p. 545-52.
17. Napoli, E., et al., *Altered zinc transport disrupts mitochondrial protein processing/import in fragile X-associated tremor/ataxia syndrome.* Hum Mol Genet, 2011. **20**(15): p. 3079-92.
18. Kaplan, E.S., et al., *Early mitochondrial abnormalities in hippocampal neurons cultured from Fmr1 pre-mutation mouse model.* J Neurochem, 2012. **123**(4): p. 613-21.
19. Lin, Y., et al., *Activation of mTOR ameliorates fragile X premutation rCGG repeat-mediated neurodegeneration.* PLoS One, 2013. **8**(4): p. e62572.

20. Loomis, E.W., et al., *Transcription-associated R-loop formation across the human FMR1 CGG-repeat region.* PLoS Genet, 2014. **10**(4): p. e1004294.
21. Todd, P.K., et al., *CGG repeat-associated translation mediates neurodegeneration in fragile X tremor ataxia syndrome.* Neuron, 2013. **78**(3): p. 440-55.
22. Green, K.M., et al., *RAN translation at C9orf72-associated repeat expansions is selectively enhanced by the integrated stress response.* Nat Commun, 2017. **8**(1): p. 2005.
23. Sellier, C., et al., *Translation of Expanded CGG Repeats into FMRpolyG Is Pathogenic and May Contribute to Fragile X Tremor Ataxia Syndrome.* Neuron, 2017. **93**(2): p. 331-347.
24. Oh, S.Y., et al., *RAN translation at CGG repeats induces ubiquitin proteasome system impairment in models of fragile X-associated tremor ataxia syndrome.* Hum Mol Genet, 2015. **24**(15): p. 4317-26.
25. Kenneson, A., et al., *Reduced FMRP and increased FMR1 transcription is proportionally associated with CGG repeat number in intermediate-length and premutation carriers.* Hum Mol Genet, 2001. **10**(14): p. 1449-54.
26. Iwahashi, C. and P.J. Hagerman, *Isolation of pathology-associated intranuclear inclusions.* Methods Mol Biol, 2008. **463**: p. 181-90.
27. Iwahashi, C.K., et al., *Protein composition of the intranuclear inclusions of FXTAS.* Brain, 2006. **129**(Pt 1): p. 256-71.
28. Greco, C.M., et al., *Neuropathology of fragile X-associated tremor/ataxia syndrome (FXTAS).* Brain, 2006. **129**(Pt 1): p. 243-55.
29. Greco, C.M., et al., *Neuronal intranuclear inclusions in a new cerebellar tremor/ataxia syndrome among fragile X carriers.* Brain, 2002. **125**(Pt 8): p. 1760-71.
30. Hagerman, P.J. and R.J. Hagerman, *The fragile-X premutation: a maturing perspective.* Am J Hum Genet, 2004. **74**(5): p. 805-16.
31. Willemsen, R., E. Mientjes, and B.A. Oostra, *FXTAS: a progressive neurologic syndrome associated with Fragile X premutation.* Curr Neurol Neurosci Rep, 2005. **5**(5): p. 405-10.
32. Arocena, D.G., et al., *Induction of inclusion formation and disruption of lamin A/C structure by premutation CGG-repeat RNA in human cultured neural cells.* Human Molecular Genetics, 2005. **14**(23): p. 3661-3671.
33. Hukema, R.K., et al., *Reversibility of neuropathology and motor deficits in an inducible mouse model for FXTAS.* Hum Mol Genet, 2015. **24**(17): p. 4948-57.
34. Jin, P., et al., *RNA-mediated neurodegeneration caused by the fragile X premutation rCGG repeats in Drosophila.* Neuron, 2003. **39**(5): p. 739-47.
35. Sellier, C., et al., *Sequestration of DROSHA and DGCR8 by expanded CGG RNA repeats alters microRNA processing in fragile X-associated tremor/ataxia syndrome.* Cell Rep, 2013. **3**(3): p. 869-80.
36. Sellier, C., et al., *Sam68 sequestration and partial loss of function are associated with splicing alterations in FXTAS patients.* EMBO J, 2010. **29**(7): p. 1248-61.
37. Krzyzosiak, W.J., et al., *Triplet repeat RNA structure and its role as pathogenic agent and therapeutic target.* Nucleic Acids Res, 2012. **40**(1): p. 11-26.
38. Haify, S.N., et al., *In silico, in vitro, and in vivo Approaches to Identify Molecular Players in Fragile X Tremor and Ataxia Syndrome.* Front Mol Biosci, 2020. **7**: p. 31.

39. Sofola, O.A., et al., *RNA-binding proteins hnRNP A2/B1 and CUGBP1 suppress fragile X CGG premutation repeat-induced neurodegeneration in a Drosophila model of FXTAS.* Neuron, 2007. **55**(4): p. 565-71.
40. Jin, P., et al., *Pur alpha binds to rCGG repeats and modulates repeat-mediated neurodegeneration in a Drosophila model of fragile X tremor/ataxia syndrome.* Neuron, 2007. **55**(4): p. 556-64.
41. He, F., et al., *TDP-43 suppresses CGG repeat-induced neurotoxicity through interactions with HnRNP A2/B1.* Hum Mol Genet, 2014. **23**(19): p. 5036-51.
42. Barreau, C., et al., *Mammalian CELF/Bruno-like RNA-binding proteins: molecular characteristics and biological functions.* Biochimie, 2006. **88**(5): p. 515-25.
43. Qurashi, A., et al., *Nuclear accumulation of stress response mRNAs contributes to the neurodegeneration caused by Fragile X premutation rCGG repeats.* PLoS Genet, 2011. **7**(6): p. e1002102.
44. Zu, T., et al., *Non-ATG-initiated translation directed by microsatellite expansions.* Proc Natl Acad Sci U S A, 2011. **108**(1): p. 260-5.
45. Krans, A., et al., *Neuropathology of RAN translation proteins in fragile X-associated tremor/ataxia syndrome.* Acta Neuropathol Commun, 2019. **7**(1): p. 152.
46. Kearse, M.G., et al., *CGG Repeat-Associated Non-AUG Translation Utilizes a Cap-Dependent Scanning Mechanism of Initiation to Produce Toxic Proteins.* Mol Cell, 2016. **62**(2): p. 314-322.
47. Ladd, P.D., et al., *An antisense transcript spanning the CGG repeat region of FMR1 is upregulated in premutation carriers but silenced in full mutation individuals.* Hum Mol Genet, 2007. **16**(24): p. 3174-87.
48. Krans, A., M.G. Kearse, and P.K. Todd, *Repeat-associated non-AUG translation from antisense CCG repeats in fragile X tremor/ataxia syndrome.* Ann Neurol, 2016. **80**(6): p. 871-881.
49. Cho, D.H., et al., *Antisense transcription and heterochromatin at the DM1 CTG repeats are constrained by CTCF.* Mol Cell, 2005. **20**(3): p. 483-9.
50. Moseley, M.L., et al., *Bidirectional expression of CUG and CAG expansion transcripts and intranuclear polyglutamine inclusions in spinocerebellar ataxia type 8.* Nat Genet, 2006. **38**(7): p. 758-69.
51. Abu-Baker, A., et al., *Involvement of the ubiquitin-proteasome pathway and molecular chaperones in oculopharyngeal muscular dystrophy.* Hum Mol Genet, 2003. **12**(20): p. 2609-23.
52. Albrecht, A.N., et al., *A molecular pathogenesis for transcription factor associated poly-alanine tract expansions.* Hum Mol Genet, 2004. **13**(20): p. 2351-9.
53. Mizielinska, S., et al., *C9orf72 repeat expansions cause neurodegeneration in Drosophila through arginine-rich proteins.* Science, 2014. **345**(6201): p. 1192-1194.
54. Kwon, I., et al., *Poly-dipeptides encoded by the C9orf72 repeats bind nucleoli, impede RNA biogenesis, and kill cells.* Science, 2014. **345**(6201): p. 1139-45.
55. Wen, X., et al., *Antisense proline-arginine RAN dipeptides linked to C9ORF72-ALS/FTD form toxic nuclear aggregates that initiate in vitro and in vivo neuronal death.* Neuron, 2014. **84**(6): p. 1213-25.
56. Yamakawa, M., et al., *Characterization of the dipeptide repeat protein in the molecular pathogenesis of c9FTD/ALS.* Hum Mol Genet, 2015. **24**(6): p. 1630-45.
57. Tao, Z., et al., *Nucleolar stress and impaired stress granule formation contribute to C9orf72 RAN translation-induced cytotoxicity.* Hum Mol Genet, 2015. **24**(9): p. 2426-41.

58. Kanekura, K., et al., *Poly-dipeptides encoded by the C9ORF72 repeats block global protein translation.* Hum Mol Genet, 2016. **25**(9): p. 1803-13.
59. Lee, K.H., et al., *C9orf72 Dipeptide Repeats Impair the Assembly, Dynamics, and Function of Membrane-Less Organelles.* Cell, 2016. **167**(3): p. 774-788 e17.
60. Yang, D., et al., *FTD/ALS-associated poly(GR) protein impairs the Notch pathway and is recruited by poly(GA) into cytoplasmic inclusions.* Acta Neuropathol, 2015. **130**(4): p. 525-35.
61. Freibaum, B.D., et al., *GGGGCC repeat expansion in C9orf72 compromises nucleocytoplasmic transport.* Nature, 2015. **525**(7567): p. 129-133.
62. Boeynaems, S., et al., *Drosophila screen connects nuclear transport genes to DPR pathology in c9ALS/FTD.* Sci Rep, 2016. **6**: p. 20877.
63. Swaminathan, A., et al., *Expression of C9orf72-related dipeptides impairs motor function in a vertebrate model.* Hum Mol Genet, 2018. **27**(10): p. 1754-1762.
64. Lopez-Gonzalez, R., et al., *Poly(GR) in C9ORF72-Related ALS/FTD Compromises Mitochondrial Function and Increases Oxidative Stress and DNA Damage in iPSC-Derived Motor Neurons.* Neuron, 2016. **92**(2): p. 383-391.
65. Shi, K.Y., et al., *Toxic PRn poly-dipeptides encoded by the C9orf72 repeat expansion block nuclear import and export.* Proc Natl Acad Sci U S A, 2017. **114**(7): p. E1111-E1117.
66. Gupta, R., et al., *The Proline/Arginine Dipeptide from Hexanucleotide Repeat Expanded C9ORF72 Inhibits the Proteasome.* 2017. **4**(1): p. ENEURO.0249-16.2017.
67. Meloni, B.P., et al., *Poly-arginine and arginine-rich peptides are neuroprotective in stroke models.* J Cereb Blood Flow Metab, 2015. **35**(6): p. 993-1004.
68. Dehay, B. and A. Bertolotti, *Critical role of the proline-rich region in Huntingtin for aggregation and cytotoxicity in yeast.* J Biol Chem, 2006. **281**(47): p. 35608-15.
69. Siwach, P., et al., *Proline repeats, in cis- and trans-positions, confer protection against the toxicity of misfolded proteins in a mammalian cellular model.* Neurosci Res, 2011. **70**(4): p. 435-41.
70. Berry-Kravis, E., et al., *Fragile X-associated tremor/ataxia syndrome: clinical features, genetics, and testing guidelines.* Mov Disord, 2007. **22**(14): p. 2018-30, quiz 2140.
71. Leehey, M.A., *Fragile X-associated tremor/ataxia syndrome: clinical phenotype, diagnosis, and treatment.* J Investig Med, 2009. **57**(8): p. 830-6.
72. Tassone, F., et al., *Neuropathological, clinical and molecular pathology in female fragile X premutation carriers with and without FXTAS.* Genes Brain Behav, 2012. **11**(5): p. 577-85.
73. Buijsen, R.A.M., et al., *FMRpolyG-positive inclusions in CNS and non-CNS organs of a fragile X premutation carrier with fragile X-associated tremor/ataxia syndrome.* Acta Neuropathologica Communications, 2014. **2**(1): p. 162.
74. Hukema, R.K., et al., *Induced expression of expanded CGG RNA causes mitochondrial dysfunction in vivo.* Cell Cycle, 2014. **13**(16): p. 2600-8.
75. Kamm, C., et al., *The fragile X tremor ataxia syndrome in the differential diagnosis of multiple system atrophy: data from the EMSA Study Group.* Brain, 2005. **128**(Pt 8): p. 1855-60.
76. Biancalana, V., et al., *FMR1 premutations associated with fragile X-associated tremor/ataxia syndrome in multiple system atrophy.* Arch Neurol, 2005. **62**(6): p. 962-6.

77. Nagele, R.G., et al., *Astrocytes accumulate A beta 42 and give rise to astrocytic amyloid plaques in Alzheimer disease brains.* Brain Res, 2003. **971**(2): p. 197-209.
78. Olabarria, M., et al., *Concomitant astroglial atrophy and astrogliosis in a triple transgenic animal model of Alzheimer's disease.* Glia, 2010. **58**(7): p. 831-8.
79. Simpson, J.E., et al., *Astrocyte phenotype in relation to Alzheimer-type pathology in the ageing brain.* Neurobiol Aging, 2010. **31**(4): p. 578-90.
80. Shin, J.Y., et al., *Expression of mutant huntingtin in glial cells contributes to neuronal excitotoxicity.* J Cell Biol, 2005. **171**(6): p. 1001-12.
81. Bradford, J., et al., *Expression of mutant huntingtin in mouse brain astrocytes causes age-dependent neurological symptoms.* Proc Natl Acad Sci U S A, 2009. **106**(52): p. 22480-5.
82. Bradford, J., et al., *Mutant huntingtin in glial cells exacerbates neurological symptoms of Huntington disease mice.* J Biol Chem, 2010. **285**(14): p. 10653-61.
83. Halliday, G.M. and C.H. Stevens, *Glia: initiators and progressors of pathology in Parkinson's disease.* Mov Disord, 2011. **26**(1): p. 6-17.
84. Bruijn, L.I., et al., *ALS-linked SOD1 mutant G85R mediates damage to astrocytes and promotes rapidly progressive disease with SOD1-containing inclusions.* Neuron, 1997. **18**(2): p. 327-38.
85. Zhang, H., et al., *TDP-43-immunoreactive neuronal and glial inclusions in the neostriatum in amyotrophic lateral sclerosis with and without dementia.* Acta Neuropathol, 2008. **115**(1): p. 115-22.
86. Forsberg, K., et al., *Glial nuclear aggregates of superoxide dismutase-1 are regularly present in patients with amyotrophic lateral sclerosis.* Acta Neuropathol, 2011. **121**(5): p. 623-34.
87. Chung, W.S. and B.A. Barres, *The role of glial cells in synapse elimination.* Curr Opin Neurobiol, 2012. **22**(3): p. 438-45.
88. Wagner, B., et al., *Neuronal survival depends on EGFR signaling in cortical but not midbrain astrocytes.* EMBO J, 2006. **25**(4): p. 752-62.
89. Brenner, M., et al., *Mutations in GFAP, encoding glial fibrillary acidic protein, are associated with Alexander disease.* Nat Genet, 2001. **27**(1): p. 117-20.
90. Li, R., et al., *Glial fibrillary acidic protein mutations in infantile, juvenile, and adult forms of Alexander disease.* Ann Neurol, 2005. **57**(3): p. 310-26.
91. Quinlan, R.A., et al., *GFAP and its role in Alexander disease.* Exp Cell Res, 2007. **313**(10): p. 2077-87.
92. Wenzel, H.J., et al., *Astroglial-targeted expression of the fragile X CGG repeat premutation in mice yields RAN translation, motor deficits and possible evidence for cell-to-cell propagation of FXTAS pathology.* Acta Neuropathol Commun, 2019. **7**(1): p. 27.
93. Wenzel, H.J., et al., *Ubiquitin-positive intranuclear inclusions in neuronal and glial cells in a mouse model of the fragile X premutation.* Brain Res, 2010. **1318**: p. 155-66.
94. Tydlacka, S., et al., *Differential activities of the ubiquitin-proteasome system in neurons versus glia may account for the preferential accumulation of misfolded proteins in neurons.* J Neurosci, 2008. **28**(49): p. 13285-95.
95. Willemsen, R., et al., *The FMR1 CGG repeat mouse displays ubiquitin-positive intranuclear neuronal inclusions; implications for the cerebellar tremor/ataxia syndrome.* Hum Mol Genet, 2003. **12**(9): p. 949-59.

96. Bergink, S., et al., *The DNA repair-ubiquitin-associated HR23 proteins are constituents of neuronal inclusions in specific neurodegenerative disorders without hampering DNA repair.* Neurobiol Dis, 2006. **23**(3): p. 708-16.
97. Hashem, V., et al., *Ectopic expression of CGG containing mRNA is neurotoxic in mammals.* Hum Mol Genet, 2009. **18**(13): p. 2443-51.
98. Riemslagh, F.W., et al., *HR23B pathology preferentially co-localizes with p62, pTDP-43 and poly-GA in C9ORF72-linked frontotemporal dementia and amyotrophic lateral sclerosis.* Acta Neuropathol Commun, 2019. **7**(1): p. 39.
99. Bertolaet, B.L., et al., *UBA domains of DNA damage-inducible proteins interact with ubiquitin.* Nat Struct Biol, 2001. **8**(5): p. 417-22.
100. Chen, L., et al., *Ubiquitin-associated (UBA) domains in Rad23 bind ubiquitin and promote inhibition of multi-ubiquitin chain assembly.* EMBO Rep, 2001. **2**(10): p. 933-8.
101. Wade, S.L. and D.T. Auble, *The Rad23 ubiquitin receptor, the proteasome and functional specificity in transcriptional control.* Transcription, 2010. **1**(1): p. 22-6.
102. Doss-Pepe, E.W., et al., *Ataxin-3 interactions with rad23 and valosin-containing protein and its associations with ubiquitin chains and the proteasome are consistent with a role in ubiquitin-mediated proteolysis.* Mol Cell Biol, 2003. **23**(18): p. 6469-83.
103. Liang, R.Y., et al., *Rad23 interaction with the proteasome is regulated by phosphorylation of its ubiquitin-like (UbL) domain.* J Mol Biol, 2014. **426**(24): p. 4049-4060.
104. Glickman, M.H. and A. Ciechanover, *The ubiquitin-proteasome proteolytic pathway: destruction for the sake of construction.* Physiol Rev, 2002. **82**(2): p. 373-428.
105. Okuda, Y., et al., *Relative levels of the two mammalian Rad23 homologs determine composition and stability of the xeroderma pigmentosum group C protein complex.* DNA Repair (Amst), 2004. **3**(10): p. 1285-95.
106. Robin, G., et al., *Calcium dysregulation and Cdk5-ATM pathway involved in a mouse model of fragile X-associated tremor/ataxia syndrome.* Hum Mol Genet, 2017. **26**(14): p. 2649-2666.
107. Ma, L., et al., *Composition of the Intranuclear Inclusions of Fragile X-associated Tremor/Ataxia Syndrome.* Acta Neuropathol Commun, 2019. **7**(1): p. 143.
108. Dubinska-Magiera, M., et al., *Xenopus LAP2beta protein knockdown affects location of lamin B and nucleoporins and has effect on assembly of cell nucleus and cell viability.* Protoplasma, 2016. **253**(3): p. 943-956.
109. Zhang, K., et al., *The C9orf72 repeat expansion disrupts nucleocytoplasmic transport.* Nature, 2015. **525**(7567): p. 56-61.
110. Gasset-Rosa, F., et al., *Polyglutamine-Expanded Huntingtin Exacerbates Age-Related Disruption of Nuclear Integrity and Nucleocytoplasmic Transport.* Neuron, 2017. **94**(1): p. 48-57 e4.
111. Etherton, M.R., et al., *Mouse neurexin-1alpha deletion causes correlated electrophysiological and behavioral changes consistent with cognitive impairments.* Proc Natl Acad Sci U S A, 2009. **106**(42): p. 17998-8003.
112. Kwon, C.H., et al., *Pten regulates neuronal arborization and social interaction in mice.* Neuron, 2006. **50**(3): p. 377-88.

113. Nakatani, J., et al., *Abnormal behavior in a chromosome-engineered mouse model for human 15q11-13 duplication seen in autism.* Cell, 2009. **137**(7): p. 1235-46.
114. Chadman, K.K., et al., *Minimal aberrant behavioral phenotypes of neuroligin-3 R451C knockin mice.* Autism Res, 2008. **1**(3): p. 147-58.
115. Tabuchi, K., et al., *A neuroligin-3 mutation implicated in autism increases inhibitory synaptic transmission in mice.* Science, 2007. **318**(5847): p. 71-6.
116. Rothwell, P.E., et al., *Autism-associated neuroligin-3 mutations commonly impair striatal circuits to boost repetitive behaviors.* Cell, 2014. **158**(1): p. 198-212.
117. Su, M., et al., *Expression specificity of GFAP transgenes.* Neurochem Res, 2004. **29**(11): p. 2075-93.
118. Eng, L.F. and R.S. Ghirnikar, *GFAP and astrogliosis.* Brain Pathol, 1994. **4**(3): p. 229-37.
119. McLendon, R.E. and D.D. Bigner, *Immunohistochemistry of the glial fibrillary acidic protein: basic and applied considerations.* Brain Pathol, 1994. **4**(3): p. 221-8.
120. Kriegstein, A.R. and M. Gotz, *Radial glia diversity: a matter of cell fate.* Glia, 2003. **43**(1): p. 37-43.
121. Miyata, T., et al., *Asymmetric inheritance of radial glial fibers by cortical neurons.* Neuron, 2001. **31**(5): p. 727-41.
122. Noctor, S.C., et al., *Dividing precursor cells of the embryonic cortical ventricular zone have morphological and molecular characteristics of radial glia.* J Neurosci, 2002. **22**(8): p. 3161-73.
123. Malatesta, P., E. Hartfuss, and M. Gotz, *Isolation of radial glial cells by fluorescent-activated cell sorting reveals a neuronal lineage.* Development, 2000. **127**(24): p. 5253-63.
124. Anthony, T.E., et al., *Radial glia serve as neuronal progenitors in all regions of the central nervous system.* Neuron, 2004. **41**(6): p. 881-90.
125. Malatesta, P., et al., *Neuronal or glial progeny: regional differences in radial glia fate.* Neuron, 2003. **37**(5): p. 751-64.
126. Casper, K.B. and K.D. McCarthy, *GFAP-positive progenitor cells produce neurons and oligodendrocytes throughout the CNS.* Mol Cell Neurosci, 2006. **31**(4): p. 676-84.
127. Westergard, T., et al., *Cell-to-Cell Transmission of Dipeptide Repeat Proteins Linked to C9orf72-ALS/FTD.* Cell Rep, 2016. **17**(3): p. 645-652.
128. Zhang, X., et al., *Potential Transfer of Polyglutamine and CAG-Repeat RNA in Extracellular Vesicles in Huntington's Disease: Background and Evaluation in Cell Culture.* Cell Mol Neurobiol, 2016. **36**(3): p. 459-70.
129. Loria, F., et al., *alpha-Synuclein transfer between neurons and astrocytes indicates that astrocytes play a role in degradation rather than in spreading.* Acta Neuropathol, 2017. **134**(5): p. 789-808.
130. Desplats, P., et al., *Inclusion formation and neuronal cell death through neuron-to-neuron transmission of alpha-synuclein.* Proc Natl Acad Sci U S A, 2009. **106**(31): p. 13010-5.
131. Garden, G.A. and A.R. La Spada, *Intercellular (mis)communication in neurodegenerative disease.* Neuron, 2012. **73**(5): p. 886-901.
132. Costanzo, M., et al., *Transfer of polyglutamine aggregates in neuronal cells occurs in tunneling nanotubes.* J Cell Sci, 2013. **126**(Pt 16): p. 3678-85.
133. Peng, C., J.Q. Trojanowski, and V.M. Lee, *Protein transmission in neurodegenerative disease.* Nat Rev Neurol, 2020. **16**(4): p. 199-212.

134. Feiler, M.S., et al., *TDP-43 is intercellularly transmitted across axon terminals.* J Cell Biol, 2015. **211**(4): p. 897-911.
135. Gallegos, S., et al., *Features of alpha-synuclein that could explain the progression and irreversibility of Parkinson's disease.* Front Neurosci, 2015. **9**: p. 59.
136. Kanouchi, T., T. Ohkubo, and T. Yokota, *Can regional spreading of amyotrophic lateral sclerosis motor symptoms be explained by prion-like propagation?* J Neurol Neurosurg Psychiatry, 2012. **83**(7): p. 739-45.
137. Nath, S., et al., *Spreading of neurodegenerative pathology via neuron-to-neuron transmission of beta-amyloid.* J Neurosci, 2012. **32**(26): p. 8767-77.
138. Ren, P.H., et al., *Cytoplasmic penetration and persistent infection of mammalian cells by polyglutamine aggregates.* Nat Cell Biol, 2009. **11**(2): p. 219-25.
139. Silverman, J.M., et al., *Disease Mechanisms in ALS: Misfolded SOD1 Transferred Through Exosome-Dependent and Exosome-Independent Pathways.* Cell Mol Neurobiol, 2016. **36**(3): p. 377-81.
140. Bellingham, S.A., et al., *Exosomes: vehicles for the transfer of toxic proteins associated with neurodegenerative diseases?* Front Physiol, 2012. **3**: p. 124.
141. Danzer, K.M., et al., *Exosomal cell-to-cell transmission of alpha synuclein oligomers.* Mol Neurodegener, 2012. **7**: p. 42.
142. Costanzo, M. and C. Zurzolo, *The cell biology of prion-like spread of protein aggregates: mechanisms and implication in neurodegeneration.* Biochem J, 2013. **452**(1): p. 1-17.
143. Yoshida, A., et al., *Morphological changes of plasma membrane and protein assembly during clathrin-mediated endocytosis.* PLoS Biol, 2018. **16**(5): p. e2004786.
144. Alberts, P., et al., *Cdc42 and actin control polarized expression of TI-VAMP vesicles to neuronal growth cones and their fusion with the plasma membrane.* Mol Biol Cell, 2006. **17**(3): p. 1194-203.
145. Hoem, G., et al., *The FMRpolyGlycine Protein Mediates Aggregate Formation and Toxicity Independent of the CGG mRNA Hairpin in a Cellular Model for FXTAS.* Front Genet, 2019. **10**: p. 249.
146. Glineburg, M.R., et al., *Repeat-associated non-AUG (RAN) translation and other molecular mechanisms in Fragile X Tremor Ataxia Syndrome.* Brain Res, 2018. **1693**(Pt A): p. 43-54.
147. Van Dam, D., et al., *Cognitive decline, neuromotor and behavioural disturbances in a mouse model for fragile-X-associated tremor/ataxia syndrome (FXTAS).* Behav Brain Res, 2005. **162**(2): p. 233-9.
148. Hunsaker, M.R., et al., *Progressive spatial processing deficits in a mouse model of the fragile X premutation.* Behav Neurosci, 2009. **123**(6): p. 1315-24.
149. Klement, I.A., et al., *Ataxin-1 nuclear localization and aggregation: role in polyglutamine-induced disease in SCA1 transgenic mice.* Cell, 1998. **95**(1): p. 41-53.
150. Saudou, F., et al., *Huntingtin acts in the nucleus to induce apoptosis but death does not correlate with the formation of intranuclear inclusions.* Cell, 1998. **95**(1): p. 55-66.
151. Arrasate, M., et al., *Inclusion body formation reduces levels of mutant huntingtin and the risk of neuronal death.* Nature, 2004. **431**(7010): p. 805-10.
152. Wang, X., et al., *Distribution of CaMKIIα expression in the brain in vivo, studied by CaMKIIα-GFP mice.* Brain Research, 2013. **1518**: p. 9-25.

153. Clark, H.B. and H.T. Orr, *Spinocerebellar ataxia type 1--modeling the pathogenesis of a polyglutamine neurodegenerative disorder in transgenic mice.* J Neuropathol Exp Neurol, 2000. **59**(4): p. 265-70.
154. Williams, A.J. and H.L. Paulson, *Polyglutamine neurodegeneration: protein misfolding revisited.* Trends Neurosci, 2008. **31**(10): p. 521-8.
155. Cummings, C.J., et al., *Mutation of the E6-AP ubiquitin ligase reduces nuclear inclusion frequency while accelerating polyglutamine-induced pathology in SCA1 mice.* Neuron, 1999. **24**(4): p. 879-92.
156. Gray, D.A., *Damage control--a possible non-proteolytic role for ubiquitin in limiting neurodegeneration.* Neuropathol Appl Neurobiol, 2001. **27**(2): p. 89-94.
157. Yoo, S.Y., et al., *SCA7 knockin mice model human SCA7 and reveal gradual accumulation of mutant ataxin-7 in neurons and abnormalities in short-term plasticity.* Neuron, 2003. **37**(3): p. 383-401.
158. Bowman, A.B., et al., *Neuronal dysfunction in a polyglutamine disease model occurs in the absence of ubiquitin-proteasome system impairment and inversely correlates with the degree of nuclear inclusion formation.* Hum Mol Genet, 2005. **14**(5): p. 679-91.
159. Watase, K., et al., *A long CAG repeat in the mouse Sca1 locus replicates SCA1 features and reveals the impact of protein solubility on selective neurodegeneration.* Neuron, 2002. **34**(6): p. 905-19.
160. Slow, E.J., et al., *Absence of behavioral abnormalities and neurodegeneration in vivo despite widespread neuronal huntingtin inclusions.* Proc Natl Acad Sci U S A, 2005. **102**(32): p. 11402-7.
161. Rodriguez-Revenga, L., et al., *Penetrance of FMR1 premutation associated pathologies in fragile X syndrome families.* Eur J Hum Genet, 2009. **17**(10): p. 1359-62.
162. Jacquemont, S., et al., *Aging in individuals with the FMR1 mutation.* Am J Ment Retard, 2004. **109**(2): p. 154-64.
163. Hunter, J., et al., *Epidemiology of fragile X syndrome: a systematic review and meta-analysis.* Am J Med Genet A, 2014. **164A**(7): p. 1648-58.
164. Group, T.R.a.N.R.R.I.o.t.A.s.A.a.t.N.I.o.A.W., *Consensus report of the Working Group on: "Molecular and Biochemical Markers of Alzheimer's Disease".* . Neurobiol Aging, 1998. **19**(2): p. 109-16.
165. Brunberg, J.A., et al., *Fragile X premutation carriers: characteristic MR imaging findings of adult male patients with progressive cerebellar and cognitive dysfunction.* AJNR Am J Neuroradiol, 2002. **23**(10): p. 1757-66.
166. Jacquemont, S., et al., *Fragile X premutation tremor/ataxia syndrome: molecular, clinical, and neuroimaging correlates.* Am J Hum Genet, 2003. **72**(4): p. 869-78.
167. Cohen, S., et al., *Molecular and imaging correlates of the fragile X-associated tremor/ataxia syndrome.* Neurology, 2006. **67**(8): p. 1426-31.
168. Shelton, A.L., et al., *Middle Cerebellar Peduncle Width-A Novel MRI Biomarker for FXTAS?* Front Neurosci, 2018. **12**: p. 379.
169. Hashimoto, R., et al., *A voxel-based morphometry study of grey matter loss in fragile X-associated tremor/ataxia syndrome.* Brain, 2011. **134**(Pt 3): p. 863-78.
170. Rivera, S., G. Stebbins, and J. Grigsby, *Radiological findings in FXTAS*. 2010. p. 55-66.
171. Apartis, E., et al., *FXTAS: new insights and the need for revised diagnostic criteria.* Neurology, 2012. **79**(18): p. 1898-907.

172. Famula, J.L., et al., *Presence of Middle Cerebellar Peduncle Sign in FMR1 Premutation Carriers Without Tremor and Ataxia.* Front Neurol, 2018. **9**: p. 695.
173. Hall, D.A., et al., *The Corpus Callosum Splenium Sign in Fragile X-Associated Tremor Ataxia Syndrome.* Mov Disord Clin Pract, 2017. **4**(3): p. 383-388.
174. Quattrone, A., et al., *MR parkinsonism index predicts vertical supranuclear gaze palsy in patients with PSP-parkinsonism.* Neurology, 2016. **87**(12): p. 1266-73.
175. Giulivi, C., et al., *Plasma Biomarkers for Monitoring Brain Pathophysiology in FMR1 Premutation Carriers.* Front Mol Neurosci, 2016. **9**: p. 71.
176. Giulivi, C., et al., *Plasma metabolic profile delineates roles for neurodegeneration, pro-inflammatory damage and mitochondrial dysfunction in the FMR1 premutation.* Biochem J, 2016. **473**(21): p. 3871-3888.
177. Yuan, A., et al., *Neurofilament subunits are integral components of synapses and modulate neurotransmission and behavior in vivo.* Molecular Psychiatry, 2015. **20**(8): p. 986-994.
178. Omary, M.B., P.A. Coulombe, and W.H. McLean, *Intermediate filament proteins and their associated diseases.* N Engl J Med, 2004. **351**(20): p. 2087-100.
179. Zastrow, M.S., S. Vlcek, and K.L. Wilson, *Proteins that bind A-type lamins: integrating isolated clues.* J Cell Sci, 2004. **117**(Pt 7): p. 979-87.
180. Hutchison, C.J. and H.J. Worman, *A-type lamins: guardians of the soma?* Nat Cell Biol, 2004. **6**(11): p. 1062-7.
181. Bacioglu, M., et al., *Neurofilament Light Chain in Blood and CSF as Marker of Disease Progression in Mouse Models and in Neurodegenerative Diseases.* Neuron, 2016. **91**(1): p. 56-66.
182. Meeter, L.H., et al., *Neurofilament light chain: a biomarker for genetic frontotemporal dementia.* Ann Clin Transl Neurol, 2016. **3**(8): p. 623-36.
183. Pijnenburg, Y.A., et al., *Discriminative and prognostic potential of cerebrospinal fluid phosphoTau/tau ratio and neurofilaments for frontotemporal dementia subtypes.* Alzheimers Dement (Amst), 2015. **1**(4): p. 505-12.
184. Scherling, C.S., et al., *Cerebrospinal fluid neurofilament concentration reflects disease severity in frontotemporal degeneration.* Ann Neurol, 2014. **75**(1): p. 116-26.
185. Rohrer, J.D., et al., *Serum neurofilament light chain protein is a measure of disease intensity in frontotemporal dementia.* Neurology, 2016. **87**(13): p. 1329-36.
186. Skillback, T., et al., *CSF neurofilament light differs in neurodegenerative diseases and predicts severity and survival.* Neurology, 2014. **83**(21): p. 1945-53.
187. Landqvist Waldo, M., et al., *Cerebrospinal fluid neurofilament light chain protein levels in subtypes of frontotemporal dementia.* BMC Neurol, 2013. **13**: p. 54.
188. Wilke, C., et al., *Neurofilament light chain in FTD is elevated not only in cerebrospinal fluid, but also in serum.* 2016. **87**(11): p. 1270-1272.
189. Khalil, M., et al., *Neurofilaments as biomarkers in neurological disorders.* Nat Rev Neurol, 2018. **14**(10): p. 577-589.
190. Hansson, O., et al., *Blood-based NfL: A biomarker for differential diagnosis of parkinsonian disorder.* Neurology, 2017. **88**(10): p. 930-937.

191. Rojas, J.C., et al., *Plasma neurofilament light chain predicts progression in progressive supranuclear palsy.* 2016. **3**(3): p. 216-225.
192. Lu, C.H., et al., *Neurofilament light chain: A prognostic biomarker in amyotrophic lateral sclerosis.* Neurology, 2015. **84**(22): p. 2247-57.
193. Bonapace, G., et al., *Intracellular FMRpolyG-Hsp70 complex in fibroblast cells from a patient affected by fragile X tremor ataxia syndrome.* Heliyon, 2019. **5**(6): p. e01954.
194. Bonapace, G., et al., *Intracellular FMRpolyG-HSP70 complex: Possible use as biochemical marker of Fragile X Tremor Ataxia Syndrome.* 2018: p. 278416.
195. Gendron, T.F., et al., *Poly(GP) proteins are a useful pharmacodynamic marker for C9ORF72-associated amyotrophic lateral sclerosis.* Sci Transl Med, 2017. **9**(383).
196. Lehmer, C., et al., *Poly-GP in cerebrospinal fluid links C9orf72-associated dipeptide repeat expression to the asymptomatic phase of ALS/FTD.* EMBO Mol Med, 2017. **9**(7): p. 859-868.
197. Su, Z., et al., *Discovery of a biomarker and lead small molecules to target r(GGGGCC)-associated defects in c9FTD/ALS.* Neuron, 2014. **83**(5): p. 1043-50.
198. El-Agnaf, O.M., et al., *Detection of oligomeric forms of alpha-synuclein protein in human plasma as a potential biomarker for Parkinson's disease.* FASEB J, 2006. **20**(3): p. 419-25.
199. Humpel, C., *Identifying and validating biomarkers for Alzheimer's disease.* Trends Biotechnol, 2011. **29**(1): p. 26-32.
200. Childs-Disney, J.L. and M.D. Disney, *Approaches to Validate and Manipulate RNA Targets with Small Molecules in Cells.* Annu Rev Pharmacol Toxicol, 2016. **56**: p. 123-40.
201. Sobczak, K., et al., *RNA structure of trinucleotide repeats associated with human neurological diseases.* Nucleic Acids Research, 2003. **31**(19): p. 5469-5482.
202. Kozlowski, P., M. de Mezer, and W.J. Krzyzosiak, *Trinucleotide repeats in human genome and exome.* Nucleic Acids Res, 2010. **38**(12): p. 4027-39.
203. Sobczak, K., et al., *Structural diversity of triplet repeat RNAs.* J Biol Chem, 2010. **285**(17): p. 12755-64.
204. Disney, M.D., et al., *A small molecule that targets r(CGG)(exp) and improves defects in fragile X-associated tremor ataxia syndrome.* ACS Chem Biol, 2012. **7**(10): p. 1711-8.
205. Tran, T., et al., *Targeting the r(CGG) repeats that cause FXTAS with modularly assembled small molecules and oligonucleotides.* ACS Chem Biol, 2014. **9**(4): p. 904-12.
206. Yang, W.Y., et al., *Inhibition of Non-ATG Translational Events in Cells via Covalent Small Molecules Targeting RNA.* J Am Chem Soc, 2015. **137**(16): p. 5336-45.
207. Annear, D.J., et al., *Abundancy of polymorphic CGG repeats in the human genome suggest a broad involvement in neurological disease.* Sci Rep, 2021. **11**(1): p. 2515.
208. Green, K.M., et al., *High-throughput screening yields several small-molecule inhibitors of repeat-associated non-AUG translation.* Journal of Biological Chemistry, 2019. **294**(49): p. 18624-18638.
209. Eckstein, F., *Phosphorothioate oligodeoxynucleotides: what is their origin and what is unique about them?* Antisense Nucleic Acid Drug Dev, 2000. **10**(2): p. 117-21.
210. Crooke, S.T., T.A. Vickers, and X.H. Liang, *Phosphorothioate modified oligonucleotide-protein interactions.* Nucleic Acids Res, 2020. **48**(10): p. 5235-5253.

211. Crooke, S.T., *Molecular Mechanisms of Antisense Oligonucleotides.* Nucleic Acid Ther, 2017. **27**(2): p. 70-77.
212. Eckstein, F., *Phosphorothioates, essential components of therapeutic oligonucleotides.* Nucleic Acid Ther, 2014. **24**(6): p. 374-87.
213. Monia, B.P., et al., *Evaluation of 2'-modified oligonucleotides containing 2'-deoxy gaps as antisense inhibitors of gene expression.* J Biol Chem, 1993. **268**(19): p. 14514-22.
214. Kordasiewicz, H.B., et al., *Sustained therapeutic reversal of Huntington's disease by transient repression of huntingtin synthesis.* Neuron, 2012. **74**(6): p. 1031-44.
215. Wheeler, T.M., et al., *Targeting nuclear RNA for in vivo correction of myotonic dystrophy.* Nature, 2012. **488**(7409): p. 111-5.
216. Smith, R.A., et al., *Antisense oligonucleotide therapy for neurodegenerative disease.* J Clin Invest, 2006. **116**(8): p. 2290-6.
217. Winer, L., et al., *SOD1 in cerebral spinal fluid as a pharmacodynamic marker for antisense oligonucleotide therapy.* JAMA Neurol, 2013. **70**(2): p. 201-7.
218. Miller, T.M., et al., *An antisense oligonucleotide against SOD1 delivered intrathecally for patients with SOD1 familial amyotrophic lateral sclerosis: a phase 1, randomised, first-in-man study.* Lancet Neurol, 2013. **12**(5): p. 435-42.
219. Scoles, D.R., et al., *Antisense oligonucleotide therapy for spinocerebellar ataxia type 2.* Nature, 2017. **544**(7650): p. 362-366.
220. Moore, L.R., et al., *Evaluation of Antisense Oligonucleotides Targeting ATXN3 in SCA3 Mouse Models.* Mol Ther Nucleic Acids, 2017. **7**: p. 200-210.
221. Bagni, C. and B.A. Oostra, *Fragile X syndrome: From protein function to therapy.* Am J Med Genet A, 2013. **161A**(11): p. 2809-21.
222. Agrawal, S., *Importance of nucleotide sequence and chemical modifications of antisense oligonucleotides.* Biochim Biophys Acta, 1999. **1489**(1): p. 53-68.
223. Southwell, A.L., et al., *Antisense oligonucleotide therapeutics for inherited neurodegenerative diseases.* Trends Mol Med, 2012. **18**(11): p. 634-43.
224. Whitesell, L., et al., *Stability, clearance, and disposition of intraventricularly administered oligodeoxynucleotides: implications for therapeutic application within the central nervous system.* Proc Natl Acad Sci U S A, 1993. **90**(10): p. 4665-9.
225. Butler, M., et al., *Spinal distribution and metabolism of 2'-O-(2-methoxyethyl)-modified oligonucleotides after intrathecal administration in rats.* Neuroscience, 2005. **131**(3): p. 705-15.
226. McClorey, G. and S. Banerjee, *Cell-Penetrating Peptides to Enhance Delivery of Oligonucleotide-Based Therapeutics.* Biomedicines, 2018. **6**(2).
227. Boisguerin, P., et al., *Delivery of therapeutic oligonucleotides with cell penetrating peptides.* Adv Drug Deliv Rev, 2015. **87**: p. 52-67.
228. Goyenvalle, A., et al., *Functional correction in mouse models of muscular dystrophy using exon-skipping tricyclo-DNA oligomers.* Nat Med, 2015. **21**(3): p. 270-5.
229. Alyautdin, R., et al., *Nanoscale drug delivery systems and the blood-brain barrier.* Int J Nanomedicine, 2014. **9**: p. 795-811.

230. Evers, M.M., L.J. Toonen, and W.M. van Roon-Mom, *Antisense oligonucleotides in therapy for neurodegenerative disorders.* Adv Drug Deliv Rev, 2015. **87**: p. 90-103.
231. Komor, A.C., A.H. Badran, and D.R. Liu, *CRISPR-Based Technologies for the Manipulation of Eukaryotic Genomes.* Cell, 2017. **168**(1-2): p. 20-36.
232. Cong, L., et al., *Multiplex genome engineering using CRISPR/Cas systems.* Science, 2013. **339**(6121): p. 819-23.
233. Batra, R., et al., *Elimination of Toxic Microsatellite Repeat Expansion RNA by RNA-Targeting Cas9.* Cell, 2017. **170**(5): p. 899-912 e10.
234. Mali, P., K.M. Esvelt, and G.M. Church, *Cas9 as a versatile tool for engineering biology.* Nat Methods, 2013. **10**(10): p. 957-63.
235. Dastidar, S., et al., *Efficient CRISPR/Cas9-mediated editing of trinucleotide repeat expansion in myotonic dystrophy patient-derived iPS and myogenic cells.* Nucleic Acids Res, 2018. **46**(16): p. 8275-8298.
236. Huai, C., et al., *CRISPR/Cas9-mediated somatic and germline gene correction to restore hemostasis in hemophilia B mice.* Hum Genet, 2017. **136**(7): p. 875-883.
237. Long, C., et al., *Postnatal genome editing partially restores dystrophin expression in a mouse model of muscular dystrophy.* Science, 2016. **351**(6271): p. 400-3.
238. Nelson, C.E., et al., *In vivo genome editing improves muscle function in a mouse model of Duchenne muscular dystrophy.* Science, 2016. **351**(6271): p. 403-7.
239. Park, C.Y., et al., *Functional Correction of Large Factor VIII Gene Chromosomal Inversions in Hemophilia A Patient-Derived iPSCs Using CRISPR-Cas9.* Cell Stem Cell, 2015. **17**(2): p. 213-20.
240. Tabebordbar, M., et al., *In vivo gene editing in dystrophic mouse muscle and muscle stem cells.* Science, 2016. **351**(6271): p. 407-411.
241. Park, C.Y., et al., *Reversion of FMR1 Methylation and Silencing by Editing the Triplet Repeats in Fragile X iPSC-Derived Neurons.* Cell Rep, 2015. **13**(2): p. 234-41.
242. Xie, N., et al., *Reactivation of FMR1 by CRISPR/Cas9-Mediated Deletion of the Expanded CGG-Repeat of the Fragile X Chromosome.* PLoS One, 2016. **11**(10): p. e0165499.
243. Liu, X.S., et al., *Rescue of Fragile X Syndrome Neurons by DNA Methylation Editing of the FMR1 Gene.* Cell, 2018. **172**(5): p. 979-992 e6.
244. Niu, Y., et al., *Generation of gene-modified cynomolgus monkey via Cas9/RNA-mediated gene targeting in one-cell embryos.* Cell, 2014. **156**(4): p. 836-43.
245. Liang, P., et al., *CRISPR/Cas9-mediated gene editing in human tripronuclear zygotes.* Protein Cell, 2015. **6**(5): p. 363-372.
246. Kang, X., et al., *Introducing precise genetic modifications into human 3PN embryos by CRISPR/Cas-mediated genome editing.* J Assist Reprod Genet, 2016. **33**(5): p. 581-588.
247. Marchione, M., *Chinese researcher claims first gene-edited babies*, in *Associated Press News*. 2018, AP News: Internet AP News Website.
248. Press, A. *A Chinese researcher claims that he helped make the world's first gene-edited babies. But not everyone supports this controversial experiment.* YouTube [Video]. Nov. 26 2018; Available from: https://www.youtube.com/watch?v=C9V3mqswbv0.

249. Hagerman, R.J., et al., *Treatment of fragile X-associated tremor ataxia syndrome (FXTAS) and related neurological problems.* Clin Interv Aging, 2008. **3**(2): p. 251-62.
250. Polussa, J., A. Schneider, and R. Hagerman, *Molecular Advances Leading to Treatment Implications for Fragile X Premutation Carriers.* Brain Disord Ther, 2014. **3**.
251. Hall, D.A., et al., *Symptomatic treatment in the fragile X-associated tremor/ataxia syndrome.* Mov Disord, 2006. **21**(10): p. 1741-4.
252. Hall, D.A., et al., *Update on the Clinical, Radiographic, and Neurobehavioral Manifestations in FXTAS and FMR1 Premutation Carriers.* Cerebellum, 2016. **15**(5): p. 578-86.
253. Weiss, D., et al., *Long-term outcome of deep brain stimulation in fragile X-associated tremor/ataxia syndrome.* Parkinsonism Relat Disord, 2015. **21**(3): p. 310-3.
254. Rosselot, H. *Fragile X-Associated Tremor/Ataxia Syndrome (FXTAS): Consensus of the FXTAS Task Force and the Fragile X Clinical & Research Consortium*. Consensus of the FXTAS Task Force and the Fragile X Clinical & Research Consortium 2011 3-1-2018; Available from: https://fragilex.org/fxtas-consensus-document/.
255. Jacobs, B.L., H. van Praag, and F.H. Gage, *Adult brain neurogenesis and psychiatry: a novel theory of depression.* Mol Psychiatry, 2000. **5**(3): p. 262-9.
256. Santarelli, L., et al., *Requirement of hippocampal neurogenesis for the behavioral effects of antidepressants.* Science, 2003. **301**(5634): p. 805-9.
257. Bourgeois, J.A., et al., *A review of fragile X premutation disorders: expanding the psychiatric perspective.* J Clin Psychiatry, 2009. **70**(6): p. 852-62.
258. Seritan, A.L., et al., *Memantine for fragile X-associated tremor/ataxia syndrome: a randomized, double-blind, placebo-controlled trial.* J Clin Psychiatry, 2014. **75**(3): p. 264-71.
259. Jain, K.K., *Evaluation of memantine for neuroprotection in dementia.* Expert Opin Investig Drugs, 2000. **9**(6): p. 1397-406.
260. Hill, E.J., et al., *Placebo Response in Fragile X-associated Tremor/Ataxia Syndrome.* Mov Disord Clin Pract, 2020. **7**(3): p. 298-302.
261. Goetz, C.G., et al., *Objective changes in motor function during placebo treatment in PD.* Neurology, 2000. **54**(3): p. 710-4.
262. Witek, N., G.T. Stebbins, and C.G. Goetz, *What influences placebo and nocebo responses in Parkinson's disease?* Mov Disord, 2018. **33**(8): p. 1204-1212.
263. Grigsby, J., et al., *Clinically significant psychiatric symptoms among male carriers of the fragile X premutation, with and without FXTAS, and the mediating influence of executive functioning.* Clin Neuropsychol, 2016. **30**(6): p. 944-59.
264. Keller, E.A., et al., *Role of allopregnanolone on cerebellar granule cells neurogenesis.* Brain Res Dev Brain Res, 2004. **153**(1): p. 13-7.
265. Napoli, E., et al., *Allopregnanolone Treatment Improves Plasma Metabolomic Profile Associated with GABA Metabolism in Fragile X-Associated Tremor/Ataxia Syndrome: a Pilot Study.* Mol Neurobiol, 2019. **56**(5): p. 3702-3713.
266. Wang, J.Y., et al., *Open-Label Allopregnanolone Treatment of Men with Fragile X-Associated Tremor/Ataxia Syndrome.* Neurotherapeutics, 2017. **14**(4): p. 1073-1083.

267. Conde, V., et al., *Abnormal GABA-mediated and cerebellar inhibition in women with the fragile X premutation.* J Neurophysiol, 2013. **109**(5): p. 1315-22.
268. D'Hulst, C., et al., *Expression of the GABAergic system in animal models for fragile X syndrome and fragile X associated tremor/ataxia syndrome (FXTAS).* Brain Res, 2009. **1253**: p. 176-83.
269. Kim, J.M., et al., *Distinct roles of the hippocampus and perirhinal cortex in GABAA receptor blockade-induced enhancement of object recognition memory.* Brain Res, 2014. **1552**: p. 17-25.
270. Prut, L., et al., *A reduction in hippocampal GABAA receptor alpha5 subunits disrupts the memory for location of objects in mice.* Genes Brain Behav, 2010. **9**(5): p. 478-88.
271. Mellon, S.H. and H. Vaudry, *Biosynthesis of neurosteroids and regulation of their synthesis.* Int Rev Neurobiol, 2001. **46**: p. 33-78.
272. Cao, Z., et al., *Clustered burst firing in FMR1 premutation hippocampal neurons: amelioration with allopregnanolone.* Hum Mol Genet, 2012. **21**(13): p. 2923-35.
273. Griffin, L.D., et al., *Niemann-Pick type C disease involves disrupted neurosteroidogenesis and responds to allopregnanolone.* Nat Med, 2004. **10**(7): p. 704-11.
274. He, J., S.W. Hoffman, and D.G. Stein, *Allopregnanolone, a progesterone metabolite, enhances behavioral recovery and decreases neuronal loss after traumatic brain injury.* Restor Neurol Neurosci, 2004. **22**(1): p. 19-31.
275. Karout, M., et al., *Novel analogs of allopregnanolone show improved efficiency and specificity in neuroprotection and stimulation of proliferation.* J Neurochem, 2016. **139**(5): p. 782-794.
276. Wang, J.M. and R.D. Brinton, *Allopregnanolone-induced rise in intracellular calcium in embryonic hippocampal neurons parallels their proliferative potential.* BMC Neuroscience, 2008. **9**(2): p. S11.
277. Singh, C., et al., *Allopregnanolone restores hippocampal-dependent learning and memory and neural progenitor survival in aging 3xTgAD and nonTg mice.* Neurobiol Aging, 2012. **33**(8): p. 1493-506.
278. Djebaili, M., et al., *The neurosteroids progesterone and allopregnanolone reduce cell death, gliosis, and functional deficits after traumatic brain injury in rats.* J Neurotrauma, 2005. **22**(1): p. 106-18.
279. Timby, E., et al., *Pharmacokinetic and behavioral effects of allopregnanolone in healthy women.* Psychopharmacology (Berl), 2006. **186**(3): p. 414-24.
280. Hall, D.A., et al., *Open-label pilot clinical trial of citicoline for fragile X-associated tremor/ataxia syndrome (FXTAS).* PLoS One, 2020. **15**(2): p. e0225191.
281. Qurashi, A., et al., *Chemical screen reveals small molecules suppressing fragile X premutation rCGG repeat-mediated neurodegeneration in Drosophila.* Hum Mol Genet, 2012. **21**(9): p. 2068-75.
282. Alvarez, X.A., et al., *Double-blind placebo-controlled study with citicoline in APOE genotyped Alzheimer's disease patients. Effects on cognitive performance, brain bioelectrical activity and cerebral perfusion.* Methods Find Exp Clin Pharmacol, 1999. **21**(9): p. 633-44.
283. Hunter, J.E., et al., *Capturing the fragile X premutation phenotypes: a collaborative effort across multiple cohorts.* Neuropsychology, 2012. **26**(2): p. 156-64.
284. Belanger, M. and P.J. Magistretti, *The role of astroglia in neuroprotection.* Dialogues Clin Neurosci, 2009. **11**(3): p. 281-95.

ADDENDUM

A

Addendum

Summary

Fragile X-associated tremor and ataxia syndrome (FXTAS) is a late-onset X-linked neurodegenerative disorder caused by a 55-200 CGG-repeat expansion in the 5′ untranslated region (UTR) of the *Fragile X Mental Retardation 1* (*FMR1*) gene. FXTAS patients are clinically characterized by intention tremors and cerebellar gait ataxia. Two main disease mechanisms have been proposed for FXTAS. The first hypothesis is an RNA gain-of-function mechanism caused by elevated levels of *FMR1* mRNA containing the expanded CGG-repeat that can form secondary structures (*i.e.,* hairpins or G-quadruplexes) able to sequester RNA-binding proteins. It is hypothesized that the sequestered RNA-binding proteins are depleted from the cell. This depletion may disturb cellular functions and eventually might lead to neurodegeneration. The second more recent discovered disease mechanism is caused by repeat-associated non-AUG (RAN) protein gain-of-function translation where downstream sequence of the expanded CGG-repeat initiates sense and antisense translation, which results in toxic polypeptides including the polyglycine-containing peptide called FMRpolyG.

In **chapter 1** several *in vitro* protein prediction models and *in vivo* mouse models are summarized that have contributed to our current understanding of the disease mechanisms underlying FXTAS. *In vitro* prediction tools allow us to discover new protein-RNA interactions that take place with the expanded CGG-repeat. Moreover, these tools help us understand why these particular proteins interact with the expanded CGG-repeat while other proteins don't. These *in vitro* approaches have yielded an extensive list of RNA-binding proteins including HNRNP A2/B1, DGCR8, SAM68 and Pur-α and their (co)-localization with ubiquitin in nuclear inclusions in different disease models. All these interactions may help us understand some of the disease phenotypes observed in animal disease models. **Chapter 1** also summarizes many mouse models that have been generated to advance our understanding of the PM and FXTAS pathology. FXTAS mouse models show many similarities to PM carriers with FXTAS including elevated levels of *FMR1/Fmr1* mRNA and the formation of ubiquitin-positive and FMRpolyG-positive inclusions in neurons and astrocytes, but also in systemic organs. Moreover, these mice show neurobehavioral deficits that may be associated with the presence of FMRpolyG and/or inclusions in affected brain regions. Mouse models are essential for the pre-clinical development of targeted therapeutic interventions to improve neurological and behavioral function in FXTAS individuals.

Characteristic neuropathology associated with FXTAS includes the formation of ubiquitin-positive intranuclear inclusions in neurons and astrocytes. Previous studies nicely recapitulate these histopathological features in neurons in a knock-in mouse model, but without significant astroglia associated pathology. To study the role of astroglia in FXTAS

pathogenesis, we generated a new transgenic mouse model (*Gfa2*-CGG99-eGFP) that selectively expresses a 99xCGG-repeat expansion linked to an enhanced green fluorescent protein (eGFP) reporter in astroglia throughout the brain, including cerebellar Bergmann glia. In **chapter 2** we show that our mice specifically express the expanded CGG-repeat in GFAP and S-100β positive cells but not in NeuN, Iba1, or MBP positive cells, indicating that expression of the 99xCGG-eGFP is specific to astroglia. FMRpolyG-positive and ubiquitin-positive intranuclear inclusions were found in astroglia but not in oligodendrocytes and microglia. Behaviorally these mice displayed impaired motor performance on the ladder-rung test, but paradoxically better performance on the rotarod. Intriguingly, immunofluorescence staining revealed FMRpolyG-positive intranuclear inclusions in neurons. The presence of FMRpolyG-positive inclusions in neurons suggests a spread of pathology from astrocytes to neurons by yet unknown mechanisms.

To date, it is a matter of debate whether intranuclear inclusions in neurons and astrocytes contribute to cellular pathology in FXTAS, or may slow down the disease process by sequestering RNA and toxic proteins. In **chapter 3** we generated a new inducible transgenic brain-specific mouse model expressing expanded CGG-repeat RNA coupled to eGFP under the control of the Tet-On system, to study the role of inclusion formation in FXTAS pathology. We showed that the *CamKII-α* promoter drives expression of the expanded CGG-repeat in all expected tissues after doxycycline (DOX)-induction. Neuronal intranuclear inclusions were observed 4 weeks after DOX-induction and after 12 weeks, FMRpolyG-positive intranuclear inclusions were abundantly present in the hippocampus and the striatum. Interestingly, no clear signs of behavioral deficits related to these specific brain regions were found in these mice. This suggests that there is a clear lack of correlation between the (early) presence of FMRpolyG-positive intranuclear inclusions in these brain regions and a behavioral phenotype.

In **chapter 4** we report for the first time about primary hippocampal neurons derived from the hnRNP-rtTA inducible mouse model and inducible mice that can be used as *in vitro* and *in vivo* drug screening tools for targeted interventions. Such a promising candidate for a future therapy is the small chemical compound *1a*. Analyte *1a* shields the expanded CGG-repeat from RNA-binding proteins being sequestered to the CGG-repeat and prevents RAN translation of the expanded CGG-repeat into the toxic FMRpolyG protein. Primary hippocampal neurons could form FMRpolyG-positive inclusions and upon treatment with small molecule *1a*, the number of FMRpolyG-positive inclusions and FMRpolyG protein levels reduced in these cells. We also describe for the first time the formation of FMRpolyG-positive inclusions in the liver of this mouse model. Treatment with small molecule *1a* reduced FMRpolyG protein levels in the liver, but not the number of inclusions. Interestingly, we were able to reduce both number of Rad23b-positive inclusions and Rad23b protein levels. Rad23b is associated with shuttling of toxic and

misfolded proteins to the ubiquitin-proteasome system. These findings suggest that targeted small molecule therapy is effective in a PM mouse model and may have potential to treat CGG-repeat mediated toxicity, including FXTAS.

Ubiquitin-positive intranuclear inclusions in neurons and astrocytes is a major post-mortem neuropathological hallmark for FXTAS. However, it remains challenging to diagnose PM carriers with FXTAS as the clinical features seen in FXTAS overlap with other neurodegenerative diseases. In **chapter 5** we describe two male cases with fragile X-associated neuropsychiatric condition related symptoms and mild movement impairments. Both donors did not show characteristic white matter lesions on MRI, however, vascular infarcts in cortical- and subcortical brain regions were present. High number of FMRpolyG-positive intranuclear inclusions throughout the brain and the vasculature were found to co-localize with ubiquitin-positive intranuclear inclusions. We report a novel pathological vascular phenotype with inclusions present in pericytes and endothelial cells in post-mortem FXTAS brain tissue. Although these results need to be confirmed in more cases, we propose that these vascular lesions in the brain could contribute to the complex symptomology of PM carriers with FXTAS. Moreover, FMRpolyG-positive inclusions can be used as post-mortem hallmark for FXTAS to identify unidentified PM carriers with and without FXTAS.

Currently it is unknown whether a PM carrier will develop FXTAS. Prognostic biomarkers that predict disease onset and disease progression are necessary. Until now, accurate measurements of FMRpolyG protein levels were not possible. In **chapter 6** we developed a new sandwich enzyme-linked immunosorbent assay (ELISA). This ELISA allowed us to accurately measure soluble FMRpolyG protein fractions in transfected COS7 cells and the insoluble FMRpolyG protein fractions in post-mortem hippocampus tissue from a female FXTAS patient. We were able to isolate the insoluble FMRpolyG protein fractions using high concentrations of urea. This proof-of-principle ELISA is promising; however, further validation and optimization are necessary. Beside the fact that post-mortem FXTAS brain tissue is very scarce, it is not possible to use brain tissue for prognostic testing. Therefore, non-invasive collection of peripheral blood mononuclear cell (PBMC) fractions or blood plasma from PM carriers with and without FXTAS would aid in the development of a reliable prognostic tool. If FMRpolyG cannot be detected in PBMC fractions or blood plasma, more invasive methods such as cerebrospinal fluid could be used. Also, this ELISA opens new avenues to investigate the potential role of FMRpolyG as a fluid prognostic or pharmacodynamic biomarker for FXTAS.

Finally, in **chapter 7** all findings reported in this manuscript are discussed in respect to what is currently published in literature.

Samenvatting

Fragiele X-geassocieerde tremor en ataxie syndroom (FXTAS) is een X-gebonden neurodegeneratieve aandoening die op latere leeftijd tot uiting komt. FXTAS wordt veroorzaakt door een verlengde CGG-herhaling (50-200; premutatie) in de 5'-UTR regio van het *fragiele X Mentale Retardatie 1* (*FMR1*) gen. FXTAS patiënten worden klinisch voornamelijk gekenmerkt door intentie tremors en cerebellaire ataxie (*i.e.,* moeite met gecoördineerde bewegingen). Er zijn twee moleculaire ziektemechanismen beschreven die FXTAS kunnen veroorzaken. Het eerste mechanisme is een RNA gain-of-function waarbij het *FMR1* mRNA met een verlengde CGG-herhaling verhoogd tot expressie komt en secundaire RNA-structuren vormt, zoals een haarspeld of een G-quadruplex. RNA-bindende eiwitten kunnen aan deze secundaire RNA-structuren binden, waardoor ze niet meer vrij in de cel voorkomen en dus niet meer hun normale functie in de cel kunnen uitvoeren. Dit zorgt ervoor dat cellulaire processen worden verstoord, wat mogelijk leidt tot neurodegeneratie. Een tweede mechanisme dat recent is beschreven is repeat geassocieerde niet-AUG geïnitieerde (RAN) translatie. RAN translatie kan zowel van 5'-zijde van het RNA naar de 3'-zijde plaatsvinden en andersom. Bij dit eiwit gain-of-function mechanisme wordt de verlengde CGG-herhaling vertaald in een toxisch polyglycine bevattend eiwit, genaamd FMRpolyG.

In **hoofdstuk 1** worden verschillende laboratoriumtechnieken en muismodellen beschreven die een belangrijke bijdrage hebben geleverd aan de huidige kennis over FXTAS en de onderliggende ziektemechanismen. De laboratoriumtechnieken maken het mogelijk om nieuwe eiwitten te beschrijven die een interactie aangaan met de verlengde CGG-herhaling. Deze technieken helpen ons beter te begrijpen waarom bepaalde eiwitten wel een interactie aangaan met de verlengde CGG-herhaling, terwijl andere eiwitten dat niet doen. Met behulp van deze technieken zijn vele RNA-bindende eiwitten beschreven die samen ophopen in insluitsels in de kern van de cel. Door deze interacties te beschrijven kunnen we hopelijk beter het gedrag in de verschillende diermodellen verklaren. **Hoofdstuk 1** vat daarnaast ook de vele muismodellen samen die zijn gegenereerd om de pathogenese FXTAS beter te begrijpen. Deze muismodellen vertonen veel overeenkomsten met FXTAS patiënten, zoals de aanwezigheid van verhoogde *FMR1*/*Fmr1* mRNA levels en de vorming van ubiquitine-positieve en FMRpolyG-positieve insluitsels in zenuwcellen en astrocyten, maar ook in vele systemische organen. Ook vertonen deze muismodellen gedragsafwijkingen die mogelijk geassocieerd kunnen worden met de aanwezigheid van het toxische FMRpolyG en/of de aanwezigheid van insluitsels in aangetaste hersengebieden. Muismodellen zijn belangrijk in het preklinisch onderzoek bij de ontwikkeling van therapeutische interventies, specifiek gericht tegen de ziekmakende verlengde CGG-herhaling, om zo de neurologische functies en klinische verschijnselen van patiënten met FXTAS te verbeteren.

De neuropathologie van FXTAS wordt gekenmerkt door de vorming van ubiquitine-positieve nucleaire insluitsels in zenuwcellen en astrocyten (*i.e.,* een van de astroglia cellen). Voorgaande studies in een knock-in muismodel beschrijven de insluitsels enkel in de zenuwcellen. De astroglia cellen worden buiten beschouwing gelaten. Om de rol van astroglia in de pathogenese van FXTAS te bestuderen, hebben we een nieuw transgeen muismodel (*Gfa2*-CGG99-eGFP) gemaakt, die een verlengde 99xCGG-herhaling gefuseerd met het enhanced green fluorescent protein (eGFP) merker eiwit enkel tot expressie brengt in de astrocyten en Bergmann glia in het brein. In **hoofdstuk 2** laten we zien dat de verlengde CGG-herhaling alleen in GFAP- en S-100β-positieve cellen tot expressie komt in deze muizen, maar niet in NeuN-, Iba1-, of MBP-positieve cellen. Dit betekent dat expressie van het transgen alleen in astroglia tot expressie komt en niet in zenuwcellen. FMRpolyG-positieve en ubiquitine-positieve nucleaire insluitsels waren aanwezig in de astroglia. Gedragsafwijkingen in deze muizen zoals verslechterde motoriek op de ladderrung test waren aanwezig, maar paradoxaal presteerden deze muizen beter op de rotarod test. Zeer verrassend was de aanwezigheid van FMRpolyG-positieve nucleaire insluitsels in zenuwcellen, ondanks dat in deze cellen het eGFP mRNA en eGFP fluorescentie signaal niet aanwezig waren. De aanwezigheid van FMRpolyG-positieve insluitsels in zenuwcellen suggereert dat de neuropathologie die gepaard gaat met de aanwezigheid van FMRpolyG in astroglia via zenuwcellen verspreid kan worden door een nog onbekend mechanisme.

Tot op heden is het niet duidelijk of nucleaire insluitsels in zenuwcellen en astrocyten bijdragen aan de pathogenese in FXTAS, of dat insluitsels het ziekteproces vertragen in FXTAS door RNA en toxische eiwitten weg te vangen. In **hoofdstuk 3** hebben we een nieuw induceerbaar transgeen muismodel ontwikkeld, waarbij de verlengde CGG-herhaling gekoppeld aan het eGFP eiwit enkel in het brein tot expressie komt. Dit muismodel maakt het mogelijk om de rol van insluitsels in de pathogenese van FXTAS te bestuderen. We laten zien dat na toedienen van doxycycline (DOX) de *CamKII-α* driver de verlengde CGG-herhaling tot expressie brengt in verschillende hersengebieden. Vier weken na DOX-inductie waren insluitsels in de zenuwcellen aanwezig en na 12 weken waren velen FMRpolyG-positieve nucleaire insluitsels aanwezig in de hippocampus en het striatum. Ondanks de aanwezigheid van het groot aantal FMRpolyG-positieve nucleaire insluitsels, waren er geen gedragsafwijkingen gerelateerd aan deze hersengebieden aanwezig. Dit suggereert in ieder geval dat er geen ziekmakend verband is tussen de vroege aanwezigheid van insluitsels in het brein en gedragsafwijkingen die mogelijk gepaard gaan met defecten van deze specifieke hersengebieden.

In **hoofdstuk 4** hebben we een primaire hippocampale zenuwcellenkweek opgezet afkomstig van een induceerbaar muismodel met algehele expressie van de CGG-herhaling. Zowel de primaire hippocampale zenuwcellenkweek als de induceerbare muizen kunnen worden gebruikt om nieuwe potentiële compounds te onderzoeken op

effectiviteit als therapeutische interventie voor FXTAS. Een veelbelovende behandeling is het gebruik maken van kleine synthetische moleculen zoals compound *1a*. Compound *1a* bindt aan de haarspeld structuur ontstaan door de verlengde CGG-herhaling en voorkomt dat RNA-bindende eiwitten gaan binden. Daarnaast voorkomt compound *1a* dat er RAN translatie van de verlengde CGG-herhaling kan plaatsvinden en dus ook geen aanmaak van het FMRpolyG. Wij laten in hoofdstuk 4 zien dat de primaire hippocampale zenuwcellen FMRpolyG-positieve insluitsels kunnen vormen en dat na behandeling met compound *1a* het aantal FMRpolyG-positieve insluitsels en FMRpolyG eiwit levels omlaag gaan. Wij beschrijven ook voor de eerste keer dat FMRpolyG-positieve insluitsels in de lever van deze induceerbare muizen worden gevormd. Na behandeling van deze muizen met compound *1a*, zien we dat FMRpolyG levels omlaaggaan, maar het aantal insluitsels niet. Als we de invloed bestuderen op een ander eiwit dat veel voorkomt in insluitsels, namelijk Rad23b, zien we dat behandeling met compound *1a* ervoor zorgt dat zowel het aantal Rad23b-positieve insluitsels als Rad23b eiwit levels omlaaggaan. Rad23b is een belangrijk eiwit dat betrokken is bij het transport van toxische en verkeerd gevouwen eiwitten naar het proteasoom om afgebroken te worden. Deze bevindingen laten zien dat kleine synthetische moleculen effectief zijn in dit FXTAS muismodel en mogelijk gebruikt kunnen worden om toxiciteit, veroorzaakt door de CGG-herhaling, in FXTAS patiënten te behandelen.

Het blijft lastig om premutatie dragers met FXTAS in de kliniek te diagnosticeren, aangezien de klinische ziekteverschijnselen veel overlap vertonen met andere neurodegeneratieve aandoeningen. Ubiquitine-positieve nucleaire insluitsels in zenuwcellen en astrocyten wordt post-mortem voornamelijk gebruikt als het belangrijkste neuropathologische kenmerk om FXTAS patiënten te identificeren. In **hoofdstuk 5** beschrijven we twee mannen met fragile X-geassocieerde neuro-psychiatrische verschijnselen en milde bewegingsproblemen. Beide donoren hadden op de MRI geen karakteristieke witte stof laesies. Echter, in de corticale en subcorticale hersengebieden waren veelvuldig vasculaire infarcten zichtbaar. Daarnaast werden veel FMRpolyG-positieve nucleaire insluitsels gevonden die co-lokaliseren met ubiquitine-positieve nucleaire insluitsels in het brein en de bloedvaten. We rapporteren hier voor het eerst over een mogelijk nieuw vasculair pathologisch fenotype met de aanwezigheid van insluitsels in pericyten en endotheelcellen in post-mortem FXTAS breinweefsel. Ondanks dat deze bevindingen in meer FXTAS gevallen bevestigd moeten worden, veronderstellen wij in dit onderzoek dat deze vasculaire laesies in het brein bijdragen aan de symptomen in premutatie dragers met FXTAS. Daarnaast kunnen FMRpolyG-positieve insluitsels in het brein gebruikt worden om bij ongeïdentificeerde premutatie dragers met en zonder FXTAS alsnog achteraf een diagnose vast te stellen.

Op dit moment is het niet mogelijk om te voorspellen welke premutatie drager in de toekomst FXTAS zal ontwikkelen. Prognostische biomarkers die de eerste symptomen en ziekteverloop van FXTAS kunnen voorspellen zijn noodzakelijk. Tot nu toe was het niet mogelijk om accuraat FMRpolyG eiwit levels in weefsels te bepalen. In **hoofdstuk 6** hebben we een nieuw sandwich enzyme-linked immunosorbent assay (ELISA) ontwikkeld. Met behulp van deze ELISA hebben wij zeer nauwkeurig de oplosbare FMRpolyG eiwit fracties kunnen bepalen in getransfecteerde COS7 cellen en de niet-oplosbare FMRpolyG eiwit fracties in post-mortem breinweefsel van een vrouwelijke FXTAS patiënt. Met behulp van hoge concentraties urea hebben wij de onoplosbare FMRpolyG eiwit fracties kunnen isoleren. Deze proof-of-principle ELISA is veelbelovend, echter is het noodzakelijk om deze ELISA verder te valideren en te optimaliseren. Behalve dat FXTAS post-mortem patiëntmateriaal zeer schaars is, is het bovendien geen goed weefsel om te gebruiken voor het ontwikkelen van een prognostische test. Daarom stellen wij voor om perifere mononucleaire bloedcel (PMBC) fracties en/of bloedplasma van premutatie dragers met en zonder FXTAS af te nemen aangezien dit op een non-invasieve methode kan gebeuren. Indien het niet mogelijk is om FMRpolyG in PMBC fracties of bloedplasma te detecteren, kan cerebrospinaal vocht een alternatief bieden. Dit zou enorm kunnen bijdragen aan het ontwikkelen van een betrouwbare prognostische techniek. Daarnaast maakt deze nieuwe ELISA techniek het mogelijk om de rol van FMRpolyG te onderzoeken als potentieel nieuw fluïde prognostische biomarker of als farmacodynamische biomarker voor FXTAS.

Tot slot, worden in **hoofdstuk 7** alle bevinden uit dit proefschrift besproken in het licht van bestaande gepubliceerde literatuur.

Curriculum Vitae

Personal information

Name: Saif Nadim Nasser Haify
Date of birth: June 9th 1990
Place of birth: Baghdad
E-mail address: s.n.haify@gmail.com

Professional carrier

2016 – 2021 **Ph.D candidate** in the group of prof. dr. Rob Willemsen and dr. Renate K. Hukema at the Department of Clinical Genetics at the Erasmus Medical Center, Rotterdam, the Netherlands

2019 – current **Co-Founder** of Woonryck B.V. located in Rotterdam, the Netherlands

2016 **Associate research scientist** at Janssen Research and Development, a division of Janssen Pharmaceutical N.V. companies of Johnson & Johnson at the Department of Preclinical Development and Safety, Beerse, Belgium

Internships

2015 – 2016 **Master internship,** supervisor dr. Nicolas Darville: the development of an *in vitro* model to study (pro-)drug release after intramacrophagic accumulation of nano/microcrystals of poorly water-soluble (pro-)drugs at Janssen Research and Development, a division of Janssen Pharmaceutical N.V. companies of Johnson & Johnson, Beerse, Belgium

2015 – 2016 **Master internship,** supervisor dr. Lieselot Croes: studying the role keratoconus at the Center for Medical Genetics, Edegem, Belgium

2013 – 2014 **Bachelor internship,** supervisor dr. Christophe Casteleyn: mucosal vaccination in the pig at the Department of Diergeneeskundige Wetenschappen at the University of Antwerp, Antwerp, Belgium

Education

2016 – 2021 Doctor of Philosophy (Ph.D) at Erasmus Medical Center, Rotterdam, the Netherlands

2014 – 2016 Master of Science (M.Sc.), Biomedical Sciences, Molecular and Cellular Sciences and minor in Research, University of Antwerp, Antwerp, Belgium

- FELASA Laboratory Animal Sciences Category C (Article 9/12)

2010 – 2014 Bachelor of Science (B.Sc.), Biomedical Sciences, University of Antwerp, Antwerp, Belgium

List of publications

Wenzel HJ, Murray KD, **Haify SN**, Hunsaker MR, Schwartzer JJ, Kim K, La Spada AR, Sopher BL, Hagerman PJ, Raske C, Severijnen LWFM, Willemsen R, Hukema RK, Berman RF. Astroglial-targeted expression of the fragile X CGG repeat premutation in mice yields RAN translation, motor deficits and possible evidence for cell-to-cell propagation of FXTAS pathology. Acta Neuropathol Commun. 2019 Feb 26;7(1):27. doi: 10.1186/s40478-019-0677-7.

Haify SN, Botta-Orfila T, Hukema RK, Tartaglia GG. *In silico, in vitro*, and *in vivo* Approaches to Identify Molecular Players in Fragile X Tremor and Ataxia Syndrome. Front Mol Biosci. 2020 Mar 11;7:31. doi: 10.3389/fmolb.2020.00031.

Haify SN, Mankoe RSD, Boumeester V, van der Toorn EC, Verhagen RFM, Willemsen R, Hukema RK, Bosman LWJ. Lack of a Clear Behavioral Phenotype in an Inducible FXTAS Mouse Model Despite the Presence of Neuronal FMRpolyG-Positive Aggregates. Front Mol Biosci. 2020 Dec 14;7:599101. doi: 10.3389/fmolb.2020.599101.

Dijkstra AA, **Haify SN**, Verwey NA, Prins ND, van der Toorn EC, Rozemuller AJM, Bugiani M, Dunnen den WFA, Todd PK, Charlet-Berguerand N, Willemsen R, Hukema RK, Hoozemans JJM, Neuropathology of *FMR1*-premutation carriers presenting with dementia and neuropsychiatric symptoms, *Brain Communications*, Volume 3, Issue 1, 2021, fcab007, https://doi.org/10.1093/braincomms/fcab007.

Haify SN, Buijsen RAM, Verwegen L, Severijnen LWFM, de Boer H, Boumeester V, Monshouwer R, Yang WY, Cameron MD, Willemsen R, Disney MD, Hukema RK. Small molecule *1a* reduces FMRpolyG-mediated toxicity in *in vitro* and *in vivo* models for *FMR1* premutation. Manuscript accepted for Human Molecular Genetics, 2021.

Haify SN, Verhagen RFM, van der Toorn, EC, Hukema RK, Charlet-Berguerand N, Willemsen R. An Enzyme-Linked Immunosorbent Assay (ELISA) to detect FMRpolyG levels in post-mortem brain tissue from FXTAS patients. Manuscript in preparation.

Nguyen V, **Haify SN**, Darville N, De Backker P, Vermeulen A. The use of *in vitro* macrophage drug release as surrogate for the in vivo behavior of aqueous nano-/microsuspensions. Manuscript in preparation.

Ph.D Portfolio

Name PhD student: Saif Haify
Department: Clinical Genetics
Research School: Medical Genetics Centre South-West Netherlands (MGC)
PhD period: 2016 - 2021
Promotor: Prof. dr. R. Willemsen
Co-promotor: Dr. R.K. Hukema

PhD training	Year(s)	Workload (ECTS)
Courses and tranings		
Laboratory Animal Science (FELASA C certificate)	2016	3 ECTS
Safely working in the laboratory	2017	0.3 ECTS
Genetics	2017	3 ECTS
The ins and outs of CRISPR-Cas	2017	2 ECTS
Genetic Engineering in Model Organisms	2017	1 ECTS
Animal handling course (IVC)	2017	0.2 ECTS
Gelijkstelling FELASA C: Legislation and Animal Experimentation + Ethics 1	2017	1 ECTS
Animated Science: explaining research in a short video	2017	1 ECTS
Theorie - en praktijktraining 'kleine blusmiddelen en ontruiming'	2018	0.2 ECTS
Biomedical English Writing and Communication (Leiden)	2019	2 ECTS
Research Integrity	2019	0.3 ECTS
Statistics (CC02a)	2020	2 ECTS
Seminars and workshops		
FXTAS/ALS/FTD group journal club	2016 - 2018	1 ECTS
FXTAS group work discussions	2016 - 2021	4 ECTS
Clinical Genetics Lectures	2016 – 2021	2 ECTS
Clinical Genetics Research Meetings (oral presentations)	2016 – 2021	2.8 ECTS
The microscopic Image Analysis seminar	2017	0.8 ECTS
Innovative Mouse Models (IMM) workshop	2017	0.8 ECTS
Introduction to the confocal microscope	2017	0.2 ECTS
MGC PhD workshop Leuven	2017	1 ECTS
FXTAS patient day	2017	0.2 ECTS
MGC PhD workshop Texel	2018	1 ECTS
Department PhD journal club	2018 - 2020	1 ECTS
Sophia Research Days (oral presentation in 2017)	2017 & 2019	0.7 ECTS

(Inter)national conferences		
3rd International Conference on FMR1 Premutation: Basic Mechanisms and Clinical Involvement, Jerusalem, Israel - Oral presentation	2017	2 ECTS
9th International Conference on Unstable Microsatellites & Human Disease, Capri, Italy - Poster presentation	2018	2.2 ECTS
1st Dutch Ataxia Symposium, Groningen, The Netherlands - Oral presentation	2018	0.7 ECTS
4th International Conference on FMR1 premutation: Basic Mechanisms, Clinical Involvement and Therapy, Rotterdam, The Netherlands - Oral presentation	2019	2 ECTS
29th MGC Symposium in Rotterdam	2019	0.2 ECTS

Teaching activities		
Workshop bachelor Medicine students: 'Overervering in de praktijk'	2017 - 2018	0.4 ECTS
Junior Med. School – 'KLGN Onderzoek over erfelijke aandoeningen, genen en vissen'	2017 - 2019	1 ECTS
Supervisor Bachelor students		
Yousif Saoor, Saxion University, Deventer	2017	2 ECTS
Valerie Boumeester, Rotterdam University of Applied Sciences, Rotterdam	2018 - 2019	1 ECTS
Robin Dirks, Avans University, Breda	2018 - 2019	1 ECTS
Renee van Buuren, Avans University, Breda	2018 - 2019	1 ECTS
Ruchira Mankoe, Rotterdam University of Applied Sciences, Rotterdam	2019	0.5 ECTS

Supervisor Master students		
Lucas Verwegen, Erasmus University, Rotterdam	2017 - 2018	1 ECTS
Bram Kuppens, Erasmus University, Rotterdam	2017 - 2018	0.5 ECTS
Benjamin Tak, Amsterdam University, Amsterdam	2018	0.5 ECTS

Institutional Responsibilities		
Supervisor ML-I laboratory (cell culture lab	2016 - 2017	1 ECTS

Totaal	**48.5 ECTS**

Dankwoord

Ik kan nog steeds niet geloven dat het gaat gebeuren maar ik ga promoveren! Whaaaaaaaaaat!! :) Het is echt waar en het voelt ontzettend goed! Voordat ik de mensen om mij heen in het zonnetje zet, wil ik eerst benadrukken dat ik de afgelopen jaren met heel veel plezier onderzoek heb gedaan op de afdeling Klinische Genetica. Promoveren was niet altijd even leuk. En zeker niet altijd even makkelijk. Maar dit promotietraject heeft enorm bijgedragen aan mijn persoonlijke en wetenschappelijke ontwikkeling. Het heeft me op geweldige plekken gebracht zoals in Jerusalem en op Capri in Italië. Daar ben ik in contact gekomen met vele uitstekende onderzoekers die direct of indirect hebben bijgedragen aan mijn promotie. Al vanaf het begin kreeg ik tegenslagen te verduren, zowel op het lab als in mijn privéleven en later kwamen daar nog meer tegenslagen bij maar altijd was er de motivatie om dit hoofdstuk in mijn leven succesvol af te ronden want opgeven zit gewoonweg niet in mijn aard. Ik ben blij dat ik door heb gezet. Promoveren is een team-effort en daarom was promoveren zeker ook niet mogelijk zonder de hulp van mijn collega's, familie en vrienden die ik hieronder wil bedanken.

Allereerst mijn promotor en copromotor, Rob W. en Renate. Ik weet nog precies de dag toen ik kwam solliciteren op de afdeling. Ik was ontzettend zenuwachtig, het zweet brak me overal uit maar jullie zorgden ervoor dat ik me op mijn gemak voelde. Ondanks de kritische bevraging voelde het voor mij als thuiskomen! Lieve Renate, het was heel erg fijn om met jou samen te werken. Zoveel leuke momenten samen meegemaakt. Bij de koffieautomaat brainstormen over nieuwe ideeën, nieuwe papers bespreken of lekker klagen over het geneuzel binnen de politiek. Er was altijd de ruimte om alles uit te spreken en belangrijke of minder belangrijke zaken te bespreken. Jouw deur stond letterlijk en figuurlijk altijd open voor mij (en voor iedereen trouwens). Ik heb ook jouw lieve familie mogen ontmoeten met als hoogtepunt spelen met Nelson en Robin in de tuin. Wat heb ik ontzettend veel gelachen toen! Je hebt een prachtig gezinnetje. Natuurlijk hebben we ook minder leuke momenten samen doorgemaakt met als dieptepunt jouw vertrek in 2019. Dat was op z'n zachts gezegd klote. Ik verloor mijn begeleidster en vriendin op de afdeling. Gelukkig ben jij daarna goed terechtgekomen als docente aan de Hogeschool Rotterdam en heb je volgens mij heel veel plezier in je werk! Dankjewel voor alles! Beste Rob, ook jij hebt veel voor mij betekend sinds het vertrek van Renate maar ook daarvoor toen het stoef ging op het lab. Toen het in 2018 niet goed ging met mij hebben jij en Birgit mij hartelijk ontvangen bij jullie thuis met kerst. Het was een gezellige kerstavond samen met James erbij. We hebben een apart laatste anderhalf jaar achter de rug met Covid19 en het 'nieuwe normaal' wat natuurlijk geen nieuwe normaal is maar een hele vervelende situatie die hopelijk heel snel voorbijgaat. Misschien al wel voorbij is als de promotie achter de rug is. Hoe dan ook, mede dankzij jouw adviezen en inbreng is dit boekje tot stand gekomen. Bedankt voor je begeleiding. Ook wil ik graag de overige leden

van de commissie, prof. dr. F. Kooy, prof. dr. M. Kros en prof. dr. I. Huitinga bedanken voor het kritisch lezen van mijn proefschrift en onderdeel uit te maken van mijn openbare verdediging. Tevens wil ik ook dr. F. de Vrij en prof. dr. Y. Elgersma bedanken voor hun tijd om deel te nemen aan de grote commissie.

Lies-Anne, Esmay en Rob V., zonder jullie harde werk was dit boekje niet mogelijk geweest! Julie hebben ieder op jullie eigen manier enorm bijgedragen aan het eindresultaat! Ontzettend bedankt voor al jullie harde werken! Lies-Anne, jij bent een alleskunner! Je hebt zoveel prachtige foto's gemaakt voor onze groep en voor anderen op de afdeling. Voor ieder klein (of groot) dingetje wist jij waar het stond, wanneer het besteld was en eventueel wie het had geleend, alweer terug heeft gebracht en wie het opnieuw heeft geleend. Je was de levende database van de afdeling. Ik ben dan ook ontzettend verdrietig geweest toen jij vertrok maar heb altijd begrip gehad voor je keuze! We hebben buiten het lab ook hele leuke momenten meegemaakt zoals in Blijdorp met de afdeling, escape room met de groep, gezellige etentjes bij Renate thuis en gezellig bij jou thuis op de koffie! Dankjewel voor de gezellige tijden op het lab maar ook zeker daarbuiten. Lieve Esmay, toen ik begon was jij nog bezig met je stage bij Renate en nu zijn we collega's. Dat getuigt van het feit dat je heel goed bent in wat je doet! Ook al verschillen we qua karakters en begrijpen we elkaar soms niet goed, heb ik veel waardering voor je werk. Ik heb veel van je geleerd! Dankjewel! And last but definitely not the least, Rob! Wij hebben het laatste jaar een veel hechtere band gekregen omdat ik met jou ook over andere dingen kan praten dan alleen werk. Je bent een ontzettend fijn en sympathiek mens, een harde werker, altijd op zoek naar oplossingen en geeft nooit op; pas als oude Rob aangeeft dat het genoeg is. Je bent heel behulpzaam, naar mij maar ook naar anderen op de afdeling. Ik heb heel veel bewondering voor jou. Je bent authentiek en dat maakt je bijzonder. Ik ga vooral missen dat tijdens carnaval jij graag carnavalsmuziek luistert terwijl eraan wil geloven. Stiekem vond ik het wel leuk Rob! Haha! Dankjewel Rob!

De afgelopen jaren zijn er ook een heleboel mensen buiten onze groep op de afdeling bij gekomen en een aantal zijn ook weer vertrokken. Met velen ik leuke momenten meegemaakt! Lieve Helen, bedankt voor je geduld. Jij hebt mij geleerd om primaire hippocampale neuronen te isoleren en te kweken wat uiteindelijk tot een prachtig hoofdstuk (en mogelijk publicatie) heeft geleid. Lieve Herma, bedankt voor je geduld en adviezen, vooral tijdens mijn eerste jaar toen we een nieuw muismodel probeerden te maken en nieuwe constructen kloneerden! Dat was een bevalling. Ik weet nog dat we op een bepaald moment eindelijk het construct hadden, getransformeerd en alles en toen moest het geïsoleerd worden.. De maxi filters bleven vastlopen en uiteindelijk om 10 uur 's avonds was het paniek in mijn hoofd. Hoe ga ik dit oplossen? Kan ik dit bewaren tot morgen? Lies-Anne appte me jouw nummer en jij hebt mij toen telefonisch stap voor stap geholpen! Dat was echt ontzettend lief. Zodra alles in de koelkast en ik naar huis

kon, kreeg ik een melding op mijn telefoon dat er een blikseminslag was op het spoor waardoor ik die dag uiteindelijk pas 1 uur 's nachts thuis was MAAAAR, de maxi's waren gered!! Goed, lang verhaal kort, muis maken uiteindelijk mislukt maar wel een grappige ervaring rijker! Lieve Fenne! Met jou was er direct een klik op het lab. De vele journal clubs samen, gezellige (soms pittige) discussies, de koffie in de ochtend en alle gezelligheid tijdens de MGC-workshops en de WIDM avondjes met pizza. In de vissenkom was het ook altijd heel gezellig met Gerben, Atze en Judith! Heel veel leuke gesprekken en roddels! Samen hebben we nog een educatief filmpje gemaakt over RAN-translatie die op YouTube staat en op het Erasmus MC website. Het was een hele eer om op jouw bruiloft aanwezig te zijn. Het was een gezellige avond met heel veeeel bier en waar ik natuurlijk ook Willem heb leren kennen! Echt een leuke gozer! Echt cool dat jij je postdoc in Amerika ging doen en dat jullie samen de stap hebben gezet om in Amerika te gaan wonen! Ik wens jullie samen een prachtige toekomst toe! Ronald, jij was al weg voordat ik op de afdeling kwam maar jouw naam galmde nog na door de gangen op de 9e. Jij hoort bij het meubilair van de afdeling klinische genetica! Bedankt voor jouw kritische blik op mijn onderzoek en de discussies die we hebben gehad. Samen met Lodewijk heb jij mij geleerd om de dotblot te gebruik en uiteindelijk samen met Lucas hebben we er een werkend protocol van gemaakt om FMRpolyG te kunnen detecteren! Dankjewel!

Ik heb met velen op de afdeling klinische genetica een leuke tijd gehad. Van laser gamen en escape rooms tot gezellige etentjes en stappen in Rotterdam en Utrecht! Het voordeel, en tegelijk ook een nadeel van interne verhuizingen is dat je vertrouwde kamergenoten moet achterlaten en nieuwe kamergenoten krijgt. Mijn lieve kamergenoten Fenne, Gerben, Judith, Atze, Stefan, Roy, Martyna, Ana en Christina! Thank you very much for the joyful years together! With you guys I could share my frustrations in the lab after an experiment failed for the 100th time as well as my successes and conferences I attended. More importantly, we could always have a chat about the important stuff in life like soccer games and the Dutch national team after a fuck-up, about politics, holidays but also weddings and birthdays! So much! I really had a blast with all of you, thanks! Goodluck with your PhDs, post-docs and careers! Madeleine, bedankt voor het organiseren van alle MGC workshops en cursussen in Leiden. Alle PhDs bedankt voor de gezellige MGC workshops and the good parties. In het bijzonder de 'kamer 202' groep: Fenne, Annemarie, Esther, Inge, Laura V., Roy en Wojtek! Tijdens de MGC uitstapjes hebben wij de gekste dingen gedaan en dat creëert een band. Na MGC zijn we in contact gebleven en zelfs vrienden geworden. De gezellige etentjes, drankjes en dansjes ga ik nooit meer vergeten! Tjakko, bedankt voor je adviezen en de gezellige gesprekken samen met Gerben! Gerben, je bent echt een toffe gozer! Vol humor en gezelligheid, ook in voor een gekke foto ;-). Ellis, wij hebben elkaar het laatste jaar heel goed leren kennen. Je bent zo lief en slim! Blijf in jezelf geloven ongeacht wat men tegen je zegt. Bedankt voor de gezellige gesprekken en de koffietjes! Alle andere (ex)collega's, bedankt voor de gezellige labdagen, borrels en

discussies op het lab: Pim, Vincenzo, Wim M., Erwin, Guido, Bianca, Rachel, Rodrigo, Pablo, Kyra, Natasha, Stijn, Leslie, Jordy, Joon, Monica, Laura, Eva, Mike, Shami, Tom, Soheil, Elena, Anita, Jonathan, Douglas, Yuying, Almira, Katherine, Maria, Michelle, Marianne, Leontine, Stefanie and Demy. Beste Rachel, Bep, Jeannette, Marike, Charlotte en Marjoleine, bedankt voor jullie administratieve ondersteuning! Jullie lieten ingewikkelde vraagstukken vaak zo ontzettend simpel lijken. Dank voor al jullie hulp! Jeannette, geniet van je pre-pensioen! Hopelijk is corona snel voorbij en kun je erop uit. Beste Tom en Ruud, bedankt voor alle mooie (en minder mooie) foto's! Als jullie de groepsfoto's maakten voor onze groep was het altijd genieten en trollen! Zeker wanneer Tom Lies-Anne op de foto wilde krijgen! Tom, geniet van je vrije tijd! Het was leuk om op de afdeling te werken en met iedereen in contact te zijn! Bedankt voor de leuke tijd.

Met mensen buiten onze afdeling heb ik natuurlijk ook contact gehad met leuke samenwerkingen (collaborations). Beste Laurens, het was prettig om met je samen te werken. Bedankt voor het opzetten van de gedragsexperimenten met de CamKII-muizen en voor de begeleiding van Ruchira. Dat heeft in een mooie publicatie geresulteerd. Beste Anke, bedankt dat ik langs mocht komen om een obductie mee te maken en samen met jou FXTAS cases te bespreken. Bedankt voor alle uitleg en het patiëntmateriaal dat je met ons deelt. Het is prettig om met jou samen te werken. Beste Gert en Suzanne, bedankt voor jullie ondersteuning bij het maken van transgene wormen. Bedankt dat Benjamin bij jullie op de afdeling mocht werken voor ons. Dear Gian and Teresa, thanks for collaboration that resulted in a very nice review. Dear prof. dr. M. Disney and dr. WY. Yang, thank you for collaborating with us and for sharing your compounds with us resulting in a nice publication in Human Molecular Genetics journal. Beste Alex Maas en John, bedankt voor alle injecties die jullie voor ons hebben gedaan en Alex bedankt dat jij mij meenam om de injecties van dichtbij mee te maken. Ook een dikke vette shout-out naar alle dierenverzorgers: Ineke, Sandra, Michelle, Jenny, Charlotte, Jennifer, Jessica, Jolien en Kim. Het contact was altijd heel prettig en jullie waren ontzettend behulpzaam en geïnteresseerd in wat wij deden! Beste Gert-Jan en Alex van het OIC, bedankt voor de introducties tot de microscopen en jullie adviezen om de beste plaatjes te kunnen schieten. Beste Koos en Leo, bedankt voor alle bestellingen en het rondbrengen van alle pakketjes. Beste Sjozef en Ton, bedankt voor de technische ondersteuning!

In de afgelopen 4.5 jaar heb ik ook met heel veel plezier 8 studenten mogen begeleiden tijdens hun bachelor- en masterstages. Allemaal hebben jullie een bijdrage geleverd aan mijn promotie waarvoor ontzettend bedankt! Yousif, jij was mijn eerste student. Ze zeggen dat de eerste altijd bijzonder is, nou dat was het zeker! Ik kende je natuurlijk al van buiten het onderzoek. Toen je kwam met de vraag of ik je kon helpen omdat het met de vorige stagebegeleider niet lekker liep, wilde ik je heel graag helpen maar dat was eventjes spannend want ik was toen zelf nog maar een paar maanden bezig. Uiteindelijk was dat

een hele leuke, geslaagde stage. Je bent een top gozer en harde werker! Bedankt! Bram K., met jou heb ik echt veel gelachen terwijl je eigenlijk niet voor mijn project werkte. Je begeleiden in de celkweek was echt leerzaam voor ons allebei! Succes met je specialisatie! Lucas, wat heb jij top werk geleverd tijdens je stage! Man! Je bent zo gedreven dat het mij nog steeds verbaast dat je geen PhD wilt doen maar goed, dat begrijp ik ook heel erg goed nu ik je beter heb leren kennen. Plannen ben je heel goed in maar vervolgens de planning uitvoeren blijkt nog steeds soms lastig te zijn. Ondanks de vele behandelingen die je moest ondergaan, heb je tijdens je stage zo goed werk geleverd dat je gedeelde eerste auteur staat op het compound 1a paper. En meer dan terecht. Je bent nu al ruim 2 jaar werkzaam op EMC als analist bij celbiologie. Ze boffen met jou. Mijn advies Lucas blijft staan en dat is overweeg die PhD als het op je pad komt ;-) Heel veel succes! Benjamin, meeste van jouw tijd zat je bij celbiologie om de juiste transgene wormen te maken. Sowieso geen gemakkelijke klus. Maar als helemaal niet omdat je best wel eigenwijs kon zijn en dingen alleen op je eigen manier wilde doen. Desondanks is het wel gelukt, ook omdat je in jezelf bleef geloven en dankzij de zeer goede ondersteuning van Suzanne Rademakers! Succes met alles Benjamin. Valerie, Robin en Renee! Jullie begonnen alle drie gelijktijdig aan jullie stage. Jullie waren vrij rustig aan het begin van de stage maar naarmate jullie je meer op je gemak voelden, hebben wij dat geweten haha! Renee, jij bent eigenlijk vanaf start tot einde de stabiele factor geweest met de meiden. Af en toe een tikkeltje onzeker, en het hielp dan ook niet mee dat het maken van RNA maar bleef mislukken. Je bent ontzettend leergierig en een echte doorzetter. RNA maken is uiteindelijk niet gelukt zoals we hadden gewild maar we wisten na jouw stage wel in welke hoek we het moesten zoeken. Een uitstekende verdediging van je thesis met een 9 als eindresultaat. Je twijfelde over een master doen maar ontzettend stoer dat je hebt doorgezet! Heel veel succes met je master! Robin, de druktemaker van de drie (alhoewel Valerie ook een pluim verdient). Jij zat weliswaar voornamelijk bij celbiologie om verder te werken aan de wormen van Benjamin maar het was meteen hoorbaar als je bij ons het lab opliep. Je bent heel slim, ontzettend energiek, je bruist van de energie. Het was dan ook altijd heel gezellig om samen met jou te lunchen want je had van alles en nog wat meegemaakt tijdens je weekend. Het was echt leuk! Dankjewel en heel veel succes met je carrière! Valerie, de kwebbelkont op het lab. Jij kon onze oren al om 9 uur 's ochtends eraf lullen want jouw leven was nooit saai haha. Toen ik de kamer naast het lab zat, kon ik je altijd horen lachen maar dat is minder geworden toen ik verhuisde mijn huidige kamer terwijl dat toch een stuk verder was. Je unieke lach is vreugde op de afdeling. Je bent heel erg goed in je werk op lab. Ook jij staat op de compound 1a paper en dat heb je helemaal zelf verdiend. En als kerst op de taart ben je na je stage in de groep van Vincenzo Bonifati aangenomen als analist. Ik wens je heel veel succes met alles! Ruchira, het was heel prettig om samen met jou te werken. Je bent rustig van aard en bewaart het overzicht in tijden van onrust. Heel fijn dat je bij Laurens Bosman terecht kon om de gedragsexperimenten uit te voeren. Ook jij hebt uitstekend werk geleverd met als resultaat een publicatie en

een 2e auteurschap voor jou! Je hebt sinds kort een nieuwe baan bij Eurofins. Heel veel geluk! Sanne, ik heb jou niet begeleidt tijdens je stage maar je verdient wel een bedankje voor jouw bijdrage aan het project met de zebravissen. Met de kennis die we hadden opgedaan bij Renee en de begeleiding van Esmay en Rob, is het jou wel gelukt om RNA te maken. Ook jij bent na je stage aan de slag gegaan bij het Erasmus op de afdeling klinische genetica bij de diagnostiek. Succes en bedankt!

Lieve vrienden en kennissen, bedankt voor jullie interesse in mijn onderzoek. In het bijzonder mijn drie beste vrienden Job, Thijs en Bram. Wij kennen elkaar sinds dat wij in Altforst kwamen wonen. Sindsdien zijn we onafscheidelijk. Onze kaart- en spelletjes avonden zijn echt momenten waar ik naar uitkijk! Met jullie kan ik lachen, heel veel lachen, veel discussiëren, ruzie maken, maar ook zware momenten in mijn leven delen en vrijuit huilen. Bij jullie ben ik mezelf en dat betekent heel veel voor me. Bram, wij hebben in 2019 onze eigen BV opgericht omdat wij beiden heel erg ondernemen zijn! Man wat vind ik dat leuk! De balans tussen vriend en zakenpartner was in het begin lastig. Zeker omdat we anders werken maar ik zou je voor geen goud inruilen (misschien wel voor een Bitcoin, just kidding bro!). Ik hou van jullie! We ride together, we die together. Best friends for life!

Woutje, liefje, wij hebben elkaar 2 jaar geleden leren kennen op de afdeling. Jij was visjes aan het inbedden. Ik was de pH aan het meten. We raakten aan de praat. Ik vroeg je om wat te gaan drinken en dat vond je wel leuk. Voor mij was dat overduidelijk een date, heel spannend natuurlijk. Voor jou was dat gezellig wat drinken met een collega. En sindsdien hebben we de grootste lol samen. Ik kan mijn hart bij jou luchten zoals ik dat bij niemand anders kan. We hebben onze ups en downs gehad. Afgelopen jaar werd ik geopereerd aan mijn knieën. Dat was heel zwaar, zowel voor jou als voor mij. Jij hebt nooit geklaagd en hebt me dag (en nacht) verzorgt totdat ik weer kon lopen. Ook tijdens het schrijven heb je er alles aan gedaan om voor mij een zo'n prettig mogelijke schrijfomgeving te creëren terwijl jij zelf natuurlijk ook aan het promoveren bent. Het kost jou geen enkele moeite om zorgzaam te zijn! En dat vind ik zo ontzettend mooi aan jou. Het is heel fijn en warm om met jou samen te zijn! Tijdens corona zijn we nog meer naar elkaar toe gegroeid en iedere dag word ik een stukje meer verliefd op je. Ik ben een zeer gelukkig mens, een zeer gelukkige vriend en ik kan niet wachten om de toekomst met jou te ontdekken!! Ik hou ontzettend veel van jou. Een hele dikke kus van mij!

Lieve pap en mam, jullie zijn ruim 20 jaar geleden gevlucht uit Irak om mij een betere toekomst te geven in Nederland en kijk waar we nu staan. Het is toch echt waar, ik ga ruim 20 jaar later promoveren! Ik weet dat studeren en een goede toekomst hebben voor jullie heel belangrijk is. Jullie zijn ook altijd mijn motivatie geweest om te blijven studeren en het maximale uit mezelf. Soms vond ik dat ook heel lastig want het voelde alsof het hele leven om studeren draaide. Nu weet ik dat dat niet zo is. Jullie hebben heel veel

opgeofferd in jullie leven voor mij. De lijst is veel te lang maar een ding dat ik nooit zal vergeten is dat jullie met het klein beetje geld dat jullie hadden, CDs voor mij kochten zodat ik beter werd in de Nederlandse taal, in rekenen, in aardrijkskunde en nog wel 10 andere dingen waarvan jullie vonden dat die belangrijk waren voor mijn ontwikkeling. Altijd ten koste van jullie. Lieve papa, jouw adviezen over het volwassen leven kwamen al heel vroeg, soms iets te vroeg maar nu 31 jaar later realiseer ik me iedere dag meer en meer hoe belangrijk die adviezen zijn geweest. Dankzij jouw begeleiding ben ik de man die ik vandaag de dag ben. Ik hou van je ouwe reus! Lieve mama, jouw liefde en zorgzaamheid is met geen woorden te beschrijven. Jouw toewijding om samen met mij tijdens toetsweken tot 's avonds laat woordjes van Duits, Frans, Latijn en Grieks te overhoren was enorm. Het was alsof jij een toets moest maken. Pas als ik alle woordjes foutloos kon opschrijven, twee keer, dan pas ging je slapen want je geloofde het dan wel. Je maakt de lekkerste gerechten, soms iets te veel kruiden maar altijd heeerlijk. Je hebt een ongelofelijk goed hart vol met liefde, naar iedereen toe! Je bent de meest liefdevolle en vergevingsgezinde persoon die ik ken! Mijn allergrootste voorbeeld! Ik hou van je!! Samen maakten jullie het mogelijk dat ik kon gaan studeren! Eerst een bachelor. Dan een master en ook al twijfelden jullie een klein beetje of een PhD wel de juiste volgende stap zou zijn, ook daarin hebben jullie mij gesteund. Daar ben ik jullie eeuwig dankbaar voor. Wonen en leven in Nederland was en is nog steeds voor jullie niet altijd even makkelijk door het verschil in cultuur. Soms zijn jullie veel te bezorgd maar dat hoeft echt niet meer. En ook al weet ik dat jullie niet gaan luisteren (die koppigheid heb ik ergens vandaan geërfd), wil ik toch echt zeggen dat het nu de hoogste tijd is om met z'n drieën van het leven te genieten, alle zorgen achter ons te laten en vooruit te kijken! Probeer dit advies aan te nemen. Dan is de cirkel helemaal rond. Ik kan het niet vaak genoeg blijven zeggen maar ik hou van jullie!

Ik wil graag ook de Fragiele X Vereniging Nederland en al haar leden bedanken dat ik aanwezig mocht zijn op jullie FXTAS dag! Door te luisteren naar jullie problemen, denk ik dat wij als wetenschappers beter ons werk kunnen doen. Soms is de wetenschap gefocust op het meest praktische en haalbare terwijl premutatiedragers en FXTAS patiënten worstelen met hele andere dingen. Dat was voor mij een absolute eye-opener! Ik hoop dat het werk dat we hier als groep hebben neergezet weer een klein beetje kan bijdragen aan het ultieme doel, namelijk een therapie vinden. Bedankt voor jullie verhalen!

En als laatste wil ik graag Robert Hofstra bedanken. Bedankt voor jou werk op de afdeling. Ik vond het heel spannend om mijn project de eerste keer bij jou op kantoor te bespreken maar na die ontmoeting vond ik je wel heel stiekem een coole afdelingshoofd. Je was altijd geïnteresseerd in wat we deden en je maakte altijd een praatje met iedereen over van alles en nog wat. Je hebt je met hart en ziel voor de afdeling ingezet, en natuurlijk kon je het niet altijd goed doen en was er af en toe kritiek maar je wist waarvoor je had

getekend. En als we nu kijken waar we staan als afdeling, dan kunnen we denk ik wel stellen dat je top werk hebt geleverd. Ik vond het heel erg leuk om tijdens de retraite met je te kletsen over kunst en je hobby's. En het was heel erg leuk om je samen met je vrouw bij de Van Nelle fabriek tegen te komen bij een kunsttentoonstelling. Afgelopen jaar kregen we allemaal het vreselijke nieuws te horen, namelijk dat die vreselijke ziekte jou te pakken had gekregen. Voor iedereen op de afdeling was het schrikken. Therapie sloeg niet meteen aan maar gelukkig kregen we al snel dat de situatie stabiel was. Ik was dan ook enorm verrast dat je alweer 2-3 maanden na je diagnose op de afdeling zag rondlopen. Maar eigenlijk verbaasde me dat niks. Dat onderschrijft namelijk jouw liefde voor de kliniek, voor de research en de afdeling klinische genetica. 'Ik wens jou en je familie heel veel sterkte toe Robert!'

Houdoe en bedankt!

Saif